Cell wall recycling in *Staphylococcus aureus* and *Bacillus subtilis*

Dissertation
der Mathematisch-Naturwissenschaftlichen Fakultät
der Eberhard Karls Universität Tübingen
zur Erlangung des Grades eines
Doktors der Naturwissenschaften
(Dr. rer. nat.)

vorgelegt von
Robert Maria Kluj
aus Zwickau

Tübingen
2022

Gedruckt mit Genehmigung der Mathematisch-Naturwissenschaftlichen Fakultät der Eberhard Karls Universität Tübingen.

Tag der mündlichen Qualifikation:	15.02.2023
Dekan:	Prof. Dr. Thilo Stehle
1. Berichterstatter:	Apl. Prof. Dr. Christoph Mayer
2. Berichterstatter:	Prof. Dr. Hannes Link

Erklärung

Ich erkläre hiermit, dass ich die zur Promotion eingereichte Arbeit mit dem Titel: „Cell wall recycling in *Staphylococcus aureus* and *Bacillus subtilis*“ selbständig verfasst, nur die angegebenen Quellen und Hilfsmittel benutzt und wörtlich oder inhaltlich übernommene Stellen als solche gekennzeichnet habe. Eine detaillierte Abgrenzung meiner eigenen Leistungen von den Beiträgen meiner Kooperationspartner habe ich in den Abschnitten 4.1.1 und 4.2.1 vorgenommen. Ich erkläre, dass die Richtlinien zur Sicherung guter wissenschaftlicher Praxis der Universität Tübingen (Beschluss des Senats vom 25.05.2000) beachtet wurden. Ich versichere an Eides statt, dass diese Angaben wahr sind und dass ich nichts verschwiegen habe. Mir ist bekannt, dass die falsche Abgabe einer Versicherung an Eides statt mit Freiheitsstrafe bis zu drei Jahren oder mit Geldstrafe bestraft wird.

Zusammenfassung

Die bakterielle Zelle ist von einer schützenden Zellwand umgeben, welche sie von ihrer Umgebung abschirmt und als Gegenkraft zum intrazellulären Turgor wirkt. Der bakterielle Lebenszyklus aus Zellwachstum und -teilung erfordert eine ständige Anpassung der Zellwand, genauer gesagt ihrer Kernstruktur, des Peptidoglykans. Während dieser Umstrukturierungsprozesse werden Bestandteile des Peptidoglykans freigesetzt. Viele Bakterien haben Strategien zur Wiederverwertung von Zellwandzuckern und -peptiden entwickelt, um den Verlust von Ressourcen zu kompensieren. In *Bacillus subtilis* umfasst die Wiederverwertung des Aminozuckers *N*-Acetylmuraminsäure (MurNAc) die Bildung von MurNAc-6P, gefolgt von der intrazellulären Umwandlung in GlcNAc-6P durch die Etherase MurQ. GlcNAc-6P kann schließlich über weitere Zwischenschritte entweder in die Peptidoglykansynthese oder in die Glykolyse eingeführt werden. *Staphylococcus aureus* und das gramnegative Bakterium *Escherichia coli* verfügen über homologe Enzyme, die die Gewinnung von extrazellulärem MurNAc ermöglichen. Beide Organismen setzen jedoch andere Fragmente des Peptidoglycans als *B. subtilis* frei. Während in *E. coli* Disaccharide mit daran gebundenen Peptiden freigesetzt und wiederverwertet werden, ist über den Wiederverwertungsprozess in *S. aureus* wenig bekannt.

In *S. aureus* werden während der Autolyse offenbar eher Disaccharide als Monosaccharide produziert, und MurNAc-GlcNAc als Hauptumsatzprodukt freigesetzt. Die vorliegende Arbeit stellt diese Tatsache in den Kontext des MurNAc-Recyclingweges.

In dieser Arbeit wurde gezeigt, dass der PTS-Transporter MurP nicht nur der Aufnahme des Monosaccharids MurNAc dient, sondern auch die Aufnahme und Phosphorylierung des Disaccharids MurNAc-GlcNAc bewerkstelligt. Das entstehende MurNAc-6P-GlcNAc ist jedoch kein direktes Substrat für die Etherase MurQ. In *S. aureus* umfasst das MurNAc-Recycling-Operon ein zusätzliches Gen, dessen theoretisches Translationsprodukt weder in *E. coli* noch in *B. subtilis* eine Entsprechung hat. Hier wurde gezeigt, dass das Gen für eine Phosphomuramidase kodiert, welche das Disaccharid MurNAc-6P-GlcNAc in MurNAc-6P und GlcNAc spaltet. Entsprechend wurde das Enzym MupG (für MurNAc-6P-Glycosidase) genannt. Das von MupG produzierte MurNAc-6P wird anschließend von MurQ prozessiert. MupG stellt somit eine Anpassung des MurNAc-Recyclingweges an die Bedürfnisse von *S. aureus* dar. MupG ist der erste charakterisierte Vertreter einer Proteinfamilie, die die Domäne mit unbekannter Funktion DUF871 enthält.

Bakterien haben nicht nur für Zellwandzucker, sondern auch für Zellwandpeptide Wiederverwertungsstrategien entwickelt. *E. coli* importiert Zellwandpeptide über einen ABC-Transporter und verarbeitet sie intrazellulär in mehreren Schritten. In dieser Arbeit wurde gezeigt, dass *B. subtilis* Enzyme kodiert, die den Abbau auf ähnliche Art und Weise ermöglichen. Die γ-D-Glu-*meso*-Dpm-Endopeptidase YkfC hydrolysiert unverzweigte und verzweigte Zellwandpeptide in L-Ala-D-Glu und Dpm-haltige Reste. Das Dipeptid kann nach Epimerisierung zu L-Ala-L-Glu weiter verstoffwechselt werden. Im Gegensatz zu *E. coli*, liegt *meso*-Dpm in *B. subtilis* fast ausschließlich amidiert vor. Diese Besonderheit erfordert die Aktivität von DppA, welches *meso*-Dpm deamidiert und dadurch YkfA ermöglicht, die LD-Bindung zwischen *meso*-Dpm und

D-Ala in den Dpm-haltigen Resten zu spalten. Das Endprodukt *meso*-Dpm dieses sequenziellen Abbaus, kann schließlich in der Peptidoglykansynthese wiederverwendet werden.

Zusammengefasst, ermöglichen diese Ergebnisse weitere Einblicke in den grundlegenden Wiederverwertungsprozess der bakteriellen Zellwand. Sie zeigen auch, dass grampositive Bakterien, obwohl sie keine äußere Membran besitzen und daher nicht in der Lage sind, Zellwandumsatzprodukte in einem Periplasma zurückzuhalten, ähnliche Strategien zur Wiederverwertung von Zellwandzuckern und -peptiden anwenden wie gramnegative Bakterien.

Abstract

The bacterial cell is surrounded by a protective cell wall, which shields the cell from its environment and acts as a counterforce to the turgor. The bacterial life cycle of cell growth and division requires continuous adaptation of the cell wall, more specifically of its core structure, the peptidoglycan. During these restructuring processes, components of the peptidoglycan are released. Many bacteria have developed strategies for recycling of cell wall sugars and peptides to cope with a loss of resources. In *Bacillus subtilis*, recycling of the amino sugar *N*-acetylmuramic acid (MurNAc) involves the formation of MurNAc 6P, followed by intracellular conversion into GlcNAc 6P by the etherase MurQ. GlcNAc 6P can finally be introduced via further intermediate steps either into peptidoglycan synthesis or into glycolysis. *Staphylococcus aureus* and the Gram-negative organism *Escherichia coli* possess homologous enzymes that allow the recovery of extracellular MurNAc. However, both organisms release fragments of the peptidoglycan different than *B. subtilis*. Whilst in *E. coli* disaccharides with peptides attached are released and recycled, little is known about recycling in *S. aureus*.

In *S. aureus*, apparently disaccharides rather than monosaccharides are produced during autolysis and MurNAc-GlcNAc is released as the main turnover product. This work puts this fact in the context of the MurNAc recycling pathway.

In this work, it was shown that the PTS transporter MurP not only serves the uptake of the monosaccharide MurNAc, but also accomplishes the uptake and phosphorylation of the disaccharide MurNAc-GlcNAc. The resulting MurNAc 6P-GlcNAc, however, is not a direct substrate for the etherase MurQ. In *S. aureus* the MurNAc recycling operon comprises an additional gene whose theoretical translation product has no equivalent in either *E. coli* or in *B. subtilis*. The gene was shown to encode a phosphomuramidase that cleaves the disaccharide MurNAc 6P-GlcNAc to MurNAc 6P and GlcNAc. Accordingly, the enzyme was named MupG (for MurNAc 6P-glycosidase). The MurNAc 6P produced by MupG is subsequently processed by MurQ. MupG thereby represents an adaptation of the MurNAc recycling pathway to the needs of *S. aureus*. MupG is the first characterised representative of a protein family containing the domain of unknown function DUF871.

Bacteria have developed recycling strategies not only for cell wall sugars but also for cell wall peptides. *E. coli* imports cell wall peptides via an ABC transporter and processes them intracellularly in several steps. In this work, it was shown that *B. subtilis* encodes enzymes that enable degradation in a similar way. The γ-D-Glu-*meso*-Dpm endopeptidase YkfC hydrolyses unbranched and branched cell wall peptides into L-Ala-D-Glu and Dpm-containing residues. The dipeptide can be further metabolised after epimerisation into L-Ala-L-Glu. In contrast to *E. coli*, *meso*-Dpm in *B. subtilis* is almost exclusively amidated. This particular feature requires the activity of DppA, which de-amidates *meso*-Dpm and thereby enables YkfA to cleave the LD-bond between *meso*-Dpm and D-Ala in the Dpm-containing residues. The end product *meso*-Dpm of this sequential degradation can eventually be reused in peptidoglycan synthesis.

In conclusion, these findings provide further insights into the basic process of cell wall recycling. They also show that Gram-positive bacteria, despite lacking an outer membrane

and thus are not able to retain cell wall turnover products in a periplasm, use similar recycling strategies as Gram-negative bacteria to salvage cell wall sugars and peptides.

Contents

Abbreviations

2P	dipeptide (L-Ala-D-Glu)
3P	tripeptide (L-Ala-D-Glu-*meso*-Dpm)
4P	tetrapeptide (L-Ala-D-Glu-*meso*-Dpm-D-Ala)
5P	pentapeptide (L-Ala-D-Glu-*meso*-Dpm-D-Ala_2)
6P	6-phosphate
AMC	7-amido-4-methylcoumarin
anhMurNAc	*N*-acetylmuramic acid
API	application programming interface
BPC	base peak chromatogram
CFU	colony forming unit
CLI	command line interface
CM	cytoplasmic membrane
CV	column volume
DC	difference chromatogram
DUF	domain of unknown function
EIC	extracted ion chromatogram
ESI	electrospray ionisation
FWHM	full width at half height
GlcNAc	*N*-acetylglucosamine
GUI	graphical user interface
Lipid II	UDP-MurNAc-Pentapeptid
M-G	MurNAc-GlcNAc
ManNAc	*N*-acetylmannosamine
MurNAc	*N*-acetylmuramic acid
OM	outer membrane
OPA	o-phthalaldehyde
PBP	Penicillin-binding protein
PTS	phosphotransferase system
SEC	size exclusion chromatography
TIC	total ion chromatogram

1. Introduction

1.1. The peptidoglycan cell wall characterises the domain Bacteria

Life on earth is classified into the three domains Archaea, Bacteria and Eukaryota [1]. Besides archaea, bacteria are among the oldest life forms on earth and account for the largest proportion of terrestrial biomass after plants [2]. Bacteria are multifaceted organisms whose enormous diversity manifests itself in different cell shapes, cellular organisation (unicellular or multicellular) and in different abilities. Some bacteria prefer higher temperatures, some live in water, others are not reliant on oxygen and still others can synthesise unusual compounds. These properties and capabilities allow them to colonise a wide variety of habitats and make them interesting for industrial applications. The human body is also colonised by bacteria. Some supply the body with nutrients that it cannot obtain itself, whereas others can cause infections.

Escherichia coli and *Bacillus subtilis* are the two most studied model organisms and representatives of the Gram-negative and Gram-positive lineages of bacteria. Both are characterised by a rod-shaped appearance and are of biotechnological importance. However, whilst *E. coli* is a common coloniser of the intestinal tract of mammals, *B. subtilis* is a ubiquitous habitant of soils and a plant fertiliser. Its ability to sporulate allows it to survive even extreme environmental conditions. The coccoid-shaped *Staphylococcus aureus* is a natural component of the human microbial flora, but can also cause severe infections [3, 4]. In this work, the single-cell organisms *B. subtilis* and *S. aureus* serve as models for investigating enzymatic processes for recycling the Gram-positive bacterial cell wall.

Regardless of their great diversity, most bacterial cells are surrounded by a protective envelope, the cell wall. It shields bacteria from the environment and counteracts the intracellular turgor pressure [5]. The integrity of this extracellular barrier is therefore of particular importance for bacterial life. The foundation of the cell wall is formed by the peptidoglycan (or murein) sacculus, which surrounds the entire cell as one huge macromolecule.

1.2. Composition and structure of the peptidoglycan cell wall

The structure and composition of the peptidoglycan is similar in all known bacteria. The backbone is formed by interconnected glycan strands, which are composed of repeating units of β-1,4-linked amino sugars. Namely, it is a sequence of *N*-acetylglucosamine (GlcNAc) and *N*-acetylmuramic acid (MurNAc). In some bacteria, the glycan strands are terminated by 1,6-anhydro-*N*-acetylmuramic acid (anhMurNAc) [6] as shown in Figure 1.1. In others, like in *S. aureus*, anhMurNAc is absent, but MurNAc is commonly *O*-acetylated [7–9]. This secondary modification confers resistance to muramidases such as lysozyme [8, 9]. In *B. subtilis*, the glycan part of the peptidoglycan is partially deacetylated – either at the GlcNAc or MurNAc residue [10, 11]. The deacetylation of the amino sugars also results in resistance to lysozyme

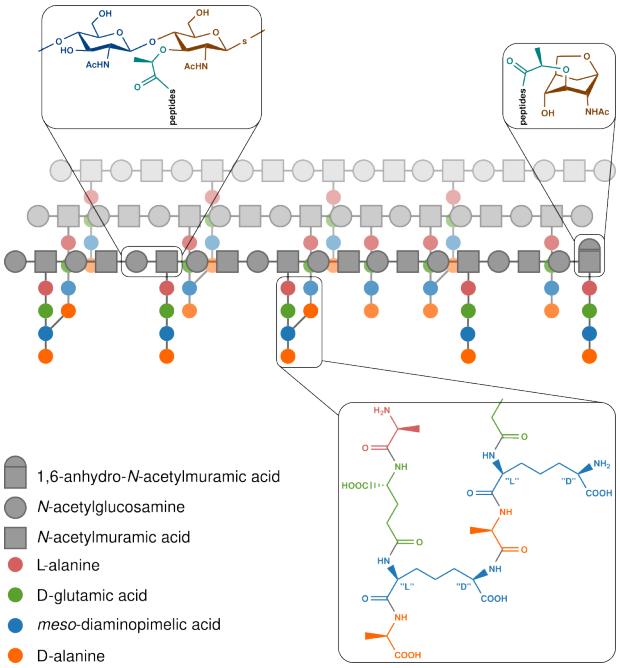

Figure 1.1.: Schematic representation of the peptidoglycan matrix in *E. coli* and *B. subtilis*. The glycan strands are composed of repeating units of the β-1,4-linked *N*-acetylglucosamine (GlcNAc) and *N*-acetylmuramic acid (MurNAc), terminating in 1,6-anhydro-*N*-acetylmuramic acid (anhMurNAc). Short peptides connect adjacent glycan chains, resulting in a mesh-like structure. Other organisms may deviate from the composition shown. In *S. aureus*, for example, anhMurNAc is not present, iso-D-glutamine and L-lysine replace D-glutamic acid and *meso*-diaminopimelic acid, and stem peptides are cross-linked via a pentaglycine bridge. Figure based on [11, 17, 18].

[8–10]. However, *B. subtilis* is not resistant to lysozyme, but other Bacilli with a higher degree of deacetylation are [9, 10]. The length of the glycan strands and thus the number of GlcNAc and MurNAc residues also varies. In *S. aureus* and some other bacteria the glycan chains consist of 5 to 10 disaccharides in average. In contrast, in *B. subtilis*, the glycan chains are comparatively long, comprising in average of over 50 disaccharides [7, 12–14]. The glycan strands are often (as in *S. aureus*), but not always, cross-linked via short peptides forming a mesh-like structure of layers [11, 15–17]. The short peptides interconnecting adjacent glycan strands, are called 'stem peptides' and are bound to MurNAc (Figure 1.1). Typically, the stem peptides consist of L-alanine (L-Ala), D-glutamic acid (D-Glu), *meso*-diaminopimelic acid (*meso*-Dpm) and D-alanine (D-Ala), as it is the case in *E. coli* and *B. subtilis* [11, 17]. Some bacteria, like *S. aureus*, deviate from this amino acid composition. Then, iso-D-glutamine (D-Gln) is found instead of D-Glu and L-lysine (L-Lys) instead of *meso*-Dpm. In this regard, *S. aureus* has another special feature: stem peptides are indirectly linked via a pentaglycine bridge between L-Lys and D-Ala [15, 16]. *E. coli* and *B. subtilis* link their stem peptides directly between *meso*-Dpm and D-Ala [11, 17]. In *E. coli*, this results in a high abundance of tetra-tetrapeptide cross-links [17]. Contrary to this, in *B. subtilis* the terminal D-Ala of one stem peptide is cleaved off which is why tri-tetrapeptides are most frequently found [11].

Based on the number of layers and the resulting thickness of the cell wall, bacteria can be

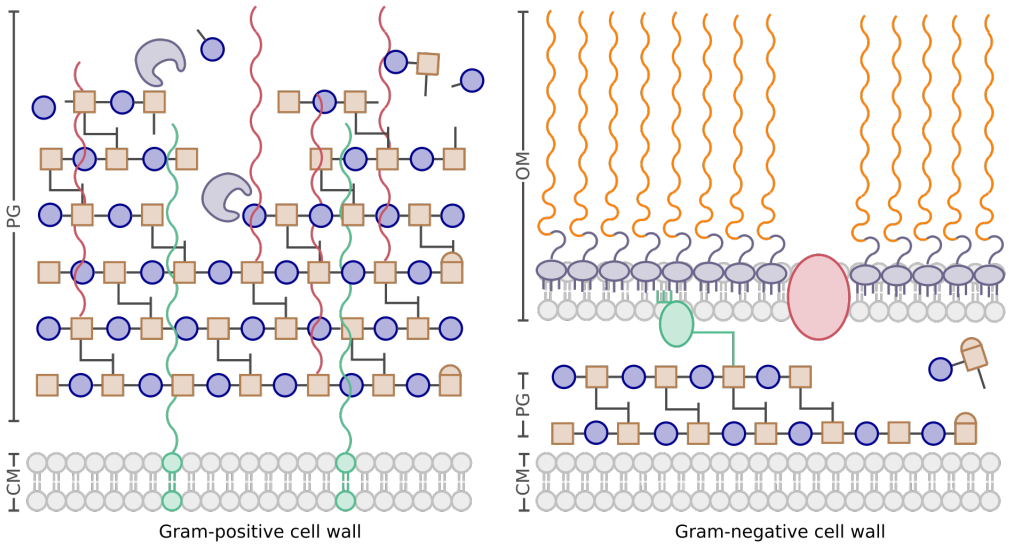

Figure 1.2.: Schematic representation of the Gram-positive and Gram-negative cell wall. A more or less thick peptidoglycan layer (PG) builds up on the cytoplasmic membrane (CM) enclosing the cell interior. In Gram-positive cells, this layer is permeated by wall teichoic acids (red lines) and lipoteichoic acids (green lines). In Gram-negatives, a second membrane (OM, outer membrane) lies on top of the peptidoglycan layer. Figure adapted from [18].

divided into two groups (see Figure 1.2). Gram-negative bacteria, like *E. coli*, feature a thin peptidoglycan layer which is encased in an outer membrane. In contrast, Gram-positives, like *B. subtilis* and *S. aureus*, generally have a thicker cell wall due to the large number of layers and lack an outer membrane [16]. In addition, the peptidoglycan of Gram-positive bacteria is permeated by two types of teichoic acids. Wall teichoic acids, covalently attached to the peptidoglycan, are glycopolymers consisting of GlcNAc, *N*-acetylmannosamine and repetitive ribitol phosphate or glycerol phosphate units [19, 20]. Lipoteichoic acids are similarly composed of repetitive glycerol phosphate units, but are anchored to the cytoplasmic membrane [21, 22].

As if variations in composition and cross-linking of the stem peptides did not already offer extensive possibilities for adapting the cell wall, bacteria make use of further modifications. *B. subtilis*, for example, amidates the majority of *meso*-Dpm residues via AsnB to control peptidoglycan degradation [11, 23, 24]. Interestingly, *E. coli*, as described before, also possesses Dpm but does not make use of Dpm-amidation [17].

Despite the similarity in the overall structure and its building blocks, the bacterial cell wall exists in a variety of forms, which reflects the bacterial diversity.

1.3. The continuous adaptation of the cell wall to the bacterial life cycle

The peptidoglycan sacculus structure with the purpose to protect the bacteria from the environment and to maintain a counter-pressure to the intracellular turgor pressure may lead to the impression that the cell wall is a rigid construct. However, the bacterial life cycle of growth and cell division requires a highly flexible cell wall [25]. Indeed, the cell wall is subject

to continuous remodelling and degradation (cell wall turnover).

As described before, the basic structure of the cell wall and the peptidoglycan are known, but the enzymatic processes responsible for its remodelling and degradation have hardly been unveiled. At least, autolytic enzymes are known to be of great importance; essential processes such as cell morphogenesis, growth and cell division rely on autolytic remodelling of the peptidoglycan [26, 27]. At the same time, the integrity of the cell wall must be maintained to ensure the survival of the cell. Precise regulation and a neatly balanced equilibrium between degradation and synthesis is essential, as uncontrolled and undirected autolysis would lead to cell death. Thus, autolysins are enzymes specialised for certain types of glycan, amide or peptide bonds within the peptidoglycan matrix.

Two different cleavage mechanisms that target the β-1,4-glycosidic bonds of the sugar backbone have been identified: via intramolecular transglycosylation and via hydrolysis. Enzymes that catalyse the former reaction are called lytic transglycosylases. In this reaction, an anhydro structure is established by linking the positions C1 and C6 within the MurNAc molecule. This results in the scission of the MurNAc-GlcNAc bond [28]. In Gram-negative bacteria, these enzymes are often redundant [25], which suggests their physiological significance. For example, the model organism *E. coli* encodes eight different lytic transglycosylases [28–30]. Less is known about lytic transglycosylases from Gram-positive bacteria, although some candidates were suggested based on sequence similarity [31–34]. In contrast, hydrolysis of the glycosidic bonds seems to be more widespread in Gram-positive than in Gram-negative bacteria. Depending on whether hydrolysis occurs between MurNAc and GlcNAc or between GlcNAc and MurNAc, a distinction is made between muramidases and glucosaminidases. Lysozyme and mutanolysin from Streptomyces sp. belong to the former [35], whereas the exo-active NagZ from *E. coli* and *B. subtilis* [36, 37] or the endo-active Atl^{Glc} from *S. aureus* [38, 39] are representatives of the latter.

Both, the flexibility and integrity of the peptidoglycan is mainly attributed to the peptide cross-linking [40, 41]. As a consequence, these connecting peptides are also object of cleavage in order to allow remodelling of the peptidoglycan. Conceptually, two types of peptide-cleaving enzymes can be distinguished. Amidases such as AmiA, AmiB, AmiC and AmiD of *E. coli* [42, 43], LytC of *B. subtilis* [44, 45] or Atl^{Am} [39, 46] of *S. aureus* cleave the amide bond between L-Ala and anhMurNAc (not in *S. aureus*) or MurNAc. Peptidases, on the other hand, cleave bonds within peptides, i. e. between amino acids. Since the stem peptides consist of L- and D-amino acids, D,L, L,D and D,D bonds are found within the peptidoglycan matrix. Autolytic peptidases are subdivided into LD-carboxy-, DD-carboxy- and DD-endopeptidases. *E. coli* possesses a whole series of peptidases. Among those are the penicillin-sensitive DD-endopeptidases Pbp4 and Pbp7 [47] and the penicillin-insensitive metalloproteases MepA [48, 49] and MepM [50] as well as MepH and MepS [50]. Whereas Pbp4 and Pbp7 are D-alanyl-D-alanine carboxypeptidases, the Mep enzymes hydrolyse the bond between D-Ala and *meso*-Dpm of cross-linked stem peptides.

1.4. Recycling of peptidoglycan in *E. coli*

The continuous adaptation of such a large construct as the bacterial cell wall to environmental conditions and cell growth is an elaborate process that requires complex regulation mechanisms. Since the synthesis of new peptidoglycan building blocks is energy-consuming, it is not surprising that strategies for recycling of peptidoglycan degradation products have evolved in

bacteria. The Gram-negative model organism *E. coli* releases about 45 % of its peptidoglycan in one generation, most of which is derived from the lateral cell wall [51, 52]. Since the cell poles are to a large extent inert to degradation, mostly lateral peptidoglycan is released [53]. Only 5 % to 8 % of degraded peptidoglycan fragments are released into the medium, whereas the majority remains in the periplasm and is transported back into the cell [51, 54].

Figure 1.3 gives a schematic overview of the steps of cell wall recycling in *E. coli*. Muropeptides, which are mainly released by the combined autolytic activity of lytic transglycosylases and DD-endopeptidases are imported by the permease AmpG [54, 55]. In the cytoplasm, cleavage into disaccharides and peptides occurs via the cytoplasmic amidase AmpD [54].

The disaccharide GlcNAc-anhMurNAc is cleaved by the exo-*N*-acetylglucosaminidase NagZ [36, 53]. The anhMurNAc thus released is converted into MurNAc 6-phosphate (MurNAc 6P) by the anhMurNAc kinase AnmK [56]. MurNAc 6P, in turn, is processed into GlcNAc 6-phosphate (GlcNAc 6P) by MurQ via cleavage of the lactyl ether residue [57, 58]. Additionally, free MurNAc can also be taken up by the phosphotransferase system (PTS) transporter MurP [59]. Inside the cell, it is introduced to the recycling process as MurNAc 6P [59] (see Figure 1.3). Similarly, GlcNAc can be incorporated by NagE [60–62]. The product of this import, GlcNAc 6P, is converted into glucosamine 6P (GlcN 6P) by the GlcNAc 6P deacetylase NagA [57, 58]. GlcNAc released by NagZ is phosphorylated by the GlcNAc kinase NagK into GlcNAc 6P [63]. GlcNAc 6P either serves as substrate for peptidoglycan synthesis or is used for energy production in glycolysis, which requires further cleavage into fructose 6P by NagB [57, 58, 63]. The outlined pathway to import and utilise MurNAc requires the presence of a PTS transporter and a MurNAc etherase. In the genome of *E. coli*, the genes encoding the transporter MurP and the etherase MurQ are organised in an operon with the regulator MurR and a penicillin binding protein [57, 64]. In the absence of MurNAc 6P, which is the substrate of MurQ, MurR represses the expression of MurQ [64].

Free peptides derived from the peptidoglycan can be imported through the ABC transporter Opp in interaction with the binding protein MppA [71]. These peptides as well as stem peptides derived from the cleavage of muropeptides, are truncated to tripeptides by the LD-carboxypeptidase LdcA by cleavage of the terminal D-Ala from tetrapeptides [65, 66]. The tripeptides are introduced into peptidoglycan synthesis by the ligase Mpl [67]. The majority of the absorbed stem peptides follow the route of peptidoglycan synthesis. However, tripeptides can also be degraded to single amino acids via another metabolic pathway, as explained later.

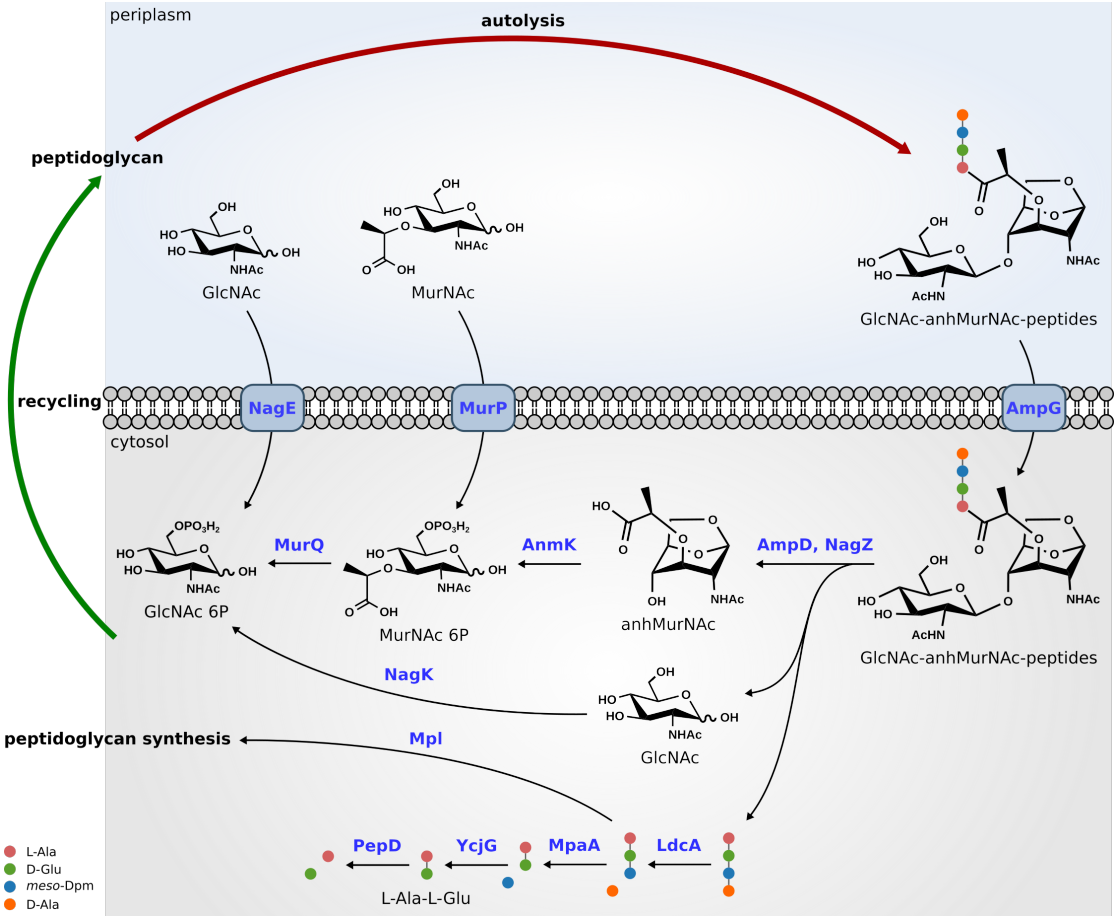

Figure 1.3.: Schematic representation of cell wall recycling and MurNAc catabolism in *E. coli*. The autolytic activity of lytic transglycosylases and DD-endopeptidases releases muropeptides, which are imported by AmpG [54, 55]. In the cytoplasm, the imported muropeptides are degraded into GlcNAc, anhMurNAc, and peptides by the amidase AmpD [54] and the exo-*N*-acetylglucosaminidase NagZ [36, 53]. GlcNAc is phosphorylated by NagK into GlcNAc 6P, which in turn can be shuttled into peptidoglycan synthesis [63]. The anhMurNAc kinase AnmK converts anhMurNAc into MurNAc 6P [56], which is further processed by the etherase MurQ into GlcNAc 6P [57, 58]. The peptides are truncated by the LD-carboxypeptidase LdcA, yielding tripeptides [65, 66]. Tripeptide is either introduced into peptidoglycan synthesis by the ligase Mpl [67] or further degraded. The degradation occurs through the γ-D-Glu-Dpm amidase MpaA [68], the L-Ala-D/L-Glu epimerase YcjG [69], and PepD [70].

1.5. Recycling of peptidoglycan glycans in Gram-positive bacteria

With an estimated turnover of up to 50 % per generation, the cell wall turnover of Gram-positive bacteria is on a similar scale as in Gram-negative bacteria [53, 72–75]. As mentioned earlier, the periplasmic space allows Gram-negative bacteria to capture the products of cell wall turnover. Although there is a compartment that may reflect a periplasmic space in Gram-positive bacteria [76, 77], degradation products are assumed to get more easily lost due to the lack of an outer membrane. Certainly interesting many Gram-positive bacteria possess sequence homologues of MurP, MurQ and MurR, but lack the recycling enzymes AmpG, AmpD and AnmK known from *E. coli*.[74, 75]. Studies in *B. subtilis*, *S. aureus* and the Gram-positive bacteria *Steptomyces coelicolor* showed that deletion of the putative MurQ homologues led to intracellular accumulation of MurNAc 6P [75]. In addition, if the putative MurP (transporter) homologues were deleted, MurNAc uptake ceased [75]. Consequently, some Gram-positive bacteria are believed to use the same metabolic pathway as the Gram-negative bacterium *E. coli* for recycling MurNAc [75]. Like *E. coli*, *B. subtilis* possesses a PTS transporter for GlcNAc (named NagP) [78, 79] and and is thus probably also able to utilise GlcNAc.

Opposite to *E. coli*, the predicted operon *murQRP* in *B. subtilis* comprises three additional genes, which are located immediately downstream of *murP*: *amiE*, *nagZ* and *namZ* [75]. The gene *amiE* encodes an amidase, *nagZ* a homologue to the aforementioned NagZ of *E. coli* and *namZ* (previously named *ybbC*) was recently described to encode an endo-*N*-acetylmuramidase [80]. Theoretically, NagZ, NamZ and AmiE would be sufficient to completely degrade the peptidoglycan of *B. subtilis* [80].

The suggested *murQRP* operon in *S. aureus* encodes an additional gene compared to *E. coli* (*sausa300_0192*; [75]). It codes for an unknown translation product with a sequence length of 351 amino acids [81]. Potential orthologs are widely distributed within the genus Staphylococcus, but there is no similarity to known proteins at sequence level. Due to its genetic position, an involvement in the recycling process of peptidoglycan is conceivable. However, *sausa300_0192* apparently serves a purpose for which there is no equivalent in *E. coli*. This hypothesis is strengthened if one considers that in *S. aureus* the product of the main autolysin Atl is not MurNAc as in *E. coli*, but the disaccharide MurNAc-GlcNAc [38, 82].

1.6. Recycling of peptidoglycan peptides in Gram-positive bacteria

As explained in Section 1.4, *E. coli* recycles peptides from cell wall turnover for use in peptidoglycan synthesis. However, the peptides can also be broken down into individual amino acids. Tetrapeptides are trimmed to tripeptides by LdcA (see section 1.4). Starting from the tripeptide L-Ala-γ-D-Glu-*meso*-Dpm, the bond between γ-D-Glu and *meso*-Dpm is cleaved by the γ-D-Glu-Dpm amidase MpaA [68]. The released dipeptide L-Ala-D-Glu is epimerised by YcjG into its L,L form [69], which in turn can be cleaved by PepD into L-Ala and L-Glu [70].

Since Gram-positive bacteria import and utilise MurNAc similarly to *E. coli*, it is assumed that they also possess mechanisms for utilising cell wall peptides. A candidate gene cluster for this is *dppABCDE ykfABCD* in *B. subtilis* [83]. It encodes a transporter and several peptidases. The Dpp transporter resembles the Opp transporter of *B. subtilis* (a homologue of the Opp transporter in

E. coli) and the canonical structure of an ABC transporter comprising two membrane domains (DppB and DppC), a nucleotide binding domain (DppD) and a binding protein (DppE) [84, 85]. Interestingly, YkfD, the translation product of the last gene, *ykfD*, shows high sequence similarity to ATPase domains of ABC transporters and therefore probably complements the Dpp transporter with a second nucleotide binding domain [85]. Although DppBCDE has been characterised as a dipeptide transporter and named accordingly [84, 86], it could represent a possible counterpart for the uptake of cell wall peptides to the Opp transporter and the binding protein MppA in *E. coli*.

Downstream of *dppE* lies a potential transcription terminator, which divides the cluster into the two operons *dppABCDE* and *ykfABCD* [83]. However, a weak termination effect was suspected [83]. That is, since YkfD is possibly part of the Dpp transporter, and *ykfABCD* is apparently co-regulated with *dppABCDE*, which in turn is regulated by the global repressor CodY [83, 87]. YkfA is assigned to the S66 serine peptidases such as LdcA from *E. coli*. Belonging to the same protein family does not necessarily mean a high sequence similarity or exhibiting the same activity, but these two proteins have a sequence identity of 30 % and therefore, a comparable activity suggests itself. YkfB has already been characterised as an L-Ala-D/L-Glu epimerase and thus as a homologue of YcjG from *E. coli* [69]. YkfC has been studied quite extensively and, based on its crystal structure and enzymatic activity, has been identified as a member of a subgroup of the NlpC/P60 family. The latter is distinguished from the rest of the NlpC/P60 family by two highly conserved amino acid residues [88–90]. YkfC specifically cleaves the bond between D-Glu and *meso*-Dpm [69]. DppA, encoded by the first gene of the gene cluster, is not part of the transporter. Instead, it appears to be a D-stereo-specific aminopeptidase [91]. Apart from its hydrolytic activity on terminal D-alanine, its physiological function is unknown. Enzymes with comparable activity have been studied mainly in relation to vancomycin resistance of Gram-positive bacteria [92–94]. Gram-negative bacteria, however, do not rely on enzymatically mediated glycopeptide resistance, since their outer membrane hinders vancomycin from entering the cell. This is why the VanX homologue DdpX of *E. coli* has been proposed to function in adaptation to the nutrient deficiency prevailing the stationary growth phase [95]. At sequence level, there is no similarity between DdpX of *E. coli* and DppA of *B. subtilis* [96]. In fact, DppA has an N-terminal sequence motif, SXDXEG, which identifies a separate family of metalloproteases [91, 96]. Nevertheless, DdpX and DppA have certain similarities. Both enzymes are zinc-dependent peptidases [91, 95]. Moreover, the co-localisation of DdpX with a peptide transporter [95] is very reminiscent of the genetic context of DppA.

Based on the findings described above, the prerequisites for the utilisation of cell wall peptides in Gram-positive bacteria seem to be given. Indeed, a degradation pathway including YkfA, YkfB and YkfC was proposed, even though in the context of β-lactam resistance [97]. According to this, a cytoplasmic intermediate of peptidoglycan degradation leads to the synthesis of a β-lactamase. Under normal conditions in the absence of penicillin stress, tetrapeptide is taken up into the cell via an ABC transporter (with YkfD as ATPase) as a product of cell wall turnover. Intracellularly, YkfA generates tripeptide from this by cleavage of the terminal D-Ala. The tripeptide is further cleaved by YkfC into the dipeptide L-Ala-D-Glu, which can be epimerised by YkfB. Amoroso *et al.* [97] postulated that penicillin stress leads to increased cell wall turnover. Consequently, tripeptide produced by YkfA is cleaved by a penicillin-activated receptor into γ-D-Glu-*meso*-Dpm, which in turn acts as an inducer to inactivate a repressor of a β-lactamase.

2. Research objective

Although the remodelling of their cell wall allows bacteria to adapt to different and changing environmental conditions, the constant loss of breakdown products would be a waste of resources. To alleviate this, bacteria evolved pathways to re-utilise cell wall sugars and peptides, which are products of the degradation process. Studies of enzymatic processes responsible for the recycling of PG mainly focused on Gram-negative bacteria, whilst these processes are still poorly investigated and understood in Gram-positive bacteria. Considering its usefulness and the discovery of homologues of recycling enzymes known from Gram-negative bacteria in some Gram-positive bacteria, the existence of recycling pathways in the latter is likely. This work aims to answer the so far unsolved question about how Gram-positive bacteria recycle their cell wall.

The coccoid non-sporulating Gram-positive bacterium *S. aureus* USA300 and the rod-shaped sporulating bacterium *B. subtilis* subsp. *subtilis* 168 served as model organisms. *S. aureus* USA300 is primarily known in a medical context as methicillin-resistant *S. aureus* (MRSA), because it can cause severe infections. *B. subtilis* is an environmental bacterium that serves as a biotechnologically important producer strain.

The capability of *S. aureus*, to recycle the cell wall sugar MurNAc via the PTS transporter MurP and the etherase MurQ was demonstrated recently in our group [75]. However, in *S. aureus*, the putative MurNAc recycling operon *murQRP* comprises an additional gene of unknown function, located upstream of *murQ*: *sausa300_0192*. The hypothetical protein contains a domain of unknown function (DUF871) and, intriguingly, is not present in either *E. coli* or *B. subtilis*. Therefore, it should be clarified whether a possible translation product is related to MurNAc recycling. If so, the pathway of MurNAc recycling should be examined.

B. subtilis has sequence homologues to enzymes that enable *E. coli* to import and degrade its cell wall peptides. This includes the ABC transporter DppBCDE and the potential degradation enzymes YkfA (an LD-carboxypeptidase), the epimerase YkfB and the γ-D-Glu-*meso*-Dpm endopeptidase YkfC. In the genome of *B. subtilis*, the encoding genes are organised as a cluster of the two operons *dppABCDE* and *ykfABCD*. The question therefore arises whether *B. subtilis* uses a metabolic pathway for the utilisation of cell wall peptides via these enzymes. In this context, and as another aim of this work, the physiological role of DppA, the first gene of the gene cluster, should also be revealed.

3. Material and methods

3.1. Cloning and construction of strains

The genes *dppA*, *ykfA* and *ykfC* were amplified from genomic DNA of *B. subtilis* subsp. *subtilis* 168 by PCR. Using the primers listed in Table 3.2, overlapping ends complementary to the plasmid pET28a were generated. *ykfA* and *ykfC* were amplified without stop codon to express them with a hexahistidine-tag. DppA was amplified with stop codon (see Section 3.2). The PCR products were isolated from the reaction mix with GeneJET Plasmid Miniprep Kit (Thermo Fisher Scientific). The plasmid was linearised with the restriction enzymes NcoI and XhoI and subsequently isolated from the gel of an agarose gel analysis. The purified PCR products and the linearised plasmid were fused via isothermal assembly ("One-step isothermal DNA assembly", [98]). Chemically competent E. coli DH5α cells were transformed with the constructed plasmids. The cloning success was verified by sequencing the plasmids isolated from the transformed E. coli DH5α strains. For expression of DppA, YkfA and YkfC, *E. coli* BL21(DE3) cells were transformed with the created plasmids pET28a-*dppA*, pET28a-*ykfA* and pET28a-*ykfC* respectively.

To investigate the capability of MurP to transport the disaccharide MurNAc-GlcNAc in *B. subtilis*, a double mutant deficient in *murP* and *namZ* was generated. A Δ*murQRP* mutant strain [75] was used to prepare competent cells as described by Schönert [99]. The erythromycin cassette was amplified via PCR from genomic DNA of a Δ*namZ::erm* mutant strain (Bacillus Genetic Stock Center, [100]) using namZ_500_fw and namZ_500_rev as primers (listed in Table 3.2). Following the protocol by Schönert [99], competent Δ*murQRP* cells were transformed with the purified PCR product and plated on lysogeny broth (LB, $5\,g\,L^{-1}$ NaCl, $5\,g\,L^{-1}$ yeast extract, $10\,g\,L^{-1}$ tryptone) agar ($15\,g\,L^{-1}$ agar) supplemented with $5\,\mu g\,mL^{-1}$ erythromycin. The plates were incubated at 37 °C over night. To verify the insertion of the erythromycin cassette, colony PCRs were performed using either namZ_500_fw and namZ_500_rev or namZ_500_fw and erm-rev (Table 3.2) as primer pair. Genomic DNA was isolated from clones whose PCR product indicated a correct insertion. The isolated DNA served as template in a second PCR, using the primer pair namZ_500_fw and namZ_500_rev. The product of this reaction was subsequently sequenced with the same primer pair, confirming the correct insertion of the erythromycin cassette and replacement of *namZ*.

Strains used or created in this work are listed in Table 3.1. Oligonucleotides and plasmids are listed in Table 3.2.

Table 3.1.: Strains used in this work.

Name	Genotype	Reference	Strain number
E. coli MC4100	F– *[araD139]$_{B/r}$ Δ(argF–lac)169 λ$^-$ e14–flhD5301 Δ(fruK-yeiR)725(fruA25) relA1 rpsL150*(strR) *rbsR22 Δ(fimB–fimE)632(::IS1) deoC1*	[101]	21830
E. coli DH5α	F– *Δ(argF–lac)169* φ80d*lacZ58*(M15) *ΔphoA8 glnX44*(AS) *λ$^-$ deoR481 rfbC1 gyrA96*(NalR) *recA1 endA1 thiE1 hsdR17*	[102]	22049
	DH5α pET28a-*dppA*	This work	22134
	DH5α pET28a-*ykfA*	This work	22034
	DH5α pET28a-*ykfC*	This work	22036
E. coli BL21(DE3)	F– *lon-11 Δ(ompT–nfrA)885 Δ(galM–ybhJ)884 λDE3 [lacI, lacUV5-T7 gene 1, ind1, sam7, nin5] Δ46 [mal$^+$]$_{K-12}$*(λ$^-$) *hsdS10*	[103]	
	BL21(DE3) pET28a-*cwlC*	[80]	22012
	BL21(DE3) pET28a-*atl^{Glc}*	Marina Borisova, unpublished	21713
	BL21(DE3) pET28a-*dppA*	This work	22135
	BL21(DE3) pET28a-*ykfA*	This work	22061
	BL21(DE3) pET28a-*ykfC*	This work	22063
B. subtilis subsp. *subtilis* 168	*trpC2*	Bacillus Genetic Stock Center [100]	22018
	trpC2 Δ*murQRP*	[75]	21856
	trpC2 Δ*murQRP*Δ*namZ::erm*	This work	22076
	trpC2 Δ*dacA::erm*	Bacillus Genetic Stock Center [100]	11445
	trpC2 Δ*amyE::kan*	Bacillus Genetic Stock Center [100]	22154
	trpC2 Δ*dppA::kan*	Bacillus Genetic Stock Center [100]	22155
	trpC2 Δ*ykfA::kan*	Bacillus Genetic Stock Center [100]	22160
	trpC2 Δ*dppABCDE::kan*	Marjorie Dauvin, unpublished	22113
	trpC2 Δ*ykfABCD::kan*	Marjorie Dauvin, unpublished	22114
	trpC2 Δ*dppABCDE::kan* Δ*ykfABCD::spc*	Marjorie Dauvin, unpublished	22115

Table 3.2.: Oligonucleotides and plasmids used in this work.

Construct	Sequence (5′–3′) or properties	Reference	Plasmid number
	Oligonucleotides		
RK-34	TGTTTAACTTTAAGAAGGAGATATACCATGAAATTGTACATGTCAGTAGATATG	This work	
RK-94	AGTGGTGGTGGTGGTGGTGCTCGAGTTAGCAGAATGATGTCCGCA	This work	
RK-38	TGTTTAACTTTAAGAAGGAGATATACCATGATGAAAGGAGTGTTTTCGTTG	This work	
RK-39	AGTGGTGGTGGTGGTGGTGCTCGAGTGTCTTCAGCGCCCCTTC	This work	
RK-42	TGTTTAACTTTAAGAAGGAGATATACCATGATGCACACTGTCATATCAG	This work	
RK-43	AGTGGTGGTGGTGGTGGTGCTCGAGTTCTGAAAAACAGCGGCG	This work	
namZ_500_fw	GCTTCAGTTTGGCTAATTCCG	[80]	
namZ_500_rev	CAAACCCGTATCCCTCAGC	[80]	
erm-rev	TTACTTATTAAATAATTTATAGCTATTGAAAAGAG	Maraike Müller, unpublished	
	Plasmids		
pET28a(+)	Expression vector for *E. coli*	Novagen	14
pET28a-*cwlC*	Overexpression of CwlC	[80]	3185
pET28a-atl^{Glc}	Overexpression of Atl^{Glc}	Marina Borisova, unpublished	2124
pET28a-*dppA*	Overexpression of DppA	This work	3207
pET28a-*ykfA*	Overexpression of YkfA with C-terminal hexahistidine-tag	This work	3203
pET28a-*ykfC*	Overexpression of YkfC with C-terminal hexahistidine-tag	This work	3205

3.2. Protein expression

Overnight cultures of *E. coli* BL21(DE3) cells carrying recombinant expression plasmids were diluted to an OD_{600} of 0.05 with 400 mL autoinduction medium (modified recipe of ZYM-5052 without traces elements [104, 105]) supplemented with 50 µg kanamycin. The cultures were grown for 18 h at room temperature in 2-L baffled flasks under continuous shaking at 130 rpm. After that, the cells were sedimented by centrifugation for 20 min with 5000 rpm at 4 °C.

The recombinant proteins Atl^{Glc}, CwlC, YkfA and YkfC were purified by their hexahistidine-tag via nickel affinity chromatography and afterwards by size exclusion chromatography (SEC). DppA was expressed with its complete coding sequence including its stop codon. Consequently, the enzyme was expressed without hexahistidine-tag and therefore was purified by ion exchange chromatography and SEC. This was needed, as the tagged enzyme appeared to be inactive in a previous attempt. The corresponding purification programmes were programmed and automatically executed in an ÄKTApurifier connected to a collector for 96-well plates. All purification steps were done at 4 °C. The detailed procedure is described in the following.

Sedimented *E. coli* BL21(DE3) cells that carried pET28a-*cwlC* or pET28a-atl^{Glc} (listed in Table 3.2) were suspended in 30 mL buffer A (20 mM imidazole, 20 mM Na_2HPO_4 dihydrate, 500 mM NaCl, pH = 7.6). The cells were broken by ultrasonic disruption (3 repetitions of 2 min each at level 5 and a pulse duration of 0.5 s). To prevent heating and thus denaturation of the recombinant proteins, the cells were cooled during this procedure with a mixture of ice water and ethanol. Cell debris was removed by centrifugation (30 min 38 000 *g* at 4 °C) followed by filtration of the supernatant (pore size of the filter: 0.22 µm). The filtrate was purified by nickel affinity chromatography. For this, a 1 mL HisTrap HP (GE Healthcare GmbH) column and a stepwise programme with a flow rate of 1 mL min^{-1} were used: 10 column volumes (CV) with 100 mM imidazole (corresponding to 20 % buffer B, which is buffer A supplemented with 500 mM imidazole), 10 CV with 250 mM imidazole (corresponding to 50 % buffer B) and finally 10 CV with 500 mM imidazole (corresponding to 100 % buffer B). Eluted fractions that showed a signal at a wavelength of 280 nm (UV_{280}) were analysed by SDS-PAGE. Fractions that showed bands with correct protein size were further purified via SEC. This was achieved by separating them on a HiLoad 16/600 Superdex 75 prep grade column (GE Healthcare) and eluting them with buffer C (20 mM Na_2HPO_4 dihydrate, 500 mM NaCl, pH = 7.6) at a flow rate of 1 mL min^{-1}. Again, eluted fractions that showed activity at 280 nm were also examined by discontinuous SDS-PAGE and fractions selected for correct protein size were mixed. The purified enzyme was slightly concentrated by ultrafiltration (Vivaspin 20 column with 10 kDa cut off, Sartorius), glycerol was added to a final concentration of 10 % and frozen at −80 °C.

Sedimented cells that carried either pET28a-*ykfA* or pET28a-*ykfC* were suspended in 30 mL buffer A. The cells were lysed by treating them three times in a French press with a pressure of 110.3 MPa (SLM-AMINCO Spect. Inst.). Cell debris was removed by centrifugation and filtration of the supernatant as described above for CwlC. The purification process was conducted on a 1 mL HisTrap HP (GE Healthcare GmbH) column applying a gradient of 0 % to 100 % buffer B over 30 CV at a flow rate of 1 mL min^{-1}. The further processing, including analysis by SDS-PAGE, purification by SEC, ultrafiltration and generation of stock solutions was as described for CwlC.

DppA was purified following the protocol by Cheggour *et al.* [91] with some modifications. Cells carrying pET28-*dppA* were solved in 30 mL 50 mM KPi pH = 6.5 and broken by ultrasonic disruption (see CwlC). As described above, cell debris was removed by centrifugation and

subsequent filtration of the supernatant. The filtered supernatant was first purified with a 20 mL HiPrep Q HP 16/10 column (GE Healthcare) at a flow rate of 3 mL min^{-1}. Therefore, the column was pre-equilibrated with 5 CV 50 mM KPi pH = 6.5. After sample injection, unbound molecules were washed out with 5 CV Kpi buffer. The elution was achieved by using a linear gradient of 0 M to 1 M NaCl (50 mM KPi supplemented with 1 M NaCl, pH = 6.5) over 15 CV. Any remaining residues were eluted with 5 CV 100 % NaCl-KPi buffer. UV_{280}-active fractions were tested for hydrolytic activity with D-alanine 7-amido-4-methylcoumarin trifluoroacetate (D-Ala-AMC TFA, CAS 201847-52-1, BLD Pharmatech). As described above for the other enzymes, selected fractions were further purified by SEC, but on a HiLoad 16/600 Superdex 200 prep grade column (GE Healthcare). Ultrafiltration and generation of stock solutions were carried out as described for CwlC.

3.3. Generation of peptide and muropeptide substrates

The racemic peptides D-Ala-*rac*-2,6-Dpm and *rac*-2,6-Dpm-D-Ala_2 were obtained from EMC and dissolved to 100 mM in ultra-pure water before use.

Peptides of *E. coli* and *B. subtilis* were released from crude preparations of peptidoglycan of *E. coli* MC4100, *B. subtilis* subsp. *subtilis* 168 and *B. subtilis* subsp. *subtilis* 168 Δ*dacA::erm* as described hereinafter. 400 mL LB medium was inoculated with overnight cultures of the respective strains to an OD_{600} of 0.05. The cultures were grown at 37 °C with a shaking frequency of 150 rpm until an OD_{600} of 1.8 to 2 was reached. Afterwards, the cultures were cooled on ice and centrifuged at 4 °C and 5000 rpm for 20 min. The sedimented cells were suspended in 30 mL ice-cold ultra-pure water and subsequently dropped into 30 mL boiling ultra-pure water. The suspensions were boiled for 45 min under continuous stirring. After the suspensions had cooled to room temperature, the cells were further broken up by freezing (−20 °C) and thawing (room temperature). The suspensions of broken cells were centrifuged at 4000 *g* for 20 min. Afterwards, the sediments were solved in 10 mL of 50 mM Tris buffer with pH = 8. To this, 600 µg α-amylase, 250 U RNAse, 240 U DNAse I, and 0.5 mmol $MgSO_4$ were added. After incubation at 37 °C for 2 h, the suspensions were boiled and centrifuged again. The sediments were solved in 1 mL Tris buffer. The suspensions thus produced were treated with either recombinant amidase (CwlC from *B. subtilis)* or recombinant glucosaminidase (Atl^{Glc} from *S. aureus*). In both cases, 5 µM enzyme was added and incubated overnight at 37 °C. This procedure was repeated once and the enzymes were then inactivated by heating at 95 °C for 15 min. The supernatants finally obtained by centrifugation (5 min at 17 000 *g*) served as substrates for in vitro studies of DppA, YkfA and YkfC.

3.4. Analysis of intracellular and extracellular accumulation

Overnight cultures were used to inoculate 100 mL LB medium to an initial OD_{600} of 0.05. In 500-mL baffled flasks, the cultures were grown for 24 h at 37 °C under continuous shaking at 130 rpm.

To analyse the intracellular accumulation of metabolites, acetone extracts of disrupted cells were generated. Accumulation was examined in cells from exponential growth phase (cultivation for 3 h to 4 h) and stationary growth phase (24 h). For this, 50 mL of the cultures were centrifuged for 15 min with 4000 *g* at room temperature and the sediments were washed with ultra-pure

water. This step was repeated two times in total and the sediments were finally frozen at −80 °C. The thawed samples were adjusted to an OD_{600} of 6 with ultra-pure water. Of these suspensions, 800 µL were disrupted with 0.25 g glass beads (0.25 mm to 0.5 mm in diameter) at 6000 rpm at 4 °C in a cell disrupter (FastPrep-24 5G, MP Biomedicals). The disruption procedure was repeated four times in total, with 30 s break after each repetition. The disrupted cells were centrifuged (10 min with 17 000 *g* at room temperature) and 200 µL of supernatant mixed with 800 µL ice-cold acetone. This suspension was frozen for 30 min at −20 °C. The samples were centrifuged (same as before) and the supernatant was dried under vacuum at 45 °C (vacuum concentrator RVC 2-18, Martin Christ Gefriertrocknungsanlagen, coupled to a vacuum system MZ 2C NT + AK + EK, Vacuubrand).

For analysis of extracellular accumulation, 1 mL of the culture supernatant was frozen at −20 °C. Of thawed supernatants, 200 µL were precipitated with acetone and dried as described above. Prior to LC-MS (liquid chromatography coupled with mass spectrometry) analysis, dried samples were solved in 50 µL ultra-pure water.

3.5. Determination of substrate specificity with synthetic peptides

3.5.1. Fluorescence-based assay for DppA

The stereospecificity and zinc dependence of recombinant DppA were investigated using a fluorescence-based assay. For this, D-Ala- or L-Ala-AMC TFA (7-amido-4-methylcoumarin trifluoroacetate) was solved in 100 mM $NaPO_4$ (pH = 8) to a final concentration of 250 µM. $ZnSO_4$ was added to yield a concentration of 40 µM if appropriate. Of these solutions, 180 µL were subsequently incubated with 10 µL (corresponds to 2.2 µM in reaction mix) of SEC-purified DppA at 37 °C for 2 h. The fluorescent (excitation wavelength of 341 nm, emission wavelength of 441 nm) was excited with a ultraviolet lamp with a fixed wavelength of 366 nm and photographed.

3.5.2. Determination of substrate specificity

The synthetic peptides D-Ala-*rac*-2,6-Dpm and *rac*-2,6-Dpm-D-Ala_2 were used to investigate the enzymatic activity of DppA and YkfC with defined substrates. Briefly, 1 µM recombinant enzyme was incubated with 1 mM synthetic substrate (D-Ala-*rac*-2,6-Dpm or *rac*-2,6-Dpm-D-Ala_2) in 50 mM Tris buffer with pH = 8 at 37 °C. When DppA was used, the reaction mixture was supplemented with 40 µM $ZnSO_4$. Incubation was carried out for 17 h (DppA) respectively 1 h (YkfA), and then heated at 95 °C for 15 min. The readout was done by LC-MS as described below in Section 3.6.

3.5.3. Determination of stereospecificity

To analyse the stereospecificity of DppA in more detail, HPLC with pre-column derivatisation with OPA reagent was performed. For this, recombinant DppA was incubated with D-Ala-*rac*-2,6-Dpm as described above. The steps for pre-column derivatisation were programmed and conducted for each sample automatically as followed. First, 340 µL of the sample were mixed with 145 µL borate buffer (50 mM boric acid, pH = 9.5) and 77 µL OPA-NAc reagent (30 mg o-phthalaldehyde, 30 mg *N*-acetyl-L-cysteine, 0.5 mL borate buffer, 4.5 mL methanol). Next,

100 µL of this mixture were added to 400 µL buffer A (40 mM monosodium phosphate, pH = 7.8). Of this, 5 µL were finally injected onto the column. Norvaline served as internal standard and to verify the derivatisation procedure and was thus added to each sample.

As for the LC-MS analysis, a reversed-phase C18 column was used to separate the samples in a Chromaster HPLC system coupled to a fluorescence detector (PU5160, ASU5260, O5310, FLD 5440; VWR Hitachi). Therefore, a programme with three linear gradients at a flow rate of 1 mL min^{-1} and a temperature of 40 °C was applied. Starting with a 56 min linear gradient from 10 % to 33 % solvent B (mixture of acetonitrile, methanol, water with volume fractions of 45 %, 45 % and 10 % respectively), the concentration of solvent B was increased to 40 % within 1 min. In two following gradients, the concentration of solvent B was further increased to 48 % over 23 min and to 100 % over 20 min, respectively. The run was concluded by washing the column for 5 min with 100 % solvent B and re-equilibrating for 5 min with 100 % solvent A. A wavelength of 330 nm was used for excitation, whereas the the emitted fluorescence was detected at 440 nm.

3.6. Determination of substrate specificity with cell wall peptides and muropeptides by LC-MS

The previously generated peptide suspensions served as substrates to investigate the specificity of DppA, YkfA and YkfC with peptides naturally occurring in the cell walls of *E. coli* and *B. subtilis*. For this purpose, 30 µL of the suspension were supplemented with 40 µM $ZnSO_4$. The enzymes were used at a concentration of 1 µM and the volumes of the preparations were adjusted with Tris buffer (see Section 3.3). Incubation was carried out for 20 h at 37 °C and stopped by incubation at 95 °C for 15 min. YkfC was incubated analogously with muropeptides from *E. coli* and *B. subtilis*, but without $ZnSO_4$.

The solved samples were separated on a reversed-phase C18 column (Gemini 5 µm C18 110 Å 150 mm × 4.6 mm, Phenomenex) in a HPLC (UltiMate 3000, Dionex) coupled to an electrospray ionisation (ESI) mass spectrometer equipped with a time-of-flight (TOF) detector (microTOF II, Bruker Daltonics). A 30-minute gradient of 0 % to 40 % acetonitrile at a flow rate of 0.2 mL min^{-1} was applied to elute the samples. Depending on whether the subsequent MS analysis was performed in positive ionisation mode or in negative ionisation mode, two different LC programmes were used. Both were identical in terms of flow rate and gradient, but differed in the equilibration and elution times. The total running time was therefore 45 min (45-min-programme, [106]) and 61 min (61-min-programme) respectively. In brief, the column was first equilibrated with 0.1 % formic acid and 0.05 % ammonium formate (aqueous phase, pH = 3.3), followed by the 30-minute gradient. The run was concluded with an elution step with 40 % acetonitrile (45-min-programme) or 60 % acetonitrile (61-min-programme) and re-equilibration with the aqueous phase.

The data evaluation and generation of extracted ion chromatograms (EICs, mass tolerance of 0.02 *m/z*) and base peak chromatograms (BPCs) was done with the programme DataAnalysis (Bruker Daltonics). Difference chromatograms (DCs) were obtained with the programme MetaboliteDetect (Bruker Daltonics) with a minimum difference of intensity in the ratio four. The exact masses and theoretical isotope patterns were calculated using the sum formulae with IsotopePattern (Bruker Daltonics, see Table 3.3 for list of calculated masses). The area of the peaks (area under the curve) was calculated using the composite trapezoidal rule with

the Python package NumPy. The data were plotted and annotated with the Python package Matplotlib.

Table 3.3.: Exact masses of compounds of interest for this work. Values calculated based on theoretical sum formulae. Quantitative designations refer to canonical peptides consisting of L-Ala, D-Glu, *meso*-Dpm and D-$Ala_{(2)}$ (ordered from N-terminus to C-terminus). Asterisks indicate amidated Dpm residues.

Compound	Sum formulae	Exact mass $[M]$ (Da)	$[M-H]^-$ (Da)	$[M+H]^+$ (Da)
	Amino sugars			
GlcNAc	$C_8H_{15}NO_6$	221.0899	220.0816	222.0972
MurNAc 6P	$C_{11}H_{20}NO_{11}P$	373.0774	372.0690	374.0847
MurNAc-GlcNAc (M-G)	$C_{19}H_{32}N_2O_{13}$	496.1904	495.1821	497.1977
MurNAc 6P-GlcNAc	$C_{19}H_{33}N_2O_{16}P$	576.1568	575.1484	577.1640
	Cell wall peptides			
Dipeptide	$C_8H_{14}N_2O_5$	218.0903	217.0819	219.0975
Tripeptide*	$C_{15}H_{27}N_5O_7$	389.1910	388.1827	390.1983
Tripeptide	$C_{15}H_{26}N_4O_8$	390.1751	389.1667	391.1823
[Gly^4]Tetrapeptide*	$C_{17}H_{30}N_6O_8$	446.2125	445.2041	447.2198
[Gly^4]Tetrapeptide	$C_{17}H_{29}N_5O_9$	447.1965	446.1882	448.2038
Tetra*	$C_{18}H_{32}N_6O_8$	460.2282	459.2198	461.2354
Tetra	$C_{18}H_{31}N_5O_9$	461.2122	460.2038	462.2195
[Gly^5]Pentapeptide*	$C_{20}H_{35}N_7O_9$	517.2496	516.2413	518.2569
[Gly^5]Pentapeptide	$C_{20}H_{34}N_6O_{10}$	518.2336	517.2253	519.2409
Pentapeptide*	$C_{21}H_{37}N_7O_9$	531.2653	530.2569	532.2726
Pentapeptide	$C_{21}H_{36}N_6O_{10}$	532.2493	531.2409	533.2566
Tripeptide*-Ala-Dpm*	$C_{25}H_{45}N_9O_{10}$	631.3289	630.3206	632.3362
(Tripeptide-Ala-Dpm)*	$C_{25}H_{44}N_8O_{11}$	632.3130	631.3046	633.3202
Tripeptide-Ala-Dpm	$C_{25}H_{43}N_7O_{12}$	633.2970	632.2886	634.3042
Tetrapeptide-Ala-Dpm	$C_{28}H_{48}N_8O_{13}$	704.3341	703.3257	705.3414
$Tripeptide_2$**	$C_{30}H_{52}N_{10}O_{13}$	760.3715	759.3632	761.3788
$Tripeptide_2$*	$C_{30}H_{51}N_9O_{14}$	761.3555	760.3472	762.3628
$Tripeptide_2$	$C_{30}H_{50}N_8O_{15}$	762.3396	761.3312	763.3468
Tri*-tetrapeptide*	$C_{33}H_{57}N_{11}O_{14}$	831.4086	830.4003	832.4159
(Tri-tetrapeptide)*	$C_{33}H_{56}N_{10}O_{15}$	832.3927	831.3843	833.3999
Tri-tetrapeptide	$C_{33}H_{55}N_9O_{16}$	833.3767	832.3683	834.3840
$Tetrapeptide_2$**	$C_{36}H_{62}N_{12}O_{15}$	902.4458	901.4374	903.4530
$Tetrapeptide_2$*	$C_{36}H_{61}N_{11}O_{16}$	903.4298	902.4214	904.4371
$Tetrapeptide_2$	$C_{36}H_{60}N_{10}O_{17}$	904.4138	903.4054	905.4211
[Gly^5]Penta*-tetrapeptide*	$C_{38}H_{65}N_{13}O_{16}$	959.4672	958.4588	960.4745
([Gly^5]Penta-tetrapeptide)*	$C_{38}H_{64}N_{12}O_{17}$	960.4512	959.4429	961.4585
[Gly^5]Penta-tetrapeptide	$C_{38}H_{63}N_{11}O_{18}$	961.4353	960.4269	962.4425
Penta*-tetrapeptide*	$C_{39}H_{67}N_{13}O_{16}$	973.4829	972.4745	974.4902
(Penta-tetrapeptide)*	$C_{39}H_{66}N_{12}O_{17}$	974.4669	973.4585	975.4742
Penta-tetrapeptide	$C_{39}H_{65}N_{11}O_{18}$	975.4509	974.4425	976.4582

Continued on the next page

Table 3.3.: Continued. Quantitative designations refer to canonical peptides consisting of L-Ala, D-Glu, *meso*-Dpm and D-$Ala_{(2)}$ (ordered from N-terminus to C-terminus). Asterisks indicate amidated Dpm residues.

Compound	Sum formulae	Exact mass [M] (Da)	[M – H]$^-$ (Da)	[M + H]$^+$ (Da)
Tri*-tetrapeptide*-Ala-Dpm*	$C_{43}H_{75}N_{15}O_{17}$	1073.5465	1072.5382	1074.5538
(Tri-tetrapeptide-Ala-Dpm)**	$C_{43}H_{74}N_{14}O_{18}$	1074.5306	1073.5222	1075.5378
Tri*-$tetrapeptide_2$**	$C_{51}H_{87}N_{17}O_{21}$	1273.6262	1272.6179	1274.6335
(Tri-$tetrapeptide_2$)**	$C_{51}H_{86}N_{16}O_{22}$	1274.6103	1273.6019	1275.6175
(Tri-$tetrapeptide_2$)*	$C_{51}H_{85}N_{15}O_{23}$	1275.5943	1274.5859	1276.6016
Tri-$tetrapeptide_2$	$C_{51}H_{84}N_{14}O_{24}$	1276.5783	1275.5699	1277.5856
$Tetrapeptide_3$	$C_{54}H_{89}N_{15}O_{25}$	1347.6154	1346.6070	1348.6227
Tri*-$tetrapeptide_3$***	$C_{69}H_{117}N_{23}O_{28}$	1715.8438	1714.8355	1716.8511
(Tri-$tetrapeptide_3$)***	$C_{69}H_{116}N_{22}O_{29}$	1716.8279	1715.8195	1717.8351
(Tri-$tetrapeptide_3$)**	$C_{69}H_{115}N_{21}O_{30}$	1717.8119	1716.8035	1718.8191
(Tri-$tetrapeptide_3$)*	$C_{69}H_{114}N_{20}O_{31}$	1718.7959	1717.7875	1719.8032
Tri-$tetrapeptide_3$	$C_{69}H_{113}N_{19}O_{32}$	1719.7799	1718.7715	1720.7872
Ala-Gly	$C_5H_{10}N_2O_3$	146.0691	145.0608	147.0764
Ala_2	$C_6H_{12}N_2O_3$	160.0848	159.0764	161.0921
Dpm*	$C_7H_{15}N_3O_3$	189.1113	188.1030	190.1186
Dpm	$C_7H_{14}N_2O_4$	190.0954	189.0870	191.1026
Dpm*-Ala	$C_{10}H_{20}N_4O_4$	260.1485	259.1401	261.1557
Dpm-Ala	$C_{10}H_{19}N_3O_5$	261.1325	260.1241	262.1397
Dpm*-Ala-Gly	$C_{12}H_{23}N_5O_5$	317.1699	316.1615	318.1772
Dpm-Ala-Gly	$C_{12}H_{22}N_4O_6$	318.1539	317.1456	319.1612
Dpm*-Ala_2	$C_{13}H_{25}N_5O_5$	331.1856	330.1772	332.1928
Dpm-Ala_2	$C_{13}H_{24}N_4O_6$	332.1696	331.1612	333.1769
Dpm*-Ala_3	$C_{16}H_{30}N_6O_6$	402.2227	401.2143	403.2300
Dpm-Ala_3	$C_{16}H_{29}N_5O_7$	403.2067	402.1983	404.2140
Dpm_2**-Ala	$C_{17}H_{33}N_7O_6$	431.2492	430.2409	432.2565
Dpm_2*-Ala	$C_{17}H_{32}N_6O_7$	432.2332	431.2249	433.2405
Dpm_2-Ala	$C_{17}H_{31}N_5O_8$	433.2173	432.2089	434.2245
Dpm_2**-Ala_2	$C_{20}H_{38}N_8O_7$	502.2863	501.2780	503.2936
Dpm_2*-Ala_2	$C_{20}H_{37}N_7O_8$	503.2704	502.2620	504.2776
Dpm_2-Ala_2	$C_{20}H_{36}N_6O_9$	504.2544	503.2460	505.2617
Dpm_2**-Ala_2-Gly	$C_{22}H_{41}N_9O_8$	559.3078	558.2994	560.3151
Dpm_2*-Ala_2-Gly	$C_{22}H_{40}N_8O_9$	560.2918	559.2835	561.2991
Dpm_2-Ala_2-Gly	$C_{22}H_{39}N_7O_{10}$	561.2758	560.2675	562.2831
Dpm_2**-Ala_3	$C_{23}H_{43}N_9O_8$	573.3235	572.3151	574.3307
Dpm_2*-Ala_3	$C_{23}H_{42}N_8O_9$	574.3075	573.2991	575.3148
Dpm_2-Ala_3	$C_{23}H_{41}N_7O_{10}$	575.2915	574.2831	576.2988
Dpm_3-Ala_3	$C_{30}H_{53}N_9O_{13}$	747.3763	746.3679	748.3836
Muropeptides				

Continued on the next page

Table 3.3.: Continued. Quantitative designations refer to canonical peptides consisting of L-Ala, D-Glu, *meso*-Dpm and D-Ala$_{(2)}$ (ordered from N-terminus to C-terminus). Asterisks indicate amidated Dpm residues.

Compound	Sum formulae	Exact mass $[M]$ (Da)	$[M-H]^-$ (Da)	$[M+H]^+$ (Da)
M-G-tripeptide*-Ala-Dpm*	$C_{44}H_{75}N_{11}O_{22}$	1109.5088	1108.5004	1110.5161
M-G-(tripeptide-Ala-Dpm)*	$C_{44}H_{74}N_{10}O_{23}$	1110.4928	1109.4845	1111.5001
M-G-tripeptide-Ala-Dpm	$C_{44}H_{73}N_9O_{24}$	1111.4768	1110.4685	1112.4841
M-G-tetrapeptide-Ala-Dpm	$C_{47}H_{78}N_{10}O_{25}$	1182.5140	1181.5056	1183.5212
M-G-tri*-tetrapeptide*	$C_{52}H_{87}N_{13}O_{26}$	1309.5885	1308.5801	1310.5958
M-G-(tri-tetra)peptide*	$C_{52}H_{86}N_{12}O_{27}$	1310.5725	1309.5642	1311.5798
M-G-tri-tetrapeptide	$C_{52}H_{85}N_{11}O_{28}$	1311.5566	1310.5482	1312.5638
M-G-tetrapeptide$_2$	$C_{55}H_{90}N_{12}O_{29}$	1382.5937	1381.5853	1383.6009

3.7. Lipid II assay

In order to elucidate whether YkfC interferes with cell wall synthesis, Lipid II (*meso*-Dpm) was used. Lipid II (2 nmol) was incubated with 2 µM YkfC in 40 µL MOPS buffer (50 mM, pH = 7.5, supplemented with 0.1 % Triton) at 37 °C overnight. Pbp6 of *Chlamydia pneumoniae* GiD was used as control with DD-carboxypeptidase activity. After incubation, the reactions were heated at 100 °C for 5 min. For the TLC analysis of Lipid II, 20 µL of a mixture of n-butanol and pyridine acetate (amount fractions of 2 and 1 respectively, pH = 4.2) were added to 20 µL of the reaction. The solution was applied on a HPTLC alumina silica gel 60 plate (Merck) using a mixture of chloroform, methanol, water and ammonia (amount fractions of 88, 48, 10 and 1 respectively) as mobile phase. Hanessian's staining was used for visualisation. For analysis of peptides, 20 µL of the reaction was sedimented (5 min at 17 000 *g*) and the supernatant applied on a TLC plate of the same type as above. A mixture of 2-butanol, pyridine, ammonia and water (amount fractions of 39, 34, 10 and 26 respectively) was used as mobile phase. Ninhydrin was used for staining.

3.8. Analysis of growth behaviour

B. subtilis 168 wild-type, Δ*amyE::kan*, Δ*dppABCDE::kan*, Δ*ykfABCD::kan* and Δ*dppABCDE::kan* Δ*ykfABCD::spc* were grown for 72 h in 100 mL LB at 37 °C with an initial OD_{600} of 0.05. Meanwhile, the optical density at 600 nm was monitored. To determine colony forming units (CFU), the strains were incubated for 72 h in 10 mL LB at 37 °C with an initial OD_{600} of 0.05. After 10 h, 24 h, 48 h and 72 h 100 µL of the cultures were diluted with 0.9 % NaCl. Of these dilutions, 10 µL were dropped on LB agar and after incubation at 30 °C over night colonies were counted. To analyse the morphology of single cells, liquid cultures of the mentioned strains were grown in the same manner as it is described above for the measurement of the optical density. After 24 h, 48 h and 72 h 15 µL of the culture were spotted onto an agarose-coated microscopy slide and imaged with 100x/1.3 oil objective lens of a Leica DM5500 B microscope connected to a Leica DFC360FX camera.

3.9. Computational analysis of genomic context

A set of 125 protein sequences taken from the seed alignment of Pfam entry PF05913 and manually added sequences was aligned using the MAFFT algorithm L-INS-i with a gap penalty offset of 0.123 [107]. The maximum likelihood tree was inferred with IQ-TREE [108] using the LG model in combination with the FreeRate model and ultrafast bootstrapping [109]. The substitution model and the number of categories of rate heterogeneity across sites was selected with ModelFinder [110] based on the minimal Bayesian information criterion.

The occurrence of putative homologues of MupG of *S. aureus* (UniProt accession number A0A0H2XHV5); MurQ (P77272), MurP (P77272), MurR (P77245) of *E. coli*; MurK (Q97ML3) of *Clostridium acetobutylicum* as well as of the 6-phospho-β-glucosidases Bgl (P40740, glycoside hydrolase family 1) and LicH (P46320, glycoside hydrolase family 4) of *B. subtilis* as representatives of hydrolases which cleave C6-phosphorylated disaccharides was determined using MultiGeneBlast. The programme was run in "architecture search" mode with thresholds set to 20 kb for maximum distance, 50 % for minimum sequence coverage and 20 % for minimum sequence identity. The phylogenetic tree was visualised and annotated with the online service iTOL [111].

4. Results

4.1. Recovery of the cell wall sugar MurNAc-GlcNAc in *S. aureus*

4.1.1. Declaration

Section 4.1.2 is a summary of the publication (see Appendix A):

> Kluj, R. M., Ebner, P., Adamek, M., Ziemert, N., Mayer, C. & Borisova, M. Recovery of the Peptidoglycan Turnover Product Released by the Autolysin Atl in *Staphylococcus aureus* Involves the Phosphotransferase System Transporter MurP and the Novel 6-phospho-*N*-acetylmuramidase MupG. *Frontiers in Microbiology* **9** (2018)

Marina Borisova and Christoph Mayer formulated the research question and conceptualised the study. The cloning of pET28a-mupG and the overexpression of MupG were planned by me and Marina Borisova, and carried out by me. The cloning of the complementation plasmid pCtufamp-mupG was planned by me, Marina Borisova and Patrick Ebner, and conducted by me. The LC-MS analyses were performed and evaluated by me in cooperation with Marina Borisova. The phylogenetic analysis of the DUF871 protein family was done by Martina Adamek, me and Nadine Ziemert. The result of this analysis was visualised by me. The manuscript was written by Marina Borisova, Christoph Mayer and myself, with the final version of the publication formulated by Marina Borisova. All authors were involved in the revision process. References to figures in Section 4.1.2 refer to this publication.

4.1.2. The role of MupG and MurP

The MurNAc recycling operon of *S. aureus* USA300 comprises genes encoding for homologues of the MurNAc etherase MurQ, the regulator MurR and the PTS transporter MurP known from *E. coli* and *B. subtilis*. Downstream of *murP*, an additional gene is located within this operon that has no counterpart in either *E. coli* or *B. subtilis*. The gene, annotated as *sausa300_0192*, is hereafter referred to as *mupG*. Its hypothetical translation product contains a domain of unknown function (DUF871) and was predicted to be a cytoplasmic protein.

To get first hints on the function of the unknown protein, a *mupG* deletion mutant was examined in a growth experiment. Compared to *S. aureus* wild-type and a Δ*murQ* mutant, the Δ*mupG* mutant reached slightly lower optical densities at 600 nm (OD_{600}) during transition and stationary growth phase in liquid culture (see Figure 1 in [106] or Appendix A). This indicated a possible involvement in processes maintaining the cells' constitution or fitness in later growth phases.

Since *mupG* is located in proximity to a transporter in the genome, it was investigated whether a loss of *mupG* leads to an accumulation. Indeed, LC-MS analyses showed an intracellular accumulation of a compound in the Δ*mupG* mutant (Figure 2 in [106] or Appendix A). The accumulation product was found in the exponential growth phase in lower levels that increased

in the stationary phase. An accumulation of the same product was observed for a *S. aureus* Δ*mupGmurQ* double mutant, but not for the wild-type (Figure 2 in [106] or Appendix A). *S. aureus* mutants deficient in *murQ* accumulate MurNAc 6P intracellularly [75], which was not observed in the Δ*mupGmurQ* double mutant here. This indicated sequential activity of MupG and MurQ within the same pathway.

The ratio of mass number to charge number (*m/z*) of the accumulation product corresponded to a phosphorylated disaccharide composed of GlcNAc and MurNAc. To determine the structure of the accumulation product, chemically reduced and non-reduced samples were analysed by HPLC-MS (Figure 3 in [106] or Appendix A). The reduced sample showed a mass difference of 2 *m/z* (Figure 3B in [106] or Appendix A), which may result from the reduction of a hemiacetal sugar, like GlcNAc and MurNAc, to a sugar alcohol. During the ionisation process of mass spectrometric analyses, molecules can be fragmented due to the energy influx. This characteristic allowed to determine the chemical structure of the accumulation product. In mass spectra of both, the reduced and the non-reduced sample, a fragment ion with a *m/z* of a phosphorylated MurNAc was found. However, only in the reduced sample a neutral loss of reduced GlcNAc was observed (Figure 3B in [106] or Appendix A). Likewise, the inspection of the mass spectrum of the non-reduced sample showed a neutral loss of non-reduced GlcNAc (Figure 3A in [106] or Appendix A). In summary, this demonstrated that GlcNAc was located at the reducing end and thus the accumulation product was MurNAc 6-phosphate-GlcNAc.

Next, it was investigated whether MupG can cleave the accumulated MurNAc 6-phosphate-GlcNAc. Hence, recombinant MupG was overexpressed and purified. As expected, it was able to cleave MurNAc 6P-GlcNAc into MurNAc 6P and GlcNAc. MurNAc 6P can be used as substrate for recombinant MurQ, which was monitored in the detection of GlcNAc 6P (Figure 4B in [106] or Appendix A). This finding further supports the conclusion that both enzymes are active in the same peptidoglycan recycling pathway and catalyse sequential reactions.

On the one hand, and as described in the introduction, the PTS transporter MurP is known to import the monosaccharide MurNAc in *E. coli*, *B. subtilis* as well as in *S. aureus*. On the other hand, in *S. aureus*, the product of peptidoglycan cleavage by the major autolysin Atl is the disaccharide MurNAc-GlcNAc. If the phosphorylated disaccharide MurNAc 6P-GlcNAc was found intracellularly in a *mupG* mutant, MurP may not be exclusively specific for the monosaccharide MurNAc. To elucidate this, the supernatant of a *murP::Tn* and a Δ*mupGmurQPR* mutant were compared to the supernatant of wild-type cells. And indeed, MurNAc-GlcNAc and not MurNAc was found to accumulate extracellularly in cultures of both mutants as indicated by HPLC-MS and fragmentation pattern analysis (Figure 6 in [106] or Appendix A). The localisation of MurNAc at the non-reducing end was also supported by the fact that the exo-*N*-acetylglucosaminidase NagZ of *B. subtilis* was not able to cleave the accumulation product (result not shown), which is thus not GlcNAc-MurNAc [37]. These findings showed that MurP of *S. aureus* besides MurNAc also transports the disaccharide MurNAc-GlcNAc. Since the accumulation was not observed intracellularly of a Δ*mupGmurQPR* mutant, it was also concluded that MurNAc-GlcNAc serves as primary substrate for the *mupGmurQPR* operon in *S. aureus*.

A phylogenetic analysis using sequences of other DUF871 proteins from various species revealed a partition into two distinct clades (Figure 8 in [106] or Appendix A). One clade, grouping with MupG of *S. aureus*, probably represents more close homologues with similar or identical function, while the other clade probably comprises more distant homologues with altered substrate specificity or activity in a different physiological context.

4.1.3. Genome context of DUF871 proteins

By analysing the phylogenetic relationship within the family of DUF871 proteins, it became evident that this family is not homogeneous but instead forms two groups. MupG proteins, named by their grouping within the same phylogenetic clade as MupG of *S. aureus*, were assumed to fulfil the same physiological function as phosphomuramidases in the recycling of MurNAc 6-phosphate-GlcNAc. Representatives of the second group, called MupG-like proteins, may have different substrates or physiological roles.

To take a closer look, the genome context of genes coding for putative MupG homologues was investigated. The result is illustrated in Figure 4.1. With a few exceptions, genes encoding putative MupG proteins were found in proximity to genes coding for homologues of the etherase MurQ and the PTS transporter MurP. Putative homologues of the regulator MurR were less frequently found, but if present within a species, the encoding genes were also located in proximity to the previously mentioned. The exceptions were MupG proteins from archaea, one *Thermaerobacter* and three *Lactobacillus* species. Notably, in some species, genes encoding putative MurK homologues were found in vicinity to genes encoding MupG proteins. MurK phosphorylates the amino sugars GlcNAc and MurNAc at the C6 position in *Clostridium acetobutylicum* [112]. Genes for putative homologues of 6P-β-glucosidases were found just as frequently near MupG-encoding genes. However, the presence of genes coding for MurK or 6P-β-glucosidases appeared to be mutually exclusive, as both never occurred simultaneously.

A contrasting picture emerged when looking at the second clade, which presumably comprises more distant homologues of MupG (MupG-like proteins). Here, co-localisation with *murQ* was observed only in three species from the classes Bacilli and Clostridia. However, PTS systems that were annotated as transporters for cellobiose and a few for lactose, fructose or lichenan were commonly found in proximity or vicinity of genes encoding putative MupG homologues (indicated by blue outlined squares in Figure 4.1). Compared to MupG-like proteins, 6P-β-glucosidases as well as putative MurK homologues were also more often, sometimes even simultaneously (e. g. in *Bacillus megaterium* and *Lactobacillus plantarum*) present.

Strikingly, some species even encoded proteins of both groups, MupG homologues and MupG-like. Examples include *B. megaterium* and *L. plantarum*, both of which belong to the class of Bacilli. In *B. megaterium*, both the MupG homologue and the MupG-like protein co-located with putative MurQ homologues, but only the MupG homologue also co-located with a putative MurP homologue. The MupG-like protein grouped with a putative 6P-β-glucosidase and a putative MurK homologue instead. *L. plantarum* possesses four putative homologues, of which only one belongs to MupG homologues. Similar to *B. megaterium*, one of the MupG-like proteins clustered with putative homologues of MurQ and, additionally, of MurP, whereas another was found in proximity of a PTS transporter for cellobiose and in vicinity of putative homologues of MurP. Next to the third putative MupG-like protein only 6P-β-glucosidases were found.

Taken together, of the examined species those encoding MupG-like proteins commonly also encode putative homologues for MurQ, MurP and often MurR. This suggests their ability to facilitate a recycling pathway for MurNAc 6P-GlcNAc similar to *S. aureus*, since all enzymes necessary for this are present. The absence of MurR should not eliminate this possibility as it acts as repressor [64]. The MupG homologues probably more distantly related might serve as glycoside hydrolases to utilise other phosphosugars as their common genetic co-localisation with PTS transporters for sugars suggest.

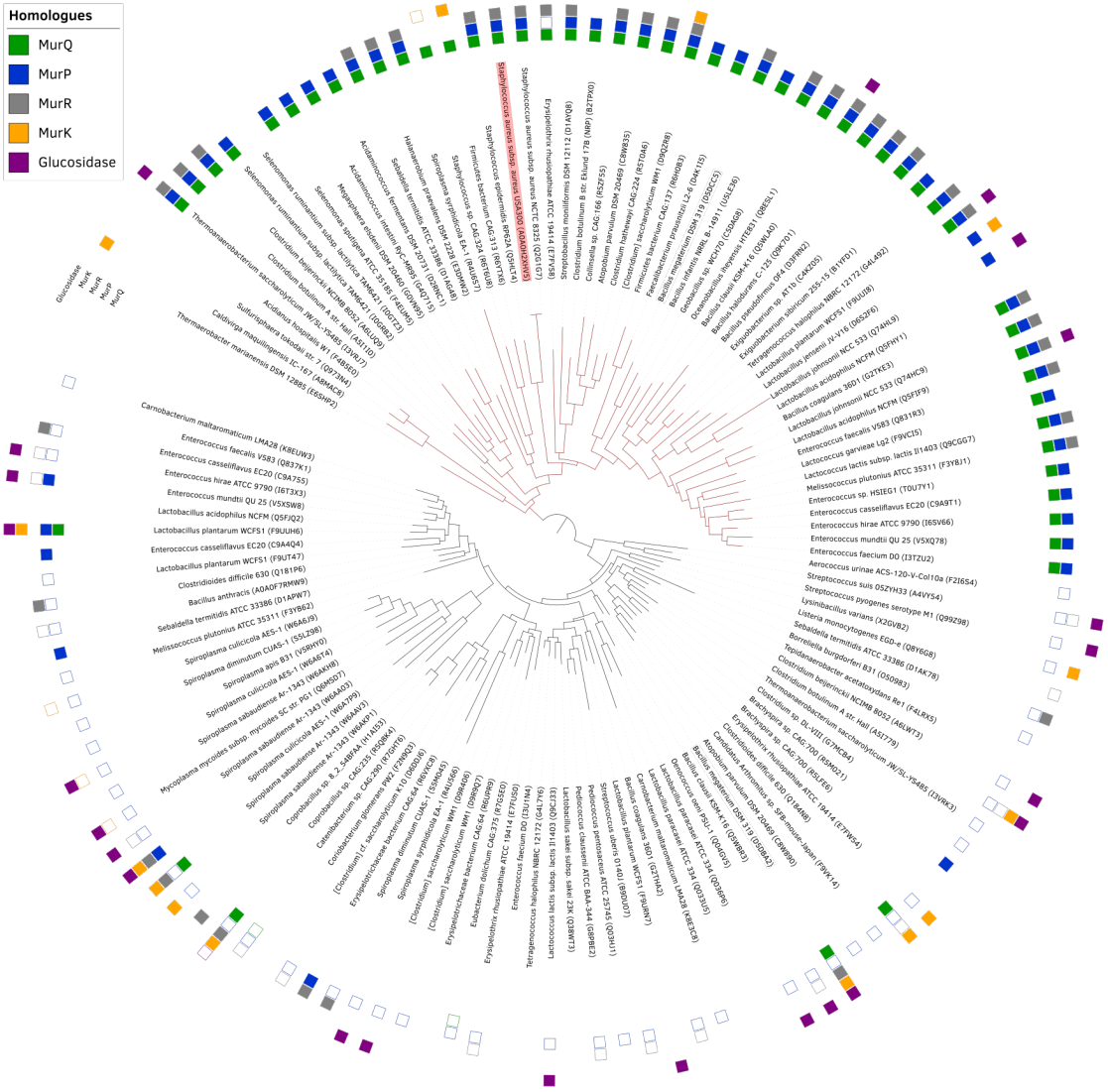

Figure 4.1.: Genomic context of genes encoding putative homologues of MupG. The phylogenetic tree shown was constructed based on a multiple sequence alignment of putative MupG homologues. The presence of putative homologues of the etherase MurQ (green), the PTS transporter MurP (blue), the regulator MurR (grey), the kinase MurK (orange) and a Glucosidase (purple) is indicated by coloured squares. Filled squares indicate sequence homologues, whereas outlined squares indicate related but not homologous proteins. The clade of proteins grouping with MupG of *S. aureus* is depicted with red lines, whereas more distant homologues are shown with black lines. MupG of *S. aureus* is shown with red coloured background.

4.1.4. Investigation of MurP in *B. subtilis*

The observations made by Kluj *et al.* [106] showed that in *S. aureus* the PTS transporter MurP ($MurP_{Sa}$) not only facilitates the transport of the monosaccharide MurNAc, but also the disaccharide MurNAc-GlcNAc, which, in fact, is the major turnover product in *S. aureus*. $MurP_{Sa}$ and MurP of *B. subtilis* ($MurP_{Bs}$) share a sequence identity of 45.3 %, which raised the question, if the disaccharide may also be transported by MurP in *B. subtilis*. To address this question, a Δ*murQRP*Δ*namZ::erm* double mutant was generated, and together with a Δ*namZ::erm* mutant examined in respect of accumulation products. MurNAc-GlcNAc is not a physiologically occurring recycling product in *B. subtilis*, but was recently identified as minimal natural substrate of NamZ [80]. Therefore, a mutant deficient in *namZ* should cause arbitrary accumulation of MurNAc-GlcNAc, and, by doing so, provide the potential substrate for $MurP_{Bs}$.

First hints towards a potential capability to transport disaccharides derived from LC-MS analyses of acetone extracts of culture supernatants of both mutants (see Figure 4.2 and Table 4.1 for retention times, accurate masses, and mass error). No accumulation of MurNAc-GlcNAc was detected in the supernatant of the *namZ* mutant. In contrast, a compound with a retention time of 21.3 min and a mass corresponding to either GlcNAc-MurNAc or MurNAc-GlcNAc accumulated in the *murQRP namZ* double mutant. Since both molecules consist of the same sugars, they have the same exact mass and isotope pattern. Whilst the addition of recombinant NagZ caused no change, the compound disappeared after the addition of recombinant NamZ. Furthermore, MurNAc was detected additionally. A cleavage of MurNAc from one of the two disaccharides should also release GlcNAc. However, GlcNAc was not detected. This might be caused by poor ionisation or NamZ bound GlcNAc. Nonetheless, cleavage by NamZ showed that the accumulation product was MurNAc-GlcNAc. GlcNAc-MurNAc is a substrate of NagZ, which, however, showed no enzymatic activity towards the accumulation product. Taken together, the analyses of the supernatants and enzymatic digestion showed that the disaccharide MurNAc-GlcNAc accumulated in the Δ*murQRP*Δ*namZ::erm* double mutant.

As seen in *S. aureus* and analogue to MurNAc, MurNAc-GlcNAc is phosphorylated when transported across the inner membrane by $MurP_{Sa}$. Therefore, intracellular accumulation was investigated. Indeed, a compound with the mass of phosphorylated MurNAc-GlcNAc (or GlcNAc-MurNAc) accumulated in the *namZ* mutant (Figure 4.3). This compound was not detected in the wild-type and in the *murQRP namZ* double mutant. As described previously, MupG of *S. aureus* cleaves MurNAc 6P-GlcNAc [106]. The addition of MupG led to degradation of the accumulation product in the acetone extract of the *namZ* mutant. Consequently, after incubation with MupG, both phosphorylated MurNAc and GlcNAc were detected. Interestingly, another compound accumulated in the *namZ* mutant that neither was found in the wild-type nor in the double mutant. The mass of this compound corresponded to MurNAc-GlcNAc (or GlcNAc-MurNAc). The compound vanished upon incubation with recombinant NamZ and subsequently MurNAc and GlcNAc were found (Figure 4.4B), identifying the compound as MurNAc-GlcNAc. Presumably, this product was generated by a so far unknown phosphatase.

In summary, the results indicated an extracellular accumulation of MurNAc-GlcNAc in a *B. subtilis* Δ*murQRP*Δ*namZ::erm* double mutant. The phosphorylated disaccharide MurNAc 6P-GlcNAc was found to accumulate in the *B. subtilis* Δ*namZ::erm* mutant, but not in the Δ*murQRP*Δ*namZ::erm* double mutant. These observations suggest $MurP_{Bs}$ to be the PTS transporter responsible for transporting the disaccharide MurNAc-GlcNAc, although unphosphorylated MurNAc-GlcNAc was found to some extent in the Δ*namZ::erm* mutant.

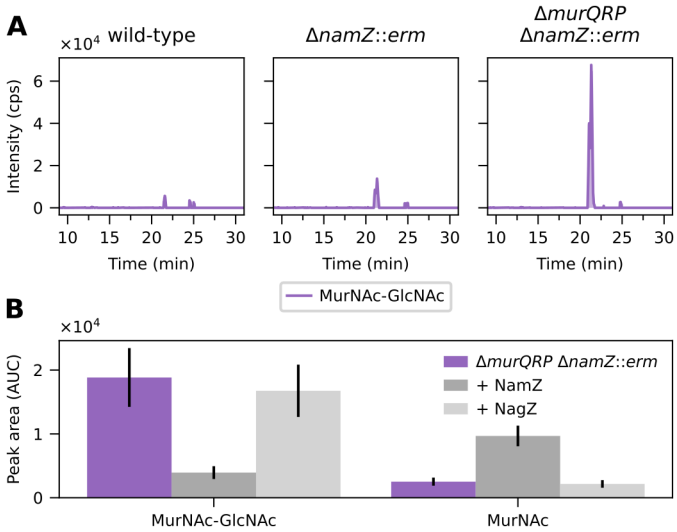

Figure 4.2.: Accumulation of MurNAc-GlcNAc in the supernatant of a *murQRP namZ* double mutant. *B. subtilis* wild-type, Δ*namZ::erm* and Δ*murQRP*Δ*namZ::erm* cells were grown for 24 h in LB medium. Acetone extracts of cytosolic fractions were analysed by LC-MS. A) Result of the LC-MS analysis with EICs for MurNAc-GlcNAc (purple). B) Result of the LC-MS analysis of the acetone extract of the double mutant (blue) treated with recombinant NamZ (orange) and NagZ (green). Data presented as mean (n = 3) area under the curve (AUC).

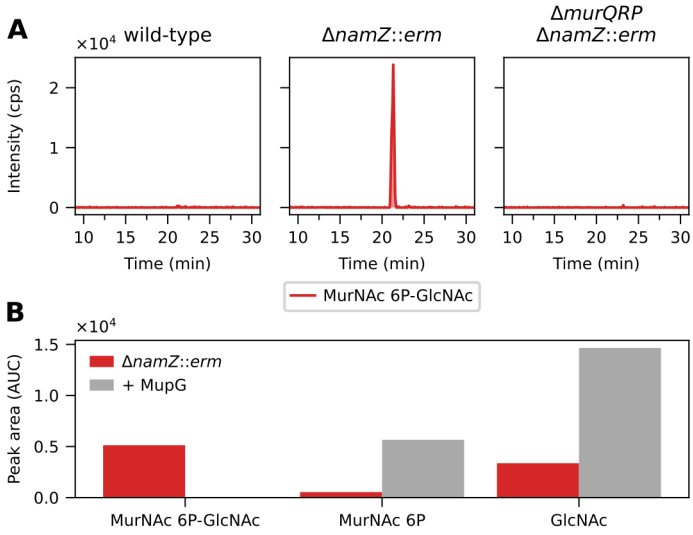

Figure 4.3.: Intracellular accumulation of MurNAc 6P-GlcNAc in a *namZ* mutant. *B. subtilis* wild-type, Δ*namZ::erm* and Δ*murQRP*Δ*namZ::erm* cells were grown for 24 h in LB medium. Acetone extracts of cytosolic fractions were analysed by LC-MS. A) Result of the LC-MS analysis with extracted ion chromatograms (EICs) for MurNAc 6P-GlcNAc (red). B) Result of the LC-MS analysis of the acetone extract of a *namZ* mutant (blue) treated with recombinant MupG (orange). Data presented as area under the curve (AUC). The two measurements derived from independent experiments.

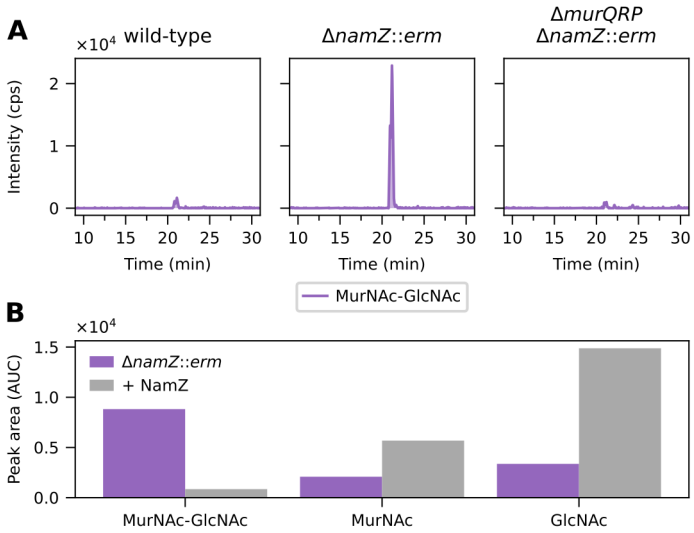

Figure 4.4.: Intracellular accumulation of MurNAc-GlcNAc in a *namZ* mutant. *B. subtilis* wild-type, Δ*namZ::erm* and Δ*murQRP*Δ*namZ::erm* cells were grown for 24 h in LB medium. Acetone extracts of cytosolic fractions were analysed by LC-MS. A) Result of the LC-MS analysis with EICs for MurNAc-GlcNAc (purple). B) Result of the LC-MS analysis of the acetone extract of a *namZ* mutant (blue) treated with recombinant NamZ (orange). Data presented as area under the curve (AUC). The two measurements were performed in independent experiments.

Table 4.1.: Retention time (min), accurate mass (*m/z*), and mass error (ppm) of extra- and intracellular accumulation products in *B. subtilis* wild-type, *namZ* and *murQRP namZ* mutants. See Table 3.3 for exact masses.

	Wild-type			Δ*namZ::erm*			Δ*murQRP* Δ*namZ::erm*		
Peptide	min	*m/z*	ppm	min	*m/z*	ppm	min	*m/z*	ppm
				Extracellular					
MurNAc-GlcNAc	21.5	497.205	14.9	21.3	497.200	5.1	21.4	497.197	0.9
MurNAc (+ NamZ)							22.1	294.120	4.7
				Intracellular					
MurNAc 6P-GlcNAc	21.2	575.155	11.7	21.3	575.151	5.0			
MurNAc-GlcNAc	21.1	495.185	5.9	21.1	495.185	5.3	21.1	495.182	2.9
MurNAc 6P (+ MupG)				21.9	374.078	16.8			
GlcNAc (+ MupG)				10.0	222.093	19.0			
MurNAc (+ NamZ)				21.7	294.114	15.8			
GlcNAc (+ NamZ)				10.0	222.092	22.1			

4.2. Utilisation of cell wall peptides in *B. subtilis*

As described in the introduction (Section 1.6), *E. coli* possesses enzymes, which allow the sequential degradation of cell wall peptides. *B. subtilis* harbours orthologs of the L-Ala-D/L-Glu epimerase YcjG, named YkfB (sequence identity of 31.2 %), and of the LD-carboxypeptidase LdcA, named YkfA (sequence identity of 30 %) [69, 97]. Furthermore, the protein YkfC was characterised as a γ-D-Glu-Dpm endopeptidase, and D-aminopeptidase activity was demonstrated for DppA (which has no counterpart in *E. coli*) [69, 91]. The corresponding genes are organised in the gene cluster *dppABCDE ykfABCD* in the genome of *B. subtilis*. Besides the aforementioned enzymes, the cluster contains genes encoding components of an ABC peptide transporter (*dppBCDE* and *ykfD*) [84, 85]. To better understand the function of DppA, YkfA and YkfC in respect to the process of peptide recycling, different cell wall peptides obtained from *E. coli* and *B. subtilis* were incubated with recombinant versions of these enzymes and analysed via LC-MS.

Difference chromatograms (DCs) and extracted ion chromatograms (EICs) from LC-MS analyses were evaluated and used for the analysis of the substrate specificities of DppA, YkfA and YkfC. Cell wall-derived peptides are assigned and identified based on their *m/z* values, isotope patterns and, where available, retention times. It is important to note that, in general, no definitive statements can be made about the constitution of compounds based on the LC-MS measurements carried out here. The assignments therefore represent assumptions based on known structures of the peptidoglycan of *E. coli* and *B. subtilis* (see Table 3.3 for list of exact masses). Retention times, accurate masses and mass error are summarised at the end of the respective parent section.

4.2.1. Declaration

The experiments described in Section 4.2 were performed by me with the following exceptions: Simon Friz (University of Tübingen, group of Christoph Mayer) conducted the HPLC with pre-column derivatisation by OPA reagent for the analysis of the substrate specificity of DppA (Section 4.2.3); Jula Reuter (University of Bonn, group of Beate Henrichfreise) performed the Lipid II assay with YkfC expressed and purified by me (Section 4.2.5); Marjorie Dauvin (University of Liège, group of Bernard Joris) generated the *B. subtilis* Δ*dppABCDE::kan*, Δ*ykfABCD::kan*, and Δ*dppABCDE::kan* Δ*ykfABCD::spc* mutants for her own studies, but provided them for my experiments (Section 4.2.7). Corresponding notes can be found in the descriptions of the respective experiments.

4.2.2. Generation of cell wall peptides

Peptides were generated by incubating crude cell wall preparations of *E. coli* MC4100 and *B. subtilis* 168 cells from the stationary growth phase with the amidase CwlC of *B. subtilis*. The amidase was heterologously overexpressed and purified by SEC to apparent purity (see Figure 4.5). In addition, peptides were prepared from *B. subtilis* Δ*dacA::erm* cells to obtain substrates with unusual pentapeptide-containing structures. The supernatants of the mixtures of various peptides were analysed by LC-MS to determine their composition as depicted in Figure 4.6.

The peptides released by CwlC found in the suspension of *E. coli* cell walls are listed in Table 4.2. The tetrapeptide L-Ala-iso-D-Glu-*meso*-Dpm-D-Ala and cross-linked tetrapeptide

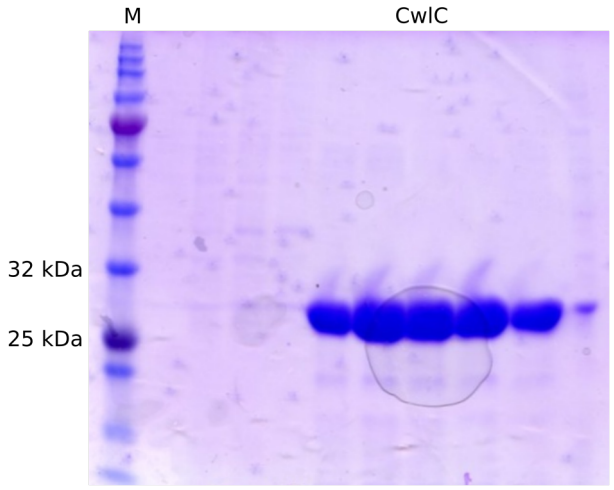

Figure 4.5.: SDS-PAGE analysis of purified recombinant CwlC (calculated molecular weight of 28.3 kDa).

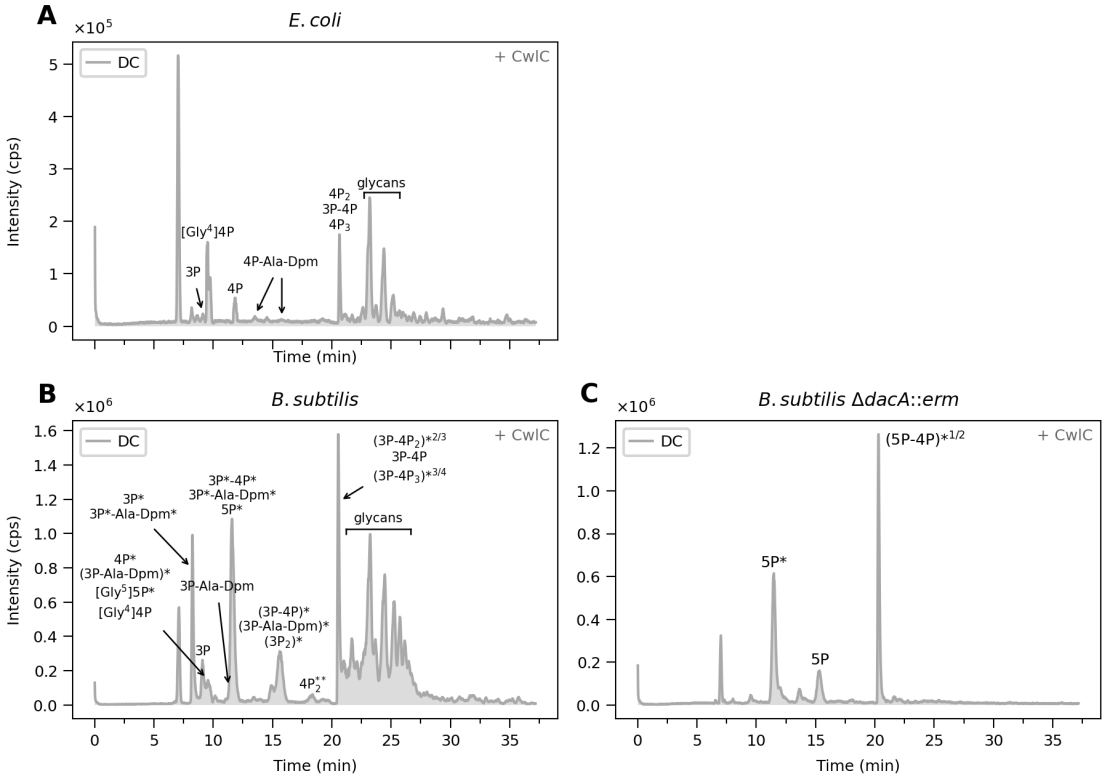

Figure 4.6.: Products released by the amidase CwlC from peptidoglycan preparations of *E. coli* MC4100 (A), *B. subtilis* 168 (B), and *B. subtilis* 168 Δ*dacA::erm* (C). Crude cell wall preparations of *E. coli* MC4100, *B. subtilis* 168, and *B. subtilis* 168 Δ*dacA::erm* from stationary growth phase were treated with CwlC. The result of the subsequent LC-MS analysis of the supernatant is shown with DCs. Asterisks indicate amidations. Peptides are abbreviated based on their number of amino acids (3P: tripeptide, 4P: tetrapeptide, 5P: pentapeptide). See Table 4.2 for accurate masses and mass errors as well as Table 3.3 for exact masses.

dimers were found with high intensity. With lower intensities, the tripeptide L-Ala-iso-D-Glu-*meso*-Dpm, tetrapeptide-Ala-Dpm, tri-tetrapeptide, tetra-tetra-tetrapeptide were also identified based on their accurate masses, which can be found in Table 3.3 in Section 3.6. Interestingly, the EIC of tetrapeptide-Ala-Dpm showed two peaks with a retention time of 13.5 min and 15.8 min respectively. The mass spectra of both peaks exhibited the same isotope pattern and accurate masses. Thus, the two peaks might resulted from a chromatographic separation of two stereoisomers. Peptide-free, multimeric glycans of the peptidoglycan eluted from the column after 23 min. With very low intensity and just two isotopes, a compound with a *m/z* value corresponding to a tetrapeptide with one Ala exchanged for Gly (referred to as [Gly^4]Tetrapeptide from now on and in Table 4.2) was also observed.

In contrast to *E. coli*, the number of CwlC-released peptides identified in the suspension of *B. subtilis* cell walls was much higher and included peptides with varying degree of Dpm-amidation (see Table 4.2). The most abundant peptides were tri-tetrapeptide with either two Dpm residues or one Dpm residue amidated as well as tripeptide, both, amidated and non-amidated. A cross-linked, trimeric peptide composed of one tri- and two tetrapeptides (tri-tetra-tetrapeptide) was also found with reasonable abundance. The number and positions of amidations, however, could not be determined unambiguously because the mass spectrum (Figure 4.7 showed an isotope pattern that corresponded to two variants with different degree of amidation. In one variant, all three Dpm residues were amidated, in the other two (the third possible variant without amidation was not detected). Unfortunately, the separation on the HPLC column was insufficient to distinguish these isoforms. Furthermore, the isotope pattern observed in the mass spectrum could not be definitely assigned to one of the two amidated isomers of tri-tetra-tetrapeptide. A higher resolving power of the mass spectrometer would have been helpful for this, as will be discussed later. Therefore, it could only be assumed that mostly two to three of three Dpm residues were amidated. Interestingly, and reminiscent of *E. coli*, two peaks were observed with retention times of 8.2 min and 11.6 min, whose mass spectra showed similar isotope patterns. The *m/z* values of both peaks matched a twice amidated tripeptide-Ala-Dpm (compare Figure 4.8 and Table 4.2 with Table 3.3). This was endorsed by the paired occurrence of further peaks with retention times of 9.4 min and 15.6 min. Each of these peaks showed similar isotope patterns with *m/z* values matching tripeptide-Ala-Dpm with one amidation. In the respective first peak of both forms (8.2 min and 9.4 min), the relative abundance of individual isotopes deviated somewhat from the calculated values. Despite a difference of 1.2 min in retention time, the EICs partially overlapped, indicating insufficient separation. Another peak with a retention time of 11.3 min was observed, which showed an accurate mass and isotope pattern corresponding to non-amidated tripeptide-Ala-Dpm. A second peak corresponding to tripeptide-Ala-Dpm was not found. Amidated [Gly^5]pentapeptide and completely amidated [Gly^5]pentapeptide-tetrapeptide were additionally identified. The canonical pentapeptide Ala-Glu-Dpm-Ala_2, in contrast, was only found in traces. This was also true for amidated tetrapeptide. In addition, a compound with a mass corresponding to a tetrapeptide with one Ala exchanged by Gly was detected (referred as [Gly^4]Tetra in Table 4.2). It seemed to be not amidated and might be the same peptide as in *E. coli* (see above). As observed with peptidoglycan from *E. coli*, peptide-free, multimeric sugars eluted from the column after 23 min.

Pentapeptide and cross-linked pentapeptide-tetrapeptide were obtained from peptidoglycan of a *B. subtilis* Δ*dacA::erm* mutant strain. Pentapeptide was found both non-amidated and amidated. For penta-tetrapeptide, no definite number of amidations could be determined for the

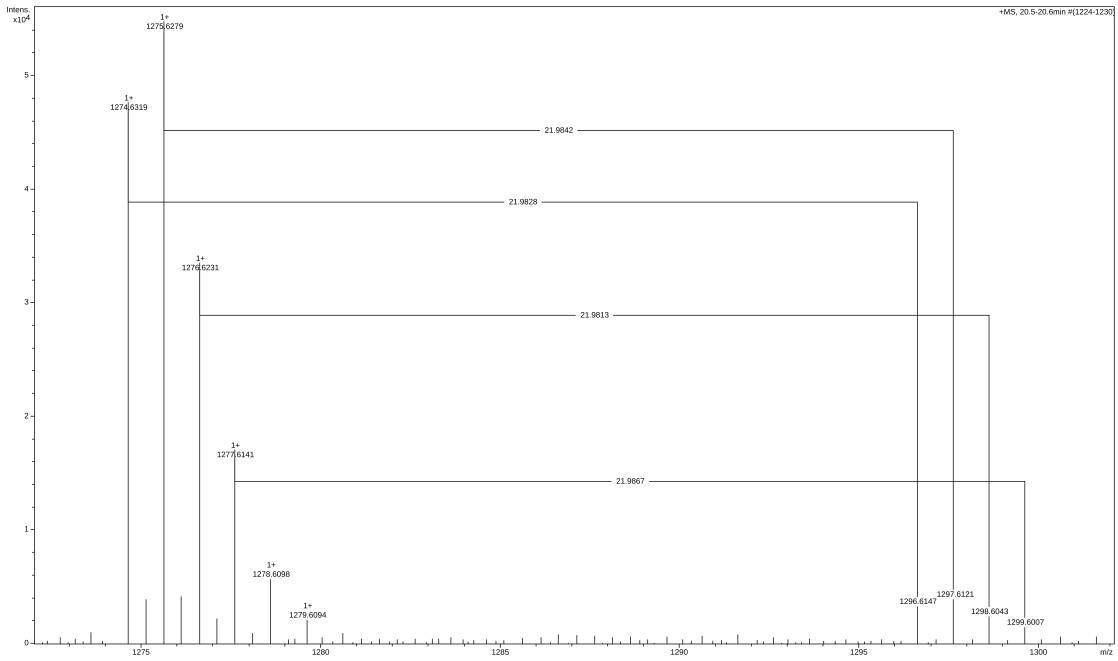

Figure 4.7.: Tri-tetra-tetrapeptide found in CwlC-treated suspension of *B. subtilis* cell walls. Crude cell wall preparations of *B. subtilis* 168 from stationary growth phase were treated with CwlC. The result of the subsequent LC-MS analysis of the supernatant is shown with a mass spectrum. The corresponding sodium adducts ($[M + \mathrm{Na}]^+$) are annotated.

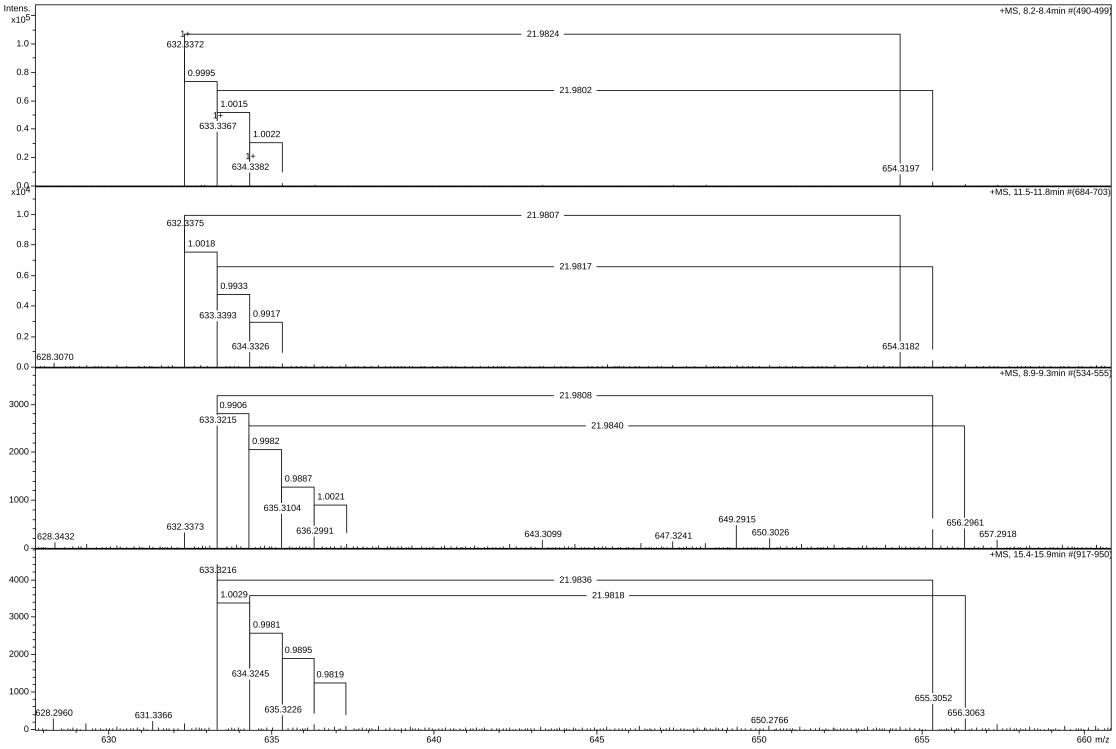

Figure 4.8.: Tripeptide-Ala-Dpm found in CwlC-treated suspension of *B. subtilis* cell walls. Crude cell wall preparations of *B. subtilis* 168 from stationary growth phase were treated with CwlC. The result of the subsequent LC-MS analysis of the supernatant is shown with mass spectra. The corresponding sodium adducts ($[M + \mathrm{Na}]^+$) are annotated.

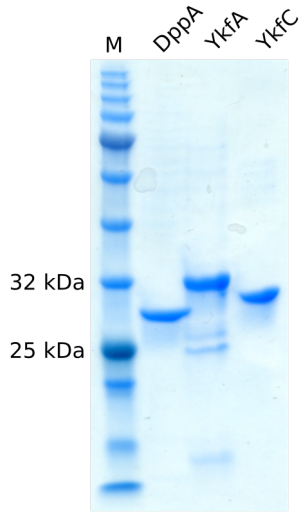

Figure 4.9.: SDS-PAGE analysis of purified recombinant DppA (calculated molecular weight of 30.2 kDa), YkfA (35.8 kDa) and YkfC (34.1 kDa).

same reason as for tri-tetra-tetrapeptide, but it was likely that either one or both Dpm residues were amidated.

These findings and the masses listed in Table 4.2 demonstrated that the amidase CwlC of *B. subtilis* was able to release unbranched as well as branched peptides from crude cell suspensions of *E. coli*, *B. subtilis* wild-type and *B. subtilis* Δ*dacA::erm*. The suspensions generated this way were used for subsequent in vitro analyses of recombinant DppA, YkfA and YkfC.

The retention times given in Table 4.2 may differ somewhat from the retention times given below. The same gradient was used for all LC-MS analyses, but the equilibration and rinsing steps differed between the substrate analysis described above and the in vitro experiments with the recombinant enzymes described below.

4.2.3. Characterisation of DppA

DppA was previously described as zinc-dependent D-aminopeptidase specifically cleaving D-Ala-p-Na [91]. To confirm the previous results, DppA was overexpressed with its complete coding sequence without His-tag, purified to apparent purity (see Figure 4.9), and its specificity was investigated with different, fluorogenic and non-fluorogenic substrates.

Zinc dependency and stereospecificity

First, the described dependence of DppA on zinc was evaluated with D- and L-isomers of fluorogenic Ala-7-amido-4-methylcoumarin trifluoroacetate (Ala-AMC) as shown in Figure 4.10. A cleavage of the substrate is indicated by release of the fluorescent product AMC. Without zinc, no change in fluorescence was observed with either D-Ala-AMC or L-Ala-AMC. When zinc was added, an increase in fluorescence was observed with the D-isomer. With the L-isomer, however, no change was observed in any condition. Thus, the results obtained by Cheggour *et al.* [91] could be confirmed.

Table 4.2.: Peptides released by the amidase CwlC from peptidoglycan preparations of *E. coli* MC4100, *B. subtilis* 168, and *B. subtilis* 168 Δ*dacA::erm* cells. The peptides are sorted by their exact mass and asterisks indicate amidations.

Peptide	Retention time (min)	Accurate mass (*m/z*)	Mass error (ppm)
	E. coli		
Tripeptide	9.1	391.183	2.7
[Gly^{4}]Tetrapeptide	9.5	448.208	9.4
Tetrapeptide	11.8	462.220	1.6
Tetrapeptide-Ala-Dpm (A)	13.5	705.345	4.9
Tetrapeptide-Ala-Dpm (B)	15.8	705.343	2.8
Tri-tetrapeptide	20.7	834.383	0.9
Tetra-tetrapeptide	20.7	905.421	6.5
Tetra-tetra-tetrapeptide	20.7	1348.608	5.5
	B. subtilis		
Tripeptide*	8.3	390.199	1.5
Tripeptide	9.1	391.183	1.9
[Gly^{4}]Tetrapeptide	9.5	448.207	6.5
Tetrapeptide*	9.6	461.237	3.8
[Gly^{5}]Pentapeptide*	9.6	518.257	1.0
Pentapeptide*	11.5	532.275	4.2
Tripeptide*-Ala-Dpm* (A)	8.2	632.337	1.7
Tripeptide*-Ala-Dpm* (B)	11.6	632.337	1.7
(Tripeptide-Ala-Dpm)* (A)	9.4	633.322	2.0
(Tripeptide-Ala-Dpm)* (B)	15.6	633.322	2.6
Tripeptide-Ala-Dpm	11.3	634.308	6.2
(Tri-tripeptide)*	15.6	762.364	2.1
Tri*-tetrapeptide*	11.6	832.416	0.3
(Tri-tetrapeptide)*	15.6	833.401	1.3
Tri-tetrapeptide	20.6	834.386	2.0
Tetra*-tetrapeptide*	18.2	903.456	12.5
[Gly^{5}]Penta*-tetrapeptide*	18.4	960.476	6.5
Tri*-tetrapeptide*-Ala-Dpm*	10.1	1074.556	8.7
(Tri-tetra-tetrapeptide)*$^{2/3}$	20.5	1275.628	7.1
(Tri-tetra-tetra-tetrapeptide)*$^{3/4}$	20.6	1717.834	4.5
Pentapeptide* (Δ*dacA::erm*)	11.5	532.271	3.5
Pentapeptide (Δ*dacA::erm*)	15.3	533.255	3.7
(Penta-tetrapeptide)*$^{1/2}$ (Δ*dacA::erm*)	20.3	974.484	6.5

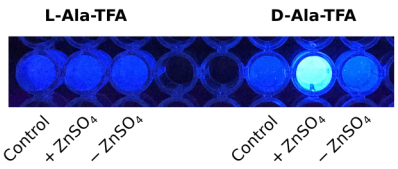

Figure 4.10.: DppA acts as zinc-dependent D-alanine aminopeptidase. Recombinant DppA (13 ng) was incubated with 0.5 mM L-alanine 7-amido-4-methylcoumarin trifluoroacetate (L-Ala-AMC) and D-Ala-AMC with (+) and without (−) zinc sulphate ($ZnSO_4$).

To investigate the specificity of DppA in more detail, chemically synthesised racemic mixtures of D-Ala-*rac*-2,6-Dpm and *rac*-2,6-Dpm-D-Ala_2 were used. In these peptides, D-Ala is linked to a mixture of isoforms of 2,6-Dpm, which includes the D-Ala-*meso*-Dpm cross-link occurring in the peptidoglycan.

DppA was incubated for 0 h to 17 h with D-Ala-*rac*-2,6-Dpm and subsequently analysed by LC-MS. As shown in Figure 4.12 (see Table 4.3 for retention times, accurate masses and mass error as well as Table 3.3 for exact masses), D-Ala-*rac*-2,6-Dpm appeared as relatively broad peak in an EIC for Ala-Dpm and in the BPC. In samples treated with DppA, the signal detected for Ala-Dpm hardly differed from the control (Figure 4.11). However, a release of Dpm was observed, which increased with incubation time (Figure 4.11). The Dpm released was initially very little, as shown by very low signals after 1 h to 2 h of incubation. However, a clear signal was detected after 17 h of incubation, indicating a release of significant amounts of Dpm. The second product of this cleavage was expected to be Ala. Due to its small mass, however, it could not be detected with the LC-MS method used here. In summary, product formation occurred with DppA, although no decrease in substrate was observed.

The incubation of *rac*-2,6-Dpm-D-Ala_2 with recombinant DppA for 17 h led to a minor release of products (Dpm and Ala_2), as shown in Figure 4.13 (see Table 4.3 for overview of retention times, accurate masses, and mass error as well as Table 3.3 for exact masses). *rac*-2,6-Dpm-D-Ala_2 appeared as one peak and was detected with the same abundance in both the control and the DppA-treated sample. Nonetheless, Dpm occurred with higher abundance in the DppA-treated sample. The same was found for Ala_2. However, both peptides were also detected in the control in appreciable amounts (Figure 4.13). Interestingly, traces of a compound composed of Ala and Dpm (Dpm-Ala or Ala-Dpm) were also detected. Its retention time differed slightly (0.4 min) from that of the chemically synthesised D-Ala-*rac*-2,6-Dpm. However, the compound was detected with comparable intensity in both the DppA-treated sample and the control. Whether this were remnants of the chemical synthesis or products of decay remained unclear. A detailed analysis of the stereospecificity in the DppA reactions could answer this. Notwithstanding, the turnover of the synthesised substrates by DppA was very low and only visible after 17 h of incubation.

Whilst the LC-MS analyses indicated a specificity of DppA for linkages between D-Ala and 2,6-Dpm, they could not answer the question if the specificity is limited to Dpm in general or to one of its stereoisomers. Therefore a HPLC analysis with pre-column derivatisation with OPA reagent was conducted by Simon Friz (University of Tübingen, group of Christoph Mayer). This allowed the separation of the stereoisomers LL-Dpm (retention time 31.8 min), DD-Dpm (retention time 33.3 min), and *meso*-Dpm (retention time 34.9 min), as shown in Figure 4.14A. D-Ala appeared

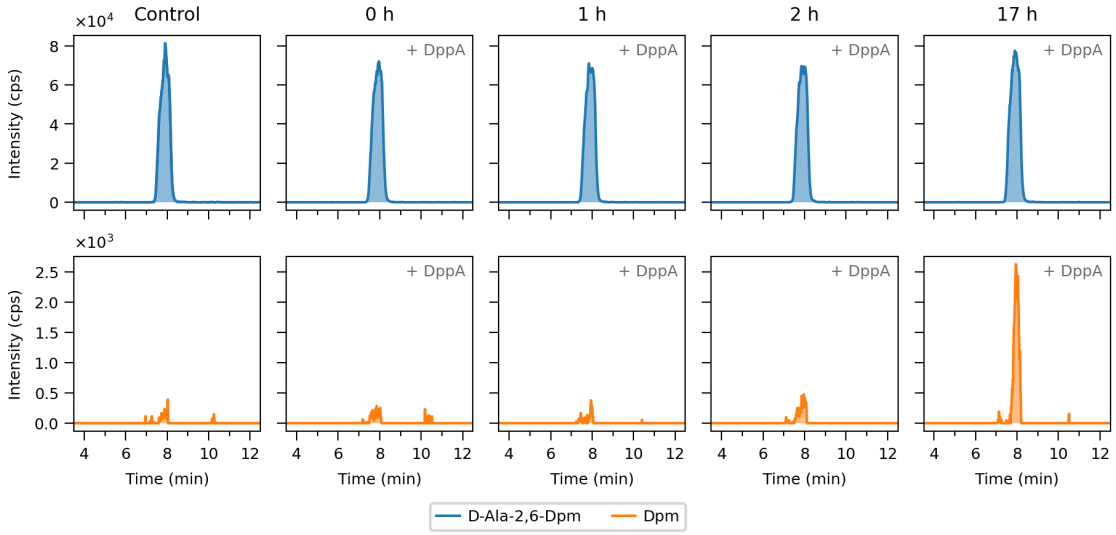

Figure 4.11.: DppA releases Dpm from D-Ala-*rac*-2,6-Dpm. D-Ala-*rac*-2,6-Dpm was incubated for 0 h to 17 h with recombinant DppA and subsequently analysed by LC-MS. Shown are EICs for Ala-Dpm (blue) and Dpm (orange). See Table 4.3 for accurate masses and mass errors as well as Table 3.3 for exact masses.

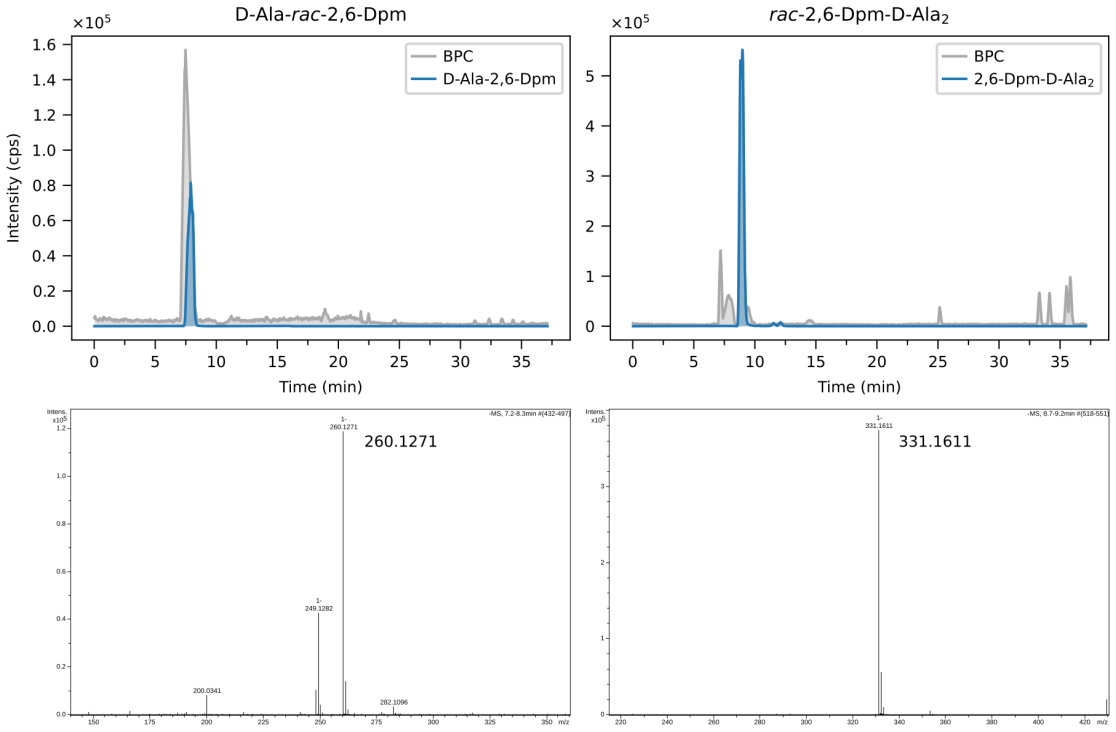

Figure 4.12.: LC-MS analyses of D-Ala-*rac*-2,6-Dpm and *rac*-2,6-Dpm-D-Ala$_2$. The racemic peptides were incubated for 0 h to 17 h without DppA and subsequently analysed by LC-MS. Shown are BPCs and mass spectra of the base peak with accurate masses (see Table 3.3 for exact masses).

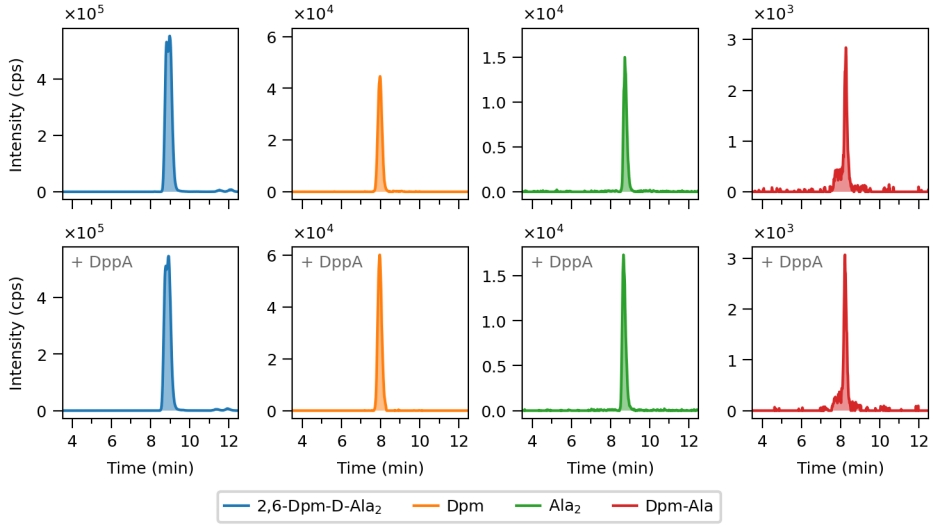

Figure 4.13.: DppA releases low amounts of Dpm and Ala_2 from *rac*-2,6-Dpm-D-Ala_2. Recombinant DppA was incubated for 17 h with *rac*-2,6-Dpm-D-Ala_2 and subsequently analysed by LC-MS. Shown are EICs for Dpm-Ala_2 (blue), Dpm (orange), Ala_2 (green) and Dpm-Ala (red). See Table 4.3 for accurate masses and mass errors as well as Table 3.3 for exact masses.

Table 4.3.: Retention time (min), accurate mass (*m/z*), and mass error (ppm) of peptides detected in the in vitro assays of DppA on chemically synthesised D-Ala-*rac*-2,6-Dpm and *rac*-2,6-Dpm-D-Ala_2. See Table 3.3 for exact masses.

	Control			DppA 17 h		
Peptide	min	*m/z*	ppm	min	*m/z*	ppm
		D-Ala-*rac*-2,6-Dpm				
D-Ala-*rac*-2,6-Dpm	7.9	260.124	1.1	7.9	260.125	4.2
Dpm				8.0	189.090	14.4
		rac-2,6-Dpm-D-Ala_2				
rac-2,6-Dpm-D-Ala_2	8.9	331.161	0.3	8.9	331.162	2.1
Dpm	8.0	189.088	4.3	8.0	189.089	8.6
Ala_2	8.7	159.075	10.8	8.7	159.076	5.8
Dpm-Ala/Ala-Dpm	8.3	260.125	3.1	8.2	260.126	8.1

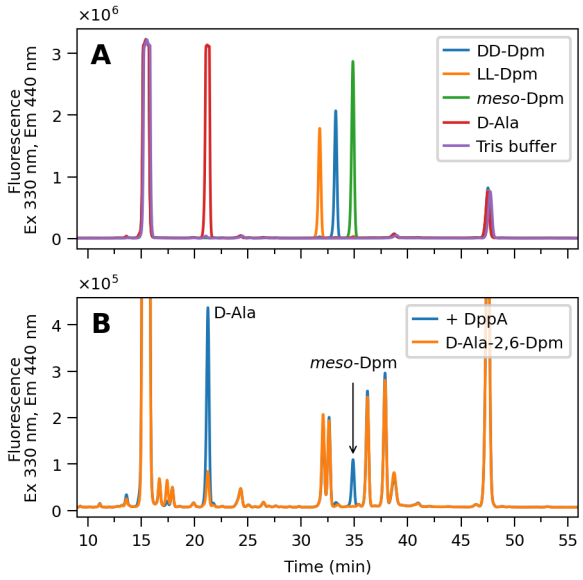

Figure 4.14.: DppA cleaves D-Ala-*meso*-Dpm. The racemic mixture D-Ala-*rac*-2,6-Dpm was incubated with recombinant DppA for 20 h. Shown are chromatograms of the subsequent HPLC analysis with pre-column derivatisation with OPA reagent. The chromatograms shown are A) standards for DD-Dpm (blue), LL-Dpm (orange), *meso*-Dpm (green), D-Ala (red), Tris buffer (violet) and B) D-Ala-*rac*-2,6-Dpm with DppA added (blue), D-Ala-*rac*-2,6-Dpm (orange).

with a retention time of 21.2 min. The chromatogram of the chemically synthesised D-Ala-*rac*-2,6-Dpm showed a number of peaks (Figure 4.14B) that could not be assigned to stereoisomers of D-Ala-*rac*-2,6-Dpm, since no corresponding standards were available. Therefore, the peaks at 17.4 min and 38.7 min that appeared lower with DppA could not be assigned to a particular product (Figure 4.14B). Nevertheless, additional peaks at 21.3 min and 34.9 min arose when DppA was added, as shown in Figure 4.14B. By comparison with the retention times of the standards, these were identified as D-Ala and *meso*-Dpm respectively. This confirmed the specificity of DppA for certain isomers of Dpm, as previously suspected from the LC-MS. DppA specifically cleaved D-Ala-*meso*-Dpm and did not release other isomers of Dpm.

In summary, these results showed the specific hydrolytic activity of DppA versus D-Ala-*meso*-Dpm. However, despite the addition of zinc, product formation was only detected after 17 h of incubation and only to a small extent. This suggests that the hydrolysis proceeded at a low rate.

Activity of DppA towards cell wall peptides

In the so far presented experiments with DppA, as well as in the study of Cheggour *et al.* [91], synthetic substrates had been used. For a more detailed analysis, DppA was next incubated with natural peptides derived from peptidoglycan of *E. coli* and *B. subtilis* cells.

Surprisingly, and although the incubation was carried out for 20 h, no changes could be noticed in chromatograms of the subsequent LC-MS analysis when peptides of *E. coli* served as substrates (data not shown). The absence of a sequence homologue to DppA in *E. coli* concedes the possibility that its cell wall peptides lack certain properties that DppA finds in cell wall

peptides of *B. subtilis*. One obvious aspect is the amidation of the Dpm, which does not occur in *E. coli* and also was absent from the synthetic substrates.

Yet, amidation seemed to be of importance for DppA. The distribution of the amidated forms of tripeptide-Ala-Dpm differed in the DppA-treated and untreated samples (Figure 4.15, see Table 4.8 for overview of retention times, accurate masses, and mass error as well as Table 3.3 for exact masses). Whilst the completely amidated form (retention time 8.4 min) was decreased in abundance, partially amidated tripeptide-Ala-Dpm was significantly increased. Non-amidated tripeptide-Ala-Dpm was also detected with a slightly higher signal than in the control. Interestingly, in both cases, the increase was confined to the respective second peak (retention time of 9.7 min for the partially amidated form and 11.6 min for the non-amidated form) whereas the respective first peak (retention time 8.7 min and 9.4 min) remained unchanged. It should be mentioned that completely amidated tripeptide Ala-Dpm appeared here as a single peak. This contrasts with the appearance of completely amidated Ala-Dpm with two peaks in the initial LC-MS analysis of the substrate (see Section 4.2.2). Moreover, both the partially amidated form as well as the non-amidated form also occurred here with two peaks as just described. The isotope distribution in the first peak (retention time 8.7 min) of the partially amidated form indicated that there was an overlapping of both the completely amidated and the partially amidated forms. The two variants of completely amidated tripeptide-Ala-Dpm were thus probably not sufficiently separated. The presumed isotopes of the completely amidated form indicated a slight decrease in the same.

Although the shift from amidated tripeptide-Ala-Dpm to less amidated tripeptide-Ala-Dpm was the only change observed, it was interesting. In contrast to tripeptide or cross-linked tri-tetrapeptide (no change observed, see Figure 4.15), the N-terminal site of the second Dpm in tripeptide-Ala-Dpm is assumed to be exposed. Tetrapeptide-Ala-Dpm of *E. coli* is assumed to share the same characteristic, but carries no amidation. The tripeptide of *B. subtilis* is often amidated, but there, the C-terminal site of Dpm is exposed. It therefore seems consistent that no change was found for either tripeptide or tri-tetrapeptide (Figure 4.15).

With these considerations, EICs were analysed for Dpm and its amidated form, as neither side is shielded by a bond. Similar to tripeptide-Ala-Dpm, amidated Dpm disappeared (retention time 7.1 min, Figure 4.15). The second peak (retention time 12.1 min) present in the EIC represents an isotope of a smaller *m/z* value and not of amidated Dpm. The EIC of non-amidated Dpm was somewhat ambiguous at first glance. From the three peaks, only the foremost one stood out from the control. A closer inspection of the mass spectra revealed an isotope pattern in agreement with Dpm in this peak. The retention time of 8.1 min also pointed to Dpm. The isotope patterns of the other two peaks and their retention times deviated from this, but do not rule out the possibility that they represent isomers of Dpm. Nevertheless, it can be stated that amidated Dpm disappeared and non-amidated Dpm became more after cell wall peptides of *B. subtilis* were incubated with DppA. At this point, an analysis of Dpm-Ala or Ala-Dpm would also have been interesting. However, since this peptide was not released by CwlC, an analysis was only carried out at a later point.

The observed amidation-dependent activity of DppA contrasts with the hydrolytic activity against the artificial peptides, but suggests a possible second function in the de-amidation of free Dpm residues. That is to say, the hydrolytic activity observed with the artificial substrates could not be confirmed neither using peptides derived from *E. coli* nor from *B. subtilis*. Yet, DppA seemed to alter the state of amidation of tripeptide-Ala-Dpm and Dpm, thereby causing a shift from an amidated to a partially or non-amidated state.

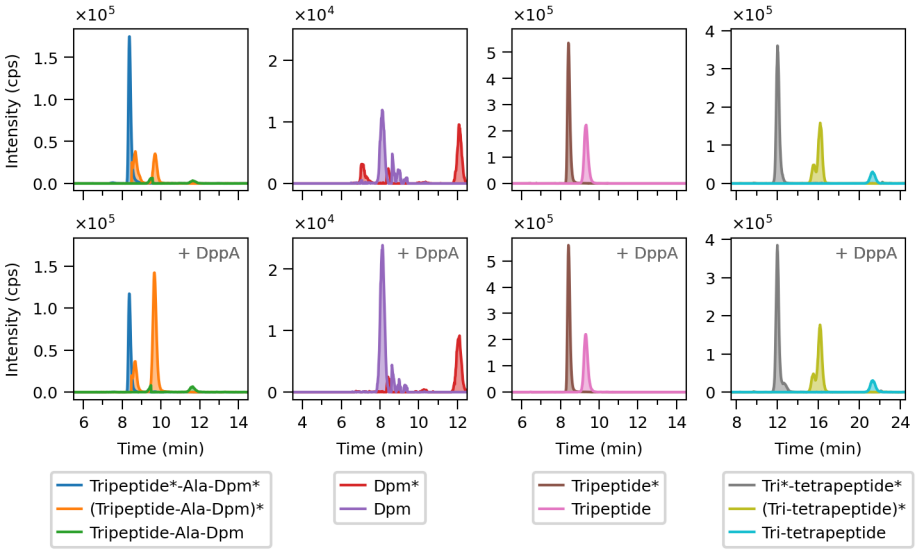

Figure 4.15.: DppA removes the amidation of amidated tripeptide-Ala-Dpm and Dpm of *B. subtilis*. Peptidoglycan of *B. subtilis* 168 was treated with an amidase and additionally with recombinant DppA (+ DppA). The result of the subsequent LC-MS analysis is shown with EICs for tripeptide-Ala-Dpm (green, partially amidated: orange, completely amidated: blue), Dpm (violet, amidated: red), tripeptide (magenta, amidated: brown), and tri-tetrapeptide (aqua, partially amidated: light olive, completely amidated: grey). The number of amidated Dpm residues is indicated with asterisks. See Table 4.8 for accurate masses and mass error as well as Table 3.3 for exact masses.

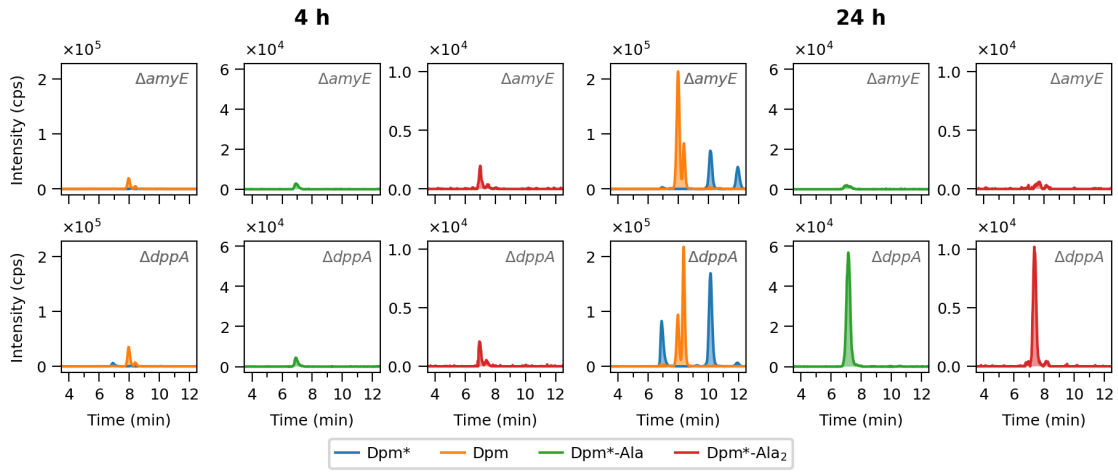

Figure 4.16.: Accumulation products in a *B. subtilis dppA* mutant. *B. subtilis* Δ*amyE::kan* and Δ*dppA::kan* mutant cells were cultivated for 4 h (exponential growth phase) and 24 h (stationary growth phase) in LB medium. Acetone extracts of cytosolic fractions were analysed by LC-MS. The result of the LC-MS analysis is shown with EICs for Dpm (orange, amidated: blue), amidated Dpm-Ala (green), and amidated Dpm-Ala_2 (red). The number of amidated Dpm residues is indicated with asterisks. See Table 4.4 for retention times, accurate masses, and Table 3.3 for exact masses.

Intracellular accumulation products of a *dppA* mutant

DppA behaved ambivalently in the in vitro experiments described before. On the one hand, it showed hydrolytic activity towards synthetic D-Ala-*rac*-2,6-Dpm and *rac*-2,6-Dpm-D-Ala_2. On the other hand, it did not show hydrolytic activity towards cell wall peptides, but instead seemed to alter their degree of amidation. To shed more light on this contradiction, a Δ*dppA::kan* mutant was examined for possible intracellular accumulation products. The result is depicted in Figure 4.16. An *amyE::kan* mutant served as a reference. AmyE is not associated with recycling processes, so the mutant should behave like the wild-type in this respect. However, the kanamycin cassette should exclude the possibility that any effects were caused solely by the introduced kanamycin resistance.

In the *dppA* mutant, an accumulation of amidated Dpm was observed, as shown in Figure 4.16. Interestingly, the EICs for amidated Dpm showed multiple peaks in both the *amyE* control and the *dppA* mutant. In the control, only the first peak (retention time of 10.5 min) showed an isotope pattern in agreement with the theoretical distribution; the second peak (retention time 12.0 min) showed a deviant isotope pattern. More specifically, the second peak represented one isotope of a compound with a smaller *m/z* value and thus did not correspond to amidated Dpm. In the *dppA* mutant, the peak at 10.5 min showed a higher intensity than in the control. In addition, a peak appeared at a retention time of 7.0 min, which also showed an isotope pattern corresponding to amidated Dpm. As in the experiments described so far, the EICs for Dpm showed more than one peak. The mass spectra of both peaks (retention time 8.0 min and 8.4 min) showed isotope patterns in agreement with the calculated distribution. Interestingly, the arrangement of a large peak in front of a small peak, as seen in the *amyE* mutant, was reversed in the *dppA* mutant. There, the rear peak was the more intense one. However, the combined abundance of both peaks remained unchanged. Furthermore, an intracellular

Table 4.4.: Retention time (min), accurate mass (*m/z*), and mass error (ppm) of intracellular accumulation products in *B. subtilis* Δ*amyE::kan* and Δ*dppA::kan* mutants. Data presented as mean (n = 3). See Table 3.3 for exact masses.

	Δ*amyE::kan*			Δ*dppA::kan*		
Peptide	min	*m/z*	ppm	min	*m/z*	ppm
Exponential growth phase (4 h)						
Dpm*				6.9	188.104	3.6
Dpm	8.0	189.088	5.4	8.0	189.089	8.0
Dpm*-Ala	6.9	259.140	2.2	6.9	259.140	2.0
Stationary growth phase (24 h)						
Dpm*				6.9	188.105	11.5
Dpm* (B)	10.2	188.105	11.3	10.1	188.105	11.7
Dpm	8.0	189.089	9.3	8.4	189.089	11.0
Dpm*-Ala	7.1	259.140	3.8	7.2	259.141	3.0
Dpm*-Ala_2				7.4	330.178	2.7

accumulation of amidated Dpm-Ala and amidated Dpm-Ala_2 was observed for the *dppA* mutant. Both peptides were absent in the *amyE* mutant. The retention times of both peptides differed from the values determined in vitro (0.5 min and 0.8 min respectively, compare Table 4.4 and 4.8). Such differences may indicate divergent constitutions. The non-amidated forms of these peptides were unaffected (data not shown). The observations described so far could already be recognised in the exponential growth phase (cultivation for 4 h), although here, the EIC for Dpm in the *dppA* mutant showed the same arrangement of peaks as the control. The peak seen in the EIC for amidated Dpm-Ala_2 in the exponential growth phase is not Dpm-Ala_2, but represents an isotope of a smaller mass.

In summary, amidated Dpm, amidated Dpm-Ala and amidated Dpm-Ala_2 accumulated in the *dppA* mutant. The EIC for Dpm showed an inverse arrangement of the double peak in the stationary growth phase, but indicated no difference in incidence. It is not known what caused this change and whether it is of physiological significance or whether it was an artefact of the LC-MS analysis.

4.2.4. Characterisation of YkfA

Activity of YkfA towards *rac*-2,6-Dpm-D-Ala_2

As described in the introduction, YkfA is assigned to the group of S66 serine peptidases due to its sequence similarity with enzymes of this protein family, including LdcA of *E. coli*. YkfA could therefore hold a similar function as LdcA and may act as LD-carboxypeptidase. This means that it potentially accomplishes the conversion of tetrapeptide (L-Ala-iso-D-Glu-*meso*-Dpm-D-Ala) into tripeptide (L-Ala-iso-D-Glu-*meso*-Dpm) through cleavage of the terminal D-Ala.

In this work, YkfA was purified by SEC to apparent purity as confirmed by SDS-PAGE (see Figure 4.9). In order to obtain an initial indication regarding its enzymatic activity, purified YkfA was incubated with the chemically synthesised, racemic peptides D-Ala-*rac*-2,6-Dpm and *rac*-2,6-Dpm-D-Ala_2. No change in the abundance of the substrate was observed when

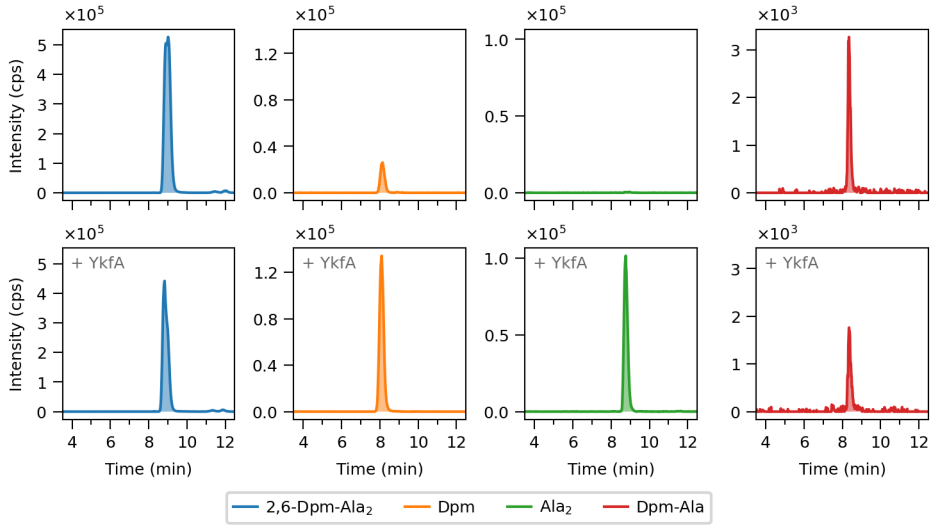

Figure 4.17.: YkfA cleaves *rac*-2,6-Dpm-D-Ala_2. Chemically synthesised *rac*-2,6-Dpm-D-Ala_2 was incubated for 1 h with recombinant YkfA (+ YkfA) and subsequently analysed by LC-MS. Shown are EICs for Dpm-Ala_2 (blue), Dpm (orange), Ala_2 (green) and Dpm-Ala (red). See Table 4.5 for accurate masses and mass errors as well as Table 3.3 for exact masses.

D-Ala-*rac*-2,6-Dpm was incubated with recombinant YkfA and also a release of Dpm was not detected (result not shown). In contrast, *rac*-2,6-Dpm-D-Ala_2 decreased in abundance after incubation with YkfA (Figure 4.17). However, *rac*-2,6-Dpm-D-Ala_2 was only partially degraded and did not disappear completely. This indicates that only one particular isomer of the racemic mixture of *rac*-2,6-Dpm-D-Ala_2 served as a substrate for YkfA. Dpm and Ala_2 appeared as products (Figure 4.17). Dpm-Ala (or Ala-Dpm) had already been detected in the substrate mixture before (see DppA) and was presumably a remnant of the chemical synthesis. The EIC for Dpm-Ala showed a reduction in its intensity with YkfA (Figure 4.17). Dpm and Ala_2 were also found initially in traces and were probably also remnants of the reactants of the chemical synthesis. See Table 4.5 for retention times, accurate masses, and mass error (see Table 3.3 for exact masses).

These results showed an enzymatic activity of YkfA towards *rac*-2,6-Dpm-D-Ala_2 with release of Dpm and Ala_2. This suggested an activity as Dpm-D-Ala peptidase. However, the activity of YkfA towards Dpm-Ala or Ala-Dpm was ambiguous. On the one hand, the synthesised racemic mixture D-Ala-*rac*-2,6-Dpm was not affected by YkfA. On the other hand, Dpm-Ala or Ala-Dpm, found in the synthesised racemic mixture *rac*-2,6-Dpm-D-Ala_2, was degraded.

Activity towards peptides of *E. coli*

Next, YkfA was incubated with the crude peptide suspension derived from *E. coli* cells to gain deeper insights into its specificity. Figure 4.18A shows the peptides that decreased in their abundance in the presence of YkfA. Besides tetrapeptide, this concerned tetrapeptide-Ala-Dpm. The latter appeared with two peaks in the EIC: one peak with a retention time of 13.9 min and a second one with a retention time of 16.1 min. The first peak appeared merely slightly different with YkfA, whereas the rear peak disappeared. In addition, a degradation of Dpm-Ala

Table 4.5.: Retention times (min), accurate masses (*m/z*), and mass errors (ppm) of peptides detected in the in vitro assays of YkfA on chemically synthesised *rac*-2,6-Dpm-D-Ala_2. See Table 3.3 for exact masses.

	Control			YkfA 1 h		
Peptide	min	*m/z*	ppm	min	*m/z*	ppm
rac-2,6-Dpm-D-Ala_2	9.0	331.160	2.4	8.9	331.162	1.5
Dpm	8.1	189.088	4.3	8.1	189.089	10.1
Ala_2	8.9	159.076	3.9	8.8	159.076	3.9
Dpm-Ala	8.4	260.123	3.1	8.4	260.125	1.5

(or Ala-Dpm) was observed. This peptide was not present in the substrate in the LC-MS analysis carried out before (see Section 4.2.2). However, the long exposure to heat during the experiment could have caused a release independent of the enzyme.

Figure 4.18B shows the peptides that were observed to increase as a result of incubation. The most obvious finding was the increased amount of tripeptide. Besides that, the finding of a compound with the mass of pentapeptide in the sample treated with YkfA was interesting. The peptidoglycan of *E. coli* does not contain pentapeptide in noteworthy amounts and this was found to be true for the substrate suspension prepared in this work as well. The compound with a retention time of 15.5 min found in the EIC for pentapeptide, was thus presumably of a different constitution than pentapeptide, as will be discussed later. Dpm was also found in larger amounts upon incubation with YkfA, whereby its EIC showed more than one peak as described before for Dpm when peptides of *B. subtilis* were incubated with DppA. The mass spectra of all three peaks showed masses in agreement with Dpm. However, only the foremost peak (retention time 8.1 min) changed as a result of incubation with YkfA.

The measurements showed that YkfA was able to cleave tetrapeptide and partially tetrapeptide-Ala-Dpm. The disappearance of Dpm-Ala (or Ala-Dpm) may seem plausible and is consistent with the results with artificial *rac*-2,6-Dpm-D-Ala_2. In this context, the observation that YkfA did not cleave D-Ala-*rac*-2,6-Dpm suggests that YkfA cleaves Dpm-Ala but not Ala-Dpm. Subsequently, tripeptide, a peptide with the mass of pentapeptide and Dpm were found to be released from cell wall peptides by YkfA. Retention times, accurate masses, and mass error of detected peptides are listed in Table 4.8 (see Table 3.3 for exact masses).

Activity towards peptides of *B. subtilis*

As an enzyme originating from *B. subtilis*, YkfA was also incubated with peptides derived from this organism. Thereupon, a decrease in tripeptide-Ala-Dpm was observed in the LC-MS analysis (Figure 4.19). Interestingly, differences depending on the degree of amidation were observed. Whilst there was only a slight decrease in completely amidated tripeptide-Ala-Dpm, a reduction of the partially and non-amidated forms was evident (Figure 4.19). When peptides from *E. coli* were digested with YkfA, the second peak corresponding to tetrapeptide-Ala-Dpm was affected in particular (see Figure 4.18). With peptides from *B. subtilis*, the second peak of both non-amidated tripeptide-Ala-Dpm (retention time 11.6 min) and the partially amidated form (9.7 min) disappeared, whereas the respective first peak (retention time 8.8 min

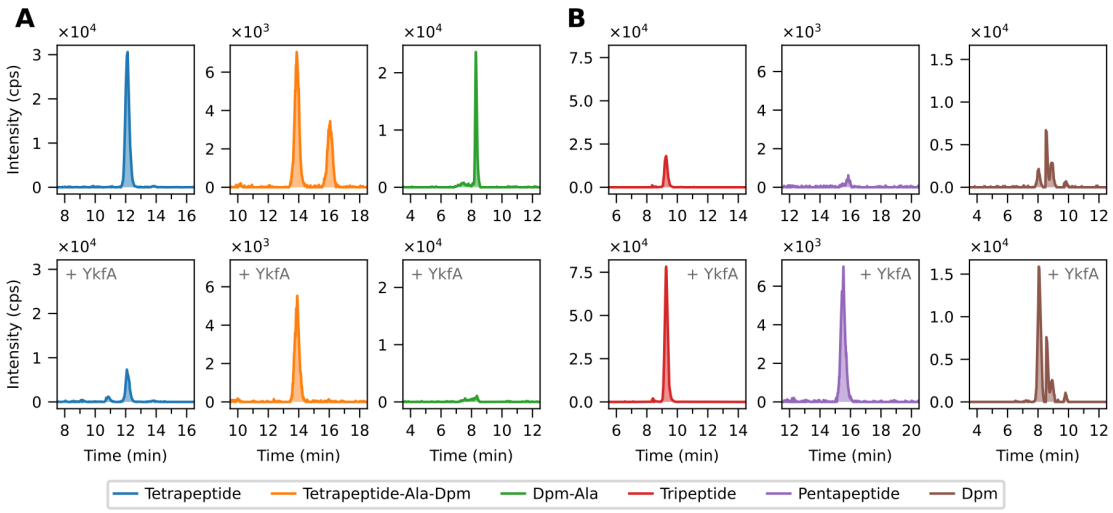

Figure 4.18.: Substrates (A) and products (B) of YkfA with cell peptides of *E. coli*. Peptidoglycan of *E. coli* MC4100 was treated with an amidase and additionally with recombinant YkfA (+ YkfA). The result of the subsequent LC-MS analysis is shown with EICs for tetrapeptide (blue), tetrapeptide-Ala-Dpm (orange), Dpm-Ala (green), tripeptide (red), pentapeptide (violet) and Dpm (brown). See Table 4.8 for accurate masses and mass errors as well as Table 3.3 for exact masses.

for partially amidated tripeptide-Ala-Dpm and 9.5 min for non-amidated tripeptide-Ala-Dpm) was only reduced in intensity. The isotope distribution in the first peak of the partially amidated form indicated that there was an overlapping of both the completely amidated and the partially amidated form. Since the EIC for the completely amidated counterpart showed only one peak, its second peak was thus probably masked by the first peak of the partially amidated form. Nonetheless, completely amidated tripeptide-Ala-dpm appeared to be slightly reduced in both peaks. In addition to tripeptide-Ala-Dpm, two other peptides disappeared as a result of incubation with YkfA: one with the mass of [Gly^4]tetrapeptide and a second with the mass of amidated [Gly^5]pentapeptide.

Tripeptide and amidated tripeptide, tetrapeptide and amidated tetrapeptide, amidated Dpm-Ala, Dpm and Ala-Gly were identified as products after incubation of cell wall peptides from *B. subtilis* with YkfA (Figure 4.20), with tripeptide (amidated and non-amidated), amidated tetrapeptide and Dpm being the most prominent ones. The differences in tetrapeptide were especially interesting. For both the control and the sample with YkfA, there was a peak with a retention time of 12.2 min, whereby the one with YkfA indicated a lower intensity. In addition, the EIC for YkfA showed another peak at 10.9 min, which was not present in the control. Thus, the respective compounds both corresponded to a tetrapeptide in their mass, but differed in their retention time. A possible indication of two different constitutions. The retention time determined for the amidated tetrapeptide (9.2 min) also deviated somewhat from the value determined in the control (9.9 min). The EIC for Dpm showed several peaks of which only the first one (retention time 8.2 min) increased. The EICs also indicated a slight increase in amidated [Gly^4]tetrapeptide as a result of YkfA addition (data not shown). The mass accuracy was 0.012 *m/z* and the isotope pattern deviated strongly with a distribution of 100 %, 46.3 %, 36.9 % and 20.7 % (distribution of the four most abundant isotopes) compared to the theoretical

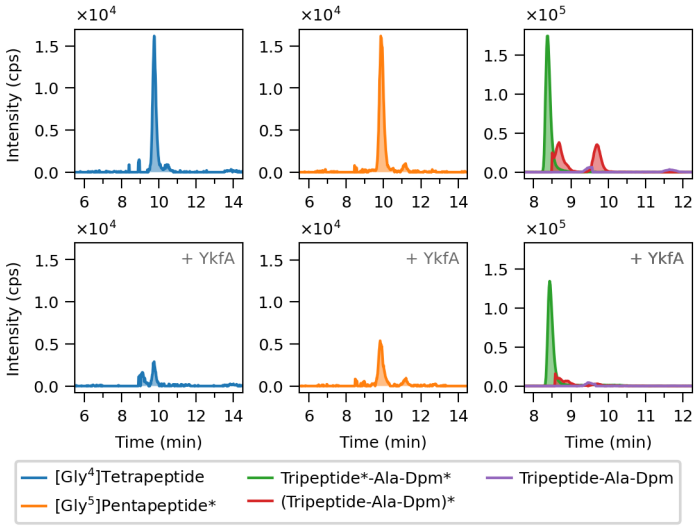

Figure 4.19.: Substrates of YkfA with cell wall peptides derived from *B. subtilis*. Peptidoglycan of *B. subtilis* 168 was treated with an amidase and additionally with recombinant YkfA (+ YkfA). The result of the subsequent LC-MS analysis is shown with EICs for [Gly^4]tetrapeptide (blue), amidated [Gly^5]pentapeptide (orange) and tripeptide-Dpm-Ala (violet, red: partially amidated, green: completely amidated). The number of amidated Dpm residues is indicated with asterisks. See Table 4.8 for accurate masses and mass errors as well as Table 3.3 for exact masses.

distribution of 100 %, 21.2 %, 3.8 % and 0.4 %. Since amidated [Gly^4]tetrapeptide occurred with a fairly low abundance and the difference between control and YkfA was also quite small, the isotope pattern made the presence of amidated [Gly^4]tetrapeptide somewhat deceptive.

In a *B. subtilis* Δ*dacA::erm* mutant, pentapeptide is incorporated into the peptidoglycan instead of tripeptide. Therefore, peptides of a *dacA* mutant were also used as substrate to investigate the impact of altered peptide structures on YkfA's activity. Although it was not present with high abundance, amidated [Gly^5]pentapeptide was found to be reduced. The same might be true for non-amidated [Gly^5]pentapeptide; there, the peak appeared smaller with YkfA, but its abundance in the control was not significant either. A decline, albeit small, was observed in non-amidated pentapeptide after incubation with YkfA (Figure 4.21), whereas amidated pentapeptide appeared unchanged (result not shown). Tripeptide, both, amidated and non-amidated, was found with reasonable abundance upon treatment with YkfA (Figure 4.21). Amidated tetrapeptide appeared with increased abundance, but in total the signal was similarly low to amidated [Gly^5]pentapeptide (Figure 4.21). Furthermore, a peak for Ala_2 was only observed after incubation of the substrate with YkfA (Figure 4.21). Retention times, accurate masses, and mass errors are listed in Table 4.8 (see Table 3.3 for exact masses).

The number of peptides affected by YkfA was considerably greater with peptides from *B. subtilis* than with peptides from *E. coli*. With the exception of tripeptide-Ala-Dpm, these were peptides which were presumably not branched. In contrast to *E. coli*, Dpm in *B. subtilis* is often amidated. An aspect that seemed to be of relevance for tripeptide-Ala-Dpm, as mainly its less amidated forms were affected by YkfA. The other peptides included both amidated and non-amidated peptides.

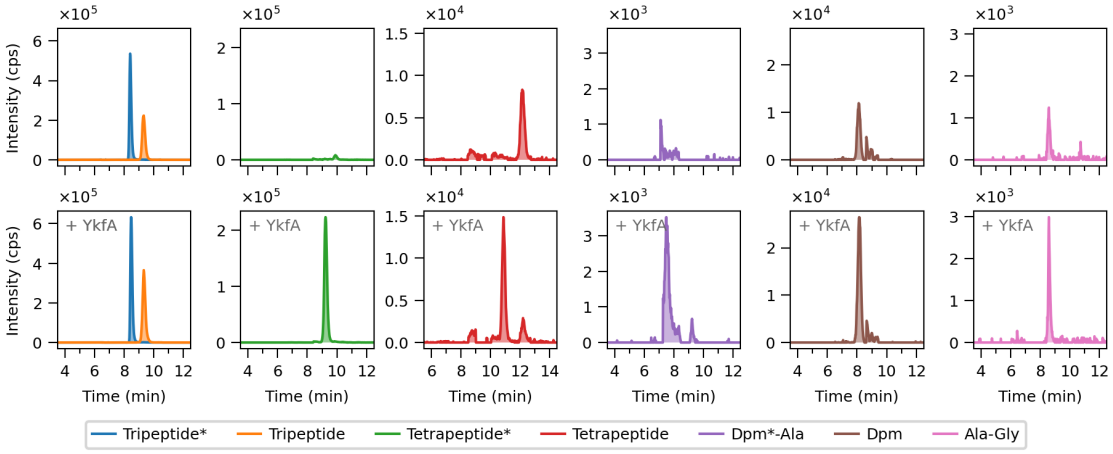

Figure 4.20.: Products of YkfA with cell wall peptides derived from *B. subtilis*. Peptidoglycan of *B. subtilis* 168 was treated with an amidase and additionally with recombinant YkfA (+ YkfA). The result of the subsequent LC-MS analysis is shown with EICs for tripeptide (orange, blue: amidated), tetrapeptide (green, red: amidated), amidated Dpm-Ala (violet), Dpm (brown), and Aly-Gly (magenta). The number of amidated Dpm residues is indicated with asterisks. See Table 4.8 for accurate masses and mass errors as well as Table 3.3 for exact masses.

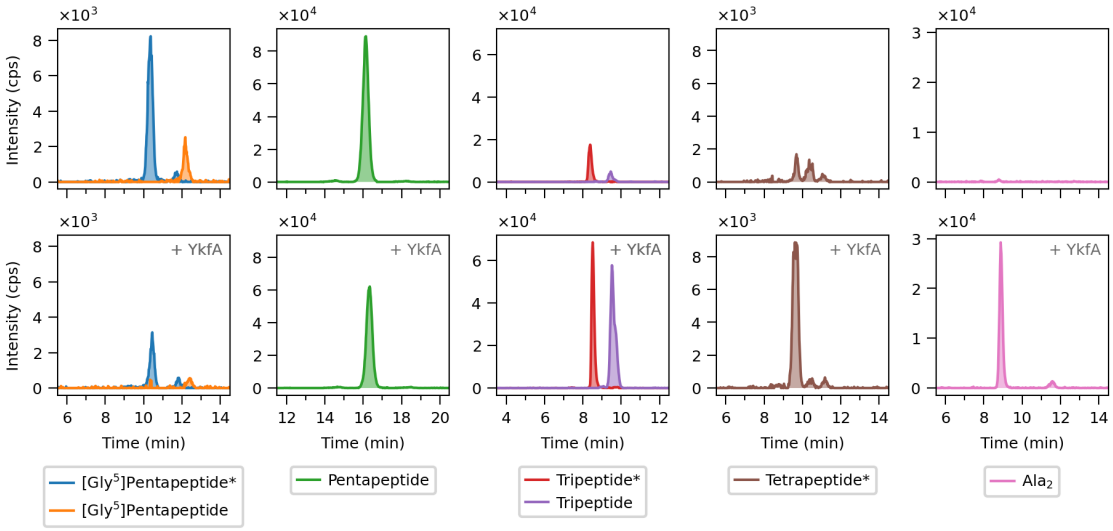

Figure 4.21.: Substrates and products of YkfA with cell wall peptides derived from a *B. subtilis* dacA mutant. Peptidoglycan of *B. subtilis* 168 Δ*dacA::erm* was treated with an amidase and additionally with recombinant YkfA (+ YkfA). The result of the subsequent LC-MS analysis is shown with EICs for [Gly^5]pentapeptide (orange, blue: amidated), pentapeptide (green), tripeptide (violet, red: amidated), amidated tetrapeptide (brown) and Ala_2 (magenta). The number of amidated Dpm residues is indicated with asterisks. See Table 4.8 for accurate masses and mass errors as well as Table 3.3 for exact masses.

Table 4.6.: Retention time (min), accurate mass (*m/z*), and mass error (ppm) of intracellular accumulation products in *B. subtilis* Δ*amyE::kan* and *ykfA::kan* mutants. Data presented as mean (n = 3). See Table 3.3 for exact masses.

	Δ*amyE::kan*			Δ*ykfA::kan*		
Peptide	min	*m/z*	ppm	min	*m/z*	ppm
Dpm	8.0	189.089	9.3	8.0	189.090	15.6
Dpm-Ala	8.1	260.124	5.8	8.2	260.125	4.6
Dpm-Ala_2				8.8	331.162	2.9
Dipeptide	10.7	217.082	5.1	10.6	217.083	5.5
Tripeptide				11.0	389.168	3.5
Dpm_2*-Ala				7.3	431.226	2.2
Dpm_2-Ala				8.0	432.211	4.0
Dpm_2*-Ala_2				7.9	502.262	2.4
Dpm_2-Ala_2				8.3	503.247	2.4

Intracellular accumulation products of a *ykfA* mutant

The in vitro studies with recombinant YkfA and cell wall peptides from *E. coli* and *B. subtilis* have already outlined the enzymatic activity of YkfA. What remains open is the physiological significance of YkfA for the cell and the effects of its functional loss. Therefore, the intracellular accumulation of a *B. subtilis* Δ*ykfA::kan* mutant was investigated. As with the *dppA* mutant, the Δ*amyE::kan* mutant served as reference.

As shown in Figure 4.22, the *ykfA* mutant showed an accumulation of Dpm-Ala as well as Dpm-Ala_2. In addition, Dpm-Ala-Gly was found with slightly increased abundance compared to the *amyE* mutant, although the signal was not considerably high (data not shown). Unexpectedly, the *amyE* mutant accumulated Dpm intracellularly. Also in this experiment, the EIC for Dpm showed a slight double peak. Both peaks showed an isotope pattern in agreement with the calculated values. However, both mutants differed only in the first peak (retention time of 8.0 min). In the *ykfA* mutant, the peak was substantially smaller. Furthermore, an increased accumulation of dipeptide and an accumulation of tripeptide was observed compared to the *amyE* mutant. Both peptides were detected with a clear signal and relatively high abundance. The retention time determined for tripeptide alone represents a certain caveat. Despite a high agreement of the isotope pattern and a high mass accuracy, the retention time deviated significantly (1.7 min) from the values determined in the in vitro experiments (compare Table 4.6 and 4.8). The in vitro assays indicated hydrolytic activity against Dpm_2-Ala and Dpm_2-Ala_2. However, an accumulation of these peptides could not be unambiguously demonstrated. The completely amidated forms were not detected at all, the partially and non-amidated forms only with very low intensities.

In summary, the *ykfA* mutant accumulated Dpm-Ala, Dpm-Ala_2, dipeptide and tripeptide. The accumulation of Dpm was reduced compared to the control. The accumulation of Dpm-Ala, Dpm-Ala_2 as well as the reduced occurrence of Dpm is consistent with the substrate specificity and activity of YkfA suggested from the in vitro experiments. An accumulation of cross-linked peptides, as released by YkfC, could not be determined beyond doubt.

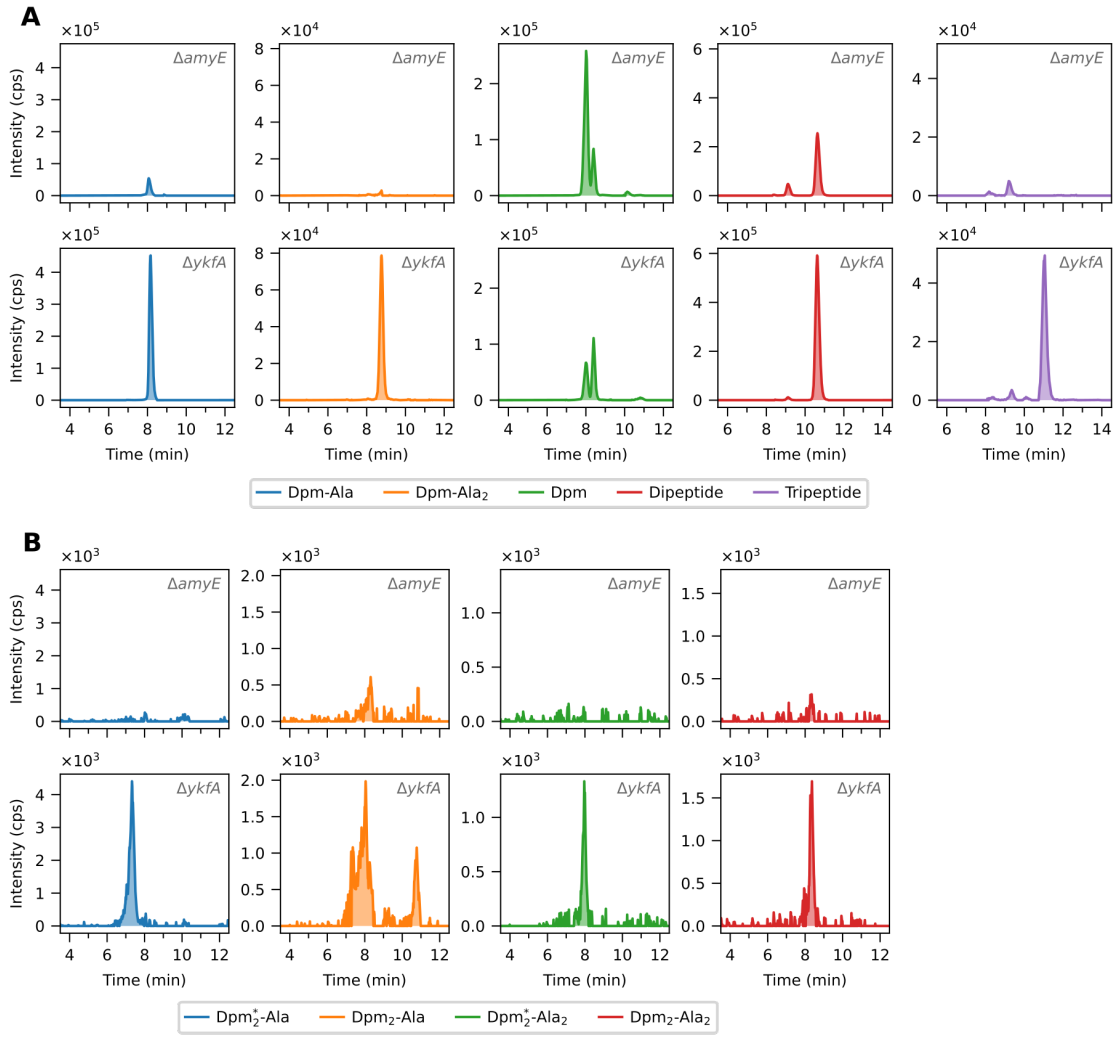

Figure 4.22.: Accumulation products in a *B. subtilis ykfA* mutant. *B. subtilis* Δ*amyE::kan* and Δ*dppA::kan* mutant cells were cultivated for 24 h (stationary growth phase) in LB medium. Acetone extracts of cytosolic fractions were analysed by LC-MS. The result of the LC-MS analysis is shown with EICs. A) Unbranched fragments: Dpm-Ala (blue), Dpm-Ala$_2$ (orange), Dpm (green), dipeptide (red), and tripeptide (violet). B) Cross-linked fragments: amidated Dpm$_2$-Ala (blue), Dpm$_2$-Ala (orange), amidated Dpm$_2$-Ala$_2$ (green), and Dpm$_2$-Ala$_2$ (red). The number of amidated Dpm residues is indicated with asterisks. See Table 4.6 for retention times and accurate masses as well as Table 3.3 for exact masses.

4.2.5. Characterisation of YkfC

YkfC was previously described as γ-D-Glu-Dpm endopeptidase (see Section 1.6 in the introduction) and cell wall peptides in *E. coli* and *B. subtilis* contain bonds of this type. Cleavage by a Glu-Dpm endopeptidase should therefore release the dipeptide Ala-Glu and the corresponding C-terminal residue, such as Dpm-Ala from a tetrapeptide. To investigate whether this could be confirmed, YkfC was incubated with crude suspensions of peptides from *E. coli* and *B. subtilis* in this work. For this, YkfC was overexpressed and purified to apparent as checked by SDS-PAGE (Figure 4.9).

Activity towards peptides of *E. coli*

Since the peptides of *E. coli* represent a less complex matrix than those of *B. subtilis*, YkfC was first incubated with them. As shown in Figure 4.23A, tripeptide and tetrapeptide disappeared when YkfC was added. Simultaneously, the dipeptide Ala-Glu was found with increased abundance (Figure 4.23B). Consistent with this and the proposed activity of a Glu-Dpm endopeptidase, increased amounts of the C-terminal peptide residues were also found. Dpm-Ala (Figure 4.23B) in particular was detected, which is consistent with the high occurrence of tetrapeptide in the peptide preparation. The retention time observed for Dpm-Ala was slightly delayed (0.5 min) compared to the retention time previously determined for D-Ala-*rac*-2,6-Dpm. Although the *m/z* value itself does not allow any statement whether Dpm-Ala or Ala-Dpm was released, it can nevertheless be assumed on the basis of the known structure of the cell wall peptides that Dpm-Ala was released by YkfC. Furthermore, the synthesised peptide was a racemic mixture, and the peptide released from peptidoglycan should be *meso*-Dpm-Ala. Whereas tripeptide was previously detected with a decent signal, the EIC for Dpm showed rather low intensities (Figure 4.23B). As before with DppA and YkfA, the EIC for Dpm showed three peaks of which only the foremost (retention time 8.1 min) stood out from the control without YkfC. Thus, Dpm was indeed released by YkfC, presumably from the tripeptide. This experiment also disclosed another interesting detail. Besides the unbranched peptides, the branched peptides tetra-tetrapeptide, tetra-tetra-tetrapeptide, tri-tetrapeptide and tetrapeptide-Ala-Dpm also disappeared upon addition of YkfC (Figure 4.23A). In turn, Dpm_2-Ala_2 and Dpm_3-Ala_3 were found as products (Figure 4.23B). The EIC for Dpm_2-Ala showed a relatively broad peak (Figure 4.23B), in whose mass spectrum no charge was indicated after deconvolution. Nevertheless, the peak contrasted clearly with the control and the isotope pattern matched the calculated distribution. Retention times, accurate masses, and mass errors of the mentioned peptides are listed in Table 4.8.

In summary, it can be stated that YkfC cleaved unbranched and branched stem peptides of the cell wall of *E. coli*. The dipeptide and various peptide fragments containing Dpm were released as products.

Activity towards peptides of *B. subtilis*

To investigate the impact of Dpm-amidation, YkfC was also incubated with a crude peptide suspension from *B. subtilis*. As opposed to *E. coli*, the peptide preparations of *B. subtilis* most notably contained tripeptide and tri-tetrapeptide. Similar to the observations with peptides from *E. coli*, peptides from *B. subtilis* disappeared upon treatment with YkfC (Figure 4.24A and 4.25A). However, another interesting observation could be made here: the peptides were

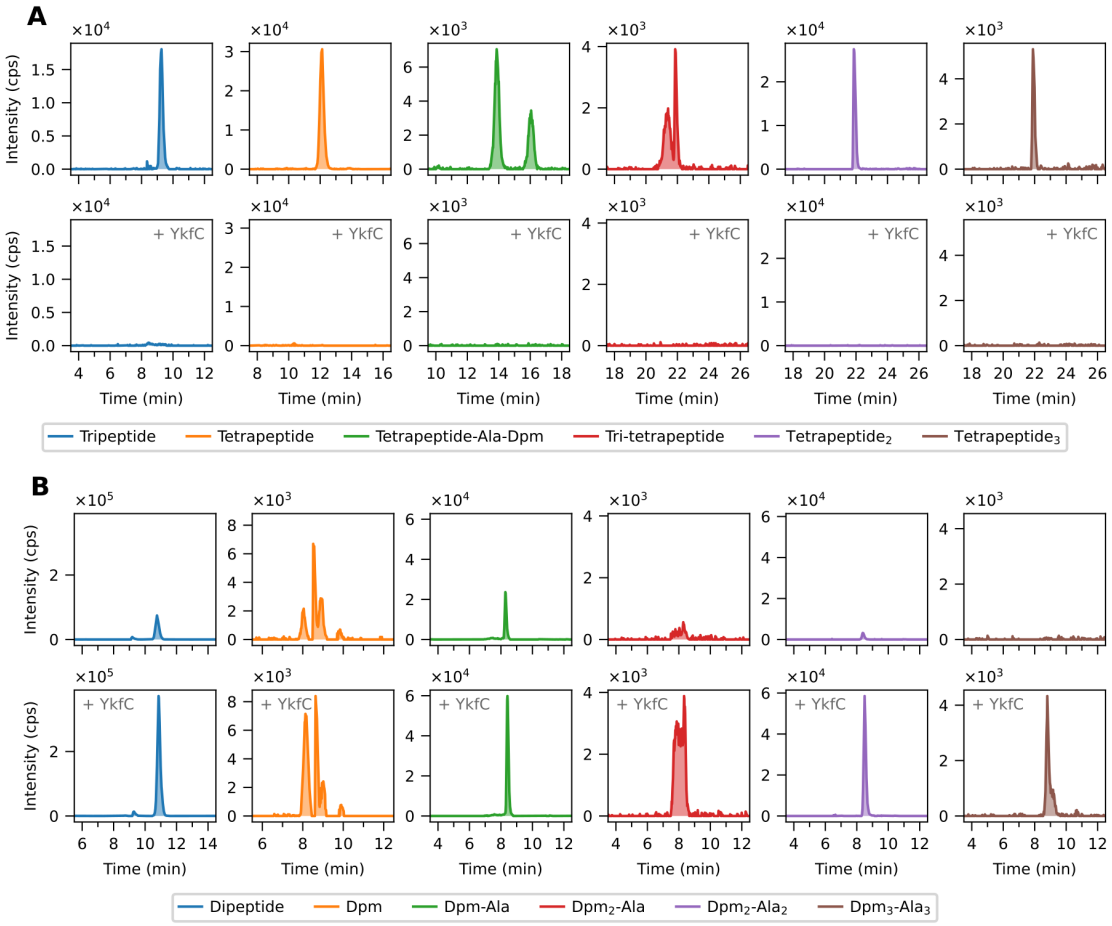

Figure 4.23.: Substrates and products of YkfC with cell wall peptides derived from *E. coli*. Peptidoglycan of *E. coli* MC4100 was treated with an amidase and additionally with recombinant YkfC (+ YkfC). The result of the subsequent LC-MS analysis is shown with EICs. Substrates (A): tripeptide (blue), tetrapeptide (orange), tetrapeptide-Ala-Dpm (green), tri-tetrapeptide (red), tetra-tetrapeptide (tetrapeptide$_2$, violet) and tetra-tetra-tetrapeptide (tetrapeptide$_3$, brown). Products (B): dipeptide (blue), Dpm (orange), Dpm-Ala (green), Dpm$_2$-Ala (red), Dpm$_2$-Ala$_2$ (violet) and Dpm$_3$-Ala$_3$ (brown). See Table 4.8 for accurate masses and mass errors.

cleaved independently of their amidation. That is, both forms of tripeptide and all three forms of tri-tetrapeptide disappeared (Figure 4.24A and 4.25A). Besides the dipeptide Ala-Glu, which was found to be increased analogous to the experiment with peptides from *E. coli*, Dpm and Dpm_2-Ala were found in (Figure 4.24B and 4.25B). Interestingly, and although amidated tripeptide is the more frequent form of tripeptide, non-amidated Dpm was detected with a more pronounced signal as cleavage product. For Dpm_2-Ala, however, the distribution was more in line with expectations and thus with the distribution of tri-tetrapeptide. Other amidated peptides were found to be processed by YkfC, as shown for [Gly^5]pentapeptide (Figure 4.24A), tripeptide-Ala-Dpm (Figure 4.25B), tetra-tetrapeptide (Figure 4.25A), [Gly^5]penta-tetrapeptide (Figure 4.25A) as well as tri-tetra-tetrapeptide (Figure 4.25A). Consequently, the data were screened for corresponding peptide fragments. Indeed, Dpm-Ala-Gly (Figure 4.24B), Dpm_2-Ala_2, Dpm_2-Ala_2-Gly were found as shown in Figure 4.25B. Moreover, YkfC was able to cleave unusual peptides. The canonical pentapeptide Ala-Glu-*meso*-Dpm-D-Ala_2 is an intermediate product of cell wall synthesis, but is virtually absent in the peptidoglycan of *B. subtilis*. To force the incorporation of pentapeptide in the peptidoglycan matrix, the D-Ala-D-Ala carboxypeptidase responsible for its cleavage must be absent – as in a *B. subtilis* Δ*dacA::erm* mutant [11]. When peptides from this strain were incubated with YkfC, no pentapeptide was found – neither amidated nor non-amidated. Instead, increased amounts of the dipeptide Ala-Glu as well as Dpm-Ala_2 were observed. Furthermore, the branched penta-tetrapeptide was cleaved regardless of its amidation degree as shown by its disappearance (Figure 4.25) and the detection of D_2-Ala_3. Both was not observed in the control without YkfC. See Table 4.8 for retention times, accurate masses, and mass errors of the LC-MS analysis.

Based on the observations described here, it can be noted that YkfC can cleave both unbranched and branched peptides. The apparent independence from a possible amidation of Dpm may seem conclusive in view of the fact that peptides are cleaved into the dipeptide and the respective Dpm residue. However, the cleavage of the pentapeptide raises the question of possible interference with cell wall synthesis.

Activity towards the peptidoglycan precursor Lipid II

Given that YkfC showed hydrolytic activity towards pentapeptide, the possibility of YkfC interfering with cell wall synthesis was investigated with muropeptides and the peptidoglycan precursor Lipid II.

First, YkfC was incubated with muropeptides derived from Atl digestion of cell wall preparations of *E. coli* and *B. subtilis* cells. The result was evaluated using DCs from a subsequent LC-MS analysis (see Figure 4.26 and Table 4.7). When muropeptides of *E. coli* were incubated with YkfC, GlcNAc-MurNAc-tri-tetrapeptide and GlcNAc-MurNAc-tetra-tetrapeptide disappeared. Dipeptide, GlcNAc-MurNAc-tripeptide-Ala-Dpm as well as GlcNAc-MurNAc-tetrapeptide-Ala-Dpm were identified as products. MurNAc-GlcNAc-tri-tetrapeptide (completely and partially amidated) disappeared when muropeptides derived from *B. subtilis* were mixed with YkfC. Furthermore, the preparation contained amidated and non-amidated tripeptide, both of which were degraded with YkfC. Instead, dipeptide was released. By targeted analysis with EICs, the release of a mass corresponding to doubly charged MurNAc-GlcNAc-tripeptide-Ala-Dpm was found. However, its abundance was very low and the mass spectra did not indicate any charge. In addition, the number of amidations could not be accurately determined because the mass spectra showed an overlap of isotope patterns of two differently amidated forms. Mass accuracy

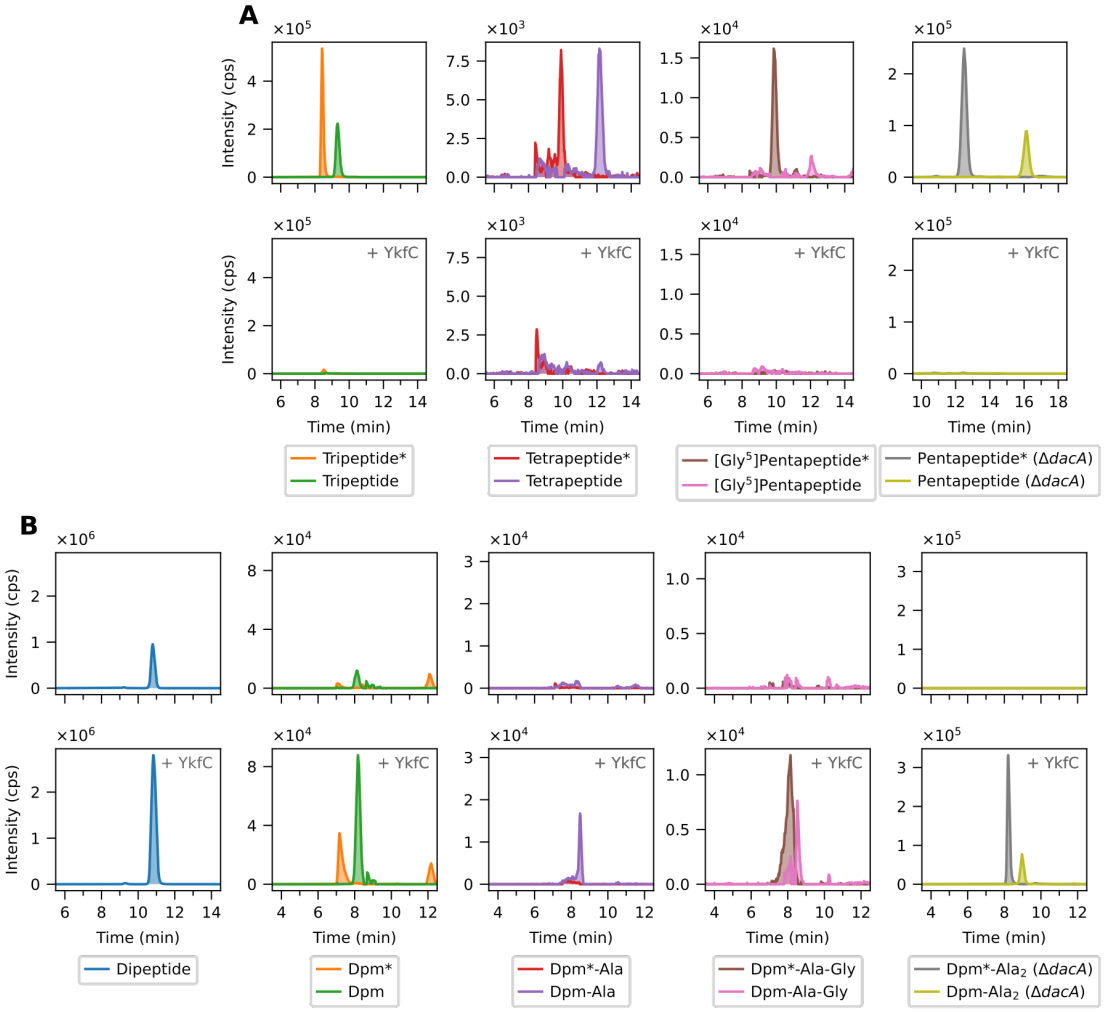

Figure 4.24.: Unbranched substrates and products of YkfC with cell wall peptides derived from *B. subtilis*. Peptidoglycan of *B. subtilis* 168 wild-type and a Δ*dacA::erm* mutant was treated with an amidase and additionally with recombinant YkfC (+ YkfC). The result of the subsequent LC-MS analysis is shown with EICs. Substrates (A): tripeptide (green, orange: amidated), tetrapeptide (violet, red: amidated), [Gly^5]pentapeptide (magenta, brown: amidated) and pentapeptide (light olive, grey: amidated). Products (B): dipeptide (blue), Dpm (green, orange: amidated), Dpm-Ala (violet, red: amidated), Dpm-Ala-Gly (magenta, brown: amidated) and Dpm-Ala_2 (light olive, grey: amidated). The number of amidated Dpm residues is indicated with asterisks. See Table 4.8 for accurate masses and mass errors.

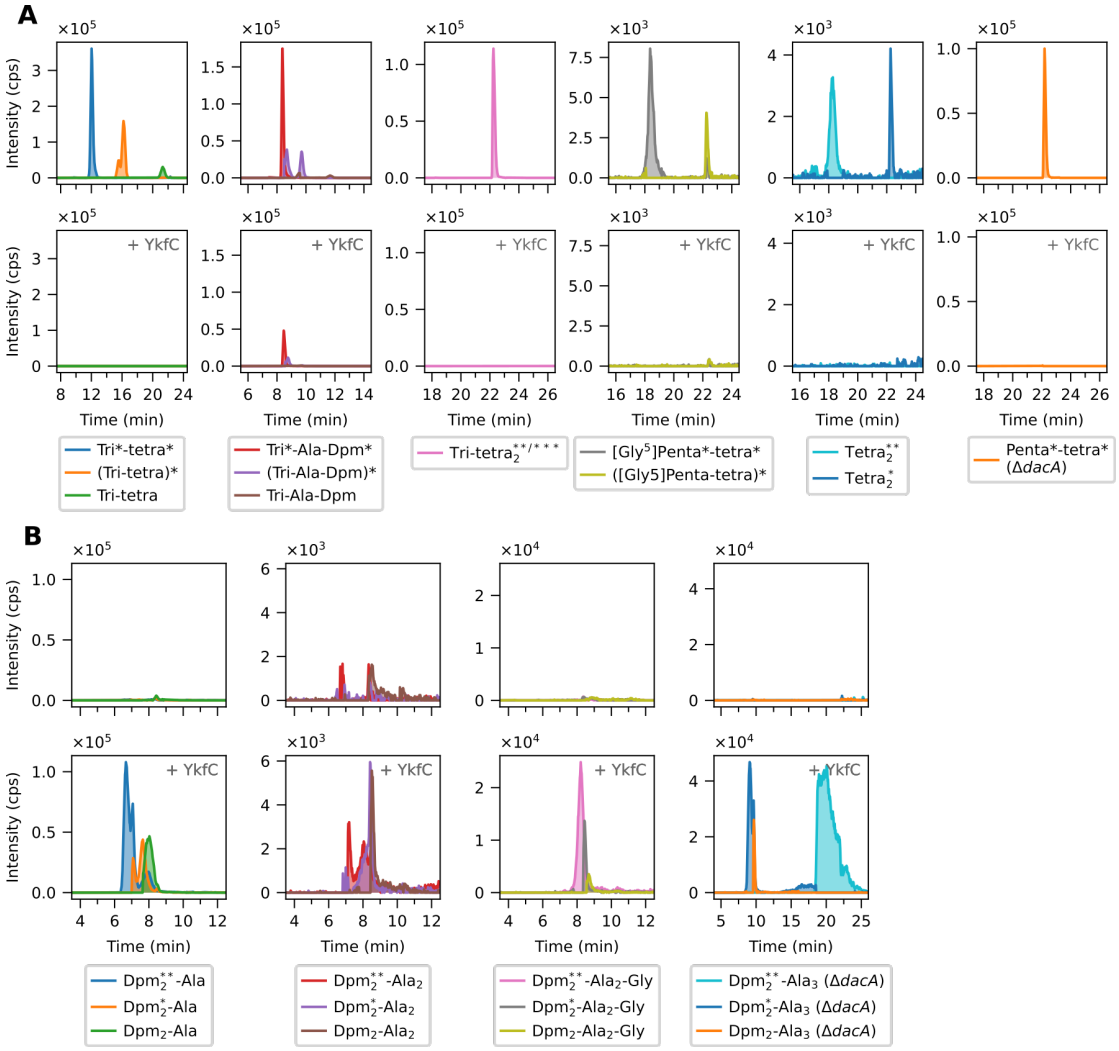

Figure 4.25.: Branched substrates and products of YkfC with cell wall peptides derived from *B. subtilis*. Peptidoglycan of *B. subtilis* 168 wild-type and a Δ*dacA::erm* mutant was treated with an amidase and additionally with recombinant YkfC (+ YkfC). The result of the subsequent LC-MS analysis is shown with EICs. Substrates (A): tri-tetrapeptide (green, orange: partially amidated, blue: completely amidated), tripeptide-Ala-Dpm (brown, violet: partially amidated, red: completely amidated), amidated tri-tetra-tetrapeptide (tri-tetra$_2$, magenta), [Gly^5]penta-tetrapeptide (light olive: partially amidated, grey: completely amidated), tetra-tetrapeptide (tetra$_2$, blue: partially amidated, aqua: completely amidated) and amidated penta-tetrapeptide (orange). Products (B): Dpm$_2$-Ala (green, orange: partially amidated, blue: amidated), Dpm$_2$-Ala$_2$ (brown, violet: partially amidated, red: amidated), Dpm$_2$-Ala$_2$-Gly (light olive, grey: partially amidated, magenta: amidated) and Dpm$_2$-Ala$_3$ (orange, blue: partially amidated, light blue: amidated). The number of amidated Dpm residues is indicated with asterisks. See Table 4.8 for accurate masses and mass errors.

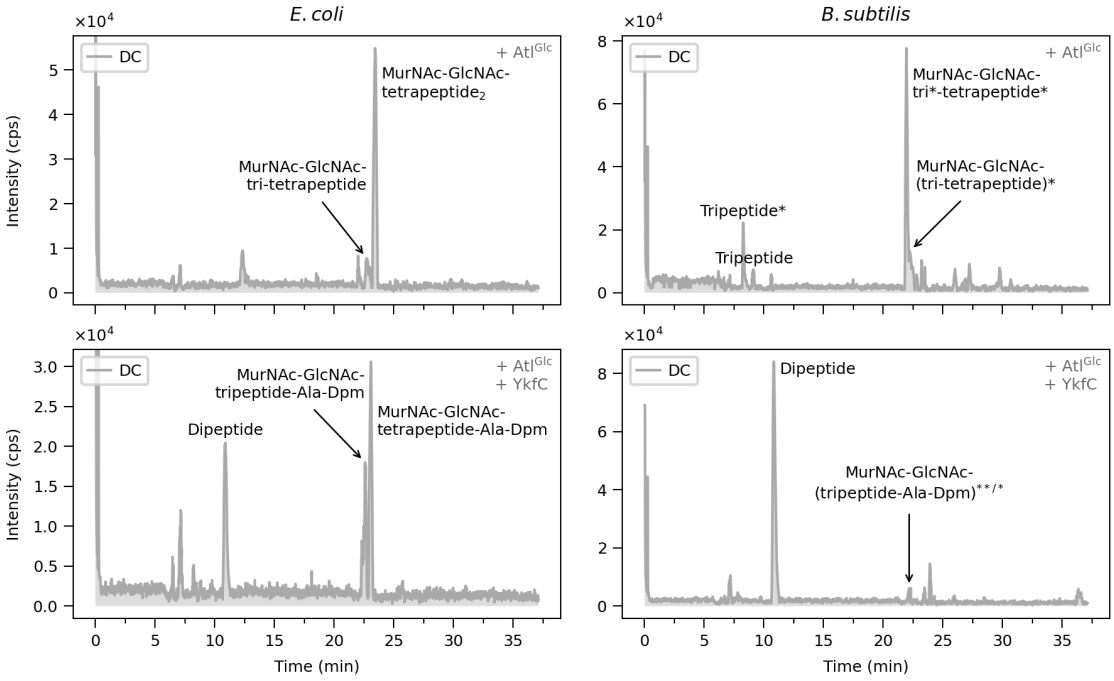

Figure 4.26.: Substrates and products of YkfC when incubated with muropeptides of *E. coli* and *B. subtilis*. Peptidoglycan of *E. coli* MC4100 and *B. subtilis* 168 was treated with the glucosaminidase Atl^{Glc}, followed by incubation with YkfC. The result of the LC-MS analysis is shown with DCs. The compounds identified are: MurNAc-GlcNAc-tri-tetrapeptide, MurNAc-GlcNAc-$tetrapeptide_2$, tripeptide, MurNAc-GlcNAc-tripeptide-Ala-Dpm, MurNAc-GlcNAc-tetrapeptide-Ala-Dpm, and dipeptide. The number of amidated Dpm residues is indicated with asterisks. See Table 4.7 for retention times and accurate masses.

and mass error were of the same order of magnitude as for the other compounds (see Table 4.7). Irrespective of that, the degradation of muropeptides that consist of two disaccharides and cross-linked peptides, was not observed.

Next, YkfC was incubated with the peptidoglycan precursor Lipid II. The DD-carboxypeptidase Pbp6 of *Chlamydia pneumoniae* GiD was used as positive control. This experiment was conducted by Jula Reuter (University of Bonn, group of Beate Henrichfreise) with recombinant YkfC expressed and purified by me.

The result of the TLC is shown in Figure 4.27. The positive control travelled a slightly longer distance than the standard for Lipid II. Furthermore, the positive control showed a band at the level of the standard for D-Ala. Both indicated a cleavage of the terminal D-Ala from Lipid II by Pbp6. In contrast, Lipid II seemed to be unaffected by YkfC. The distance travelled by the sample was consistent with the standard for Lipid II and no additional spot was found.

In summary, YkfC of *B. subtilis* was able to cleave muropeptides with a free peptide terminus, but not cross-linked muropeptides. It was further unable to cleave the peptidoglycan precursor Lipid II.

Table 4.7.: Retention time, accurate mass, and mass error of muropeptides and peptides detected with YkfC incubated with muropeptides of *E. coli* and *B. subtilis*. Asterisks indicate amidations. See Table 3.3 for exact masses.

Peptide	Retention time (min)	Accurate mass (m/z)	Mass error (ppm)
E. coli			
MurNAc-GlcNAc-tri-tetrapeptide	22.8	1310.580	12.6
MurNAc-GlcNAc-tetrapeptide$_2$	23.4	1381.615	10.9
Di	10.9	217.085	15.2
MurNAc-GlcNAc-tripeptide-Ala-Dpm	22.4	1110.498	13.6
MurNAc-GlcNAc-tetrapeptide-Ala-Dpm	22.6	1181.527	9.9
B. subtilis			
Tripeptide*	8.3	388.190	19.4
Tripeptide	9.1	389.174	17.5
MurNAc-GlcNAc-tri*-tetrapeptide*	22.0	1308.611	12.4
MurNAc-GlcNAc-(tri-tetrapeptide)*	22.2	1309.598	13.3
Di	10.9	217.086	18.4
MurNAc-GlcNAc-tripeptide*-Ala-Dpm*	22.1	1108.528	12.8

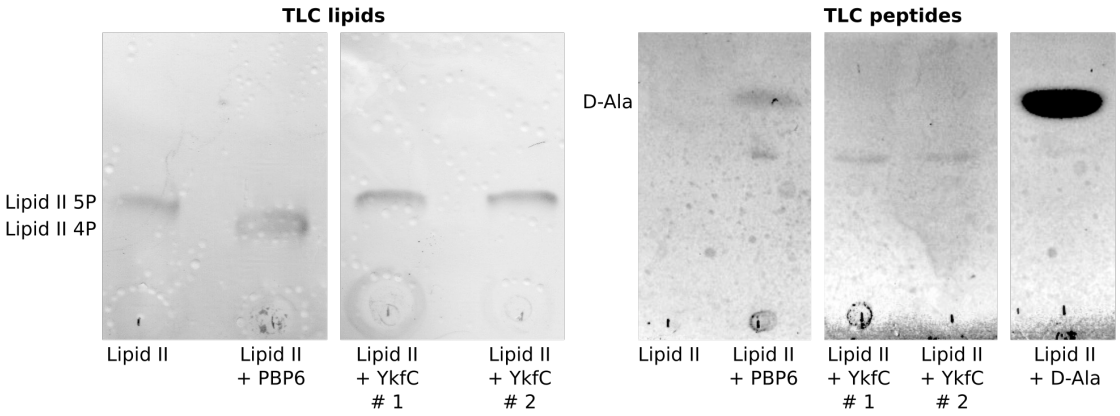

Figure 4.27.: YkfC is not active against the peptidoglycan precursor Lipid II. Lipid II was incubated with recombinant YkfC and the recombinant DD-carboxypeptidase Pbp6 of *Chlamydia pneumoniae* GiD. The result is shown with stained TLC analyses with standards for Lipid II and D-Ala.

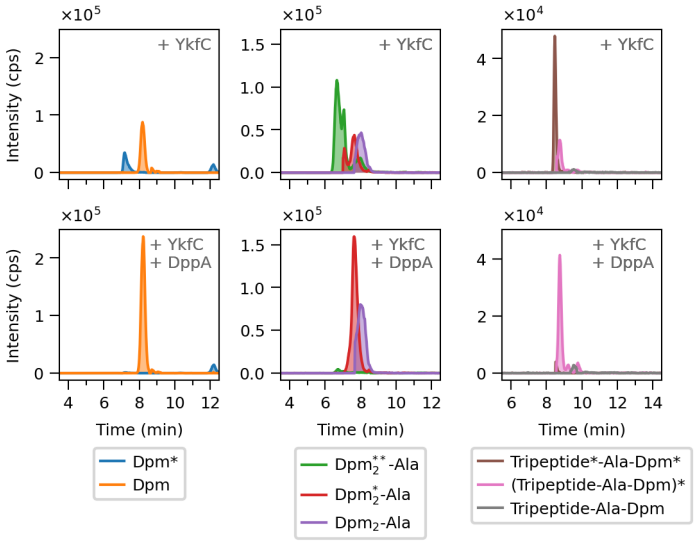

Figure 4.28.: DppA in conjunction with YkfC alters the degree of amidation of peptides of *B. subtilis*. Peptidoglycan of *B. subtilis* was treated with an amidase and incubated with recombinant YkfC or recombinant DppA in combination with YkfC. The result of the subsequent LC-MS analysis is shown with EICs for: Dpm (orange, amidated: blue), Dpm_2-Ala (violet, partially amidated: red, completely amidated: green) and tripeptide-Ala-Dpm (grey, partially amidated: magenta, completely amidated: brown). The number of amidated Dpm residues is indicated with asterisks. See Table 4.8 for accurate masses and mass errors.

4.2.6. Combined activity of DppA, YkfA and YkfC

As described in the introduction, YkfA and YkfC are encoded in a contiguous unit on the genome and DppA is encoded in close proximity. The results described so far indicated different substrate specificities and considering the genomic organisation, an activity in a concerted process is conceivable. Therefore, the extent to which the combination of the enzymes affects the degradation of the peptides and the formation of product was investigated.

The combined incubation of DppA and YkfC with peptides from *E. coli* did not reveal any difference compared to the application of YkfC alone (data not shown). Thus, even in combination with YkfC, there was no evidence of enzymatic activity of DppA against peptides from *E. coli*. In contrast, the combination of DppA with YkfC showed enzymatic activity towards peptides from *B. subtilis* (see Figure 4.28 and Table 4.8 for retention times and accurate masses). Likewise to DppA alone, a shift from the amidated to the less amidated forms was observed for Dpm and tripeptide-Ala-Dpm. In addition, completely amidated Dpm_2-Ala was identified as further substrate of DppA.

As described before, incubation of YkfC with cell wall peptides resulted in the release of Dpm_2-Ala_2 (*E. coli*) and Dpm_2-Ala with varying degrees of amidation (*B. subtilis*). In contrast, Dpm_2-Ala_2 was not found when both, YkfA and YkfC, were used as shown in Figure 4.29A. Instead, Dpm-Ala_2 was detected – a peptide which was not found when only one of the enzymes was used (*E. coli*, Figure 4.29A). As described above (Sections 4.2.4 and 4.2.5), Dpm was released by both YkfA and YkfC. Consistent with this, a release of Dpm was also observed when both enzymes were combined (Figure 4.29A). However, the amounts released by both enzymes

individually were negligible in comparison to the amount of Dpm released by the combined activities of both enzymes. Especially little Dpm was released with YkfA as the only catalyst. Given the apparent cleavage of Dpm_2-Ala, an increased release of Dpm-Ala was expected. Instead, Dpm-Ala was observed with much lower abundance (see Figure 4.29A). A detail that will be discussed later.

Similar to Dpm_2-Ala_2 of *E. coli*, Dpm_2-Ala of *B. subtilis* was apparently cleaved (see Figure 4.29B). This mainly applied to partially amidated Dpm_2-Ala and its non-amidated form, whereas only a slight reduction was noted for the completely amidated form. Although no product could be identified, the amounts of Dpm as well as amidated and non-amidated Dpm-Ala increased.

Neither the combination of DppA with YkfC nor the combination of YkfA with YkfC resulted in a complete degradation of tripeptide-Ala-Dpm or Dpm_2-Ala (see Figure 4.30). One or more differently amidated forms always remained. In this context, the combination of all three enzymes was investigated. As shown in Figure 4.30, as a result, no tripeptide-Ala-Dpm and no Dpm_2-Ala was left after the addition of all three enzymes. This was true for all forms of the respective peptides, regardless of the amidation of the Dpm residue. Furthermore, of all combinations, the highest values for amidated and non-amidated Dpm-Ala, as well as for Dpm, were observed with the reaction of all three enzymes (Figure 4.30).

From peptides of the *B. subtilis dacA* mutant, Dpm_2-Ala_3 was released by YkfC with varying degrees of amidation (see Section 4.2.5). Whilst completely amidated Dpm_2-Ala_3 was barely found with the combination of DppA and YkfC, an increase in partially and non-amidated Dpm_2-Ala_3 was observed compared to YkfC alone (Figure 4.31). In contrast, and as shown in the same figure, with YkfA and YkfC, partially and non-amidated Dpm_2-Ala_3 was hardly found, but the completely amidated form appeared unchanged compared to YkfC alone. Only the combination of DppA, YkfA and YkfC led to a significant degradation of all forms (Figure 4.31). Interestingly, a residue of partially and non-amidated Dpm_2-Ala_3 remained, and thus more than when only YkfA and YkfC were used (same figure).

Table 4.8.: Retention times, accurate masses, and mass errors of peptides detected in in vitro experiments with recombinant DppA, YkfA and YkfC on cell wall peptides of *E. coli* MC4100, *B. subtilis* 168 and *B. subtilis* Δ*dacA::erm*. Asterisks indicate amidations.

Peptide	Retention time (min)	Accurate mass (*m/z*)	Mass error (ppm)
	E. coli control		
Dipeptide	10.8	217.084	9.7
Tripeptide	9.3	389.171	10.6
Tetrapeptide	12.1	460.209	10.9
[Gly^4]Tetrapeptide	9.7	446.194	12.2
Tetrapeptide-Ala-Dpm (A)	13.9	703.334	11.2
Tetrapeptide-Ala-Dpm (B)	16.1	703.334	11.6
Tri-tetrapeptide	21.9	832.334	8.3
$Tetrapeptide_2$	21.9	903.413	8.0
$Tetrapeptide_3$	21.9	1346.625	13.9
Dpm	8.0	189.086	5.7

Continued on the next page

Table 4.8.: Retention times, accurate masses, and mass errors of peptides detected in in vitro experiments with recombinant DppA, YkfA and YkfC on cell wall peptides of *E. coli* MC4100, *B. subtilis* 168 and *B. subtilis* Δ*dacA::erm*. Asterisks indicate amidations.

Peptide	Retention time (min)	Accurate mass (*m/z*)	Mass error (ppm)
Dpm-Ala	8.3	260.128	13.1
Dpm_2-Ala_2	8.4	503.253	14.1
YkfA (*E. coli*, Section 4.2.4)			
Dpm	8.1	189.091	18.6
Tripeptide	9.3	389.171	9.8
Tetrapeptide	12.1	460.208	8.9
Pentapeptide	15.5	531.246	9.8
Tetrapeptide-Ala-Dpm (A)	13.9	703.333	9.7
YkfC (*E. coli*, Section 4.2.5)			
Dipeptide	10.9	217.084	9.2
Dpm	8.1	189.091	20.2
Dpm-Ala	8.4	260.127	10.8
Dpm_2-Ala	8.3	432.213	9.0
Dpm_2-Ala_2	8.5	503.251	10.7
Dpm_3-Ala_3	8.8	746.375	9.2
B. subtilis control			
Dipeptide	10.8	217.084	11.1
Tripeptide*	8.4	388.187	11.9
Tripeptide	9.3	389.172	13.6
Tetrapeptide*	9.9	459.226	13.3
Tetrapeptide	12.2	460.211	15.6
[Gly^4]Tetrapeptide	9.8	446.195	14.7
[Gly^5]Pentapeptide*	9.9	516.248	13.3
[Gly^5]Pentapeptide	12.1	517.234	17.5
Tripeptide*-Ala-Dpm*	8.4	630.329	14.0
(Tripeptide-Ala-Dpm)* (A)	8.7	631.314	16.0
(Tripeptide-Ala-Dpm)* (B)	9.7	632.315	14.9
Tripeptide-Ala-Dpm (A)	9.5	632.303	22.3
Tripeptide-Ala-Dpm (B)	11.7	632.298	14.7
Tri*-tetrapeptide*	12.0	830.410	11.4
(Tri-tetrapeptide)*	16.2	831.393	9.9
Tri-tetrapeptide	21.3	832.376	9.6
$Tetrapeptide_2$**	18.3	901.446	9.2
$Tetrapeptide_2$*	22.3	902.425	4.4
[Gly^5]Penta*-tetrapeptide*	18.4	958.470	11.1
([Gly^5]Penta-tetrapeptide)*	22.3	959.454	11.9
Tri*-tetrapeptide*-Ala-Dpm*	10.4	1072.555	16.1
$(Tri\text{-}tetrapeptide_2)^{*2/3}$	22.3	1272.637	15.7

Continued on the next page

Table 4.8.: Retention times, accurate masses, and mass errors of peptides detected in in vitro experiments with recombinant DppA, YkfA and YkfC on cell wall peptides of *E. coli* MC4100, *B. subtilis* 168 and *B. subtilis* Δ*dacA::erm*. Asterisks indicate amidations.

Peptide	Retention time (min)	Accurate mass (*m/z*)	Mass error (ppm)
(Tri-tetrapeptide$_3$)$^{*3/4}$	22.3	1714.857	13.0
Dpm*	7.1	188.107	21.4
Dpm	8.1	189.092	24.4
Pentapeptide* (Δ*dacA::erm*)	12.5	530.265	15.8
Pentapeptide (Δ*dacA::erm*)	16.1	531.249	16.0
(Penta-tetrapeptide)$^{*1/2}$ (Δ*dacA::erm*)	22.2	972.484	10.0
DppA (*B. subtilis*, Section 4.2.3)			
Tripeptide*-Ala-Dpm*	8.4	630.332	17.9
(Tripeptide-Ala-Dpm)* (A)	8.7	631.316	18.4
(Tripeptide-Ala-Dpm)* (B)	9.7	631.315	16.8
Tripeptide-Ala-Dpm (A)	9.4	632.306	26.8
Tripeptide-Ala-Dpm (B)	11.6	632.300	17.8
Dpm	8.1	189.092	25.7
YkfA (*B. subtilis*, Section 4.2.4)			
[Gly^5]Pentapeptide*	9.8	516.249	14.4
Tripeptide*-Ala-Dpm*	8.4	630.330	15.6
(Tripeptide-Ala-Dpm)*	8.8	631.318	20.6
Tripeptide-Ala-Dpm	9.5	632.300	17.2
Tripeptide	9.3	389.173	15.4
Tetrapeptide*	9.2	459.227	16.1
Tetrapeptide (B)	10.9	460.210	13.2
Dpm*-Ala	7.5	259.144	15.1
Dpm	8.2	189.092	23.9
Ala-Gly	8.6	145.063	12.6
[Gly^5]Pentapeptide* (Δ*dacA::erm*)	10.4	516.247	10.2
Pentapeptide (Δ*dacA::erm*)	16.3	531.249	14.8
Ala$_2$ (Δ*dacA::erm*)	8.9	159.078	8.7
Tripeptide* (Δ*dacA::erm*)	8.5	388.189	15.5
Tripeptide (Δ*dacA::erm*)	9.5	389.172	13.4
Tetrapeptide* (Δ*dacA::erm*)	9.7	459.226	14.0
YkfC (*B. subtilis*, Section 4.2.5)			
Dipeptide	10.8	217.083	6.0
Dpm*	7.2	188.107	23.0
Dpm	8.2	189.091	20.7
Dpm-Ala	8.5	260.129	18.5
Dpm*-Ala-Gly	8.1	316.165	11.2
Dpm-Ala-Gly	8.5	317.153	22.5
Dpm*-Ala$_2$ (Δ*dacA::erm*)	8.2	330.182	15.8

Continued on the next page

Table 4.8.: Retention times, accurate masses, and mass errors of peptides detected in in vitro experiments with recombinant DppA, YkfA and YkfC on cell wall peptides of *E. coli* MC4100, *B. subtilis* 168 and *B. subtilis* Δ*dacA::erm*. Asterisks indicate amidations.

Peptide	Retention time (min)	Accurate mass (*m/z*)	Mass error (ppm)
Dpm-Ala_2 (Δ*dacA::erm*)	9.0	331.166	15.7
Dpm_2**-Ala	6.7	430.246	11.5
Dpm_2*-Ala	7.6	431.231	13.7
Dpm_2-Ala	8.0	432.216	15.5
Dpm_2*-Ala_2	8.4	502.269	13.8
Dpm_2-Ala_2	8.5	503.252	11.5
Dpm_2**-Ala_2-Gly	8.2	558.306	11.9
Dpm_2*-Ala_2-Gly	8.5	559.293	16.7
Dpm_2-Ala_2-Gly	8.7	560.274	11.1
Dpm_2**-Ala_3 (Δ*dacA::erm*)	20.1	572.324	15.4
Dpm_2*-Ala_3 (Δ*dacA::erm*)	9.1	573.308	15.9
Dpm_2-Ala_3 (Δ*dacA::erm*)	9.7	574.298	25.6
DppA + YkfC (*B. subtilis*, Section 4.2.6)			
Dpm_2*-Ala	7.7	431.229	10.0
Dpm_2-Ala	8.0	432.217	17.8
Tripeptide-Ala-Dpm*	8.8	631.312	12.2
Tripeptide-Ala-Dpm	9.6	632.299	16.6
Dpm_3**-Ala_2	7.1	673.371	11.6
Dpm_3*-Ala_2	8.3	674.355	11.7
Dpm_3-Ala_2	8.5	675.342	16.0
Dpm	8.2	189.091	19.7
Dpm_2*-Ala_3 (Δ*dacA::erm*)	9.1	573.308	15.3
Dpm_2-Ala_3 (Δ*dacA::erm*)	9.7	574.295	20.5
YkfA + YkfC (*E. coli*, Section 4.2.6)			
Dpm-Ala_2	8.6	331.165	9.9
Dpm	8.2	189.090	17.0
YkfA + YkfC (*B. subtilis*, Section 4.2.6)			
Dpm_2**-Ala	6.7	430.246	11.7
Dpm	8.1	189.091	21.8
Dpm*-Ala	7.6	259.144	13.2
Dpm-Ala	8.1	260.128	15.8
Dpm_2**-Ala_3 (Δ*dacA::erm*)	20.1	572.323	14.5
Dpm*-Ala_3 (Δ*dacA::erm*)	8.4	401.219	12.4
Dpm-Ala_3 (Δ*dacA::erm*)	9.2	402.204	13.4
Dpm* (Δ*dacA::erm*)	7.3	188.107	22.5
Dpm (Δ*dacA::erm*)	8.2	189.091	22.8
DppA + YkfA + YkfC (*B. subtilis*, Section 4.2.6)			
Dpm*-Ala	7.6	259.144	16.7

Continued on the next page

Table 4.8.: Retention times, accurate masses, and mass errors of peptides detected in in vitro experiments with recombinant DppA, YkfA and YkfC on cell wall peptides of *E. coli* MC4100, *B. subtilis* 168 and *B. subtilis* Δ*dacA::erm*. Asterisks indicate amidations.

Peptide	Retention time (min)	Accurate mass (*m/z*)	Mass error (ppm)
Dpm-Ala	8.1	260.129	19.2
Dpm	8.1	189.092	23.9
Dpm_2*-Ala_3 (Δ*dacA::erm*)	9.1	573.307	12.9
Dpm_2-Ala_3 (Δ*dacA::erm*)	9.7	574.296	22.3
Dpm*-Ala_3 (Δ*dacA::erm*)	8.4	401.219	10.9
Dpm-Ala_3 (Δ*dacA::erm*)	9.2	402.203	11.9
Dpm (Δ*dacA::erm*)	8.2	189.091	20.7

4.2.7. Characterisation of *dppABCDE* and *ykfABCD* mutants

Analysis of growth and cell morphology

Since the peptidoglycan is essential for the maintenance of cell shape and growth, mutants lacking enzymes of the peptidoglycan recycling pathway were studied for their growth behaviour and cell morphology. The *B. subtilis* Δ*dppABCDE::kan*, Δ*ykfABCD::kan*, and Δ*dppABCDE::kan* Δ*ykfABCD::spc* mutants were created and provided by Marjorie Dauvin (University of Liège, group of Bernard Joris).

When the growth of *B. subtilis* wild-type, *amyE*, *dppABCDE*, *ykfABCD* and *dppABCDE ykfABCD* mutant cells was monitored, they were found to grow equally well during exponential and late exponential growth phase (8 h, Figure 4.32A). The first differences appeared with the beginning transition phase. The *dppABCDE* mutant showed reduced, albeit steady, growth, while the decreasing OD_{600} of the *ykfABCD*n mutant and the double mutant indicated incipient lysis or morphological changes (see below). In contrast, the wild-type and the *amyE* mutant continued to grow unabated for another 2 h before their OD_{600} values also decreased. Comparing the growth curves up to 24 h, the transition phase of the *dppABCDE* mutant seems to be clearly extended. From 24 h on, a constant decline in OD_{600} was observed for all cultures. Interestingly, from 48 h to 72 h, the wild-type showed a pronounced drop in OD_{600}, resulting in the lowest final values of all strains.

To see whether the cause of the decreasing OD values was cell lysis or morphological changes, the colony-forming units (CFU) were quantified and the morphological appearance was examined. As shown in Figure 4.32B, the CFU figures showed the same tendency as the OD measurements. However, the change from transition phase (10 h) to stationary phase (24 h) was much more noticeable: the values here already dropped to the low level after 48 h of cultivation. After 72 h, the values dropped again slightly. Likewise to the OD values, the strong drop of the wild-type after 48 h was remarkable in comparison with the mutants. The decreasing OD values thus correlated to a certain extent with decreasing numbers of viable colonies.

In this experiment, the *ykfABCD* mutant showed the highest number of viable colonies of all strains in long-term cultivation. The loss of the *dpp* genes, in contrast, seemed to significantly reduce the viability of the cells.

No less interesting was the difference in the morphological appearance of the colonies that

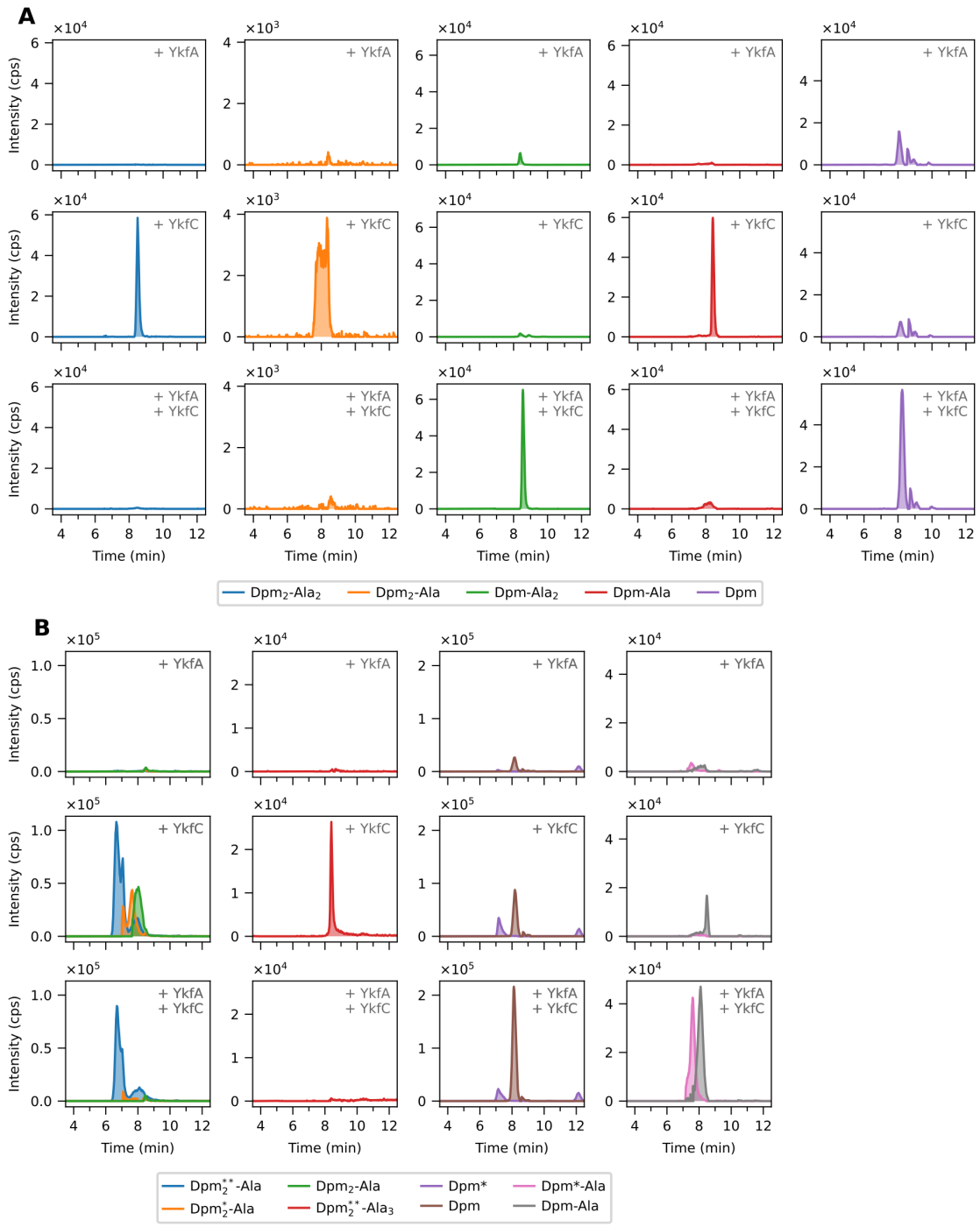

Figure 4.29.: Substrates and products of YkfA when used in conjunction with YkfC on peptides of *E. coli* and *B. subtilis*. Peptidoglycan of *E. coli* (A) or *B. subtilis* (B) was treated with an amidase and then incubated with YkfA, YkfC or YkfA in combination with YkfC. The result of the subsequent LC-MS analyses is shown with EICs. A) *E. coli*: Dpm_2-Ala_2 (blue), Dpm_2-Ala (orange), Dpm-Ala_2 (green), Dpm-Ala (red), and Dpm (violet). B) *B. subtilis*: Dpm_2-Ala_2 (green, partially amidated: orange, completely amidated: blue), amidated Dpm_2-Ala_3 (red), Dpm (brown, amidated: violet), and Dpm-Ala (grey, amidated: magenta). The number of amidated Dpm residues is indicated with asterisks. See Table 4.8 for accurate masses and mass errors.

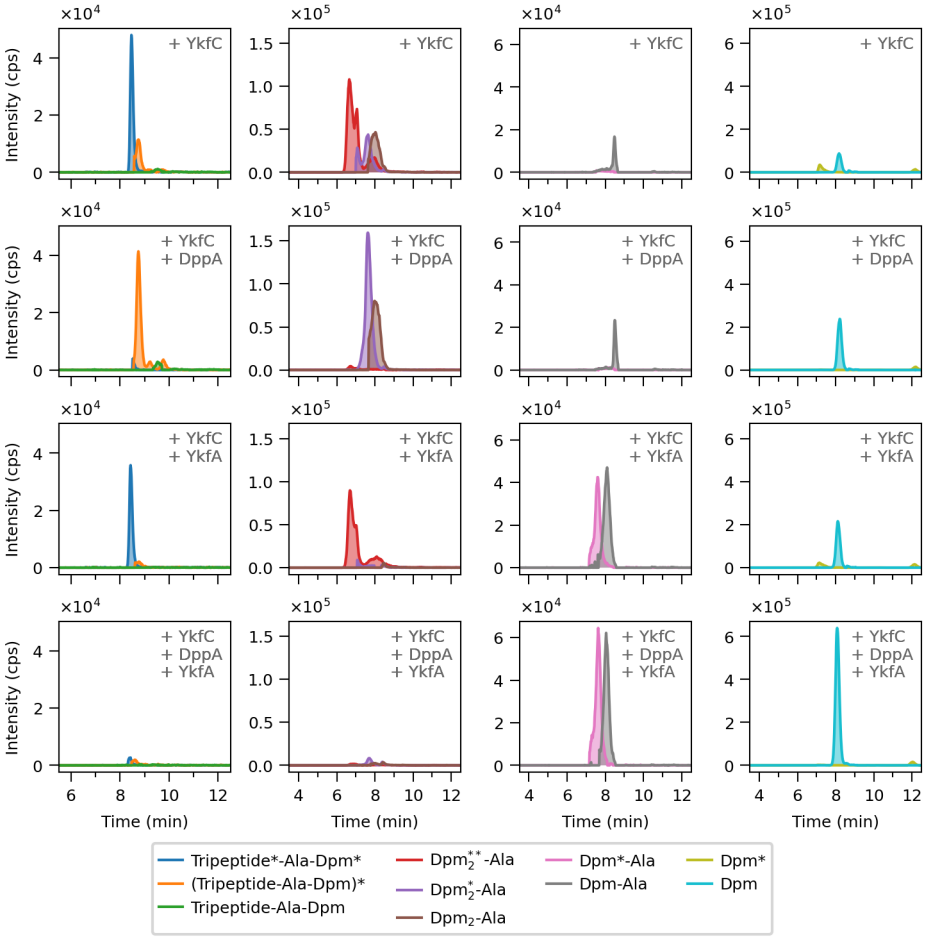

Figure 4.30.: DppA, YkfA and YkfC in conjunction degrade cross-linked peptide fragments of *B. subtilis*. Peptidoglycan of *B. subtilis* was treated with an amidase and then incubated with YkfC alone or YkfC in combination. The result of the subsequent LC-MS analysis is shown with EICs for: tripeptide-Ala-Dpm (green, partially amidated: orange, completely amidated: blue), Dpm_2-Ala (brown, partially amidated violet, completely amidated: red), Dpm-Ala (grey, amidated: magenta), and Dpm (aqua, amidated: light olive). The number of amidated Dpm residues is indicated with asterisks. See Table 4.8 for accurate masses and mass errors.

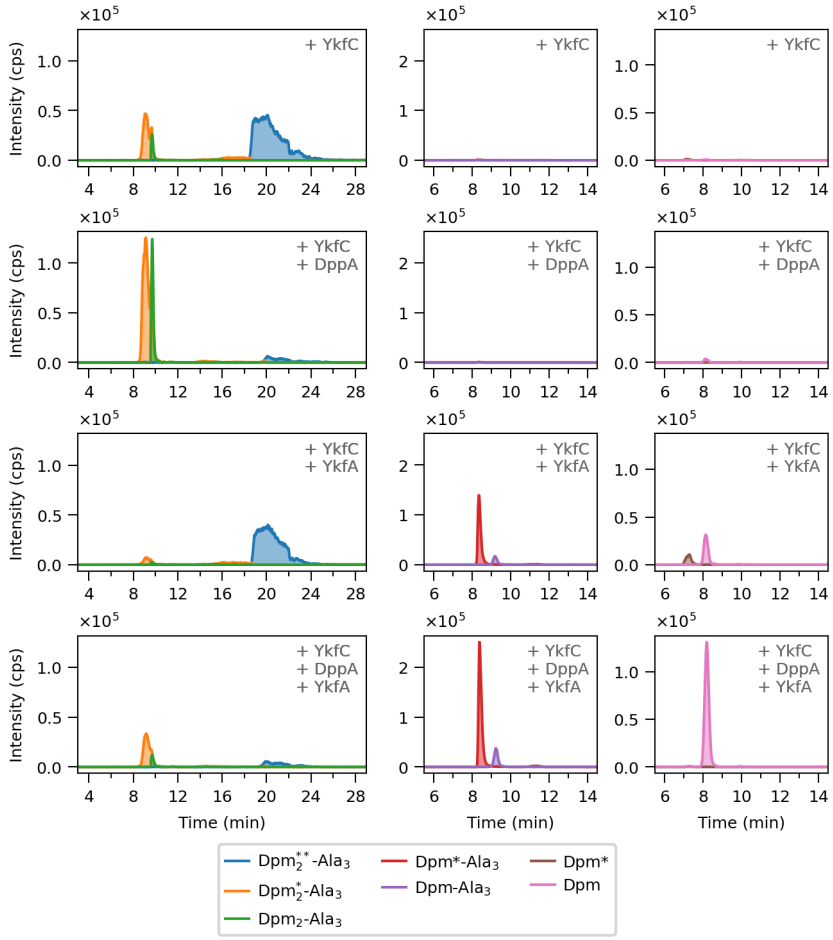

Figure 4.31.: DppA, YkfA and YkfC in conjunction degrade cross-linked Dpm_2-Ala_3 of a *B. subtilis dacA* mutant. Peptidoglycan of *B. subtilis* Δ*dacA::erm* was treated with an amidase and then incubated with YkfC alone or YkfC in combination. The result of the subsequent LC-MS analysis is shown with EICs for: Dpm_2-Ala_3 (green, partially amidated: orange, completely amidated: blue), Dpm-Ala_3 (violet, partially amidated: red), and Dpm (magenta, amidated: brown). The number of amidated Dpm residues is indicated with asterisks. See Table 4.8 for accurate masses and mass errors.

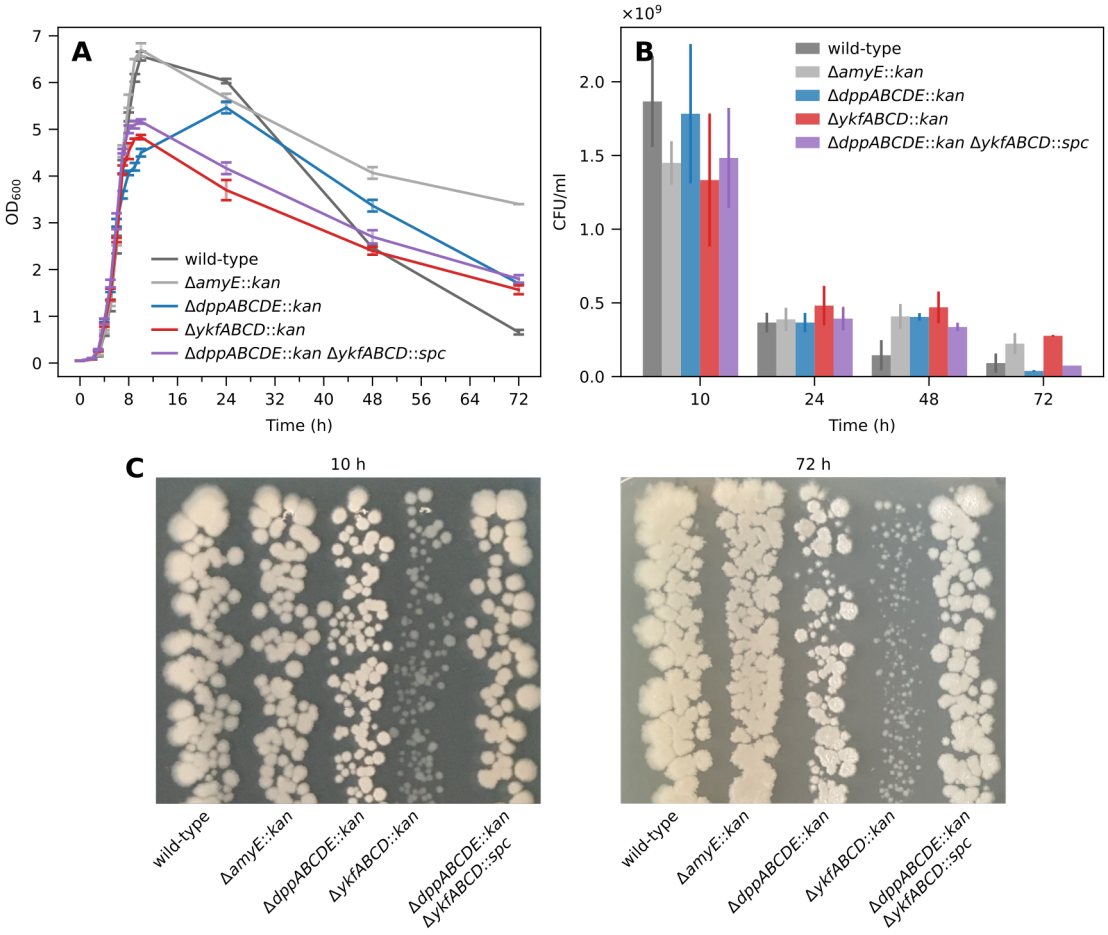

Figure 4.32.: *B. subtilis* mutants deficient in *dppABCDE* or *ykfABCD* exhibit altered morphology in colonies, but show viability comparable to the wild-type. Cells of *B. subtilis* wild-type, Δ*amyE::kan*, Δ*dppABCDE::kan*, Δ*ykfABCD::kan* and Δ*dppABCDE::kan* Δ*ykfABCD::spc* were grown for 72 h in LB medium. A) Optical density at 600 nm (OD_{600}). B) Number of colony forming units (CFU/ml). C) Cells plated for determination of CFU after 10 h to 72 h of growth. The OD and CFU values are represented as mean (n = 3) with standard deviation. The two measurements were determined in independent experiments.

were plated to quantify the CFUs (Figure 4.32C). The wild-type and the *amyE* mutant showed densely growing colonies with a light beige colouration, with the outer colonies showing a swarming phenotype. Interestingly, this was only true for those colonies that faced the edge of the agar plate and no other strain. In comparison, the dpp operon mutant had smaller colonies that were lighter in colour and had a seamed, dull surface rather than shiny and translucent. Also, colonies plated after 72 h of growth in liquid culture, appeared more heterogeneous in their size. Some were very small and other were comparable to the wild-type in size. The most striking phenotype showed the *ykf* operon mutant. With colonies that small and almost translucent that they were not visible after incubation on agar overnight, it took an additional day for them to became visible. This phenotype was already apparent after 10 h of cultivation, but was even more pronounced after 72 h. The phenotype of the double mutant, which was deficient in both operons, was therefore surprising. The morphology of corresponding cells was comparable to the wild-type and the *amyE* mutant, except for the whitish colouring observed for the *dpp* operon mutant and a slightly velvety, dull surface.

To investigate whether morphological changes of the colonies were reflected on the single cell, cells were examined under the microscope after 24 h, 48 h and 72 h of growth (Figure 4.33). In all cultures, cells were found predominantly aggregated and less as isolated, dispersed cells. The size of the cell aggregations seemed to be different, but the number of cells within a section was also not equalised. No obvious differences in cell shape and size were found. The rods were about 2.4 µm long and 0.7 µm wide. Already after 24 h, the formation of spores could be observed, as some cells were shorter, elliptical shaped and appeared opaque. Interestingly, this was most obvious for the *amyE* mutant. The sample of this mutant also contained more shaded cells, which indicated cell lysis and is conceivable with a higher number of spores. However, the mutants which were the research objects of this experiment, Δ*dppABCDE::kan*, Δ*ykfABCD::kan* and Δ*dppABCDE::kan* Δ*ykfABCD::spc*, differed not distinctively from the wild-type.

In summary, mutants deficient in *dppABCDE*, *ykfABCD* or both exhibited an impaired growth, as manifested in OD and number of CFUs in the transition phase. Although the reduced size of colonies and the altered cell surface probably impacted the measurements of the OD, a reduced growth rate was supported by the fact that the colonies of the *ykf* operon mutant only became visible on plate after prolonged incubation. Obviously, the size of the colonies was considerably reduced, but not the number of viable cells. Indeed, the *ykf* mutant showed the highest numbers of CFU in long-term growth. The functional loss of *dppABCDE* or *ykfABCD* was reflected in pronounced morphological changes at colony level whereas single cells did not differ from the wild-type.

Accumulation studies

Functional loss of the putative operons *dppABCDE* and *ykfABCD* resulted in altered colony morphology and impaired growth (see sections before). To shed some more light on this phenomenon, intracellular accumulation of peptidoglycan components was examined in a Δ*dppABCDE::kan*, a Δ*ykfABCD::kan* and a Δ*dppABCDE::kan* Δ*ykfABCD::spc* double mutant. The cells were grown in LB medium for 24 h, whereby the following findings refer to the stationary growth phase. The result is depicted in Figure 4.34A.

For the *dppABCDE* operon mutant, no intracellular accumulation of cell wall peptides could be detected, neither by evaluating DCs nor by targeted analysis using EICs. In contrast, the *ykfABCD* operon mutant showed intracellular accumulation of amidated tripeptide, tetrapeptide

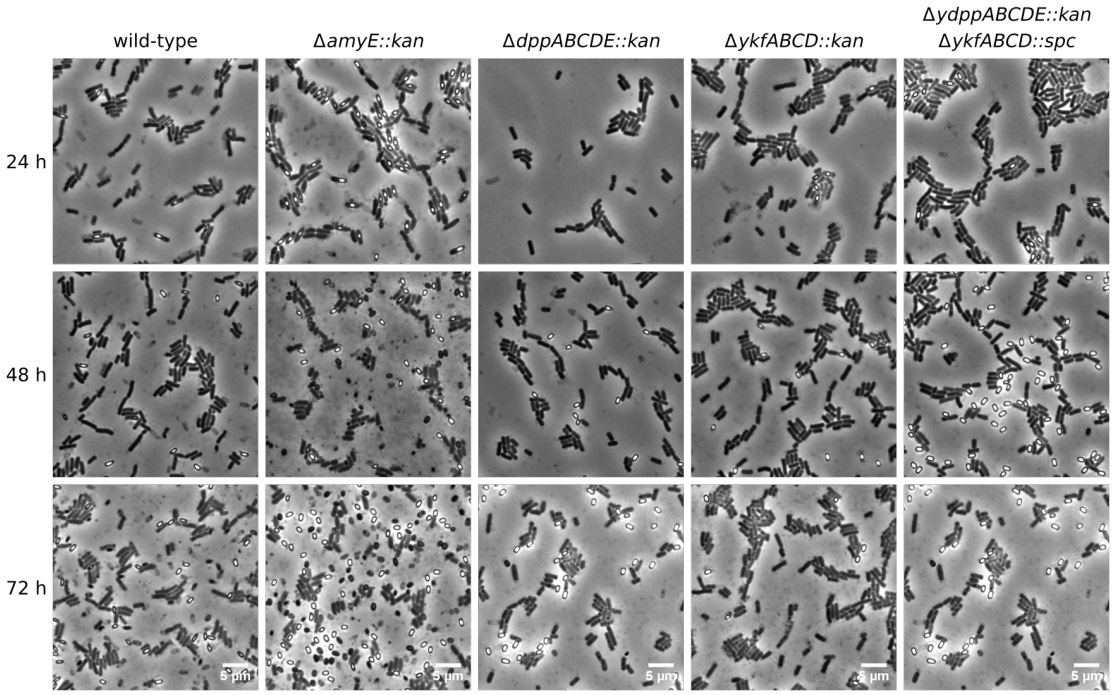

Figure 4.33.: Phase-contrast images of *B. subtilis* wild-type, Δ*amyE::kan*, Δ*dppABCDE::kan*, Δ*ykfABCD::kan* and Δ*dppABCDE::kan* Δ*ykfABCD::spc* mutant cells. Cells were grown for 72 h in LB medium and visualised by phase-contrast microscopy after 24 h, 48 h and 72 h of growth. The scale bars indicate a length of 5 µm.

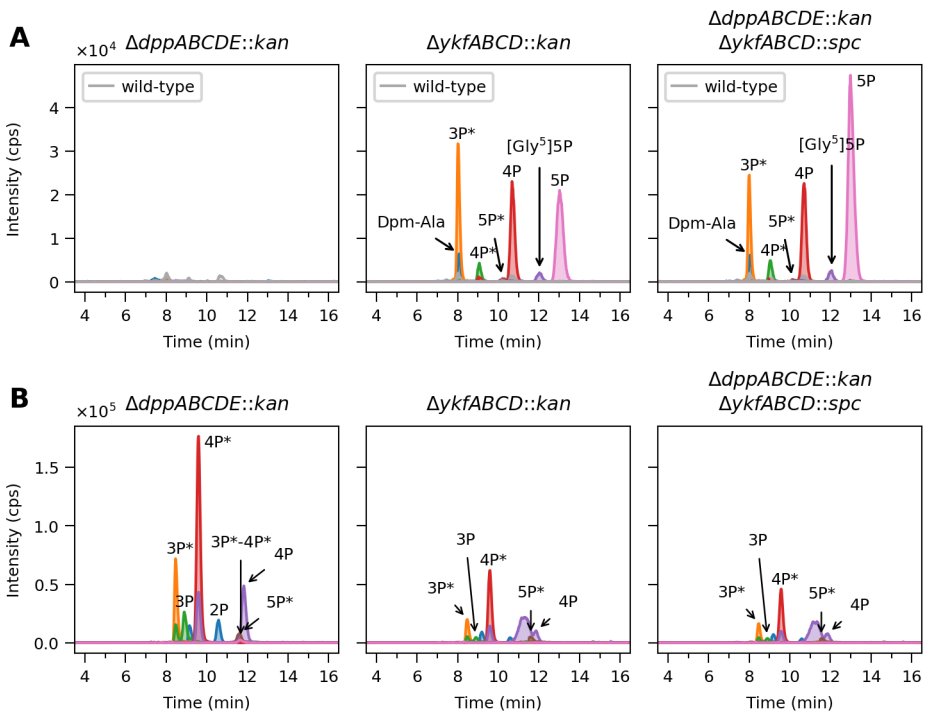

Figure 4.34.: Intracellular (A) and extracellular (B) accumulation products of *B. subtilis dppABCDE*, *ykfABCD* and *dppABCDE ykfABCD* mutants. *B. subtilis* 168 wild-type, Δ*dppABCDE::kan*, Δ*ykfABCD::kan*, and Δ*dppABCDE::kan* Δ*ykfABCD::spc* mutant cells were cultivated for 24 h (stationary growth phase) in LB medium. Acetone extracts of cytosolic fractions and supernatants were analysed by LC-MS. The result of the LC-MS analysis is shown with EICs for Dpm-Ala, tripeptide (3P), tetrapeptide (4P), [Gly^5]pentapeptide ([Gly^5]5P), pentapeptide (5P), dipeptide (2P), and tri-tetrapeptide (3P-4P). The number of amidated Dpm residues is indicated with asterisks. Both measurements were determined in independent experiments. See Table 4.9 for retention times and accurate masses.

and a compound with the mass of pentapeptide. Furthermore, Dpm-Ala, amidated tetrapeptide, and [Gly^5]pentapeptide were found with low abundance. A compound with the mass of amidated pentapeptide was detected in trace amounts. Surprisingly, the double mutant showed the same pattern with comparable intensities. Only the compound with the mass of pentapeptide appeared with an even higher signal. Somewhat unusual was the retention time observed for this peptide. With a retention time of 13 min in both mutants, it eluted significantly earlier than in the in vitro experiments with the recombinant enzymes (16 min). In none of the mutants an accumulation of cross-linked peptides such as tri-tetrapeptide, tetra-tetrapeptide or [Gly^5]penta-tetrapeptide was detected.

Moreover, the supernatants of the cultures were analysed (see Figure 4.34B). Compared to the *ykfABCD* mutant, the *dppABCDE* mutant showed a strongly increased extracellular accumulation of unbranched peptides. In particular, amidated tetrapeptide appeared with strongly increased abundance, but also tetrapeptide and amidated tripeptide were detected with significantly higher values. Dipeptide and tripeptide also were more abundant, whereas amidated pentapeptide was found with only slightly higher values. Interestingly, an accumulation of completely amidated tri-tetrapeptide was also observed, although its abundance was very low.

It was striking that the double mutant resembled the *ykf* operon mutant in its behaviour; it accumulated the same peptides in comparable amounts and thus significantly less than the *dpp* operon mutant.

Table 4.9.: Retention time (min), accurate mass (*m/z*), and mass error (ppm) of intracellular accumulation products in *B. subtilis* 168 wild-type, *ykfABCD* and *dppABCDE ykfABCD* mutants. Data presented as mean (n = 3). See Table 3.3 for exact masses.

	Wild-type			Δ*ykfABCD::kan*			Δ*dppABCDE::kan* Δ*ykfABCD::spc*		
Peptide	min	*m/z*	ppm	min	*m/z*	ppm	min	*m/z*	ppm
Tripeptide*	8.0	388.184	4.8	8.0	388.186	8.7	8.0	388.186	9.5
Tetrapeptide*	9.1	459.221	3.8	9.1	459.222	5.3	9.0	459.222	5.6
Tetrapeptide	10.7	460.204	4.3	10.7	460.207	6.1	10.7	460.207	6.2
Pentapeptide*				10.2	530.259	4.6	10.2	530.261	7.0
Pentapeptide				13.0	531.244	5.6	13.0	531.244	5.4
[Gly^5]Pentapeptide				12.0	517.228	5.1	12.0	517.228	5.7
Dpm-Ala				8.1	260.127	9.9	8.1	260.127	11.9

Table 4.10.: Retention time (min), accurate mass (*m/z*), and mass error (ppm) of intracellular accumulation products in *B. subtilis* 168 *dppABCDE*, *ykfABCD* and *dppABCDE ykfABCD* mutants. Data presented as mean (n = 3). See Table 3.3 for exact masses.

	Δ*dppABCDE::kan*			Δ*ykfABCD::kan*			Δ*dppABCDE::kan* Δ*ykfABCD::spc*		
Peptide	min	*m/z*	ppm	min	*m/z*	ppm	min	*m/z*	ppm
Dipeptide (A)	9.2	217.078	18.4	9.2	217.078	17.3	9.2	217.078	18.7
Dipeptide (B)	10.6	217.079	12.1	10.6	217.08	10	10.6	217.08	7.7
Tripeptide*	8.5	388.180	7.1	8.5	388.179	10.2	8.5	388.180	7.1
Tripeptide	8.9	389.164	6.2	8.9	389.165	3.2	8.9	389.166	2.3
Tetrapeptide*	9.6	459.217	5.9	9.6	459.217	5.9	9.6	459.218	3.8
Tetrapeptide	11.8	460.201	7.0	11.8	460.205	2.4	11.8	460.205	2.8
Pentapeptide*	11.6	530.251	12	11.6	530.245	23.3	11.6	530.244	24.2
Tri*-tetrapeptide*	11.7	830.391	10.7						

4.3. Project-related software development

4.3.1. Wühlmaus: An application to receive records from UniProt

The Universal Protein Resource (UniProt) Knowledgebase is an online database which holds an enormous amount of information on proteins from bacteria, eukaryots, archaea and viruses [113]. This includes information about the amino acid sequence, the encoding gene (or open reading frame) and their taxonomic origin. Beyond that, the UniProt database is connected with other databases like KEGG or InterPro and enriches its content with annotations provided by these databases (e. g. the existence of domains or binding sites) [114]. The UniProt Knowledgebase is divided into two sections: Swiss-Prot and TrEMBL [113]. Proteins, which have been experimentally characterised and published or whose computational analysis was manually curated, are sorted into Swiss-Prot. Proteins of which only little is known and for which only automatic computational annotations are available are sorted into TrEMBL. Due to the progress made in sequencing technologies, the number of available entries in TrEMBL is several hundred times higher than the number of entries in Swiss-Prot. It is obvious that this enormous amount of data cannot be experimentally validated in the same speed as it is generated and thus, only a small portion of proteins of living organisms is characterised. However, by automatic computational analysis, assumptions based on homologies can give some hints and insights on unknown proteins. Therefore, it is crucial to access data in databases like UniProt in an easy and convenient way. The first and important step for this is the structured organisation and presentation of this data, which is already done by UniProt itself. To unequivocally identify a protein sequence, a unique identifier (ID) is given, which is the accession number (e. g. the accession number for MupG of *S. aureus* is `A0A0H2XHV5`). Each accession number identifies one protein. Consequently, even proteins with the same or very similar sequences from the same species are assigned to different accession numbers. Another possible identifier is the entry name, the name of the actual record. It is often a combination of the protein's common name, followed by an underscore and the abbreviated organism name (e. g. `YKFC_BACSU` for YkfC of *B. subtilis*) but is not to be considered as stable as the accession number.

On the UniProt website, the whole database can be searched and accessed. And while this works great when looking for more general information, e. g. all proteins which are assigned to the Pfam family DUF871, it has its shortcomings when looking for detailed information about one specific protein. This is especially evident, when a larger numbers of protein identifiers should be queried. For example, in proteome analyses of pulldown experiments, the number of hits can sum up to several hundreds of proteins. There is, indeed, a tool which is designed to do this kind of batch queries, but it does hide some useful information by default that help to find interesting proteins (e. g. annotations about domains or protein families). Accessing these information is not self-explaining and requires some knowledge about the underlying UniProt application programming interface (API, [114]), which is described in the UniProt documentation. For this reason, I developed a small semi-interactive application written in the programming language Python. It accesses the UniProt database and retrieves information from records for given accession numbers. If available, it also retrieves the current scientific name of the organism from the NCBI database. The application was named "Wühlmaus" [115] (german name for *Arvicolinae*) and its source code is published[1].

Records of proteins (or entries) in the UniProt database are written in extensible markup language (XML). The HTML version of an entry, which is shown by default when accessed via the web interface, only resembles the information in the XML version. The topology of UniProt's XML structure was thus investigated and is used by Wühlmaus to request and process entries in this format.

When started, Wühlmaus presents either a command line interface (CLI) or a graphical user interface (GUI). The user is asked to point the application to a text file which contains accession numbers to search for, implemented as input variable. Secondly, the user is asked to specify file name and location of the output file which will be written by the application. An option to write protein sequences to a separate file in FASTA format is also included. If checked, the accession number is used as descriptive header for each sequence in the FASTA file. In addition, the CLI provides an option to write a basic mapping of accession number to gene or entry name and the organism name for further use in iTOL, an online tool to visualise and annotate phylogenetic data [111]. This option is inactive by default (commented out in the source code), because most users probably will not use this feature. Upon providing a text file, which contains the accession number(s) to search for, Wühlmaus opens a connection to the UniProt API and requests the records for the given accession numbers at once. Before readout, the records and taxa in the response's content are extracted. The extracted unique taxonomic identifiers are sent to the NCBI database, to obtain the current scientific names mapped to the identifier. The actual readout of the UniProt records is done by searching for values of given tags and attributes in the XML structure, whereas links to databases named there are not extracted from the XML, but instead from static concatenation. As mentioned, Wühlmaus can request and process multiple records at once. Therefore, the processing is done repetitively for each single record within a loop. Furthermore, the taxonomy identifier given in the UniProt record is mapped to the scientific name given in the NCBI database. The organism name given by UniProt is then replaced with the current scientific name from NCBI. This is done, because the NCBI taxonomy is usually more up to date and more precise. Finally, the report is written to a tab-separated text file and the next record is processed. If the user selected, amino acid sequences and basic mappings for iTOL are written to separate files.

[1] `https://codeberg.org/culpeo/wuehlmaus/`

The information to be extracted from a record or an entry is preset to provide a rational summary of a protein's characteristics. The selection of information cannot be changed through the interface, but in the source code by users with programming knowledge. However, this might be unsatisfying for regular users and is something to improve. The function `get_user_selection()` is intended for that, but not yet fully implemented. An option to directly enter the identifiers into the user interface as query would also be an improvement for the user experience.

Besides the previously mentioned possibilities for improvement, Wühlmaus is a functional, small and fast application which helps to review lots of proteins. It does so in a more convenient way compared to UniProt's own implementation while still providing access to the enormous knowledge resource of UniProt.

4.3.2. Chromius: An application to extract LC-MS data from text files

Raw data from the LC-MS system used in this dissertation and related publications can be analysed extensively and visualised using DataAnalysis and other applications of the *micro-TOF Compass* programme suite (Bruker Daltonics). However, these applications are not very convenient to use, when it comes to comparative analysis of a larger number of samples at once, since it requires manual adjustments and selection for every single data set. Another shortcoming is apparent, when figures should be created for use in publications. This requires high quality, clearly readable images in a universal file format. Furthermore, it is often necessary to annotate graphs. Both cannot be achieved with DataAnalysis. Yet, DataAnalysis can export raw data as text files (one per chromatogram trace), which contain the retention time in seconds and the detected intensity in counts per seconds (cps) at the given time point. The files are written into the directory of the respective sample. With these files, further processing can be done with spreadsheet applications. Depending on the analysis, the number of files might be cumbersome though.

Therefore, an application to extract the data from these exported text files was developed and written in the programming language Python (Walter, unpublished). It extracted data by opening text files with either "EIC" or "BPC" and the extension `.xy` in the file name that are located within the same directory as the application. Briefly, this was done by scanning the directory and its subdirectories in a loop. Coupled to this, the content of the text files was read. Although quite useful to simplify the processing of LC-MS data, it had some drawbacks. That is, in every iteration of the loop the whole directory was scanned, every text file was opened, and read. This caused a lot of disk activity and made the readout of LC-MS analyses with many samples slow. Furthermore, the original implementation required the user to rename the subdirectories by adding a two digit prefix to identify samples in later processing. I made some changes to the application and extended its functionality, which is described in the following. The resulting application was named Chromius [116] and its source code is available online[2].

To improve the performance and reduce the disk load, I isolated the scanning for text files from the actual readout. Using the Path library in conjunction with `glob()`, eliminated the need to iterate repetitively over directories. Subsequently, directories are searched only once and without actually opening files. Paths of files, containing "BPC", "EIC", or "TIC" in their name are stored in a generator object. In the particular LC-MS system used here, some meta

[2] `https://codeberg.org/culpeo/chromius/`

data, including sample identifier, sample name, position in the sample tray, injection volume and used method, is saved in XML files. Especially, the sample identifier is of great importance, since it serves as unique identifier and resolves the need to rename the sample directories. Thus, a function to read meta data was implemented. That is, paths for files with the extension `.xml` are also collected. Sometimes the main information file is missing, e. g. if it was accidentally deleted or only sub-directories of certain samples were copied. To ensure the readout of meta data, sample-specific XML files are also considered. The information from the XML side files is extracted with the help of regular expressions and directly reading entries from the XML files. The actual readout of raw data is done with the file paths read before as input. Similar to the original implementation, a loop is used to open the file paths. The extracted raw data is stored facilitating the sample identifier and the name of the chromatogram as descriptive and unique key. In addition, and in contrast to the original implementation, the time values of each sample are read out. Previously, only the time values of the first sample were read out and served as common time values for all samples. However, long HPLC runs or a large number of samples tend to result in shifts in retention times. To account for these shifts and to map the retention times correctly, the read out was therefore changed. If no XML file was found previously, the sample identifier and the sample name are read from the file path as measure of last resort by using regular expressions. Independently whether a sample table was present or not, the sample identifier and name of difference chromatograms is extracted from the file path. This is done, because difference chromatograms (DCs) are not samples and thus have no entry in the sample table. They are, however, analyses of samples and linked with them by using the same base ID extended with a suffix. The suffix contains a three digit number, counting the number of DCs from the specific sample. To identify a DC, a regular expression for "ID" followed by three digits is used. Since the length of the data sets within one run can vary slightly, they are aligned to the length of the shortest data set. As in the original implementation, the output is written as comma separated table to a plain text file and can be opened with spreadsheet applications like LibreOffice Calc, Microsoft Excel or GraphPad Prism. The meta data is written into a plain text file as well and serves as information file for the user. It includes mappings of the sample names to string variables for further use with the visualisation library Matplotlib.

In summary, the core functionality of extracting raw data from text files was maintained, but the listing of the text files and their readout was implemented in a different way. With these changes a perceptible increase of processing speed was achieved, whilst the disk load was reduced. The extensions made improved the further processing of extracted data by automatically mapping them to a unique identifier, including DCs and provide some meta data. The user is no longer required to manually rename sample directories in order to identify them, but to specify the input directory and the name of the output file. Finally, the application was made more accessible for users without programming knowledge by bundling the application with a GUI. The addition of a GUI also resolved the need to copy the application into the directory to be read.

5. Discussion

5.1. Recycling of the disaccharide MurNAc-GlcNAc in *S. aureus*

5.1.1. MupG and DUF871 proteins represent a family of versatile phosphoglycosidases

In this work, MupG of *S. aureus* was characterised as a unique MurNAc 6P-hydrolase and as the founding member of a new family of glycosidases – the glycoside hydrolase (GH) family 170 within the CAZy database[1] [117]. Phylogenetic analysis of MupG homologues and more distantly related enzymes (MupG-like enzymes), as discussed by Kluj *et al.* [106], suggested that the GH170 family can be divided into distinct clades with presumably different physiological functions. Thus, the family of GH170 (formerly DUF871) proteins represents a family of different phosphoglycosidases. Somewhat unexpected was the finding that some species even encode GH170 proteins of both groups, MupG homologues and MupG-like enzymes.

The majority, but not all, of GH170 proteins appear to be structured in two sub-domains as seen in crystal structures of the MupG homologue of *Enterococcus faecalis* (PDB ID: 2P0O, sequence identity of 32.2 %) and the MupG-like homologue of *Bacillus cereus* (PDB ID: 1X7F, sequence identity of 26 %). The larger N-terminal domain is reminiscent of a TIM barrel and the smaller, C-terminal one of cyclophilins. Interestingly, as mentioned earlier, some GH170 proteins lack the cyclophilin-like domain. Cyclophilins, or peptidyl-prolyl isomerases, are involved in protein folding and assembly, act as chaperones, but are also immunologically relevant [118–121]. This suggests that the cyclophilin-like domain in GH170 proteins is involved in their folding. Since cyclophilins are present in many organisms [119–121], they may support the folding of those GH170 proteins that lack the second cyclophilin-like domain.

The apparent versatility of the GH170 family is likewise reflected in the homologues within a single species and to some extent in their tertiary structure. The genomic context of GH170 proteins also differs. While MupG proteins are often encoded with enzymes of the MurQ pathway, the genomic context of MupG-like proteins is heterogeneous. In some organisms, a co-occurrence of MupG-like proteins with putative homologues of MurK was observed. As a kinase, MurK phosphorylates the monosaccharides MurNAc and GlcNAc at the C6 position [112]. MupG and MurQ together release GlcNAc and GlcNAc 6P (Figure 4 in [106] or Appendix A), the latter of which can be channelled into the peptidoglycan synthesis. The kinase activity of MurK would be useful in providing a second GlcNAc 6P molecule for peptidoglycan synthesis from the GlcNAc released by MupG and MurQ. However, few organisms with MupG-like proteins also encoded a MurQ homologue. GlcNAc may not be available as a MurK substrate in these organisms. Since the specificity of MupG-like proteins presumably differs from that of MupG homologues, it would be interesting to investigate whether this also applies to MurK homologues that co-localise with MupG-like proteins. More frequently than with MurK homologues, co-localisation of MupG-like proteins with 6P-β-glucosidases was found. Similar to MupG, 6P-β-glucosidases

[1] http://www.cazy.org/

hydrolyse disaccharides in which the C6 position of one carbohydrate is phosphorylated (EC 3.2.1.86, the ExplorEnz database [122]).

Both MupG and 6P-glucosidases frequently co-localise with PTS systems for uptake of sugars and share the specificity for C6-phosphorylated sugars. Furthermore, metabolic pathways for uptake and utilisation via PTS systems and 6P-glucosidases have been identified for various sugars [123, 124]). All 6P-glucosidases characterised so far are assigned to the GH1 or the GH4 family [125]. GH1 enzymes, like LacG of *S. aureus* [126–128] and Bgl of *B. subtilis* [129], specifically cleave β-glycosidic bonds in various sugars, releasing glucose [130]. In contrast, the GH4 family includes both α- and β-glucosidases, which are characterised by their dependence on NAD^+. The TIM barrel folding of the GH1 family [131] and the tertiary structure of MupG's (respectively its *E. faecalis* homologue's) N-terminal domain appear similar. And while these aspects suggests a relationship between MupG and 6P-glucosidases, they have nothing in common beyond this. There is no sequence similarity and in the experiments conducted here there was no evidence of NAD dependence. Hence, MupG is the founding member of a new GH family (GH170) and is not assigned to the GH1 or GH4 family as are all 6P-glucosidases characterised so far.

Encoding multiple systems for sugar uptake and utilisation is considered advantageous for bacteria, as it enables them to specifically cleave different sugars and thus access a larger amount of resources. MupG represents the pathway for the utilisation of the cell wall sugar MurNAc-GlcNAc. In this context, it would be instructive to investigate to what extent the substrate specificity of MupG and MupG-like proteins actually differ. Especially proteins from organisms that encode more than one MupG homologue or that encode proteins of both clades would be illustrative (e. g. from *B. megaterium* and *L. plantarum*).

5.1.2. MurP is a transporter for MurNAc-GlcNAc

In the context of the wide distribution of putative MupG homologues among Firmicutes, the observations on substrate specificity of the PTS transporter MurP in *B. subtilis* and *S. aureus* are also interesting. Previously, MurP was thought to only transport the monosaccharide MurNAc, as demonstrated in *E. coli*, *B. subtilis*, and *S. aureus* [59, 75]. An assumption that was challenged in view of the results described here. First, the major autolysin of *S. aureus* generates a disaccharide and not single sugars [38, 82], as already discussed in [106] (see Figures 6 and 7 in [106] or Appendix A). Second, in both *B. subtilis* and *S. aureus* MurP is capable of transporting the dissaccharide MurNAc-GlcNAc across the inner membrane. This is especially remarkable as MurNAc-GlcNAc is not a physiologically occurring recycling product in *B. subtilis*, but only in *S. aureus*. This raises the question of the usefulness of an uptake of this disaccharide for *B. subtilis*. The answer could simply be a common evolutionary origin and does not necessarily imply a physiological need. It could be an advantageous adaptation considering the accessibility of further resources, but this is contrasted by the apparent inability of *B. subtilis* to metabolise MurNAc-GlcNAc.

5.1.3. A modular recycling pathway for MurNAc-containing sugars

This work provided further insights into the process of cell wall recycling and leads to a more complete picture of the recycling pathway of MurNAc. The scheme outlined in the introduction can therefore be refined and expanded as depicted in Figure 5.1. During the

process of autolysis, amino sugars and peptides are released from the peptidoglycan. The form in which these products are released depends on the organism. Some organisms, such as *E. coli*, release anhydromuropeptides (GlcNAc-anhMurNAc-peptide) [53]. *B. subtilis*, release GlcNAc and MurNAc as single sugar molecules [80]. And in others, like in *S. aureus* through its main autolysin Atl, the disaccharide MurNAc-GlcNAc is released [38, 82]. In all three organisms, MurP serves as a PTS transporter to take up either MurNAc [59, 75] or MurNAc-GlcNAc. Uptaken MurNAc 6P-GlcNAc is first cleaved by the phosphomuramidase MupG into MurNAc 6P and GlcNAc. Irrespective of whether MurNAc 6P was formed by cleavage or direct transport, it is hydrolysed by the etherase MurQ into GlcNAc 6P [57, 58]. GlcNAc 6P, in turn, can be introduced into peptidoglycan synthesis and thus be recycled [57, 58]. Since cleavage by MupG also releases GlcNAc, its utilisation in phosphorylated form would be obvious. To my knowledge, a corresponding kinase has not yet been identified in either *S. aureus* or *B. subtilis*.

Despite the ability to utilise MurNAc via the same metabolic pathway, *E. coli*, *B. subtilis* and *S. aureus* differ significantly in cell wall recycling. In addition to the different sugars that are recycled, this also applies to the timing of recycling. *E. coli* recycles its anhydromuropeptides during exponential growth [64], *B. subtilis* and *S. aureus* recycle their turnover products primarily in the stationary growth phase [75, 106]. *B. subtilis* differs from *S. aureus* (and other firmicutes such as *B. megaterium*) further in that peptidoglycan is degraded to monosaccharides by exo-lytic enzymes (NamZ, NagZ, AmiE) [80] and is thus special among firmicutes.

Complementing the MurNAc recycling pathway with MupG enables *S. aureus* to utilise its major turnover product MurNAc-GlcNAc. Other firmicutes, like *B. megaterium* and *L. plantarum* possess MupG and MurP homologues, suggesting that the same pathway is present as in *S. aureus*. MupG-like enzymes probably fulfil related functions in disaccharide metabolism. MupG thus represents a convenient extension of the bacteria's capabilities using existing enzymatic processes. It also shows that bacteria exploit the modular organisation of their (recycling) pathways and adapt them to their needs or possibly even access further substrates.

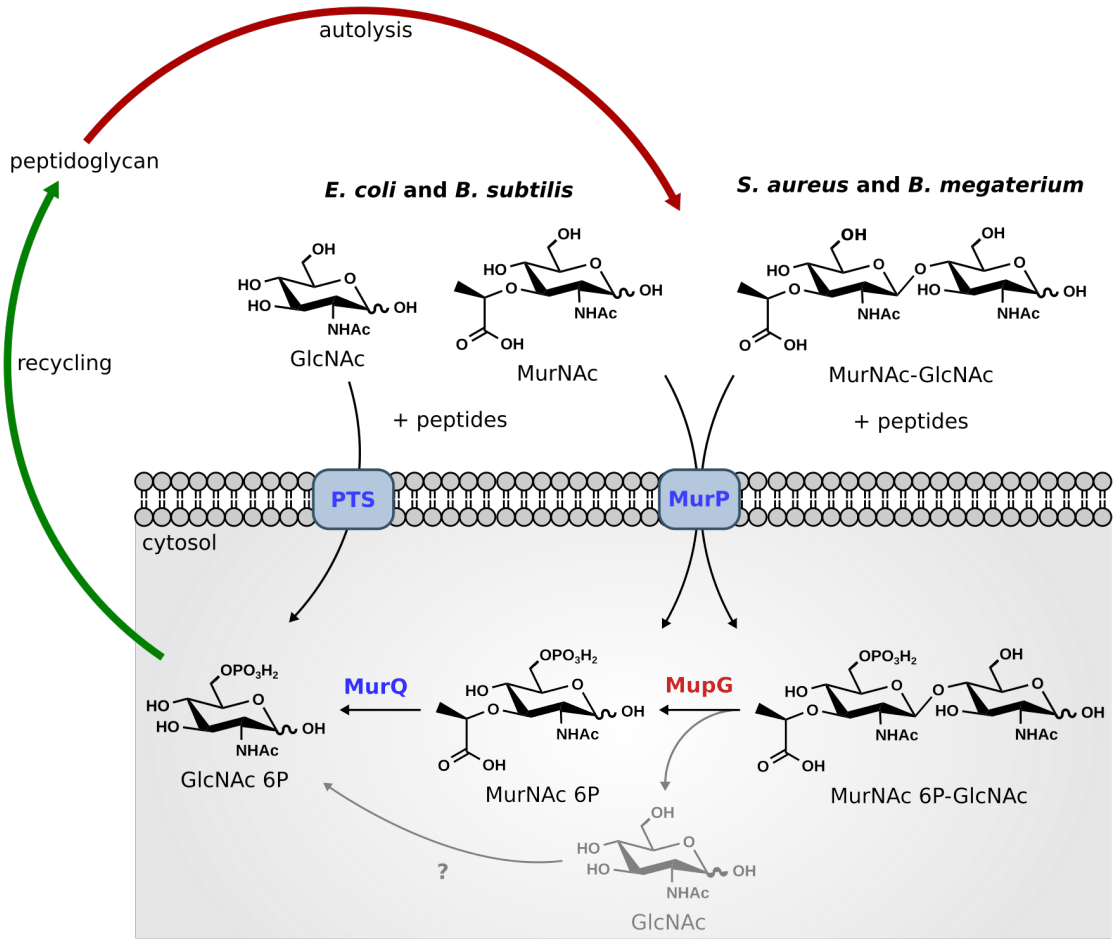

Figure 5.1.: Proposed utilisation process of MurNAc. During autolysis, amino sugars and peptides of the peptidoglycan are released, whereas sugars are degraded to either monosaccharides (*B. subtilis*, [53, 80]) or disaccharides (*S. aureus*, [38, 82]). Irrespective of whether MurNAc or MurNAc-GlcNAc was generated, they are taken up by the PTS transporter MurP and thereby get phosphorylated [59, 75, 106]. Note that in *E. coli* anhydromuropeptides are recycled [53, 54] and direct uptake of MurNAc can occur independently [57–59]. In *E. coli* and *B. subtilis*, GlcNAc is also taken up by a PTS-Transporter (NagE and NagP, respectively) [60–62, 78, 79]. Intracellularly, MurNAc 6P-GlcNAc is cleaved into MurNAc 6P and GlcNAc by the phosphomuramidase MupG [106]. MurNAc 6P is cleaved by the etherase MurQ into GlcNAc 6P, which can be shuttled into peptidoglycan synthesis [57, 58, 75, 106]. Organisms encoding putative MupG homologues like *B. megaterium* are probably able to utilise MurNAc-GlcNAc.

5.2. Recycling of cell wall peptides in *B. subtilis*

The recycling of the cell wall includes not only the carbohydrate part, but also the peptide part [53, 132]. How the cell wall sugars are recycled differs between *E. coli* and the Gram-positives *B. subtilis* and *S. aureus* [75, 132]. However, the differences are not limited to which sugars are processed, but also concern the timing. While in *E. coli* the sugar recycling takes place in the exponential growth phase, it occurs primarily in the stationary growth phase in *B. subtilis* [64, 75]. Another aspect is the presence of an outer membrane, which allows Gram-negative bacteria to retain products of peptidoglycan turnover in the periplasm [51, 74]. Gram-positive bacteria lack the outer membrane [16] and accordingly an enrichment of the turnover products was found in the medium of *B. subtilis* and *S. aureus* [75, 106]. All these differences may also be reflected in the peptide recycling. Indeed, earlier studies found that the peptide recycling-associated gene cluster *dppABCDE ykfABCD* in *B. subtilis* is repressed by CodY until the onset of the stationary growth phase [83, 84, 86, 87]. This would already imply that in *B. subtilis*, sugar and peptide recycling proceed at the same time.

5.2.1. The challenge of identifying cell wall peptides

The identification of cell wall peptides is a challenging task. Although the basic structure of the peptidoglycan is similar in different organisms, cell wall peptides occur in an enormous variety of structures. In this work, this was particularly evident in *B. subtilis*, where many peptides appeared in several variants. The presence of peptide modifications such as Gly instead of Ala and Dpm amidation was not quantified in this work. However, there are reports on the composition of the peptidoglycan of *B. subtilis* [11, 23]. The exchange of Ala to Gly was not frequently observed in this work, and according to previous reports also only accounts for a maximum of 2.7 % (6.3 % in a *dacA* mutant) [11]. Dpm was found amidated slightly less often than expected, given a reported level of amidation of 99 % [11]. This could be an artefact caused by the simplified method of peptidoglycan isolation used here.

The occurrence of amidated besides non-amidated Dpm forms increases the number of peptide turnover products that need to be distinguished. However, the challenge goes beyond the mere number of masses to be analysed. The modification of Dpm by amidation, which was identified in this work as critical for peptide recycling in *B. subtilis*, is only reflected in relatively small changes in the exact mass. Consequently, the masses of individual isotopes of differently amidated forms are often very close to each other. For example, the exact mass of tripeptide is $[M-\mathrm{H}]^- = 389.1667$ *m/z*, the exact mass of the second most abundant isotope of amidated tripeptide is $[M-\mathrm{H}]^- = 389.1859$ *m/z*. The ability of a mass spectrometer to discriminate between masses (or ions) depends on its resolution. It is defined as $R = \frac{m/z}{\Delta m/z}$ with $\Delta m/z$ commonly specified as the full peak width at half maximum height (FWHM, R_{FWHM}) [133]. In relation to a mass, the resolution indicates by how much two masses must differ in order to be detected as two distinct masses. The need for resolution consequently increases with increasing mass. To resolve the mass difference between the isotopes mentioned (0.0193 *m/z*), a mass spectrometer thus requires a resolution of $R_{FWHM} = 20200$. To distinguish the most abundant isotope of tri-tetrapeptide ($[M-\mathrm{H}]^- = 832.3683$ *m/z*) from the second most abundant isotope of partially amidated tri-tetrapeptide, a resolution of $R_{FWHM} = 43300$ is required. According to the manufacturer, the instrument used here has a resolution of 17 500 to 20 000. Therefore, it can barely discriminate the isotopes of the tripeptides, but no longer the isotopes of the mentioned

tri-tetrapptides. Amidation changes the chemistry of a peptide considerably and thus its chromatographic behaviour. Therefore, a distinction between amidated and non-amidated peptides is possible by a suitable separation method such as LC-MS. This method was also used in this work. Unfortunately, the separation of peptides using a reversed-phase column was insufficient in some cases. For example, tri-tetra-tetrapeptide eluted in two differently amidated forms at the same time, as indicated by overlapping isotope patterns (see Section 4.2.2). Hence, the described issue of insufficient resolution ($R_{FWHM} = 66500$ would have been necessary) became apparent. Another problem was the lack of suitable standards, which was also noticeable in the identification of tripeptide-Ala-Dpm. This peptide apparently existed in two structures (see Section 4.2.2). Although these could be distinguished by their retention time, the differently amidated forms also showed two peaks in most cases, which overlapped with the other forms (see Section 4.2.3). In particular, it was difficult to discriminate between the completely and partially amidated forms (Figure 4.15). To discriminate their isotopes, a resolution of at least $R_{FWHM} = 33000$ is required.

The above examples reveal the limitations of the LC-MS methods used in this work and underline the importance of effective chromatographic separation for identification of cell wall peptides, especially when amidations need to be distinguished. The resolution of the mass spectrometer becomes a critical factor if sufficient chromatographic separation of the molecules is not achieved, although the chromatography method can certainly be further optimised. However, the substrates alone exhibit a wide range of masses and retention times, whilst the products tend to be found in the lower range. Methods for simultaneous detection of substrates and products can therefore only represent a compromise. The use of isolated, clearly characterised peptides would be advantageous. Nevertheless, mass spectrometry is a valuable tool and extends the possibilities of a purely LC-based approach by the ability to identify fragments quite unambiguously by their mass.

5.2.2. DppA de-amidates *meso*-Dpm in cell wall peptides of *B. subtilis*

DppA was previously described as Zn protease with a high specificity for the D-isomer of alanine [91]. It shares these properties with VanX or VanX-like enzymes, but is not related to them, as it differs from them in structure, by the characteristic sequence motif SXDXEG, and many other features [91, 96].

The reported zinc dependence and D-Ala-specific aminopeptidase activity [91] could be confirmed in this work. In addition, D-Ala-*meso*-Dpm was shown to be a suitable substrate, albeit with a low turnover rate (Figure 4.14, Section 4.2.3). It was striking that despite long incubation times, no decrease in the substrate D-Ala-2,6-Dpm was detected and relatively little Dpm was released. The second chemically synthesised substrate, *rac*-2,6-Dpm-D-Ala_2, also contained *meso*-Dpm and D-alanine, but D-alanine constituted the C-terminal end. With this substrate, enzymatic activity of DppA was not immediately apparent (Figure 4.13, Section 4.2.3). The measured values showed a, albeit very slight, product formation. This could mean that DppA binds its products. In comparison with the observations made for YkfA with the same substrate (Figure 4.17, Section 4.2.4), the intensities determined for Dpm and Ala_2 in the controls are interesting: these were clearly higher in the experiment with DppA than with YkfA. While the incubation time in the experiment with DppA was 17 h, it was only 1 h for YkfA. Therefore, the high initial values for the products (i. e. in the control without DppA) in the experiment with DppA, could be the result of heat-induced decay. The low turnover of the

racemic substrates by DppA is interesting, as it supports the specificity for the *meso*-form of Dpm inferred by chromatographic analysis of the stereoisomers. Both chemically synthesised substrates contained the racemate 2,6-Dpm, of which *meso*-Dpm was only one isomer. Complete conversion was therefore not expected.

In addition to the specificity for only one of the Dpm isomers, the low turnover rate could, however, also indicate another, somehow related activity. It might also be the consequence of a substrate specificity for a very similar but not identical binding. No activity was observed with peptides obtained from peptidoglycan of *E. coli*. With peptides from *B. subtilis*, on the other hand, an activity was indeed observed. However, this was not a cleavage of the bond between Ala and Dpm, but a shift from predominantly amidated forms to less or non-amidated forms in individual peptides. Thus, a de-amidation, or more precisely a de-amidation of Dpm, could be observed. Remarkably, for peptides with more than one Dpm amidated (Dpm_2-Ala and tripeptide-Ala-Dpm), not all amidated Dpm residues were de-amidated. Rather only some of the amidations were removed. As shown in Figure 5.2, the amino groups of the Dpm residue are exposed depending on their bonding state. In Dpm_2-Ala and tripeptide-Ala-Dpm, one Dpm is in a LD-bond with D-Ala, the other in a DD-bond with D-Ala. Whilst in the LD-bound *meso*-Dpm the adjacent amino and amido groups on the D-side and the amino group on the L-side are exposed, the situation is different in the DD-bound *meso*-Dpm. There, the L-side amino group is either exposed (Dpm_2-Ala) or not (tripeptide-Ala-Dpm). The observation that no peptides were de-amidated by DppA in which the L-sided amino groups of all Dpm residues are involved in a bond should also be understood in this respect. This concerns the frequently occurring cross-linked tri-tetrapeptide in *B. subtilis*. The spatial accessibility of the amino groups therefore seems to be of crucial importance for DppA. Conceivably, DppA only removes the amidation on the D-side of Dpm, which also has a free NH_2 terminus. This is supported by the fact that de-amidation of tripeptide-Ala-Dpm, Dpm and Dpm_2-Ala occurred. In contrast, amidated tri-, tetra- and pentapeptide were not de-amidated by DppA, although these also have free D-amino groups. As discussed above, in tripeptide-Ala-Dpm, Dpm_2-Ala, and likewise in single Dpm, not only the D-side NH_2 group is exposed, but also the L-side.

DppA assembles in an octameric structure [91]. Both amino groups may therefore play a role in the correct positioning of the substrate in the protein's binding pockets.

The amino group of an amidation and the amino groups of non-amidated peptides are similar in principle, yet not identical. This similarity might be sufficient for DppA to accept the synthesised D-Ala-*meso*-Dpm as substrate and to cleave it slowly. However, degradation of the peptidoglycan probably does not produce D-Ala-*meso*-Dpm, but *meso*-Dpm-D-Ala only. This would explain why cell wall peptides of *E. coli* were not cleaved. In *B. subtilis*, the preferred substrate, amidated peptides, is present in excess.

The importance of Dpm amidation is further emphasised by the fact that a *dppA* deficient mutant accumulates amidated Dpm, amidated Dpm-Ala and amidated Dpm-Ala_2 intracellularly, especially in the stationary growth phase. It is debatable what necessity there is for the cell to maintain a stock of de-amidated Dpm. This aspect will be revisited below.

As already mentioned, the previously reported specificity of DppA for D-Ala [91] could be confirmed in this work. Nonetheless, the turnover rate reported there for oligopeptides indicated a rather slow hydrolysis. Here, too, only a low hydrolytic activity towards D-Ala-*meso*-Dpm was found. However, DppA was also found to be specific for *meso*-Dpm and de-amidated *meso*-Dpm in cell wall peptides of *B. subtilis*. These results give reason to reconsider the classification as a D-alanyl-aminopeptidase. A designation as de-amidase seems more appropriate in view of its

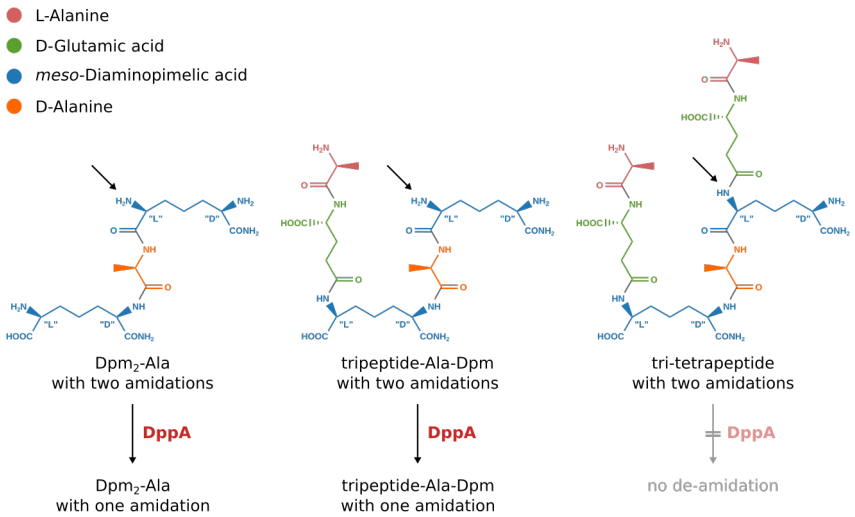

Figure 5.2.: DppA's de-amidation activity is dependent on the accessibility of the amino groups of *meso*-Dpm. Shown are the structures of Dpm_2-Ala (left), tripeptide-Ala-Dpm (middle), and tri-tetrapeptide (right) with amidated *meso*-Dpm. In *B. subtilis*, the D-side carboxy group of *meso*-Dpm is amidated by AsnB to an amido group [11, 23, 24]. De-amidation by DppA was observed for amidated Dpm_2-Ala and amidated tripeptide-Ala-Dpm only, but not for amidated tri-tetrapeptide. In the former two, the adjacent amino and amido groups on the D-side and the amino group on the L-side (marked by tilted arrows) are exposed. In amidated tri-tetrapeptide, the adjacent amino and amido groups on the D-side are exposed only.

activity.

5.2.3. YkfA cleaves LD-bonds between *meso*-Dpm-D-Ala

YkfA is assigned to the group of serine peptidases and shows sequence similarity (30 %) to LdcA of *E. coli* [65, 66] and *Pseudomonas aeruginosa* [134]. Accordingly, it was annotated as LD-carboxypeptidase in the UniProt database (UniProt accession number O34851) [113]. LdcA is part of the cell wall recycling pathway in *E. coli* and *P. aeruginosa*, and hydrolyses tetrapeptide into tripeptide in the cytoplasm by elimination of the carboxy-terminal D-Ala [65, 66].

Initial indications of its function were provided by incubating YkfA with the chemically synthesised substrates D-Ala-*rac*-2,6-Dpm and *rac*-2,6-Dpm-D-Ala_2 (Section 4.2.4). While YkfA showed no enzymatic activity towards the former (which does not possess a carboxy-terminal D-Ala), it cleaved *rac*-2,6-Dpm-D-Ala_2 into Dpm and Ala_2, although not completely (Figure 4.17). The incomplete cleavage of this racemic substrate suggests that only bonds between certain Dpm isomers and D-Ala were cleaved. As with DppA, a specificity for the *meso*-isomer would be obvious, since this occurs naturally in the peptidoglycan of *B. subtilis*. The analysis was done by LC-MS only, which is why it could not be determined which isoform of Dpm was released. A derivatisation with OPA reagent would undoubtedly be helpful to confirm or disprove the assumed specificity for *meso*-Dpm.

The observed degradation of tetrapeptide as well as the release of tripeptide with peptides from *E. coli* (Figure 4.18) seems to support the classification as LD-carboxypeptidase. It has to be taken into account, however, that mixtures of cell wall peptides served as substrate in this work. Consequently, products could not be definitively assigned to a specific substrate peptide. Nevertheless, the following assumptions can be made.

Tetrapeptide-Ala-Dpm as well as Dpm-Ala (or, less likely, Ala-Dpm) were also degraded by YkfA and a compound with the mass of pentapeptide and Dpm were released in addition to tripeptide (Figure 4.18, Section 4.2.4). Tripeptide could also have been released from tetrapeptide-Ala-Dpm. Since no Dpm_2-Ala was released, however, two different bonds would have had to be cleaved in this case: the LD-bond between *meso*-Dpm and D-Ala of the tetrapeptide and the DD-bond between *meso*-Dpm of the tetrapeptide and D-Ala of the dipeptide Dpm-Ala (see Figure 5.3). More likely, and implicating the formation of a pentapeptide, is the cleavage of the Dpm with an exposed D-side. This cleavage would release Dpm as well as a peptide with the mass of a pentapeptide – as it was observed in this work (Figure 4.18, Section 4.2.4). Depending on the constitution of tetrapeptide-Ala-Dpm (or pentapeptide-Dpm), the released pentapeptide corresponded to canonical pentapeptide (L-Ala-D-Glu-*meso*-Dpm-D-Ala_2) or to a pentapeptide which has the linear structure of tetrapeptide (L-Ala-D-Glu-*meso*-Dpm-D-Ala) and in which the D-carboxy group of the *meso*-Dpm was substituted with D-Ala (hence referred as tetrapeptide-Ala). To generate canonical pentapeptide, a LD-bond between *meso*-Dpm and *meso*-Dpm in pentapeptide-Dpm needs be cleaved, to generate tetrapeptide-Ala a LD-bond between *meso*-Dpm and D-Ala in tetrapeptide-Ala-Dpm. Although cross-links via LD-bonds between two *meso*-Dpm occur with a frequency of 1.7 % to 5.2 %, [17] in the peptidoglycan of *E. coli*, there is no experimental evidence for the presence of pentapeptide-Dpm. The cleaved compound is therefore likely to have been tetrapeptide-Ala-Dpm and the product tetrapeptide-Ala. In the context of two different constitutions, the observed occurrence of tetrapeptide-Ala-Dpm in two peaks is also interesting. Only one of the two forms was degraded by YkfA.

With peptides from *B. subtilis*, the situation was incomparably more complicated due to

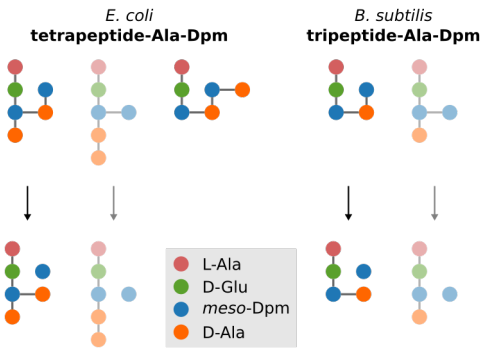

Figure 5.3.: Theoretical constitutions of tetrapeptide-Ala-Dpm from *E. coli* and tripeptide-Ala-Dpm from *B. subtilis*. For *E. coli* from left: Tetrapeptide-Ala-Dpm (with LD-cross-linking between *meso*-Dpm and D-Ala-*meso*-Dpm), pentapeptide-Dpm (with LD-cross-linking between *meso*-Dpm; faded representation, as hypothetical constitution without experimental evidence) and tripeptide-Ala_2-Dpm (with two DD-cross-links between *meso*-Dpm and D-Ala and one LD-bond between *meso*-Dpm and D-Ala). Possible constitutions considering the products of YkfA: tetrapeptide-Ala from tetrapeptide-Ala-Dpm and pentapeptide from pentapeptide-Dpm. For *B. subtilis* from left: Tripeptide-Ala-Dpm (ld cross-linking between *meso*-Dpm and D-Ala-*meso*-Dpm, [11, 23]) and tetrapeptide-Dpm (cross-linking between *meso*-Dpm; faded representation, as hypothetical constitution without experimental evidence) with simultaneous release of *meso*-Dpm. Possible constitutions of the products: Tripeptide-Ala and tetrapeptide, each with simultaneous release of *meso*-Dpm.

Dpm amidation (see Section 5.2.1), although a similar picture emerged here (Figures 4.19, 4.20, and 4.21 in Section 4.2.4). The degradation of partially and non-amidated tripeptide-Ala-Dpm, [Gly^4]tetrapeptide and amidated [Gly^5]pentapeptide resulted in the formation of tripeptide (amidated and non-amidated), Dpm, amidated Dpm-Ala, Ala-Gly and two compounds corresponding in mass to amidated and non-amidated tetrapeptide (Figures 4.19 and 4.20). Similar to tetrapeptide-Ala-Dpm from *E. coli*, two constitutions for tripeptide-Ala-Dpm are conceivable (see Figure 5.3): a cross-linking of tripeptide and Ala-Dpm via a DD-bond between *meso*-Dpm and D-Ala or a cross-linking of tetrapeptide and Dpm via a LD-bond between *meso*-Dpm and *meso*-Dpm. A hydrolysis of the LD-bond between *meso*-Dpm and D-Ala in the latter would have resulted in tripeptide-Dpm and D-Ala. Cross-links via *meso*-Dpm-*meso*-Dpm are rather uncommon, but usually occur between *meso*-Dpm and D-Ala [11, 23, 135]. Therefore, tripeptide-Ala-Dpm was probably tripeptide cross-linked via a LD-bond and D-Ala-*meso*-Dpm (Figure 5.3, [11, 23]). Cleavage products of this molecule would consequently be tripeptide-Ala and Dpm. Tripeptide-Ala differs in constitution from tetrapeptide, but their masses are identical. The two compounds released by YkfA, which were equivalent in mass to tetrapeptide, differed slightly in their retention times from those observed in the controls (Table 4.8). It is therefore not unlikely that these were indeed molecules with a deviating constitution.

The previous observations already indicated a cleavage of the bond between *meso*-Dpm and D-Ala by YkfA. Based on this, [Gly^4]tetrapeptide may have been cleaved into tripeptide and Gly, whereby the mass of the latter was too low for detection. Accordingly, the cleavage of amidated [Gly^5]pentapeptide should also have yield amidated tripeptide and Ala-Gly. Both was indeed observed, although the increase in tripeptide was small (Figure 4.20). At the same time, the amount of non-amidated tripeptide released appeared to be somewhat too high to

derive from the cleavage of [Gly^4]tetrapeptide alone (Figure 4.20). The degradation of amidated [Gly^5]pentapeptide was also observed with peptides from a *B. subtilis dacA* mutant (Figure 4.21). In contrast to its activity with cell wall peptides of the wild-type, YkfA released amidated tripeptide with peptides of the *dacA* mutant, but no Ala-Gly (Figure 4.21). Since its initial abundance was already quite low, Ala-Gly was perhaps below the detection limit. It should be taken into account that no standards for amidated or non-amidated [Gly^4]tetrapeptide and [Gly^5]pentapeptide were available. The assignment was therefore based on mass alone and the actual constitution is not known, although Atrih *et al.* [11] reported the occurrence of [Gly^5]pentapeptide in a *B. subtilis dacA* mutant. The release of amidated tetrapeptide from peptides of the *dacA* mutant by YkfA is also somewhat puzzling. The retention time pointed to a different constitution from tetrapeptide, as previously observed with peptides of the wild-type. However, tripeptide-Ala-Dpm with any degree of amidation was hardly detected among the peptides of the *dacA* mutant. Given the replacement of tripeptide by pentapeptide in a *B. subtilis dacA* mutant, the observations with tripeptide of the wild-type and pentapeptide of the *dacA* mutant are at least consistent with respect to a LD-carboxypeptidase activity. Tripeptide and Ala_2 can be considered as products.

While the observations with peptides from *E. coli* gave a fairly clear picture, conclusions with peptides from *B. subtilis* were not straightforward. Viewed as a whole, there was notwithstanding some evidence that YkfA has an enzymatic activity comparable to that of LdcA. The cleavage by YkfA occurs between Dpm and the following D-Ala, as the experiment with chemically synthesised *rac*-2,6-Dpm-D-Ala_2 showed (Figure 4.17). This is also supported by the intracellular accumulation of Dpm-Ala and Dpm-Ala_2 in a *ykfA* mutant (Figure 4.22, Section 4.2.4).

The meaning of the L-side of *meso*-Dpm in binding with D-Ala for a LD-carboxypeptidase is obvious. However, in the case of YkfA, the D-side of *meso*-Dpm also appears to be of particular importance, since enzymatic activity was only observed for peptides with a supposedly unbound D-side. Likewise, LdcA from *E. coli* and *P. aeruginosa* were reported to not cleave cross-linked peptides [66, 134]. It is conceivable that YkfA recognises substrates basically via the D-side of *meso*-Dpm and cleaves on the L-side. In contrast to LdcA from *E. coli*, YkfA in *B. subtilis* is confronted with amidated *meso*-Dpm. One of the carboxy groups (COOH) in *meso*-Dpm is thus amidated to a carbamoyl group ($CONH_2$). Usually, the D-side carboxy group is amidated [11, 23] and hence the side that is probably recognised by YkfA. The carbamoyl group shows certain similarities to peptide bonds and thereby to the bond between the L-side carboxy group of *meso*-Dpm and the amino group of D-alanine. However, while in the peptide bond the amino group is substituted and cleavage can occur through YkfA, NH_2 already represents a terminus in the carbamoyl group. Possibly, the amidation of the D-side carboxy group also masks the carboxy group and in this way hinders recognition by YkfA.

YkfA, LdcA of *E. coli* and the LdcA homologue of *P. aeruginosa* have a comparable size and are assigned to the same protein family (see above). Furthermore, the catalytically important amino acids Ser115, Glu217 and His285 identified in the homologue of *P. aeruginosa* [134] find their counterparts in YkfA (Ser116, Glu214, His284; sequence comparison with MAFFT [107]). Like LdcA [66], YkfA did not cleave cross-linked peptides, but was able to cleave LD-bonds between *meso*-Dpm and D-Ala. In contrast to LdcA [65, 66], YkfA also degraded canonical pentapeptide to a certain degree. In the same direction, the similarity between pentapeptide and the chemical substrate *rac*-2,6-Dpm-D-Ala_2 cleaved by YkfA should also be pointed out. Even if these aspects are not entirely conclusive in themselves, they somewhat tarnish the picture of YkfA as a LD-carboxypeptidase. Since in *B. subtilis*, tripeptide rather than tetrapeptide is

usually part of the peptidoglycan [11, 23], the purpose of YkfA is probably not identical to LdcA. Therefore, it would be interesting to compare the activity of LdcA towards cell wall peptides of *B. subtilis* in future studies.

5.2.4. YkfC acts as an γ-D-Glu-*meso*-Dpm-endopeptidase

YkfC was previously described as an γ-D-Glu-L-Lys endopeptidase [69]. Investigations of its crystal structure and amino acid sequence classified it as a representative of the NlpC/P60 protein family [89]. Together with homologues from other Bacilli, but also from other phyla, it forms a subgroup within this protein family [88, 89].

In this work, the enzymatic activity of YkfC was investigated for the first time with cell wall peptides. YkfC cleaved both the tripeptide typically found in *B. subtilis* as well as the tetrapeptide of *E. coli* (Figures 4.23 and 4.24, Section 4.2.5). It was particularly interesting that the enzymatic activity of YkfC was not limited to unbranched peptides but also extended to branched peptides, such as the frequently occurring tri-tetrapeptide of *B. subtilis* (Figure 4.25) and tetra-tetrapeptide of *E. coli* (Figures 4.23). Products of this cleavage were, on the one hand, the dipeptide Ala-Glu and, on the other hand, corresponding Dpm-containing counterparts. This was a clear indication that YkfC indeed cleaved the bond between Glu and *meso*-Dpm in cell wall peptides. Interestingly, and despite almost all Dpm residues are amidated in *B. subtilis* [11, 23], peptides were cleaved. When peptides from *B. subtilis* served as substrate, products appeared both amidated and non-amidated. The same applies to the unusual peptides of a *B. subtilis dacA* mutant (Figures 4.24 and 4.25). This mutant lacks the DD-carboxypeptidase necessary for shortening the pentapeptide, whereby pentapeptide instead of tripeptide is incorporated into the peptidoglycan [11]. Nevertheless, YkfC cleaved both unbranched pentapeptide and branched penta-tetrapeptide, releasing dipeptide and corresponding Dpm-containing fragments. The cleavage of pentapeptide was surprising as an intermediate of the peptidoglycan biosynthesis, Lipid II, also contains pentapeptide. An uncontrolled interference with such an essential process for cell survival would be fatal. However, these concerns could be dispelled, as YkfC showed no enzymatic activity when incubated with Lipid II (Figure 4.27). The reason probably lies in the accessibility of the N-terminus: In Lipid II, pentapeptide is linked to MurNAc via L-Ala, whereby it has an exposed C-terminus but no free N-terminus. The same is true for cross-linked muropeptides in the peptidoglycan, where both L-Ala termini are linked to a MurNAc. Consequently, YkfC showed activity towards muropeptides from *E. coli* and *B. subtilis* by cleaving dipeptide only from free termini not bound to MurNAc (Figure 4.26).

With its activity YkfC is reminiscent of LytE and CwlO, which act as autolysins during cell growth and allow cell enlargement by cleaving cross-linked peptides [136, 137]. Notwithstanding the common specificity for the γ-D-Glu-*meso*-Dpm binding and the common membership in the NlpC/P60 protein family, YkfC only cleaved peptides with free termini, i. e. not organised in the peptidoglycan mesh. This is consistent with previous studies by Xu *et al.* [89], who, by examining the crystal structure of YkfC, concluded that only peptides with exposed L-Ala termini could serve as substrates [89]. Both LytE and CwlO act extracellularly and predominantly during cell growth [136, 137], whereas YkfC appears to be active in the cytoplasm during the stationary growth phase. This assumption was based on the apparent co-regulation of *ykfABCD* with the *dppABCDE* operon, which is expressed at the onset of the stationary growth phase [83, 84, 86].

In summary, this work demonstrated that YkfC cleaves cell wall peptides of *E. coli* and

B. subtilis between Glu and Dpm. This confirmed the previous classification as a γ-D-Glu-Dpm endopeptidase on the basis of the amino acid sequence and investigations with peptide analogues [69]. Furthermore, it was shown that cleavage by YkfC occurred independently of binding state and amidation of *meso*-Dpm. YkfC is thus clearly different from DppA and YkfA in these two aspects. Due to its specificity for D-Glu-*meso*-Dpm bindings, the substrate spectrum of YkfC includes virtually all peptides occurring in the peptidoglycan.

5.2.5. *meso*-Dpm as main product of the concerted activity of DppA, YkfA and YkfC

The specific functions for each of the three enzymes DppA, YkfA and YkfC were already indicated, when they were applied individually. Both the *dppABCDE* and the *ykfABCD* operon are directly or indirectly controlled by the same regulator and are only separated by a weak transcriptional terminator [83, 87]. Based on this, it is likely that both operons are expressed at the same time. In a physiological context, DppA, YkfA and YkfC may therefore be active simultaneously, raising the question of possible synergistic effects. To investigate this, the enzymes were analysed in a combined enzymatic digest.

The combination of DppA and YkfC did not initially lead to any further findings, except that DppA also de-amidated Dpm_2-Ala released by YkfC from peptides of *B. subtilis* (Figure 4.28, Section 4.2.6). The combination of YkfA with YkfC showed that YkfA cleaves mainly the less strongly amidated products of YkfC (Figure 4.29). This behaviour was already indicated by tripeptide Ala-Dpm with YkfA alone (Figure 4.19, Section 4.2.4). Very revealing was the cleavage of Dpm_2-Ala_2 by YkfA (Figure 4.29A). This compound most likely represents the cross-linking of tetra-tetrapeptide, released by YkfC from *E. coli* peptides. The fact that the combination of both enzymes did not release Dpm-Ala but Dpm-Ala_2 proofed that YkfA only cleaves the LD-bond between D-Ala and the *meso*-Dpm whose D-side was exposed. The addition of DppA, i. e. the combination of all three enzymes, apparently also removed the obstacle of Dpm amidation (Figures 4.30 and 4.31). Namely, de-amidation of completely amidated Dpm_2-Ala (*B. subtilis* wild type) and Dpm_2-Ala_3 (*B. subtilis dacA* mutant) cleared the way for YkfA. End products of this concerted activity were, in the case of *B. subtilis* wild-type cell wall peptides, Dpm-Ala, both amidated and non-amidated, and Dpm. One product of YkfC was Dpm_2-Ala, which was probably released from tri-tetrapeptide. It can therefore be assumed that in Dpm_2-Ala D-alanine was linked to one *meso*-Dpm via a DD-bond and to the second one via a LD-bond. YkfA most likely only cleaved the latter bond, as it was previously shown for Dpm_2-Ala_2 from *E. coli*. Further cleavage of Dpm-Ala did not occur due to lack of DD-endopeptidase activity. DppA, although hydrolytically active against bonds between D-alanine and *meso*-Dpm and thus potentially active against DD-bonds between these two amino acids, showed no hydrolytic activity towards cell wall peptides. Possibly an activation factor was missing, albeit a need for zinc was reported only [91]. It therefore remains elusive whether D-Ala-*meso*-Dpm and *meso*-Dpm-D-Ala represent enantiomers that are discriminated by DppA. In analogy to the findings just described, the end products of the concerted activity of DppA, YkfA and YkfC on peptides of a *B. subtilis dacA* mutant were mainly amidated Dpm-Ala_3 and Dpm (Figure 4.31).

meso-Dpm is important for all three enzymes and ultimately the concerted activity results in the generation of *meso*-Dpm. It thus seems evident that *meso*-Dpm plays a major role in peptide recycling, if not the key role. However, this conclusion raises some questions: What is the role of amidation in the context of possible intracellular utilisation? What is the benefit of

intracellular accumulation of Dpm? Furthermore, if Dpm is so important, why is the DD-bond in Dpm-Ala not cleaved? To the best of my knowledge, no corresponding DD-endopeptidase activity is known to date in *B. subtilis*. The fate of this compound could simply be due to the lack of a DD-hydrolytic activity or very slow hydrolysis. Dpm-Ala might be reused directly for cross-linking. Assuming there is DD-endopeptidase activity, DppA, YkfA and YkfC may not face Dpm-Ala physiologically at all. Further investigations to answer these questions can be the scope for further research.

The presence of amidated Dpm influences the activity of extracellular autolytic enzymes such as LytE and CwlO, with the absence of the amidation leading to increased autolytic activity [24]. Amidation thus plays an important role in the coordination of critical processes affecting the integrity of the cell wall, such as cell division and growth [24]. This means that the amidation has a regulatory function extracellularly. In vitro, and therefore presumably also intracellularly, the importance of amidation is different. YkfC, on the one hand, did not discriminate the degree of amidation. YkfA, on the other hand, showed a certain dependence on and a strict specificity for de-amidated Dpm in order to be able to develop its full activity. Appropriately, DppA removed the amidations. Amidation was thus ultimately only important for YkfA. If cell wall peptides or fragments are present intracellularly, they do not pose a threat to the integrity of the cell wall, even without amidation of the Dpm residues. Whether Dpm is amidated or not is also considered irrelevant for the biosynthesis of peptidoglycan, albeit essential to maintain a stable cell wall and avoid uncontrolled autolysis [24, 138]. De-amidation by DppA to increase the activity of YkfA seems reasonable in this respect. It remains to be answered if this dependence on YkfA has a regulatory benefit or is merely a side effect of the fact that *B. subtilis* amidates indeed those carboxy groups that are relevant for carboxypeptidases. Likewise, substrates of YkfA could themselves fulfil a regulatory function. Besides Dpm-Ala and Dpm-Ala_2, a *ykfA* mutant also accumulated dipeptide and tripeptide. Dipeptide is a product of YkfC and is processed in the form of L-Ala-D-Glu by the epimerase YkfB into L-Ala-L-Glu [69]. Its degradation would only be visible if the LL-isomer was processed directly. Tripeptide can be cleaved by YkfC and, according to the findings of this work, does not represent a substrate for YkfA. However, other products of YkfC can be cleaved by YkfA. The accumulation of these peptides could indeed lead to a feedback inhibition of YkfC in order to regulate its hydrolytic activity. Conceivably, the cell could thus direct the flow of amino acids towards peptidoglycan synthesis or towards catabolism.

In *B. subtilis*, the aspartic acid metabolism is of central importance, as it serves as starting point for various metabolic pathways: for protein synthesis and for the formation of *meso*-Dpm for peptidoglycan synthesis [139]. This is illustrated by the fact that depletion or lack of Asp leads to the collapse of peptidoglycan synthesis [139]. Exogenously available *meso*-Dpm allows the cell to partially compensate for the devastating effects [139]. Maintaining an intracellular supply of *meso*-Dpm would help alleviate the singular dependence on Asp availability. This applies in particularly with regard to the competitive demand for Asp for protein synthesis and peptidoglycan synthesis, which is even more critical under general nutrient deficiencies.

5.2.6. Physiological importance of *dppABCDE* and *ykfABCD*

It was previously suspected that the genes of the *dppABCDE* operon and thus indirectly also the genes of the *ykfABCD* operon play a role in the adaptation of the cell to nutrient deficiency [83, 84]. Both putative operons are up-regulated in the phase of stationary growth, and thus

under conditions with potential nutrient deficiency [83, 84, 86]. The increased accumulation of intermediates found here in a *dppA*-deficient mutant is consistent with this (Figure 4.16, Section 4.2.3). Therefore, the intra- and extracellular accumulation of cell wall peptides in *dppABCDE* and *ykfABCD* mutants as well as in a *dppABCDE ykfABCD* double mutant was investigated in this work (Figure 4.34, Section 4.2.7). The *dpp* mutant accumulated no peptides intracellularly and mainly unbranched peptides extracellularly. Since this mutant, in addition to DppA, lacks the putative ABC transporter DppBCDE, these results confirm the description as peptide transporter [84]. As expected, the loss of *ykfABCD* led to the intracellular accumulation of unbranched peptides. Nevertheless, a minor extracellular accumulation was also detectable. Since both operons are adjacent and co-regulated [83], a functional link between uptake and degradation is convincing. Consequently, the *dppABCDE ykfABCD* double mutant was expected to behave like the *dppABCDE* mutant, i. e. showing extracellular but no intracellular accumulation. Instead, it behaved like the *ykfABCD* mutant. This initially suggested that the *dppABCDE* operon was not correctly deleted. In addition, the double mutant resembled the *ykfABCD* mutant in its growth behaviour and the *dppABCDE* mutant in its morphological appearance and CFU in growth experiments (Figure 4.32). The ambivalent behaviour of these mutants (kindly provided by Marjorie Dauvin) at least raises doubts, for which reason no conclusive consideration is given here in this regard. In subsequent studies, verification of the DNA sequences should be considered. In any case, the drastic changes in the morphological appearance of the *ykfABCD* mutant were striking, manifesting themselves in translucent and extremely small colonies (Figure 4.32C). Although this did not negatively affect the number of viable colonies (Figure 4.32B) or the morphology of individual cells (Figure 4.33), a certain significance can be deduced from this. Morphological changes might have gone undetected at the resolution of a light microscope and an electron microscope would be more revealing. The *dppABCDE* mutant had the lowest number of CFU after 72 h, but apart from this it did not show drastic phenotypic changes (Figure 4.32C).

Besides Dpp, *B. subtilis* encodes another ABC transporter, namely the Opp transporter [85]. It plays an important role especially for both sporulation and competence [140, 141]. Opp transports peptides consisting of 3 to 5 amino acids [140, 141]. In addition, there is a third ABC transporter, App (inactive in the laboratory strain 168), which can compensate a loss of Opp [142]. The Opp systems of the Gram-negative organisms *E. coli* and *Salmonella typhimurium* have been described as essential for the recycling of cell wall peptides [143]. It is therefore somewhat surprising that OppA from *S. typhimurium* is quite non-specific and transports di- to pentapeptides regardless of their sequence [144]. In this context, it is also interesting that *E. coli* has another binding protein besides OppA, MppA, which complements the Opp transporter to specifically take up tripeptide of the cell wall [71]. The Dpp transporter in *B. subtilis* may have a similar function, although it is not only a binding protein, but an entire ABC transporter [84, 85]. An involvement in the recycling of cell wall peptides, however, challenges the previously postulated specificity for dipeptides [84]. On the one hand, the enzymes YkfA and YkfC also degraded larger peptides and, on the other hand, a *dppABCDE* mutant also accumulated larger peptides in the supernatant. The accumulation of unbranched peptides in the *dppABCDE* mutant implies that even larger and cross-linked peptides are taken up elsewhere or that there is a yet unknown intra- or extracellular DD-endopeptidase activity. If so, the activity of YkfC towards branched peptides would presumably only be a consequence of the specificity for γ-D-Glu-*meso*-Dpm binding, which does not require intracellular regulation. A DD-endopeptidase activity also appears to make sense in that DppA, YkfA and YkfC cannot degrade Dpm-Ala even together. A

DD-endopeptidase has already been characterised for *E. coli*, which can cleave D-Ala-*meso*-Dpm bonds [48, 49] and is believed to be involved in autolysis [145, 146]. So far, no comparable enzyme has been identified in *Bacillus* or Gram-positive bacteria. Whether DppA, YkfA and YkfC are confronted with Dpm_2-Ala cross-links in vivo therefore remains open.

Taken together, each of the three enzymes DppA, YkfA and YkfC seems to fulfil a specific function: DppA removes amidations, YkfA cleaves bonds between *meso*-Dpm and D-Ala, and YkfC cleaves bonds between D-Glu and *meso*-Dpm. In a physiological context in which DppA, YkfA and YkfC are jointly active, the distribution of tasks could be outlined as follows (Figure 5.4): In the initial step, YkfC cleaves the bond between D-Glu and *meso*-Dpm within cell wall peptides, yielding dipeptide and peptide fragments with Dpm residues with a free D-side. The dipeptide is epimerised by YkfB and can thus be further utilised [69]. Dpm-containing fragments are processed depending on their degree of amidation. Amidated *meso*-Dpm residues are de-amidated by DppA, fragments with non-amidated *meso*-Dpm are cleaved by hydrolysis of the LD-bond between *meso*-Dpm and D-Ala by YkfA. The *meso*-Dpm thus released can be reused in the peptidoglycan synthesis. D-Ala is also relevant for the assembly of the peptidoglycan [147] and could therefore experience the same fate.

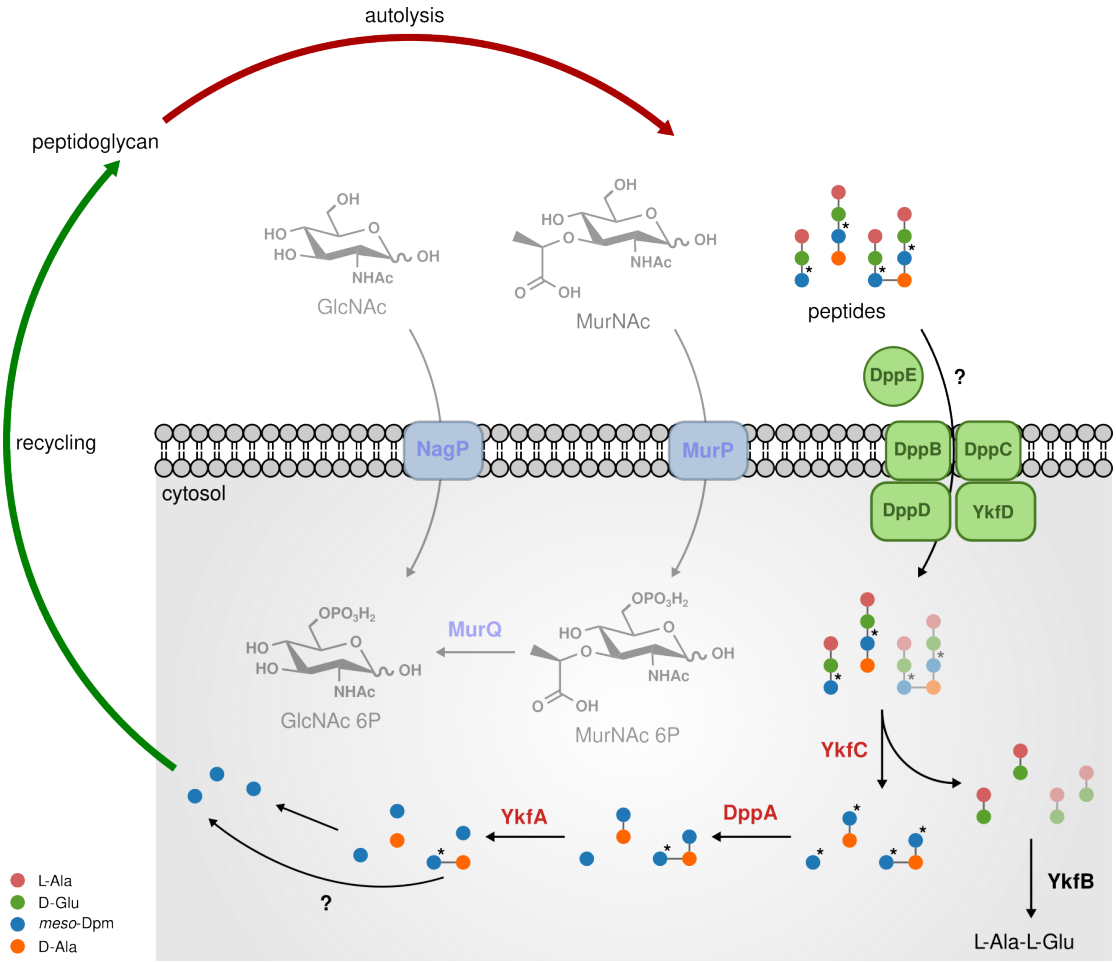

Figure 5.4.: Proposed pathway for recycling of cell wall peptides in *B. subtilis*. Peptides released by autolysis may be taken up via Dpp (possibly requiring YkfD as second nucleotide-binding domain). In the cell, YkfC cleaves the bond between D-Glu and *meso*-Dpm under formation of the dipeptide L-Ala-D-Glu and corresponding Dpm-containing fragments. YkfC does not discriminate between Dpm and amidated Dpm (asterisks indicate amidations). The dipeptide is converted into L-Ala-L-Glu by the epimerase YkfB. If present, DppA removes amidations from amidated *meso*-Dpm. Subsequently, YkfA can cleave the LD-bond between *meso*-Dpm and D-Ala. Non-amidated fragments can be cleaved directly. End products of this concerted activity are amidated *meso*-Dpm-D-Ala, *meso*-Dpm and D-Ala, of which *meso*-Dpm can be recycled in peptidoglycan synthesis. D-Ala might also be used for this purpose. Cross-linked peptides are shown faded, as it is uncertain whether they are cleaved or not. The cleavage of cross-links requires DD-endopeptidase activity for which a corresponding enzyme has not yet been described in *B. subtilis*. Irrespective of this, cross-linked peptides were cleaved in vitro by YkfC.

5.3. Closing words

All bacteria are confronted with situations of nutrient deficiency and resource scarcity in their life cycle, which is why strategies for coping with these unpleasant living conditions are indispensable. One strategy is sporulation, which is an elaborate process that involves a fundamental remodelling of the cell envelope. Once initiated, it cannot simply be reversed. Sporulation is thus a sophisticated developmental process that occurs only in a limited number of bacterial species such as *B. subtilis*. Cell wall recycling is another compelling and more adaptable strategy that many bacteria employ. Recycling in general is understood as the concept of reusing degradation products. In bacteria, this means recycling their own cellular components, including the peptidoglycan cell wall. As the effort to recycle raw materials is not higher than their synthesis, recycling is an ecological and economical process, which can reduce the demand for resources. Even more so in environmental conditions, where nutrients are limited. In this respect, it is only consistent that bacteria, especially in the stationary growth phase, recycle degradation products that are inevitably produced by autolysis of their cell wall during their life cycle. The glycan chains of the peptidoglycan are basically constructed in the same way in all known bacteria. Despite this, the present work showed that variations of the common scheme in recycling the glycan part occur in different bacteria. The composition of the peptides, on the other hand, is more diverse. Whether there is a single, universal recycling mechanism for peptides is thus questionable. Rather, it is conceivable that similar enzyme cascades for uptake and degradation of cell wall peptides have evolved in organisms with similar peptide structures. Irrespective of this, the recycling of cell wall sugars and peptides can be understood as an adaptation to changed living conditions as a result of nutrient deficiency, which ensures the survival of the individual cell in the long term.

This work revealed further aspects about the mechanisms of sugar uptake and recycling in Gram-positive bacteria. Furthermore, it presents a possible recycling pathway for cell wall peptides in *B. subtilis* in detail. These findings contribute to a better and deeper understanding of the little-studied processes of cell wall recycling in Gram-positive bacteria.

Bibliography

1. Woese, C. R., Kandler, O. & Wheelis, M. L. Towards a natural system of organisms: Proposal for the domains Archaea, Bacteria, and Eucarya. *Proceedings of the National Academy of Sciences* **87,** 4576–4579 (1990).
2. Bar-On, Y. M., Phillips, R. & Milo, R. The biomass distribution on Earth. *Proceedings of the National Academy of Sciences* **115,** 6506–6511 (2018).
3. Armstrong-Esther, C. A. & Smith, J. E. Carriage patterns of *Staphylococcus aureus* in a healthy non-hospital population of adults and children. *Annals of Human Biology* **3,** 221–227 (2009).
4. Tong, S. Y. C., Davis, J. S., Eichenberger, E., Holland, T. L. & Fowler Jr., V. G. *Staphylococcus aureus* Infections: Epidemiology, Pathophysiology, Clinical Manifestations, and Management. *Clinical Microbiology Reviews* **28,** 603–661 (2015).
5. Cabeen, M. T. & Jacobs-Wagner, C. Bacterial cell shape. *Nature Reviews Microbiology* **3,** 601–610 (2005).
6. Vollmer, W., Blanot, D. & de Pedro, M. A. Peptidoglycan structure and architecture. *FEMS Microbiology Reviews* **32,** 149–167 (2008).
7. Boneca, I. G., Huang, Z.-H., Gage, D. A. & Tomasz, A. Characterization of *Staphylococcus aureus* Cell Wall Glycan Strands, Evidence for a New β-*N*-Acetylglucosaminidase Activity. *Journal of Biological Chemistry* **275,** 9910–9918 (2000).
8. Bera, A., Herbert, S., Jakob, A., Vollmer, W. & Götz, F. Why are pathogenic staphylococci so lysozyme resistant? The peptidoglycan *O*-acetyltransferase OatA is the major determinant for lysozyme resistance of *Staphylococcus aureus*. *Molecular Microbiology* **55,** 778–787 (2004).
9. Vollmer, W. Structural variation in the glycan strands of bacterial peptidoglycan. *FEMS Microbiology Reviews* **32,** 287–306 (2008).
10. Zipperle Jr., G. F., Ezzell Jr., J. W. & Doyle, R. J. Glucosamine substitution and muramidase susceptibility in *Bacillus anthracis*. *Canadian Journal of Microbiology* **30,** 553–559 (1984).
11. Atrih, A., Bacher, G., Allmaier, G., Williamson, M. P. & Foster, S. J. Analysis of Peptidoglycan Structure from Vegetative Cells of *Bacillus subtilis* 168 and Role of PBP 5 in Peptidoglycan Maturation. *Journal of Bacteriology* **181,** 3956–3966 (1999).
12. Wheeler, R., Mesnage, S., Boneca, I. G., Hobbs, J. K. & Foster, S. J. Super-resolution microscopy reveals cell wall dynamics and peptidoglycan architecture in ovococcal bacteria. *Molecular Microbiology* **82,** 1096–1109 (2011).
13. Wheeler, R. *et al.* Bacterial Cell Enlargement Requires Control of Cell Wall Stiffness Mediated by Peptidoglycan Hydrolases. *mBio* **6** (ed Casadevall, A.) (2015).

14. Hayhurst, E. J., Kailas, L., Hobbs, J. K. & Foster, S. J. Cell wall peptidoglycan architecture in *Bacillus subtilis*. *Proceedings of the National Academy of Sciences* **105,** 14603–14608 (2008).
15. Tipper, D. J. & Berman, M. F. Structures of the Cell Wall Peptidoglycans of *Staphylococcus epidermidis* Texas 26 and *Staphylococcus aureus* Copenhagen. I. Chain length and Average Sequence of Cross-Bridge Peptides. *Biochemistry* **8,** 2183–2192 (1969).
16. Schleifer, K. H. & Kandler, O. Peptidoglycan Types of Bacterial Cell Walls and their Taxonomic Implications. *Bacteriological Reviews* **36,** 407–477 (1972).
17. Glauner, B., Höltje, J.-V. & Schwarz, U. The Composition of the Murein of *Escherichia coli*. *Journal of Biological Chemistry* **263,** 10088–10095 (1988).
18. Walter, A. & Mayer, C. in *Extracellular Sugar-Based Biopolymers Matrices* (eds Cohen, E. & Merzendorfer, H.) 237–299 (Springer International Publishing, 2019).
19. Armstrong, J. J., Baddiley, J., Buchanan, J. G., Carss, B. & Greenberg, G. R. 882. Isolation and Structure of Ribitol Phosphate Derivatives (Teichoic Acids) from Bacterial Cell Walls. *Journal of the Chemical Society (Resumed),* 4344 (1958).
20. Brown, S., Santa Maria Jr., J. P. & Walker, S. Wall Teichoic Acids of Gram-Positive Bacteria. *Annual Review of Microbiology* **67,** 313–336 (2013).
21. Fischer, W. in *Advances in Microbial Physiology* (eds Rose, A. H. & Tempest, D. W.) 233–302 (Elsevier, 1988).
22. Percy, M. G. & Gründling, A. Lipoteichoic Acid Synthesis and Function in Gram-Positive Bacteria. *Annual Review of Microbiology* **68,** 81–100 (2014).
23. Warth, A. D. & Strominger, J. L. Structure of the Peptidoglycan from Vegetative Cell Walls of *Bacillus subtilis*. *Biochemistry* **10,** 4349–4358 (1971).
24. Dajkovic, A. *et al.* Hydrolysis of peptidoglycan is modulated by amidation of *meso*-diaminopimelic acid and Mg^{2+} in *Bacillus subtilis*. *Molecular Microbiology* **104,** 972–988 (2017).
25. Höltje, J.-V. Growth of the Stress-Bearing and Shape-Maintaining Murein Sacculus of *Escherichia coli*. *Microbiology and Molecular Biology Reviews* **62,** 181–203 (1998).
26. Vermassen, A. *et al.* Cell Wall Hydrolases in Bacteria: Insight on the Diversity of Cell Wall Amidases, Glycosidases and Peptidases Toward Peptidoglycan. *Frontiers in Microbiology* **10** (2019).
27. Mueller, E. A. & Levin, P. A. Bacterial Cell Wall Quality Control during Environmental Stress. *mBio* **11** (ed Garsin, D. A.) (2020).
28. Höltje, J.-V., Mirelman, D., Sharon, N. & Schwarz, U. Novel Type of Murein Transglycosylase in *Escherichia coli*. *Journal of Bacteriology* **124,** 1067–1076 (1975).
29. Blackburn, N. T. & Clarke, A. J. Identification of Four Families of Peptidoglycan Lytic Transglycosylases. *Journal of Molecular Evolution* **52,** 78–84 (2001).
30. Yunck, R., Cho, H. & Bernhardt, T. G. Identification of MltG as a potential terminase for peptidoglycan polymerization in bacteria. *Molecular Microbiology* **99,** 700–718 (2015).
31. Sakata, N., Terakubo, S. & Mukai, T. Subcellular Location of the Soluble Lytic Transglycosylase Homologue in *Staphylococcus aureus*. *Current Microbiology* **50,** 47–51 (2004).

32. Sakata, N. & Mukai, T. Production profile of the soluble lytic transglycosylase homologue in*Staphylococcus aureus* during bacterial proliferation. *FEMS Immunology & Medical Microbiology* **49,** 288–295 (2007).

33. Stapleton, M. R. *et al.* Characterization of IsaA and SceD, Two Putative Lytic Transglycosylases of *Staphylococcus aureus*. *Journal of Bacteriology* **189,** 7316–7325 (2007).

34. Sudiarta, I. P., Fukushima, T. & Sekiguchi, J. *Bacillus subtilis* CwlQ (previous YjbJ) is a bifunctional enzyme exhibiting muramidase and soluble-lytic transglycosylase activities. *Biochemical and Biophysical Research Communications* **398,** 606–612 (2010).

35. Brönneke, V. & Fiedler, F. Production of Bacteriolytic Enzymes by *Streptomyces globisporus* Regulated by Exogenous Bacterial Cell Walls. *Applied and Environmental Microbiology* **60,** 785–791 (1994).

36. Vötsch, W. & Templin, M. F. Characterization of a β-*N*-acetylglucosaminidase of *Escherichia coli* and Elucidation of Its Role in Muropeptide Recycling and β-Lactamase Induction. *Journal of Biological Chemistry* **275,** 39032–39038 (2000).

37. Litzinger, S. *et al.* Muropeptide Rescue in *Bacillus subtilis* Involves Sequential Hydrolysis by β-*N*-Acetylglucosaminidase and *N*-Acetylmuramyl-L-Alanine Amidase. *Journal of Bacteriology* **192,** 3132–3143 (2010).

38. Oshida, T. *et al.* A *Staphylococcus aureus* autolysin that has an *N*-acetylmuramoyl-L-alanine amidase domain and an endo-β-*N*-acetylglucosaminidase domain: cloning, sequence analysis, and characterization. *Proceedings of the National Academy of Sciences* **92,** 285–289 (1995).

39. Götz, F., Heilmann, C. & Stehle, T. Functional and structural analysis of the major amidase (Atl) in *Staphylococcus*. *International Journal of Medical Microbiology* **304,** 156–163 (2014).

40. Yao, X., Jericho, M., Pink, D. & Beveridge, T. Thickness and Elasticity of Gram-Negative Murein Sacculi Measured by Atomic Force Microscopy. *Journal of Bacteriology* **181,** 6865–6875 (1999).

41. De Pedro, M. A. & Cava, F. Structural constraints and dynamics of bacterial cell wall architecture. *Frontiers in Microbiology* **6** (2015).

42. Heidrich, C. *et al.* Involvement of *N*-acetylmuramyl-L-alanine amidases in cell separation and antibiotic-induced autolysis of *Escherichia coli*. *Molecular Microbiology* **41,** 167–178 (2001).

43. Uehara, T. & Park, J. T. An Anhydro-*N*-Acetylmuramyl-L-Alanine Amidase with Broad Specificity Tethered to the Outer Membrane of *Escherichia coli*. *Journal of Bacteriology* **189,** 5634–5641 (2007).

44. Young, F. E. Autolytic Enzyme Associated with Cell Walls of *Bacillus subtilis*. *Journal of Biological Chemistry* **241,** 3462–3467 (1966).

45. Herbold, D. R. & Glaser, L. *Bacillus subtilis N*-Acetylmuramic Acid L-Alanine Amidase. *Journal of Biological Chemistry* **250,** 1676–1682 (1975).

46. Biswas, R. *et al.* Activity of the major staphylococcal autolysin Atl. *FEMS Microbiology Letters* **259,** 260–268 (2006).

47. Meberg, B. M., Paulson, A. L., Priyadarshini, R. & Young, K. D. Endopeptidase Penicillin-Binding Proteins 4 and 7 Play Auxiliary Roles in Determining Uniform Morphology of *Escherichia coli*. *Journal of Bacteriology* **186,** 8326–8336 (2004).

48. Tomioka, S. & Matsuhashi, M. Purification of Penicillin-Insensitive DD-Endopeptidase, a New Cell Wall Peptidoglycan-Hydrolyzing Enzyme in *Escherichia coli*, and Its Inhibition by Deoxyribonucleic Acids. *Biochemical and Biophysical Research Communications* **84,** 978–984 (1978).

49. Keck, W. & Schwarz, U. *Escherichia coli* Murein-DD-Endopeptidase Insensitive to β-Lactam Antibiotics. *Journal of Bacteriology* **139,** 770–774 (1979).

50. Singh, S. K., SaiSree, L., Amrutha, R. N. & Reddy, M. Three redundant murein endopeptidases catalyse an essential cleavage step in peptidoglycan synthesis of *Escherichia coli* K12. *Molecular Microbiology* **86,** 1036–1051 (2012).

51. Goodell, E. W. Recycling of Murein by *Escherichia coli*. *Journal of Bacteriology* **163,** 305–310 (1985).

52. Park, J. T. Turnover and Recycling of the Murein Sacculus in Oligopeptide Permease-Negative Strains of *Escherichia coli*: Indirect Evidence for an Alternative Permease System and for a Monolayered Sacculus. *Journal of Bacteriology* **175,** 7–11 (1993).

53. Park, J. T. & Uehara, T. How Bacteria Consume Their Own Exoskeletons (Turnover and Recycling of Cell Wall Peptidoglycan). *Microbiology and Molecular Biology Reviews* **72,** 211–227 (2008).

54. Jacobs, C., Huang, L.-j., Bartowsky, E., Normark, S. & Park, J. T. Bacterial cell wall recycling provides cytosolic muropeptides as effectors for β-lactamase induction. *The EMBO Journal* **13,** 4684–4694 (1994).

55. Cheng, Q. & Park, J. T. Substrate Specificity of the AmpG Permease Required for Recycling of Cell Wall Anhydro-Muropeptides. *Journal of Bacteriology* **184,** 6434–6436 (2002).

56. Uehara, T. *et al.* Recycling of the Anhydro-*N*-Acetylmuramic Acid Derived from Cell Wall Murein Involves a Two-Step Conversion to *N*-Acetylglucosamine-Phosphate. *Journal of Bacteriology* **187,** 3643–3649 (2005).

57. Jaeger, T., Arsic, M. & Mayer, C. Scission of the Lactyl Ether Bond of *N*-Acetylmuramic Acid by *Escherichia coli* "Etherase". *Journal of Biological Chemistry* **280,** 30100–30106 (2005).

58. Uehara, T., Suefuji, K., Jaeger, T., Mayer, C. & Park, J. T. MurQ Etherase Is Required by *Escherichia coli* in Order To Metabolize Anhydro-*N*-Acetylmuramic Acid Obtained either from the Environment or from Its Own Cell Wall. *Journal of Bacteriology* **188,** 1660–1662 (2006).

59. Dahl, U., Jaeger, T., Nguyen, B. T., Sattler, J. M. & Mayer, C. Identification of a Phosphotransferase System of *Escherichia coli* Required for Growth on *N*-Acetylmuramic Acid. *Journal of Bacteriology* **186,** 2385–2392 (2004).

60. White, R. J. The Role of the Phosphoenolpyruvate Phosphotransferase System in the Transport of *N*-Acetyl-D-Glucosamine by *Escherichia coli*. *Biochemical Journal* **118,** 89–92 (1970).

61. Jones-Mortimer, M. C. & Kornberg, H. L. Amino-sugar Transport Systems of *Escherichia coli* K12. *Microbiology* **117,** 369–376 (1980).

62. Lengeler, J. Characterisation of Mutants of *Escherichia coli* K12, Selected by Resistance to Streptozotocin. *Molecular and General Genetics MGG* **179,** 49–54 (1980).

63. Uehara, T. & Park, J. T. The *N*-Acetyl-D-Glucosamine Kinase of *Escherichia coli* and Its Role in Murein Recycling. *Journal of Bacteriology* **186,** 7273–7279 (2004).

64. Jaeger, T. & Mayer, C. The Transcriptional Factors MurR and Catabolite Activator Protein Regulate *N*-Acetylmuramic Acid Catabolism in *Escherichia coli*. *Journal of Bacteriology* **190,** 6598–6608 (2008).

65. Ursinus, A., Steinhaus, H. & Höltje, J.-V. Purification of a Nocardicin A-Sensitive LD-Carboxypeptidase from *Escherichia coli* by Affinity Chromatography. *Journal of Bacteriology* **174,** 441–446 (1992).

66. Templin, M. F., Ursinus, A. & Höltje, J.-V. A defect in cell wall recycling triggers autolysis during the stationary growth phase of *Escherichia coli*. *The EMBO Journal* **18,** 4108–4117 (1999).

67. Mengin-Lecreulx, D., van Heijenoort, J. & Park, J. T. Identification of the *mpl* Gene Encoding UDP-*N*-Acetylmuramate: L-Alanyl-γ-D-Glutamyl-*meso*-Diaminopimelate Ligase in *Escherichia coli* and Its Role in Recycling of Cell Wall Peptidoglycan. *Journal of Bacteriology* **178,** 5347–5352 (1996).

68. Uehara, T. & Park, J. T. Identification of MpaA, an Amidase in *Escherichia coli* That Hydrolyzes the γ-D-Glutamyl-*meso*-Diaminopimelate Bond in Murein Peptides. *Journal of Bacteriology* **185,** 679–682 (2003).

69. Schmidt, D. M. Z., Hubbard, B. K. & Gerlt, J. A. Evolution of Enzymatic Activities in the Enolase Superfamily: Functional Assignment of Unknown Proteins in *Bacillus subtilis* and *Escherichia coli* as L-Ala-D/L-Glu Epimerases. *Biochemistry* **40,** 15707–15715 (2001).

70. Schroeder, U., Henrich, B., Fink, J. & Plapp, R. Peptidase D of *Escherichia coli* K-12, a metallopeptidase of low substrate specificity. *FEMS Microbiology Letters* **123,** 153–159 (1994).

71. Park, J. T., Raychaudhuri, D., Li, H., Normark, S. & Mengin-Lecreulx, D. MppA, a Periplasmic Binding Protein Essential for Import of the Bacterial Cell Wall Peptide L-Alanyl-γ-D-Glutamyl-*meso*-Diaminopimelate. *Journal of Bacteriology* **180,** 1215–1223 (1998).

72. Chaloupka, J., Křečková, P. & Řfhová, L. The Mucopeptide Turnover in the Cell Walls of Growing Cultures of *Bacillus megaterium* KM. *Experientia* **18,** 362–363 (1962).

73. Mauck, J., Chan, L. & Glaser, L. Turnover of the Cell Wall of Gram-positive Bacteria. *Journal of Biological Chemistry* **246,** 1820–1827 (1971).

74. Reith, J. & Mayer, C. Peptidoglycan turnover and recycling in Gram-positive bacteria. *Applied Microbiology and Biotechnology* **92,** 1–11 (2011).

75. Borisova, M. *et al.* Peptidoglycan Recycling in Gram-Positive Bacteria Is Crucial for Survival in Stationary Phase. *mBio* **7** (ed Davies, J. E.) (2016).

76. Matias, V. R. F. & Beveridge, T. J. Cryo-electron microscopy reveals native polymeric cell wall structure in *Bacillus subtilis* 168 and the existence of a periplasmic space. *Molecular Microbiology* **56,** 240–251 (2005).

77. Matias, V. R. F. & Beveridge, T. J. Native Cell Wall Organization Shown by Cryo-Electron Microscopy Confirms the Existence of a Periplasmic Space in *Staphylococcus aureus*. *Journal of Bacteriology* **188,** 1011–1021 (2006).

78. Mobley, H. L. T., Doyle, R. J., Streips, U. N. & Langemeier, S. O. Transport and Incorporation of *N*-Acetyl-D-Glucosamine in *Bacillus subtilis*. *Journal of Bacteriology* **150,** 8–15 (1982).

79. Reizer, J. *et al.* Novel phosphotransferase system genes revealed by genome analysis – the complete complement of PTS proteins encoded within the genome of *Bacillus subtilis*. *Microbiology* **145,** 3419–3429 (1999).

80. Müller, M. *et al.* The exo-β-*N*-acetylmuramidase NamZ from *Bacillus subtilis* is the founding member of a family of exo-lytic peptidoglycan hexosaminidases. *Journal of Biological Chemistry* **296,** 100519 (2021).

81. Diep, B. A. *et al.* Complete genome sequence of USA300, an epidemic clone of community-acquired meticillin-resistant *Staphylococcus aureus*. *The Lancet* **367,** 731–739 (2006).

82. Sugai, M. *et al.* Identification of Endo-β-*N*-Acetylglucosaminidase and *N*-acetylmuramyl-L-Alanine Amidase as Cluster-Dispersing Enzymes in *Staphylococcus aureus*. *Journal of Bacteriology* **177,** 1491–1496 (1995).

83. Molle, V. *et al.* Additional Targets of the *Bacillus subtilis* Global Regulator CodY Identified by Chromatin Immunoprecipitation and Genome-Wide Transcript Analysis. *Journal of Bacteriology* **185,** 1911–1922 (2003).

84. Mathiopoulos, C. *et al.* A *Bacillus subtilis* dipeptide transport system expressed early during sporulation. *Molecular Microbiology* **5,** 1903–1913 (1991).

85. Quentin, Y., Fichant, G. & Denizot, F. Inventory, Assembly and Analysis of *Bacillus subtilis* ABC Transport Systems. *Journal of Molecular Biology* **287,** 467–484 (1999).

86. Slack, F. J., Mueller, J. R., Strauch, M. A., Mathiopoulos, C. & Sonenshein, A. L. Transcriptional regulation of a Bacillus subtilis dipeptide transport operon. *Molecular Microbiology* **5,** 1915–1925 (1991).

87. Serror, P. & Sonenshein, A. L. Interaction of CodY, a novel *Bacillus subtillis* DNA-binding protein, with the *dpp* promoter region. *Molecular Microbiology* **20,** 843–852 (1996).

88. Xu, Q. *et al.* Structural Basis of Murein Peptide Specificity of a γ-D-Glutamyl-L-Diamino Acid Endopeptidase. *Structure* **17,** 303–313 (2009).

89. Xu, Q. *et al.* Structure of the γ-D-glutamyl-L-diamino acid endopeptidase YkfC from-*Bacillus cereus* in complex with L-Ala-γ-D-Glu: insights into substrate recognition by NlpC/P60 cysteine peptidases. *Acta Crystallographica Section F Structural Biology and Crystallization Communications* **66,** 1354–1364 (2010).

90. Xu, Q. *et al.* Insights into Substrate Specificity of NlpC/P60 Cell Wall Hydrolases Containing Bacterial SH3 Domains. *mBio* **6** (eds Bernhardt, T. & Pier, G. B.) (2015).

91. Cheggour, A. *et al.* The *dppA* gene of *Bacillus subtilis* encodes a new D-aminopeptidase. *Molecular Microbiology* **38,** 504–513 (2002).

92. Reynolds, P. E., Depardieu, F., Dutka-Malen, S., Arthur, M. & Courvalin, P. Glycopeptide resistance mediated by enterococcal transposon Tn1546 requires production of VanX for hydrolysis of D-alanyl-D-alanine. *Molecular Microbiology* **13,** 1065–1070 (1994).

93. Arthur, M., Depardieu, F., Cabanié, L., Reynolds, P. & Courvalin, P. Requirement of the VanY and VanX D,D-peptidases for glycopeptide resistance in enterococci. *Molecular Microbiology* **30,** 819–830 (1998).

94. Marshall, C. G., Lessard, I. A. D., Park, I.-S. & Wright, G. D. Glycopeptide Antibiotic Resistance Genes in Glycopeptide-Producing Organisms. *Antimicrobial Agents and Chemotherapy* **42,** 2215–2220 (1998).

95. Lessard, I. A. D. & Walsh, C. T. VanX, a bacterial D-alanyl-D-alanine dipeptidase: Resistance, immunity, or survival function? *Proceedings of the National Academy of Sciences* **96,** 11028–11032 (1999).

96. Remaut, H., Bompard-Gilles, C., Goffin, C., Frère, J.-M. & van Beeumen, J. Structure of the *Bacillus subtilis* D-aminopeptidase DppA reveals a novel self-compartmentalizing protease. *Nature Structural Biology* **8,** 674–678 (2001).

97. Amoroso, A. *et al.* A Peptidoglycan Fragment Triggers β-lactam Resistance in *Bacillus licheniformis*. *PLoS Pathogens* **8** (ed Cheung, A.) e1002571 (2012).

98. Gibson, D. G. *et al.* Enzymatic assembly of DNA molecules up to several hundred kilobases. *Nature Methods* **6,** 343–345 (2009).

99. Schönert, S. *Maltose- und Maltodextrin-Verwertung in* Bacillus subtilis PhD thesis (Universität Konstanz, Konstanz, 2004). `https://kops.uni-konstanz.de/handle/123456789/8547` (2021).

100. Koo, B.-M. *et al.* Construction and Analysis of Two Genome-Scale Deletion Libraries for *Bacillus subtilis*. *Cell Systems* **4,** 291–305.e7 (2017).

101. Casadaban, M. J. Transposition and Fusion of the *lac* Genes to Selected Promoters in *Escherichia coli* using Bacteriophage Lambda and Mu. *Journal of Molecular Biology* **104,** 541–555 (1976).

102. Hanahan, D. Studies on Transformation of *Escherichia coli* with Plasmids. *Journal of Molecular Biology* **166,** 557–580 (1983).

103. Studier, F. W. & Moffatt, B. A. Use of Bacteriophage T7 RNA Polymerase to Direct Selective High-level Expression of Cloned Genes. *Journal of Molecular Biology* **189,** 113–130 (1986).

104. Matsen, J. B. *Lidstrom:Autoinduction Media* `https://openwetware.org/wiki/Lidstrom:Autoinduction_Media`.

105. Studier, F. W. Protein production by auto-induction in high-density shaking cultures. *Protein Expression and Purification* **41,** 207–234 (2005).

106. Kluj, R. M. *et al.* Recovery of the Peptidoglycan Turnover Product Released by the Autolysin Atl in *Staphylococcus aureus* Involves the Phosphotransferase System Transporter MurP and the Novel 6-phospho-*N*-acetylmuramidase MupG. *Frontiers in Microbiology* **9** (2018).

107. Katoh, K., Rozewicki, J. & Yamada, K. D. MAFFT online service: multiple sequence alignment, interactive sequence choice and visualization. *Briefings in Bioinformatics* **20,** 1160–1166 (2017).

108. Nguyen, L.-T., Schmidt, H. A., von Haeseler, A. & Minh, B. Q. IQ-TREE: A Fast and Effective Stochastic Algorithm for Estimating Maximum-Likelihood Phylogenies. *Molecular Biology and Evolution* **32,** 268–274 (2014).

109. Hoang, D. T., Chernomor, O., von Haeseler, A., Minh, B. Q. & Vinh, L. S. UFBoot2: Improving the Ultrafast Bootstrap Approximation. *Molecular Biology and Evolution* **35,** 518–522 (2017).

110. Kalyaanamoorthy, S., Minh, B. Q., Wong, T. K. F., von Haeseler, A. & Jermiin, L. S. ModelFinder: fast model selection for accurate phylogenetic estimates. *Nature Methods* **14,** 587–589 (2017).

111. Letunic, I. & Bork, P. Interactive Tree Of Life (iTOL): an online tool for phylogenetic tree display and annotation. *Bioinformatics* **23,** 127–128 (2006).

112. Reith, J., Berking, A. & Mayer, C. Characterization of an *N*-Acetylmuramic Acid/*N*-Acetylglucosamine Kinase of *Clostridium acetobutylicum*. *Journal of Bacteriology* **193,** 5386–5392 (2011).

113. The UniProt Consortium. UniProt: the universal protein knowledgebase in 2021. *Nucleic Acids Research* **49,** D480–D489 (2020).

114. Nightingale, A. *et al.* The Proteins API: accessing key integrated protein and genome information. *Nucleic Acids Research* **45,** W539–W544 (2017).

115. Kluj, R. M. *Wühlmaus* comp. software. Version 1.2.0 (2021). `https://codeberg.org/culpeo/wuehlmaus/releases/tag/v1.2.0`.

116. Kluj, R. M. *Chromius* comp. software. Version 1.2.1 (2021). `https://codeberg.org/culpeo/chromius/releases/tag/v1.2.1`.

117. Drula, E. *et al.* The carbohydrate-active enzyme database: functions and literature. *Nucleic Acids Research* **50,** D571–D577 (2021).

118. Fischer, G. & Schmid, F. X. The Mechanism of Protein Folding. Implications of in Vitro Refolding Models for de Novo Protein Folding and Translocation in the Cell. *Biochemistry* **29,** 2205–2212 (1990).

119. Stamnes, M. A., Rutherford, S. L. & Zuker, C. S. Cyclophilins: a new family of proteins involved in intracellular folding. *Trends in Cell Biology* **2,** 272–276 (1992).

120. Wang, P. & Heitman, J. The cyclophilins. *Genome Biology* **6,** 226 (2005).

121. Lee, J. & Kim, S. S. An Overview of Cyclophilins in Human Cancers. *Journal of International Medical Research* **38,** 1561–1574 (2010).

122. McDonald, A. G., Boyce, S. & Tipton, K. F. ExplorEnz: the primary source of the IUBMB enzyme list. *Nucleic Acids Research* **37,** D593–D597 (2008).

123. Schnetz, K., Toloczyki, C. & Rak, B. β-Gucoside (*bgl*) Operon of *Escherichia coli* K-12: Nucleotide Sequence, Genetic Organization, and Possible Evolutionary Relationship to Regulatory Components of Two *Bacillus subtilis* Genes. *Journal of Bacteriology* **169,** 2579–2590 (1987).

124. Hengstenberg, W. *et al.* Structure and function of proteins of the phosphotransferase system and of 6-phospho-β-glycosidases in Gram-positive bacteria. *FEMS Microbiology Reviews* **12,** 149–163 (1993).

125. Davies, G. J., Gloster, T. M. & Henrissat, B. Recent structural insights into the expanding world of carbohydrate-active enzymes. *Current Opinion in Structural Biology* **15,** 637–645 (2005).

126. Hengstenberg, W. & Morse, M. L. Synthesis of *o*-nitrophenyl β-D-galactoside 6-phosphate, a substrate of the staphylococcal β-D-galactosidase. *Carbohydrate Research* **7,** 180–183 (1968).

127. Breidt Jr., F. & Stewart, G. C. Nucleotide and Deduced Amino Acid Sequences of the *Staphylococcus aureus* Phospho-β-Galactosidase Gene. *Applied and Environmental Microbiology* **53,** 969–973 (1987).

128. Henrissat, B. A classification of glycosyl hydrolases based on amino acid sequence similarities. *Biochemical Journal* **280,** 309–316 (1991).

129. Setlow, B., Cabrera-Hernandez, A., Cabrera-Martinez, R. M. & Setlow, P. Identification of aryl-phospho-β-D-glucosidases in *Bacillus subtilis*. *Archives of Microbiology* **181,** 60–67 (2003).

130. Hill, A. D. & Reilly, P. J. Computational Analysis of Glycoside Hydrolase Family 1 Specificities. *Biopolymers* **89,** 1021–1031 (2008).

131. Henrissat, B. *et al.* Conserved catalytic machinery and the prediction of a common fold for several families of glycosyl hydrolases. *Proceedings of the National Academy of Sciences* **92,** 7090–7094 (1995).

132. Mayer, C. *et al.* Bacteria's different ways to recycle their own cell wall. *International Journal of Medical Microbiology* **309,** 151326 (2019).

133. Murray, K. K. *et al.* Definitions of terms relating to mass spectrometry (IUPAC Recommendations 2013). *Pure and Applied Chemistry* **85,** 1515–1609 (2013).

134. Korza, H. J. & Bochtler, M. *Pseudomonas aeruginosa* LD-Carboxypeptidase, a Serine Peptidase with a Ser-His-Glu Triad and a Nucleophilic Elbow. *Journal of Biological Chemistry* **280,** 40802–40812 (2005).

135. Hughes, R. C. Autolysis of Isolated Cell Walls of *Bacillus licheniformis* N.C.T.C. 6346 and *Bacillus subtilis* Marburg strain 168. Separation of the Products and Characterization of the Mucopeptide Fragments. *Biochemical Journal* **119,** 849–860 (1970).

136. Bisicchia, P. *et al.* The essential YycFG two-component system controls cell wall metabolism in *Bacillus subtilis*. *Molecular Microbiology* **65,** 180–200 (2007).

137. Hashimoto, M., Ooiwa, S. & Sekiguchi, J. Synthetic Lethality of the *lytE cwlO* Genotype in *Bacillus subtilis* Is Caused by Lack of D,L-Endopeptidase Activity at the Lateral Cell Wall. *Journal of Bacteriology* **194,** 796–803 (2012).

138. Levefaudes, M. *et al.* Diaminopimelic Acid Amidation in Corynebacteriales. *Journal of Biological Chemistry* **290,** 13079–13094 (2015).

139. Zhao, H., Roistacher, D. M. & Helmann, J. D. Aspartate deficiency limits peptidoglycan synthesis and sensitizes cells to antibiotics targeting cell wall synthesis in *Bacillus subtilis*. *Molecular Microbiology* **109,** 826–844 (2018).

140. Perego, M., Higgins, C. F., Pearce, S. R., Gallagher, M. P. & Hoch, J. A. The oligopeptide transport system of *Bacillus subtilis* plays a role in the initiation of sporulation. *Molecular Microbiology* **5,** 173–185 (1991).

141. Rudner, D. Z., LeDeaux, J. R., Ireton, K. & Grossman, A. D. The *spo0K* Locus of *Bacillus subtilis* Is Homologous to the Oligopeptide Permease Locus and Is Required for Sporulation and Competence. *Journal of Bacteriology* **173,** 1388–1398 (1991).

142. Koide, A. & Hoch, J. A. Identification of a second oligopeptide transport system in *Bacillus subtilis* and determination of its role in sporulation. *Molecular Microbiology* **13,** 417–426 (1994).

143. Goodell, E. W. & Higgins, C. F. Uptake of Cell Wall Peptides by *Salmonella typhimurium* and *Escherichia coli. Journal of Bacteriology* **169,** 3861–3865 (1987).

144. Tame, J. R. H. *et al.* The Structural Basis of Sequence-Independent Peptide Binding by OppA Protein. *Science* **264,** 1578–1581 (1994).

145. Kitano, K., Tuomanen, E. & Tomasz, A. Transglycosylase and Endopeptidase Participate in the Degradation of Murein During Autolysis of *Escherichia coli. Journal of Bacteriology* **167,** 759–765 (1986).

146. Keck, W., van Leeuwen, A. M., Huber, M. & Goodell, E. W. Cloning and characterization of *mepA*, the structural gene of the penicillin-insensitive murein endopeptidase from *Escherichia coli. Molecular Microbiology* **4,** 209–219 (1990).

147. Hoyland, C. N. *et al.* Structure of the LdcB LD-Carboxypeptidase Reveals the Molecular Basis of Peptidoglycan Recognition. *Structure* **22,** 949–960 (2014).

A. Publication

frontiers in Microbiology

ORIGINAL RESEARCH
published: 16 November 2018
doi: 10.3389/fmicb.2018.02725

Recovery of the Peptidoglycan Turnover Product Released by the Autolysin Atl in *Staphylococcus aureus* Involves the Phosphotransferase System Transporter MurP and the Novel 6-phospho-*N*-acetylmuramidase MupG

Robert Maria Kluj*[1], *Patrick Ebner*[2], *Martina Adamek*[1], *Nadine Ziemert*[1], *Christoph Mayer*[1]* *and Marina Borisova*[1]

[1] *Microbiology/Biotechnology, Department of Biology, Interfaculty Institute of Microbiology and Infection Medicine, University of Tübingen, Tübingen, Germany,* [2] *Microbial Genetics, Department of Biology, Interfaculty Institute of Microbiology and Infection Medicine, University of Tübingen, Tübingen, Germany*

OPEN ACCESS

Edited by:
Marc Bramkamp,
Ludwig-Maximilians-Universität München, Germany

Reviewed by:
Patrick Joseph Moynihan, University of Birmingham, United Kingdom
Volker F. Wendisch, Bielefeld University, Germany

****Correspondence:***
Christoph Mayer
christoph.mayer@uni-tuebingen.de
Marina Borisova
marina.borisova@uni-tuebingen.de

Specialty section:
This article was submitted to Microbial Physiology and Metabolism, a section of the journal Frontiers in Microbiology

Received: *04 June 2018*
Accepted: *24 October 2018*
Published: *16 November 2018*

Citation:
Kluj RM, Ebner P, Adamek M, Ziemert N, Mayer C and Borisova M (2018) Recovery of the Peptidoglycan Turnover Product Released by the Autolysin Atl in Staphylococcus aureus Involves the Phosphotransferase System Transporter MurP and the Novel 6-phospho-N-acetylmuramidase MupG. Front. Microbiol. 9:2725. doi: 10.3389/fmicb.2018.02725

The peptidoglycan of the bacterial cell wall undergoes a permanent turnover during cell growth and differentiation. In the Gram-positive pathogen *Staphylococcus aureus,* the major peptidoglycan hydrolase Atl is required for accurate cell division, daughter cell separation and autolysis. Atl is a bifunctional *N*-acetylmuramoyl-L-alanine amidase/endo-β-*N*-acetylglucosaminidase that releases peptides and the disaccharide *N*-acetylmuramic acid-β-1,4-*N*-acetylglucosamine (MurNAc-GlcNAc) from the peptidoglycan. Here we revealed the recycling pathway of the cell wall turnover product MurNAc-GlcNAc in *S. aureus*. The latter disaccharide is internalized and concomitantly phosphorylated by the phosphotransferase system (PTS) transporter MurP, which had been implicated previously in the uptake and phosphorylation of MurNAc. Since MurP mutant cells accumulate MurNAc-GlcNAc and not MurNAc in the culture medium during growth, the disaccharide represents the physiological substrate of the PTS transporter. We further identified and characterized a novel 6-phospho-*N*-acetylmuramidase, named MupG, which intracellularly hydrolyses MurNAc 6-phosphate-GlcNAc, the product of MurP-uptake and phosphorylation, yielding MurNAc 6-phosphate and GlcNAc. MupG is the first characterized representative of a novel family of glycosidases containing domain of unknown function 871 (DUF871). The corresponding gene *mupG* (*SAUSA300_0192*) of *S. aureus* strain USA300 is the first gene within a putative operon that also includes genes encoding the MurNAc 6-phosphate etherase MurQ,

MurP, and the putative transcriptional regulator MurR. Using mass spectrometry, we observed cytoplasmic accumulation of MurNAc 6-phosphate-GlcNAc in Δ*mupG* and Δ*mupGmurQ* markerless non-polar deletion mutants, but not in the wild type or in the complemented Δ*mupG* strain. MurNAc 6-phosphate-GlcNAc levels in the mutants increased during stationary phase, in accordance with previous observations regarding peptidoglycan recycling in *S. aureus*.

Keywords: peptidoglycan recycling, cell wall turnover, *Staphylococcus aureus*, Atl autolysin, peptidoglycan hydrolases, 6-phosphomuramidase, exo-*N*-acetylmuramidase, MurNAc-GlcNAc

INTRODUCTION

Staphylococcus aureus is a small, spherical bacterium (∼1 μm diameter) belonging to the phylum firmicutes that can cause life-threatening infections due to the emergence of multi-drug resistance (Hiramatsu et al., 2014). As a Gram-positive bacterium, *S. aureus* is encased in a thick layer of peptidoglycan (PGN), which maintains cell shape and protects the cells from rupture due to high turgor pressure (Cabeen and Jacobs-Wagner, 2005). The general structure of the PGN is conserved in all eubacteria, consisting of a glycan backbone of two alternating β-1,4-glycosidically linked sugars *N*-acetylmuramic acid (MurNAc) and *N*-acetylglucosamine (GlcNAc) and polypeptides, connected to the D-lactyl moiety of MurNAc, that are partially crosslinked (Vollmer et al., 2008). The PGN polymer is synthesized by glycosyltransferases and transpeptidases [involving shape, elongation, division and sporulation (SEDS) family peptidoglycan synthases and penicillin binding proteins (PBPs)] through polymerization of GlcNAc-β-1,4-MurNAc-peptide building blocks, provided by lipid II precursors (Cho et al., 2016; Meeske et al., 2016). The overall peptidoglycan structure of *S. aureus* is different in some aspects compared to most other bacterial species. Firstly, pentaglycine (Gly_5) bridges are attached to the ε-NH_2 group of L-lysine (L-Lys) of the stem tetrapeptide L-alanine-D-isoglutamine-L-Lys-D-alanine (L-ala-D-isoGln-L-Lys-D-Ala) that are extensively cross-linked (degree of crosslinking of about 80%, dependent on the growth phase and growth conditions) with neighboring peptide stems via their carboxyl group of D-Ala (Gally and Archibald, 1993; Litzinger and Mayer, 2010). Secondly, the glycan chains are comparatively short. About 80% of the glycan chains of the mature cell wall have a predominant length of 3–10 disaccharides, the average degree of polymerization is 6 disaccharides, and only about 15% of the glycan chains have a degree of polymerization more than 25 (Boneca et al., 2000).

The coccus-shaped *S. aureus* divides sequentially in three orthogonal planes over three consecutive division cycles (Monteiro et al., 2015). Although elongation-specific cell wall synthesis machinery is absent, the cells elongate before initiation and after completion of the division septum (Monteiro et al., 2015). The final splitting of daughter cells is accompanied by fast reshaping of the flat septum to finally yield two coccoid offspring cells. Thus, the peptidoglycan is remarkably dynamic and it is constantly degraded during the cell cycle of *S. aureus* by peptidoglycan hydrolases (potential autolysins) (Foster, 1995; Ramadurai et al., 1999; Takahashi et al., 2002; Kajimura et al., 2005; Biswas et al., 2006; Frankel et al., 2011; Wheeler et al., 2015; Chan et al., 2016). The major autolysin of *S. aureus,* called Atl, is a multi-domain enzyme, composed of a secretion signal peptide, a propeptide of still unclear function, and two catalytic domains, an N-terminal *N*-acetylmuramoyl-L-alanine amidase as well as a C-terminal endo-β-*N*-acetylglucosaminidase domain, which are interrupted by cell wall binding repeats (Sugai et al., 1995). The enzyme undergoes proteolytic processing to generate two extracellular peptidoglycan hydrolases, a 62 kDa *N*-acetylmuramoyl-L-alanine amidase (Atl_{AM}) and a 51 kDa endo-β-*N*-acetylglucosaminidase (Atl_{GL}), which localize in a ring-like structure on the cell surface at the septal region, most likely binding to lipoteichoic acids, extending from the cell membrane (Yamada et al., 1996; Götz et al., 2014). Both Atl hydrolase entities can also be secreted and are found in the culture supernatants of some strains (Sugai et al., 1995). Atl functions during cell expansion and division, and it is required for proper daughter cell separation (Sugai et al., 1995; Biswas et al., 2006). Furthermore, Atl is associated with autolysis processes, e.g., during biofilm formation (Biswas et al., 2006; Bose et al., 2012). Besides Atl_{GL}, *S. aureus* also possesses three other *N*-acetylglucosaminidases, SagA, SagB, and ScaH, which are important for proper septum formation at the final stage of cell division. SagB was also found to be responsible for shortening of newly synthesized glycan strands to their physiological length, thus ensuring flexibility during the cell elongation process (Wheeler et al., 2015; Chan et al., 2016). Interestingly, the *S. aureus* genome apparently does not encode any *N*-acetylmuramidases, with the exception of two putative lytic transglycosylases, IsaA and SceD (Stapleton et al., 2007), indicating that the processing of glycan strands in this organism involves endo-acting *N*-acetylglucosaminidases, besides peptidoglycan amidases and endopeptidases (Ramadurai et al., 1999; Kajimura et al., 2005; Frankel et al., 2011). The combined activities of these PGN hydrolases generate MurNAc-GlcNAc and peptides as final peptidoglycan turnover products.

It was calculated that during the process of PGN turnover in *S. aureus*, 15% (Wong et al., 1974) or up to 25% (Blümel et al., 1979) of cell wall material fragments are released per generation in the culture medium. However,

the ability of Gram-positive bacteria in general to recycle these fragments was questioned for a long time. We recently elucidated that recycling occurs in different Gram-positive bacteria such as *S. aureus*, *Bacillus subtilis*, and *Steptomyces coelicolor* and revealed that the MurNAc 6-phosphate (MurNAc 6P) etherase MurQ (Borisova et al., 2016), responsible for the intracellular conversion of MurNAc 6P to GlcNAc 6-phosphate and D-lactate, is required for this process. In addition, we quantified the intracellular accumulation of MurNAc 6P in the markerless Δ*murQ* mutant, showed that recycling of the MurNAc portion of peptidoglycan occurs predominantly during nutrient limitation within transition and stationary phase (Borisova et al., 2016). Furthermore we discovered that peptidoglycan recycling is essential for bacterial survival in the late stationary phase (Borisova et al., 2016). In *S. aureus* strain USA300, the *murQ* etherase gene (*SAUSA300_0193*) is encoded in an operon together with *SAUSA300_0194*, encoding the enzyme IIB and IIC domains of the MurNAc PTS-transporter MurP, *SAUSA300_0195*, encoding a MurR-like regulator, and *SAUSA300_0192*, encoding a protein with unknown function (Borisova et al., 2016).

We hypothesized that MurNAc-GlcNAc, the product of cell wall cleavage by Atl, rather than MurNAc, might be taken up and recycled in *S. aureus* and proposed a role of the gene *SAUSA300_0192* of unknown function in this process. To prove this hypothesis, we generated markerless gene deletion mutants and investigated the intracellular and extracellular accumulation of specific recycling products in different growth phases by mass spectrometry. Our study showed that MurNAc 6P-GlcNAc accumulates in *SAUSA300_0192* mutant, predominantly during stationary phase, and that this compound is generated by the uptake and phosphorylation of MurNAc-GlcNAc by the PTS transporter MurP. The *SAUSA300_0192* gene was shown to encode a novel 6-phospho-*N*-acetylmuramidase, named MupG that hydrolyses MurNAc 6P-GlcNAc yielding MurNAc 6P and GlcNAc. MupG is the first characterized protein of a so far unexplored family of proteins containing the domain of unknown function 871 (DUF871). Altogether in this study we revealed the recycling pathway of the peptidoglycan sugar turnover product of the Atl autolysin in *S. aureus*.

MATERIALS AND METHODS

Chemicals, Enzymes, and Oligonucleotides

Enzymes for DNA restriction and for cloning were purchased from New England Biolabs (Ipswich, USA) or Thermo Fischer Scientific (Waltham, MA, United States). The Gene JET plasmid miniprep kit, PCR purification kit, and Gene Ruler 1 kb marker were also purchased from Thermo Fisher Scientific and anhydrotetracycline was obtained from Biomol GmbH (Hamburg, Germany). Oligonucleotides were purchased from MWG Eurofins (Ebersberg, Germany) and are listed in **Supplementary Table 1**.

Bacterial Strains, Growth Conditions, and Plasmids

The bacterial strains and plasmids used in this study are listed in **Supplementary Table 2**. The construction of mutant strains and plasmids is also described in the **Supplementary Material**. *Staphylococcus aureus* USA300 JE2 strain was cultured aerobically in lysogeny broth (LB broth Lennox, Carl Roth) at 37°C and with continuous shaking at 160 rpm or on solid LB supplemented with 1.5% agar. *S. aureus* overnight cultures (∼16 h) were used to inoculate fresh LB medium to yield an initial optical density at 600 nm (OD_{600}) of 0.05 for growth studies and for the determination of intracellular accumulation of *N*-acetylmuramic acid 6-phosphate-*N*-acetylglucosamine (MurNAc 6P-GlcNAc) at different growth phases. BM medium (10 g/l peptone, 5 g/l yeast extract, 1 g/l glucose, 5 g/l NaCl, 1 g/l K_2HPO_4) was used to prepare electrocompetent *S. aureus* JE2 cells and for the generation of the markerless Δ*mupG* and Δ*mupGmurQ* mutants (see **Supplementary Data** in the **Supplementary Material**). Antibiotics were used, when appropriate, at the following concentrations: 100 μg/ml ampicillin and 30 μg/ml kanamycin for *E. coli* and 10 μg/ml chloramphenicol for *S. aureus*.

Generation of Cytosolic Fractions and Reduction of Samples With $NaBH_4$

Overnight cultures of *S. aureus* JE2 wild type, Δ*mupG* and Δ*mupGmurQ* mutants were used to inoculate LB medium to an initial OD_{600} of 0.05. Bacteria were grown at 37°C with constant shaking and harvested at mid-exponential growth phase (OD_{600} of 2.4, grown for ∼3–3.5 h), at transitional phase (OD_{600} of 7.2, grown for 9 h) and stationary phase (OD_{600} of 5.9, grown for 24 h). Afterward, 50 ml of the culture were transferred to Falcon tubes, bacteria were centrifuged at 4,000 × *g* for 10 min, washed with 20 ml deionized water, and pellets were frozen at −80°C. Bacterial samples were thawed at room temperature and suspended in different volumes of water to prepare cell suspensions with OD_{600} of 250 per ml in the different growth phases. Seven hundred microliters of the bacterial suspensions were transferred to new tubes containing ∼0.25 g glass beads (0.25–0.5 mm; Roth) and cells were disrupted in a cell homogenisor (Precellys Evolution, Bertin Technologies) at 6000 rpm for 30 s. This procedure was repeated 4 times, with cooling on ice for 1 min after the second cycle. Lysates were cooled briefly and subsequently centrifuged for 10 min at maximum speed in a microcentrifuge. Two hundred microliters of each supernatant was added to 800 μl of ice-cold acetone to precipitate remaining proteins. After centrifugation (12,000 × *g* for 10 min), the supernatant was transferred to a new tube, and samples were dried under vacuum for 2 h at 55°C and finally stored at 4°C prior to LC-MS measurements.

Reduction solution was freshly prepared for each experiment by adding 500 μl of 0.5 M borate buffer (pH 9) to 5 mg of sodium borohydride, as previously described (Schaub and Dillard, 2017). Thirty microliters of the cytosolic fractions or the culture supernatants were added to equal volumes

of the reduction solution and samples were incubated for 20 min at room temperature. Reactions were adjusted to pH between 3 and 4 by adding 10 µl of 8.5% phosphoric acid. Samples were dried under vacuum at 45°C and pellets were solved in 30 µl of deionized water prior to LC-MS analysis.

Analysis of MurNAc 6P-GlcNAc Accumulation by LC-MS

Sample analysis of bacterial cytosolic fractions was conducted using an electrospray ionization-time of flight (ESI-TOF) mass spectrometer (MicrOTOF II; Bruker Daltonics), operated in negative or positive ion-mode that was connected to an UltiMate 3000 high performance liquid chromatography (HPLC) system (Dionex). For HPLC-MS analysis cytosolic samples were dissolved in 50 µl deionized water and 3 µl were injected into a Gemini C18 column (150 by 4.6 mm, 5 µm, 110 Å, Phenomenex). A 45 min program at a flow rate of 0.2 ml/min was used to separate compounds in the cytosolic fractions as previously described (Gisin et al., 2013). The mass spectra of the investigated samples were presented as base peak chromatograms (BPC), differential spectra (DS, obtained by subtraction of BPC_{mutant} minus $BPC_{wildtype}$) and extracted ion chromatograms (EIC) in DataAnalysis program and were presented in Prism 6 (GraphPad). The relative amounts of MurNAc 6P-GlcNAc in different growth phases and in *mupG* complementation experiments were determined by calculating the area under the curve (AUC) of the respective EIC spectra for MurNAc 6P-GlcNAc.

Construction of pET28a-*mupG* Plasmid and Heterologous Expression and Purification of MupG-His_6

For heterologous overexpression in *E. coli*, the *mupG* gene was cloned in a pET28a(+) expression vector as a recombinant protein with a C-terminal His_6-tag. Therefore, genomic DNA from *S. aureus* USA300 JE2 strain was used to amplify the *mupG* gene by PCR using primer pair MB-67 and MB-68. Both, the PCR product and vector were digested with NcoI and XhoI restriction enzymes, ligated by T4 DNA ligase and chemically competent *E. coli* DH5α cells were transformed with the ligation reaction mixture. The pET28a-*mupG* recombinant plasmid was isolated from kanamycin-resistant *E. coli* cells and DNA sequence was verified by sequencing. BL21(DE3) cells were then transformed with the pET28a-*mupG* plasmid and protein was expressed by addition of IPTG (isopropyl-β-D-thiogalactopyranoside), controlling the T7 inducible promoter.

For expression of MupG, an overnight culture of *E. coli* BL21(DE3) pET28a-*mupG* cells was diluted to an OD_{600} of 0.05 with LB medium supplemented with 30 µg/ml kanamycin (final volume of 1 l) and cells were grown at 37°C with shaking. MupG expression was induced by addition of 1 mM IPTG after the culture reached an OD_{600} of 0.75. Three hours after induction, bacteria were harvested by centrifugation (4,000 × *g*, 4°C, 20 min) and frozen at −20°C. Then, cells were solved in phosphate buffer A (20 mM Na_2HPO_4, 500 mM NaCl, pH 8), disrupted by sonication (Branson Sonifier 250, 3 times for 2 min, output 5, duty cycle of 50%) and cell debris were removed by centrifugation (38,000 × *g*, 4°C, 20 min). The soluble fraction was filtered (0.2 µm, Sarstedt) and the His-tagged protein was purified by Ni^{2+} affinity chromatograpy system Äkta Purifier on a 1 ml HisTrap HP column (GE Healthcare). A linear gradient over 30 min from 96% buffer A and 4% buffer B (20 mM Na_2HPO_4, 500 mM NaCl, 500 mM imidazole, pH 8) to 100% buffer B was used to elute the His-tagged enzyme from the column. The UV_{280nm} active fractions were analyzed for MupG protein content on 13% SDS-PAGE gel. The MupG-His_6 containing fractions were pooled and further purified by size-exclusion chromatography (HiLoad 16/600 Superdex 75 pg, GE Healthcare) with buffer A for elution. Protein purity was analyzed by SDS-PAGE and the extinction coefficient at 280 nm of 20,860 M^{-1} cm^{-1} was calculated based on amino acid composition with the ExPASy ProtParam tool. Protein was stored at −80°C in 10% glycerol solution.

Phylogenetic Analysis

The phylogenetic tree was based on the Pfam entry PF05913. A set of 519 amino acid sequences in this entry (for a complete list of proteins see **Supplementary Table 3**) were aligned using MAFFT (Katoh and Standley, 2013) under default settings and subsequently trimmed with trimAl in automated1 mode (Capella-Gutiérrez et al., 2009). Pfam PF05913 sequences with less than 200 amino acids were removed from the analysis. The maximum likelihood phylogenetic tree was constructed with RaxML using the Gamma Blosum62 Protein model and rapid bootstrapping algorithm (Stamatakis, 2014). The visualization and annotation was done with the program interactive Tree Of Life (iTOL) v3: an online tool for the display and annotation of phylogenetic and other trees (Letunic and Bork, 2016).

RESULTS

Accumulation of MurNAc 6-phosphate-GlcNAc in Δ*mupG* and Δ*mupGmurQ* Cells

The gene *SAUSA300_0192,* named *mupG,* encodes an uncharacterized, hypothetical protein that is classified as a member of a protein family of unknown function (DUF871). It is located upstream of *murQ*, *murP* and *murR*, encoded in an operon on the genome of *S. aureus* strain USA300_FPR3757 (according to the AureoWiki database[1]) (Fuchs et al., 1990). We recently showed that the PTS transporter MurP and the MurNAc 6-phosphate etherase MurQ are required for the recovery of the cell wall sugar *N*-acetylmuramic acid (MurNAc) in *S. aureus* and other Gram-positive bacteria (Borisova et al., 2016). Thus, we assumed that the enzyme MupG of *S. aureus* might also be involved in the recycling of peptidoglycan turnover products, possibly acting sequentially with MurQ within a joint catabolic pathway. To prove this hypothesis, we generated markerless

[1]http://aureowiki.med.uni-greifswald.de/SAUSA300_0192

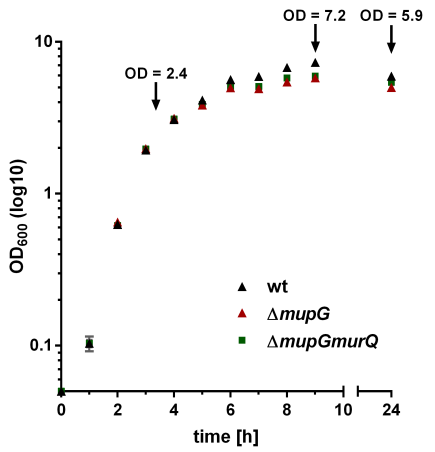

FIGURE 1 | Growth kinetics of wild type and peptidoglycan recycling mutants in LB medium. *S. aureus* wild type (wt, black triangles), Δ*mupG* mutant (red triangle), and Δ*mupGmurQ* (green squares) cells were grown in LB medium under constant shaking and the optical density was monitored at 600 nm (OD_{600}) up to 24 h. Experiment was performed in triplicates and data were presented in GraphPad Prism 6 as mean ± SD. Arrows indicate the time when samples were taken for the generation of cytosolic fractions in different growth phases.

S. aureus Δ*mupG* and Δ*mupGmurQ* deletion mutants (see **Supplementary Data** and **Supplementary Figure 1**) and we analyzed growth of these mutant strains in comparison with the parental (wild type) strain in nutrient-rich LB medium for 24 h (**Figure 1**). No significant differences in growth were detectable in all three strains during exponential growth phase, when monitoring the optical density at 600 nm (OD_{600}). However, a slight reduction in OD_{600} was observed during late exponential and stationary phase for Δ*mupG* and Δ*mupGmurQ*, compared to the wild type cultures. A *S. aureus* USA300 JE2 Δ*murQ* mutant, lacking the etherase enconding *murQ*, which is located in the same putative operon as *mupG* also showed a slight growth defect in these growth phases, as described previously in Borisova et al. (2016). Therefore, we also compared the growth of the Δ*mupG* mutant with the Δ*murQ* mutant. Interestingly, Δ*mupG* cultures reached slightly lower optical density compared to the Δ*murQ* cultures (see **Supplementary Figure 2**).

Mass spectrometric analyses of cytosolic cell fractions of Δ*mupG* and Δ*mupGmurQ* cells revealed the accumulation of an intracellular recycling product in both mutant strains, which was absent in wild type cells. The accumulation product in both mutant strains occurred at the same retention time of 21.2 min and had an identical mass within the error of mass analysis of <5 ppm (Δ*mupG* cells, $(M\text{-}H)^-$ = 575.151 m/z and Δ*mupGmurQ* cells, $(M\text{-}H)^-$ = 575.148 m/z) (**Figure 2**). The accumulation of the same compound in both mutants and the absence of MurNAc 6P accumulation in the double mutant, which has been reported to accumulate in a Δ*murQ* single mutant (Borisova et al., 2016), indicated that MupG and MurQ are indeed operating in the same peptidoglycan recovery pathway, with MupG presumably acting upstream of MurQ. The unknown accumulation product has a mass that is identical within the error of mass analysis with the theoretical mass of a phosphorylated disaccharide containing the sugars GlcNAc and MurNAc (calculated mass in negative ion mode $(M\text{-}H)^-$ = 575.1495 m/z and positive ion mode $(M+H)^+$ = 577.164 m/z). To identify the chemical structure of the phosphorylated disaccharide, i.e., which sugar resides at the reducing end and which sugar is phosphorylated, we analyzed the fragmentation patterns obtained by in-source decay during mass analysis. We analyzed the intact cytosolic extracts of the Δ*mupG* cells containing the accumulation product, as well as the same samples after reduction with $NaBH_4$ this time in positive ion-mode (**Figure 3**). As expected a mass shift of 2 Da occurred after treatment with $NaBH_4$, in agreement with the expected reduction of a sugar hemiacetal at the reducing end yielding a sugar alcohol. The accumulation product in the Δ*mupG* extract with a mass of $(M+H)^+$ = 577.166 m/z (non-reduced) was diminished [**Figure 3A**; calculated mass of a phosphorylated disaccharide containing GlcNAc and MurNAc in positive ion mode: $(M+H)^+$ = 577.164 m/z)], and a new mass appeared with $(M+H)^+$ = 579.178 m/z, corresponding to the same disaccharide reduced to sugar alcohol [calculated reduced form $(M+H)^+$ = 579.1797 m/z] (**Figure 3B**). The fact that the phosphorylated disaccharide is reduced at the anomeric position indicated that the C1 position is not phosphorylated, but most likely the C6 position carries the phosphate group. Thus, four different chemical structures are imaginable, which were presented in **Supplementary Figure 3A**.

In the non-reduced sample (**Figure 3A**), the recycling product with the mass of $(M+H)^+$ = 577.166 m/z was detected and also the Na^+ and K^+ adducts. Fragmentations included the neutral loss of GlcNAc (-221.092 Da; calculated exact mass loss of 221.089 Da), and a MurNAc 6P elimination product (see **Supplementary Figure 3B**) with a mass of $(M+H)^+$ = 356.074 m/z (which is identical with the calculated m/z of this fragment). Besides, the loss of a phosphoryl group (-79.971 Da) and the loss of water (-18.013 Da), most likely at the anomeric site, was observed. The latter fragmentations caused the formation of a dephosphorylated recycling product [$(M+H)^+$ = 497.195 m/z] and a dehydrated product [$(M+H)^+$ = 559.152 m/z], respectively. From these MS result we could conclude that MurNAc, but not GlcNAc, is phosphorylated. After sample reduction, the mass of the accumulation product changed to $(M+H)^+$ = 579.178 m/z (**Figure 3B**). Na^+ and K^+ adducts of the reduced compound were also detected. Compound fragmentation pattern included the neutral loss of GlcNAc, this time in a reduced form (measured and theoretical exact mass loss of 223.106 Da) and generated a compound, as seen in the non-reduced sample, with a m/z identical within error with a MurNAc 6P elimination product (356.072 m/z) (**Figure 3B**; see also **Supplementary Figure 3B**).

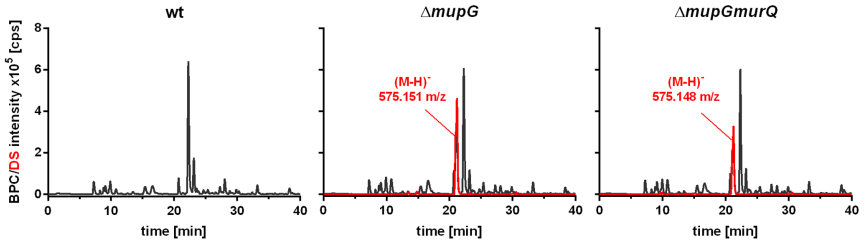

FIGURE 2 | Analysis of cytosolic extracts from wild type, Δ*mupG* and Δ*mupGmurQ* cells by LC-MS. *S. aureus* JE2 wild type (wt) and mutant strains were grown in LB medium for 24 h. Macromolecules were removed from the cytosolic fractions by acetone precipitation and soluble extracts were analyzed by LC-MS in negative ion-mode. Representative mass spectra from at least three independent experiments are presented as base peak chromatograms (BPC) ($\times 10^5$ counts per s [cps]) in black and as differential spectra (DS, $BPC_{mutant} - BPC_{wt}$) ($\times 10^5$ [cps]) in red. DS of both mutants revealed the intracellular accumulation of a compound (absent in the wt cells) with an observed mass of $(M\text{-}H)^-$ = 575.151 m/z in Δ*mupG* cells and an observed mass of $(M\text{-}H)^-$ = 575.148 m/z) in Δ*mupGmurQ* cells.

Fragments indicating the loss of phosphate (-79.968 Da, resulting in 499.211 m/z, reduced MurNAc-GlcNAc) were detected also in the reduced sample. However, a fragmentation product indicating the loss of water was absent, as expected for a compound reduced at the anomeric position. These latter results showed that after sample reduction with $NaBH_4$, the mass of the elimination product of MurNAc 6P did not change, but the mass, corresponding to GlcNAc, was changed to the reduced form. Thus, we could conclude that the investigated phosphorylated disaccharide contains a MurNAc at the non-reducing end that is phosphorylated and GlcNAc at the reducing end. Taken together, the fragmentation patterns of the non-reduced and reduced accumulation products, identified the accumulation of MurNAc 6P-GlcNAc disaccharide in the Δ*mupG* cells.

MurNAc 6P-GlcNAc Is Hydrolyzed by MupG Yielding MurNAc 6P and GlcNAc

To characterize the *in vitro* functionality of MupG from *S. aureus*, we overexpressed the enzyme in *E. coli* BL21(DE3) in the presence of IPTG as a recombinant C-terminal His_6-fusion protein (**Figure 4A**) and purified the recombinant enzyme by Ni^{2+}-affinity and gel filtration chromatography (calculated mass of 41.5 kDa). After purification, a total amount of 3 and 5 mg protein, respectively, was obtained from 1 l bacterial culture in two different experiments and purity of the purified enzyme was confirmed with SDS-PAGE (**Figure 4A**). Addition of the recombinant MupG enzyme to cytosolic extracts, prepared from wild type and Δ*mupG* mutant cells revealed the specific cleavage of the Δ*mupG* recycling product ($(M+H)^+$ = 577.166 m/z, measured in positive ion-mode, and a retention time of 21.2 min), yielding two new masses $(M+H)^+$ = 222.098 m/z and $(M+H)^+$ = 374.083 m/z (**Figure 4B**). These new masses correspond to the theoretical masses for GlcNAc [$(M+H)^+$ = 222.097 m/z] and MurNAc P [$(M+H)^+$ = 374.085 m/z], respectively. However, MupG did not affect any other compound accumulating in the cytosol of the wild type cells or Δ*mupG* cells (data not shown). Notably, in extracts of the mutant, we detected a second peak with a mass of $(M+H)^+$ = 577.165 m/z that eluted with a retention time of 25 min (**Figure 4B**). This compound was only detectable, when the MS analysis was conducted in the positive ion-mode, but was absent when samples were analyzed in negative ion-mode (see **Figures 1**, **2** for comparison). Recombinant MupG enzyme only diminished the compound with a retention time of 21.2 min but not the compound with the same m/z but a retention time of 25 min (**Figure 4B**). The identity of this compound is so far unclear, since the MS fragmentation pattern indicated that it is neither composed of non-phosphorylated nor of phosphorylated MurNAc and GlcNAc sugars (data not shown).

To unequivocally identify MurNAc 6P as the product of MupG cleavage, we incubated the MupG-treated cytosolic fraction, with the MurNAc 6P etherase MurQ, which specifically converts MurNAc 6P to GlcNAc 6P (Borisova et al., 2016). As expected, MurQ reduced the amount of MurNAc 6P about 4 times, at the same time a mass with $(M+H)^+$ = 302.062 m/z, corresponding to the theoretical mass of GlcNAc 6P ($(M+H)^+$ = 302.064 m/z) was generated (**Figure 4B**). MurQ treatment did not affect amounts of GlcNAc, the second product of MupG action. These results confirmed that the accumulating recycling product is indeed MurNAc 6P-GlcNAc and that the MupG enzyme acts as a MurNAc 6P-GlcNAc glycosidase. The recombinant enzyme was stable for several months at 4°C without losing significant activity, even in the absence of DTT reducing agent.

MurNAc 6P-GlcNAc Accumulation Primarily Occurs in Transition and Stationary Phase and Is Abolished by Plasmid-Based Complementation of MupG

We previously showed that a *murQ* mutant of *S. aureus* accumulates intracellularly MurNAc 6P predominantly in transition and stationary phases (Borisova et al., 2016). Here, we examined the growth phase-dependent accumulation of MurNAc 6P-GlcNAc. The time points used for harvesting where mid

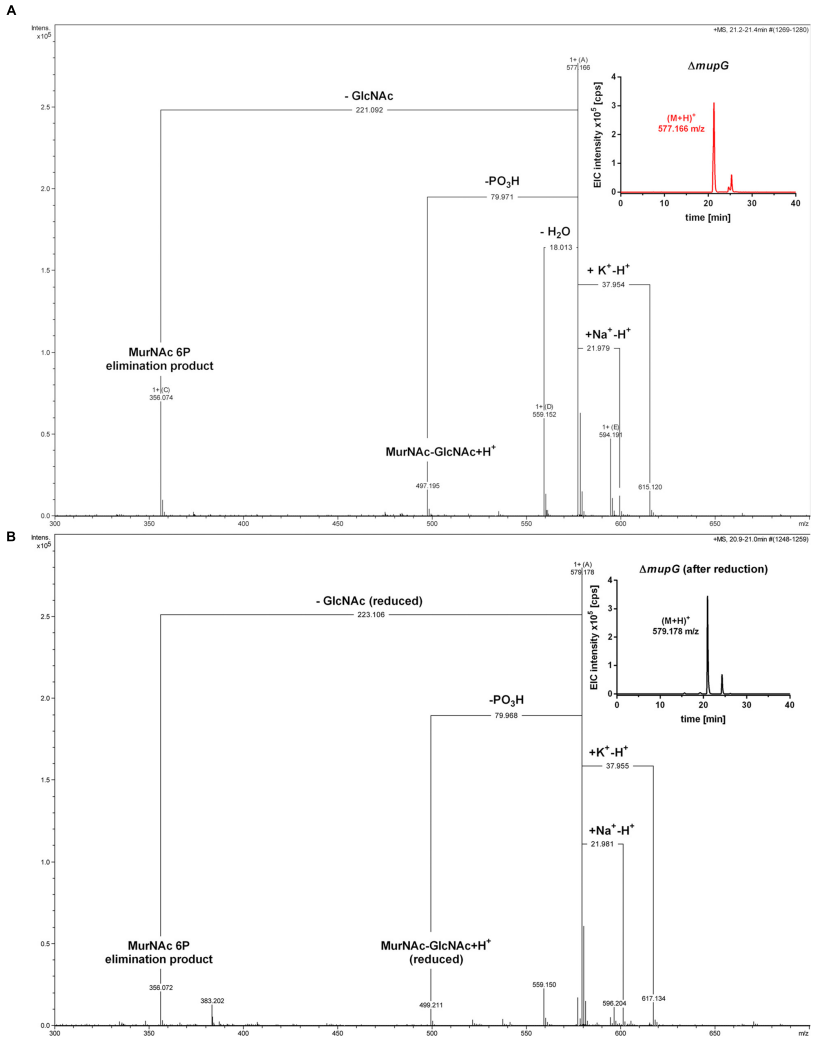

FIGURE 3 | Accumulation of MurNAc 6P-GlcNAc in Δ*mupG* cells. *S. aureus* Δ*mupG* was grown in LB medium to stationary phase (24 h). Acetone extracts of the cytosolic fractions were analyzed by LC-MS in positive ion-mode, before **(A)** and after **(B)** $NaBH_4$ reduction. **(A)** Shown are the fragmentation patterns obtained by in-source decay of the compound that accumulates specifically in Δ*mupG* mutant cells and eluates at a retention time of 21.2–21.4 min, represented as extracted ion chromatogram with an observed mass of $(M+H)^+$ = 577.166 m/z (EIC × 10^5 counts per s [cps], upper right corner). Representative mass spectra from three biological replicates are illustrated. **(B)** Shown are the fragmentation patterns after reduction of the sample with $NaBH_4$, which results in the formation of a new compound that elutes at 21.0 min, represented by an EIC with an observed mass of $(M+H)^+$ = 579.178 m/z (upper right corner). The mass spectra fragmentation patterns of both compounds were presented in Compass DataAnalysis program (Bruker) from 300 to 700 m/z. The obtained fragmentation pattern indicated that the substrate for *MupG* is MurNAc 6P-GlcNAc.

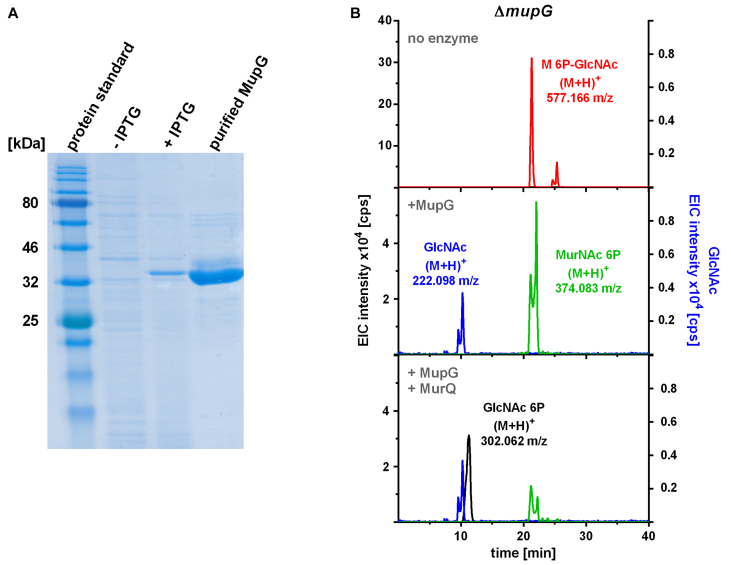

FIGURE 4 | Production of recombinant MupG and enzymatic digest of MurNAc 6P-GlcNAc extracted from Δ*mupG* cytosolic fractions. **(A)** MupG from *S. aureus* JE2 strain was heterologously expressed in *E. coli* BL21(DE3) cells. Protein expression, before (-IPTG) and after induction for 3 h (+IPTG), and purity (after purification by Ni^{2+}-affinity and size exclusion chromatography) was controlled by SDS-PAGE (5 μg of the recombinant MupG protein was loaded). MupG-His_6 protein has a calculated molecular weight of 41.5 kDa. **(B)** *S. aureus* Δ*mupG* cells were grown in LB medium for 24 h. Acetone extracts of the cytosolic fractions were analyzed by LC-MS in positive ion-mode. Fifty microliter of the cytosolic fraction from Δ*mupG* was incubated with buffer (no enzyme), with 1 μg recombinant MupG (+MupG) or with MupG and MurNAc 6P etherase MurQ (both 1 μg) for 2.5 h at 37°C. Representative mass spectra of the samples from at least three biological replicates were presented as extracted ion chromatograms (EIC × 10^4 [cps]) for MurNAc 6P-GlcNAc (observed masses of $(M+H)^+$ = 577.166 m/z) in red, GlcNAc ($(M+H)^+$ = 222.098 m/z) in blue, MurNAc 6P ($(M+H)^+$ = 374.083 m/z) in green and GlcNAc 6P ($(M+H)^+$ = 302.062) in black.

exponential growth phase (3 h), early stationary phase (9 h) and stationary phase (24 h). These growth phases were defined by a growth kinetics study with *S. aureus* wild type and Δ*mupG* mutant cells in LB medium (cf. **Figure 1**). The accumulation of MurNAc 6P-GlcNAc was low at exponential phase, increased significantly at transition phase and reached the highest level after 24 h of growth (**Supplementary Figure 4**). Thus, accumulation of MurNAc 6P-GlcNAc in Δ*mupG* cells confirmed that cell wall sugar recycling occurs predominantly in the transition and stationary phase.

We further investigated, whether accumulation of MurNAc 6P-GlcNAc in the Δ*mupG* cells can be abolished by expressing MupG on a plasmid. We used stationary phase cells for this study, since highest levels of accumulation were obtained at this stage (**Supplementary Figure 4**). *S. aureus* Δ*mupG* cells were transformed with a plasmid (named pCtufamp-*mupG*; see **Supplementary Data**) constitutively expressing MupG, or with empty plasmid (pCtufamp) as a control. Analysis of the cytosolic fractions of the Δ*mupG* cells showed that MupG expression leads to complete disappearance of MurNAc 6P-GlcNAc amounts in the cytosol after 24 h of growth (**Figure 5**).

MurNAc-GlcNAc Accumulates Extracellularly in *S. aureus* Cells Lacking the MurP Transporter

The PTS transporter MurP of *S. aureus* was shown to transport and concomitantly phosphorylate MurNAc, yielding MurNAc 6P (Borisova et al., 2016). However, MurNAc-GlcNAc rather than MurNAc is the main sugar released from the peptidoglycan by Atl and other autolysins during cell wall turnover in *S. aureus*. Thus, we proposed that MurNAc-GlcNAc might be primary the natural substrates of MurP, thereby generating intracellular MurNAc 6P-GlcNAc, the substrate of the MupG hydrolase. To test this hypothesis, we analyzed the extracellular extracts of *S. aureus* wild type and two *murP* mutant cells (*murP::Tn* insertion mutant and Δ*mupGmurQPR* markerless deletion mutant). The MS analysis of the culture supernatant indeed revealed the accumulation of a disaccharide turnover

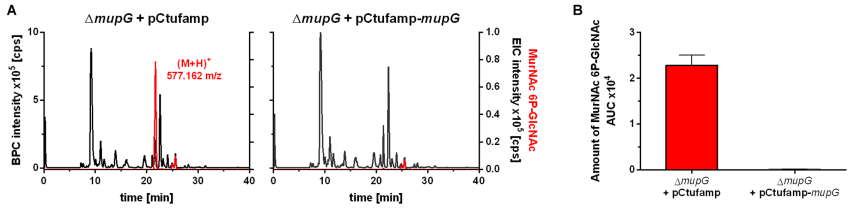

FIGURE 5 | LC-MS analysis of cell extract from MupG complemented mutant. *S. aureus* Δ*mupG* cells transformed with the control pCtufamp plasmid (Δ*mupG* + pCtufamp) or with the *mupG* complementation plasmid pCtufamp-*mupG* (Δ*mupG* + pCtufamp-*mupG*) were grown for 24 h. Cytosolic fractions were analyzed by LC-MS in positive ion-mode. **(A)** Mass spectra of the samples were presented as base peak chromatograms (BPC × 10^5 counts per s [cps]) in black and as extracted ion chromatograms (EIC × 10^5 [cps]) for MurNAc 6P-GlcNAc with observed mass of $(M+H)^+$ = 577.162 m/z in red. **(B)** MupG complementation experiment was performed in triplicates and the relative amount of the MurNAc 6P-GlcNAc in the cells was determined by calculating the area under the curve (AUC) of the respective EIC spectra.

product with a mass identical to MurNAc-GlcNAc (observed $(M+H)^+$ = 497.197 and 497.195 m/z, respectively, theoretical mass of $(M+H)^+$ = 497.198 m/z), which was lacking in the culture supernatant of the wild type cells (**Figure 6**). To confirm the identity of the disaccharide, again MS fragmentation analyses before and after reduction were conducted, as summarized in **Supplementary Figure 5**. A compound with the mass of $(M+H)^+$ = 497.197 m/z was detected also as Na^+ and K^+ adducts, as well as it was characterized by the neutral loss of GlcNAc (-221.087 Da) and the formation of a MurNAc elimination product [$(M+H)^+$ = 276.111 m/z]. In addition, we identified a fragmentation product in which water was eliminated (-18.004 Da) yielding a dehydration product [$(M+H)^+$ = 479.192 m/z] (**Supplementary Figure 5A**). After $NaBH_4$ reduction of the culture supernatant from the *murP::Tn* mutant, the mass of the disaccharide product $(M+H)^+$ = 497.197 m/z disappeared and a product in a reduced form with a mass of $(M+H)^+$ = 499.214 m/z appeared. This product was also detected as Na^+ and K^+ adducts and, in addition, the fragmentation pattern revealed a mass corresponding to a MurNAc elimination product (observed mass of 276.108 m/z) that lost a neutral mass, corresponding to the exact mass of reduced GlcNAc (-223.107 Da). The absence of a fragmentation product with a loss of water is in agreement with a reduction at the anomeric site, which precludes water elimination. The fragmentation pattern of the non-reduced and reduced extracellular accumulation products indicated that MurNAc-GlcNAc, but not GlcNAc-MurNAc, accumulates in the culture supernatant of Δ*murP* deletion mutants. This disaccharide was not cleaved by the recombinant β-1,4-*N*-acetylglucosaminidase NagZ from *B. subtilis* (Litzinger et al., 2010a,b) (data not shown), which provides a further evidence that GlcNAc-MurNAc is not the recycling product in *S. aureus*. The same MS

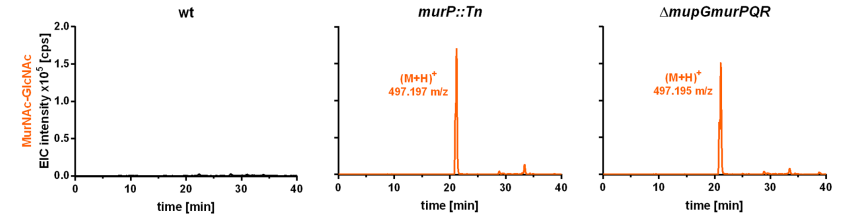

FIGURE 6 | LC-MS analysis from recycling mutants, lacking MurP transporter. *S. aureus* wild type (wt) cells, a *murP* transporter mutant (*murP::Tn*) and a *murQ*-operon mutant (Δ*mupGmurQPR*) were grown to stationary phase (24 h) in LB. Bacterial cultures were centrifuged and 1 ml of each supernatant was transferred to 500 μl of ice-cold acetone to remove macromolecules and proteins from the samples. After centrifugation, culture supernatants were dryed in the speedvac, solved in 50 μl of Millipore water and 2 μl of the samples were injected to the HPLC column. MS analysis of the culture supernatants was performed in positive-ion mode and mass spectra are presented as extracted ion chromatograms (EIC × 10^5 counts per second [cps]) in orange. In the culture supernatants of both mutants, an additional compound accumulates (*murP::Tn*, observed mass of $(M+H)^+$ = 497.197 m/z; Δ*mupGmurQPR*, observed mass of $(M+H)^+$ = 497.195 m/z). The mass of this compound in the supernatant corresponds to a disaccharide made of GlcNAc and MurNAc. This compound was further analyzed by MS fragmentation and identified as MurNAc-GlcNAc (see **Supplementary Figure 5**). MS data are shown as representative from three biological replicates.

fragmentation pattern was obtained in the culture supernatant of the Δ*mupGmurQPR* recycling mutant, before and after reduction of the supernatant (data not shown), showing that also in this mutant the recycling product MurNAc-GlcNAc accumulates. Interestingly, in the culture supernatant of the Δ*mupGmurQPR* mutant also other compounds accumulated and were absent in the supernatant of the wild type cells, which nature could not be identified so far (data not shown).

To conclude, the extracellular accumulation of MurNAc-GlcNAc in both *murP* mutants, as well as the intracellular accumulation of MurNAc 6P-GlcNAc in the *mupG* mutants and the absence of MurNAc 6P-GlcNAc and MurNAc 6P in the cytosol of Δ*mupGmurQPR* operon mutant revealed that the disaccharide MurNAc-GlcNAc is the natural substrate internalized by the PTS transporter MurP, which intracellularly yields MurNAc 6P-GlcNAc, the substrate of MupG.

DISCUSSION

We discovered in this study how *S. aureus* reutilizes the sugar part of the peptidoglycan of its cell wall. The overall scheme of this novel peptidoglycan recycling pathway is depicted in **Figure 7**. Mass spectrometric analysis of sugars compounds, accumulating in the growth medium of Δ*murP* cells (MurNAc-GlcNAc) and in the cytoplasm of Δ*mupG* cells (MurNAc 6P-GlcNAc), measured directly or after reduction of the sugars, unequivocally demonstrated the chemical nature of these compounds and allowed to establish the pathway. Thus, the principle peptidoglycan turnover product of *S. aureus* is MurNAc-GlcNAc, which results from the peptidoglycan cleavage by muramoyl-L-Ala amidases and endo-*N*-acetylglucosaminidases, whereas lysozyme-like endo-*N*-acetylmuramidases would generate GlcNAc-MurNAc products. Remarkably, the peptidoglycan of *S. aureus* is frequently *O*-acetylated at the C6 hydroxyl group of MurNAc, thereby rendered lysozyme-resistant (Bera et al., 2006; Sychantha et al., 2017). An endogenous lysozyme-like muramidase therefore would not be able to cleave the peptidoglycan of *S. aureus*. Accordingly, *S. aureus* possesses peptidoglycan-cleaving endo-*N*-acetylglucosaminidases: one of them is the well-studied major autolysin Atl (Sugai et al., 1995; Wheeler et al., 2015; Chan et al., 2016).

Since only MurNAc-GlcNAc and not MurNAc was found in the spent medium of the *murP::Tn* and Δ*mupGmurQPR* mutants during growth, the disaccharide appears to be the general peptidoglycan turnover product of *S. aureus* and natural substrate of the PTS transporter MurP. However, MurP had been shown previously to take up and phosphorylate also MurNAc, if added to the growth medium (Borisova et al., 2016). Thus, apparently MurP accepts both sugars, MurNAc and MurNAc-GlcNAc as substrates. To our knowledge, this is the first report of a PTS system that is able to take up and to specifically phosphorylate a disaccharide as well as a monosaccharide (Postma et al., 1993). Since *murP* of *S. aureus* encodes only the enzyme IIBC components, an enzyme IIA (along with the general components EI and HPr of the PTS) is required to enable MurP functioning

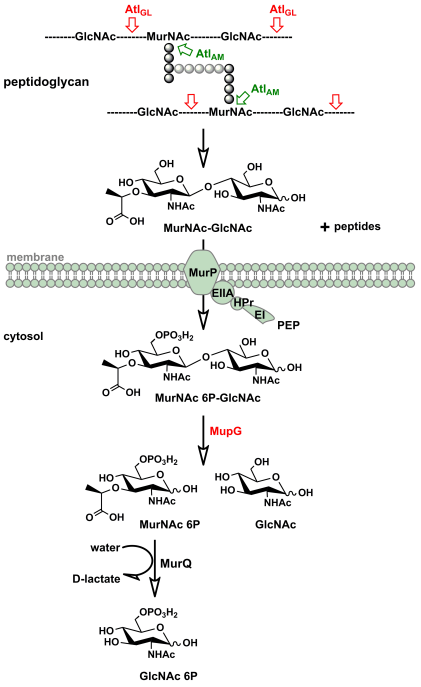

FIGURE 7 | Scheme of the peptidoglycan sugar recycling in *S. aureus*. During growth and division, *S. aureus* cells constantly degrade and resynthesize their peptidoglycan. The major autolysin Atl, a bifunctional muramoyl-L-alanine amidase and endo-*N*-acetylglucosaminidase, is able to cleave its peptidoglycan, generating MurNAc-GlcNAc and peptide turnover products. MurNAc-GlcNAc disaccharide is reutilized: transported in the cells and concommitantly phosphorylated by the MurP PTS transporter generating intracellularly MurNAc 6P-GlcNAc. Subsequently, the MurNAc 6-phosphate-GlcNAc glycosidase MupG cleaves this compound, generating the products MurNAc 6P and GlcNAc. The D-lactyl ether substituent of MurNAc 6P is specifically cleaved off by the etherase MurQ, previously characterized in our lab, forming GlcNAc 6P and D-lactate (Borisova et al., 2016). It is currently unclear how GlcNAc, the second product of the MupG reaction, is further metabolized in *S. aureus* cells.

(**Figure 7**). So far, it is unclear which enzyme IIA operates together with MurP.

The most important result of this study is the identification of a novel 6-phosphomuramidase, encoded by *SAUSA300_0192* (strain USA300), which we named MupG, for MurNAc-6P glycosidase. MurNAc 6P-GlcNAc accumulated in Δ*mupG* cells of *S. aureus* and recombinantly produced MupG cleaved MurNAc 6P-GlcNAc, releasing MurNAc 6P and GlcNAc. The former product is subsequently metabolized and was identified by

specific cleavage by the MurNAc 6P etherase MurQ, yielding GlcNAc 6P and D-lactate (Borisova et al., 2016). Moreover, accumulation of MurNAc 6P-GlcNAc in a Δ*mupG* mutant was abolished by complementation using a MupG-expressing plasmid. Since only accumulation of MurNAc 6P-GlcNAc and not of MurNAc 6P was observed in a Δ*murGmurQ* double mutant (please note that MurNAc 6P accumulates in Δ*murQ* cells; Borisova et al., 2016), it can be concluded that recycling of the sugar part of the peptidoglycan during growth of *S. aureus* in LB medium exclusively proceeds via the uptake of MurNAc-GlcNAc disaccharides.

6-phosphoglycosidases commonly act in combination with PTS glycoside transporters. Such systems were characterized with specificities for α-glucosides such as maltose, sucrose, and trehalose (EC 3.2.1.122), or for β-glycosides (EC 3.2.1.86) or β-galactosides (EC 3.2.1.85), such as cellobiose, chitobiose, and lactose (Hengstenberg et al., 1993; Mokhtari et al., 2013). For example, *S. aureus* (as well as *Lactobacillus* and *Streptococcus* sp.) imports lactose via the specific PTS LacE (enzyme IIBC), which phosphorylates the disaccharide at the C6 hydroxyl group of the β-galactose moiety (Hengstenberg et al., 1993). In addition, it possesses a cytoplasmic 6-phospho-β-galactosidase (LacG) that hydrolyzes lactose 6P to galactose 6P and glucose (Staedtler et al., 1995; Yip et al., 2007; Hill and Reilly, 2008). All of the 6P-glycosidases characterized to date are classified within the CAZy glycosidase families 1 and 4 (Davies et al., 2005), which operate by very distinct mechanisms (Witt et al., 1993; Staedtler et al., 1995; Yip et al., 2007; Hill and Reilly, 2008). MupG, however, displays no significant similarity with these glycosidases, instead it founds an entirely new enzyme family. MupG and related proteins so far had been classified as domain of unknown function proteins (IPR008589; DUF871). Although they had been grouped within the glycoside hydrolase (IPR017853) and aldolase-type TIM barrel (IPR013785) superfamilies, no clear attribution to glycosidase function had been made by bioinformatic analyses. The mechanism of members of this novel glycosidase family, i.e., the stereochemical outcome and catalytic residues remain enigmatic. Our results, however, indicate that MupG has no requirement for NAD^+ as for family 4 glycosidases (Yip et al., 2007).

Proteins displaying significant amino acid sequence identities with MupG of *S. aureus* can be found in different bacterial species. Together with MupG these proteins constitute a family (Pfam PF05913) containing domain of unknown function (DUF) 871, with MupG representing the first characterized enzyme of this protein family. The distribution of putative orthologous proteins of MupG is surprisingly narrow and mostly restricted to the phylum firmicutes. The reason for this narrow phylogenetic distribution among the firmicutes and a very selective occurrence within organisms of other phyla, is currently unclear. It may suggest a recent evolutionary event and in addition the distribution by horizontal gene transfer, however, additional studies are required to confirm these assumptions. To learn more about the distribution of MupG orthologs within bacteria, we constructed a phylogenetic tree, based on an alignment of 519 amino acid sequences extracted from the protein family entry Pfam PF05913 (**Figure 8**) that includes proteins from 115 bacterial genera as well as from five Crenarcheotae and one nematode species (see **Supplementary Table 3** for a complete list of species or genera containing putative enzymes orthologous to MupG). Intriguingly, the phylogenetic tree revealed distinct clades of proteins that include close homologs of MupG and more distinct MupG-like proteins (**Figure 8**). Potential orthologs of MupG of *S. aureus* are found in various *Staphylococcus* sp. (red rectangle, **Figure 8**) and in many other Bacilli, e.g., Bacillales such as *Listeria, Paenibacillus, and Bacillus sp.*, and also in Lactobacillales, e.g., *Streptococcus*, *Lactococcus*, *Enterococcus*, *Lactobacillus,* and *Pediococcus* sp., as well as in some Clostridiales. Intriguingly, also some few Fusobacteriales, Chlamydiales and Spirochetales species as well the nematode *Trichuris trichiura* possess a putative MupG ortholog. Some bacterial species, however, contain up to six putative paralogs of MupG (**Supplementary Table 3**), indicating that the PF05913/DUF871 protein family besides MupG orthologs might also contain proteins of distinct physiological function and with altered substrate specificity. For example, *Coprobacillus cateniformis* contains six putative paralogs, *Carnobacterium maltaromaticum* LMA28 five, *Lactobacillus plantarum* WCFS1 four, *Bacillus anthracis* and *Enterococcus faecalis* V583 three and *Lactococcus lactis* IL1403, *Bacillus megaterium* and many other bacteria contain two putative paralogs (cf. **Supplementary Table 3**). We assume that close homologs of MupG of *S. aureus* have identical function (MurNAc-6P glycosidases, see protein clade colored red in **Figure 8**) but more remotely related proteins (colored black in **Figure 8**) likely contain enzymes of different function. Remarkebly, some archaea (e.g., *Sulfolobus solfatorius* and *Sulfurisphaera tokodaii*) contain putative MupG-like orthologs. Since archaea lack a peptidoglycan cell wall it seems likely that these enzymes have a function that differs from the hydrolysis of a peptidoglycan turnover product. Many firmicutes presumably contain a MupG ortholog and supposably possess a recycling pathway for MurNAc-GlcNAc as that presented here for *S. aureus*. Notably, crystal structures of two putative orthologs of *MupG* [from *Bacillus cereus* (1×7f) and *Enterococcus faecalis* (2P0O)] were deposited to the protein structure database[2]. We are currently investigating whether these enzymes and MupG have the same specificity and function.

For a long time, the need for cell wall recycling in Gram-positive bacteria, and particularly in coccoidal bacteria such as *S. aureus*, had been questioned. Although, reports from the 1970s revealed a massive turnover of the cell wall in *S. aureus* (Wong et al., 1974; Blümel et al., 1979; reviewed in Doyle et al., 1988; Reith and Mayer, 2011). Recent studies, showed that the peptidoglycan of the cell wall in *S. aureus* undergoes a massive rearrangement during growth and division that involves glycan strand trimming by endo-*N*-acetylglucosaminidases (Wheeler et al., 2015; Chan et al., 2016), peptidoglycan degradation by autolysins such as Atl during cell division and separation (Yamada et al., 1996; Biswas, 2009; Götz et al., 2014) as well as autolysis during biofilm formation (Bose et al., 2012). We recently demonstrated that peptidoglycan recycling proceeds in Gram-positive organisms predominantly occurring during transition and stationary phases

[2]https://www.rcsb.org/

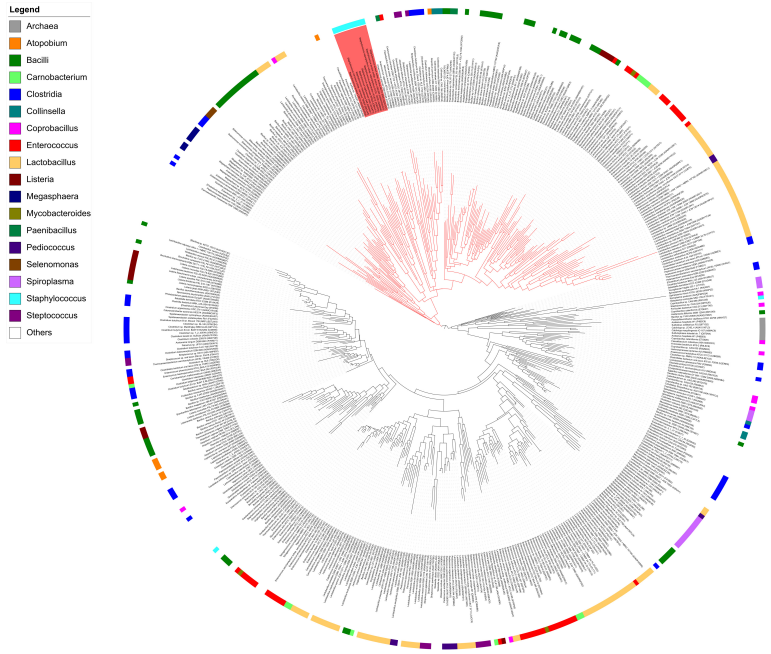

FIGURE 8 | Phylogenetic tree showing the relation of MupG orthologs. The phylogenetic tree was constructed with RaxML from an alignment of 519 amino acid sequences, based on the Pfam entry PF05913, which lists putative orthologs of MupG (DUF871 domain proteins). The genus of *Staphylococcus* is marked by a red rectangle and includes MupG of *S. aureus* USA300, which was characterized in this study as a MurNAc 6P-glycosidase. Putative MurNAc 6P glycosidase (close orthologs of MupG) constitute a distinct clade, indicated by red lines. More distantly related MupG-like proteins constitute different clades that are indicated by black lines. Bacterial genera are color coded as indicated. See **Supplementary Table 3** for a complete list of the proteins within this phylogenetic tree.

(Borisova et al., 2016). The results of the present study confirmed these previous observations. Notably, the *mupG* mutant and the Δ*mupGmurQ* double mutant showed a weak disadvantage during growth in stationary phase (cf. **Supplementary Figure 2**). This growth defect was stronger than previously observed for the Δ*murQ* mutant (Borisova et al., 2016), which might be explained by the inability of the former mutants to recycle both sugars of the peptidoglycan, GlcNAc and MurNAc, whereas the latter mutant has a defect only in the recovery of MurNAc. So far, it remains unclear how the GlcNAc part of MurNAc 6P-GlcNAc is recovered, after cleavage by MupG in the cytoplasm. GlcNAc reutilization would require either a GlcNAc kinase, or alternatively the secretion and a re-import by the GlcNAc PTS of *S. aureus*, in both cases yielding GlcNAc 6P, which can be shuttled into the amino sugar catabolic pathway (Komatsuzawa et al., 2004). Moreover, the fate of the peptide part of the peptidoglycan is currently unknown.

CONCLUSION

Here we elucidated a novel pathway for the uptake and catabolism of the disaccharide MurNAc-GlcNAc, which is a specific peptidoglycan turnover product generated by the joint action of peptidoglycan amidases and endo-*N*-acetylglucosamidases, e.g., by the bifunctional autolysin Atl of *S. aureus*. The pathway in *S. aureus* involves the PTS transporter MurP, required for the uptake and phosphorylation of the disaccharide yielding MurNAc 6-phosphate-GlcNAc, and MupG, a unique glycosidase with 6-phospho-*N*-acetylmuramidase activity. MupG is the first characterized representative of a so far unexplored protein family containing domain of unknown function DUF871, which is distributed mostly among firmicutes. As many of these organisms also possess peptidoglycan-cleaving endo-*N*-acetylglucosaminidases and MurP-like transporters, besides MupG orthologs, recycling of the peptidoglycan turnover product MurNAc-GlcNAc

is presumably a common feature among these firmicutes. Peptidoglycan recycling is crucial for stationary phase survival of Gram-positive bacteria (Borisova et al., 2016) and thus, the pathway identified in this study may serve as a novel target to treat persistent infections by *S. aureus* and selectively other bacteria.

AUTHOR CONTRIBUTIONS

RK, MB, and PE cloned MupG. RK and MB expressed and biochemically characterized MupG. RK and MB performed HPLC-MS experiments and analyzed the data. MA, RK, and NZ aligned the MupG-like protein family, constructed the phylogenetic tree based on this alignment, and prepared the **Figure 8**. MB and CM formulated the original problem and provided guidance throughout the study. MB, CM, RK, and PE designed the experiments and developed the methodology. MB, CM, and RK wrote the manuscript. MB approved the final version to be published.

FUNDING

This work was financed by the German Research Foundation (DFG; Grants SFB766/A15 and GRK1708/B2 to CM). We further acknowledge support by the DFG and the Open Access Publishing Fund of the University of Tübingen.

ACKNOWLEDGMENTS

We are very grateful to Rosmarie Gaupp, Friedrich Götz, and Heike Brötz-Oesterhelt for providing plasmids, strains, and working space.

SUPPLEMENTARY MATERIAL

The Supplementary Material for this article can be found online at: https://www.frontiersin.org/articles/10.3389/fmicb.2018.02725/full#supplementary-material

REFERENCES

Bera, A., Biswas, R., Herbert, S., and Götz, F. (2006). The presence of peptidoglycan O-acetyltransferase in various staphylococcal species correlates with lysozyme resistance and pathogenicity. *Infect. Immun.* 74, 4598–4604. doi: 10.1128/IAI.00301-06

Biswas, R. (2009). Characterization of *Staphylococcus aureus* peptidoglycan hydrolases and isolation of defined peptidoglycan structures. Ph.D. thesis, University of Tübingen, Tübingen.

Biswas, R., Voggu, L., Simon, U. K., Hentschel, P., Thumm, G., and Götz, F. (2006). Activity of the major staphylococcal autolysin Atl. *FEMS Microbiol. Lett.* 259, 260–268. doi: 10.1111/j.1574-6968.2006.00281.x

Blümel, P., Uecker, W., and Giesbrecht, P. (1979). Zero order kinetics of cell wall turnover in *Staphylococcus aureus*. *Arch. Microbiol.* 121, 103–110. doi: 10.1007/BF00689972

Boneca, I. G., Huang, Z. H., Gage, D. A., and Tomasz, A. (2000). Characterization of *Staphylococcus aureus* cell wall glycan strands, evidence for a new β-N-acetylglucosaminidase activity. *J. Biol. Chem.* 275, 9910–9918. doi: 10.1074/jbc.275.14.9910

Borisova, M., Gaupp, R., Duckworth, A., Schneider, A., Dalügge, D., Mühleck, M., et al. (2016). Peptidoglycan recycling in Gram-positive bacteria is crucial for survival in stationary phase. *mBio* 7:e00923-16. doi: 10.1128/mBio.00923-16

Bose, J. L., Lehman, M. K., Fey, P. D., and Bayles, K. W. (2012). Contribution of the *Staphylococcus aureus* Atl AM and GL murein hydrolase activities in cell division, autolysis, and biofilm formation. *PLoS One* 7:e42244. doi: 10.1371/journal.pone.0042244

Cabeen, M. T., and Jacobs-Wagner, C. (2005). Bacterial cell shape. *Nat. Rev. Microbiol.* 3, 601–610. doi: 10.1038/nrmicro1205

Capella-Gutiérrez, S., Silla-Martínez, J. M., and Gabaldón, T. (2009). trimAl: a tool for automated alignment trimming in large-scale phylogenetic analyses. *Bioinformatics* 25, 1972–1973. doi: 10.1093/bioinformatics/btp348

Chan, Y. G., Frankel, M. B., Missiakas, D., and Schneewind, O. (2016). SagB glucosaminidase is a determinant of *Staphylococcus aureus* glycan chain length, antibiotic susceptibility, and protein secretion. *J. Bacteriol.* 198, 1123–1136. doi: 10.1128/JB.00983-15

Cho, H., Wivagg, C. N., Kapoor, M., Barry, Z., Rohs, P. D., Suh, H., et al. (2016). Bacterial cell wall biogenesis is mediated by SEDS and PBP polymerase families functioning semi-autonomously. *Nat. Microbiol.* 1:16172 doi: 10.1038/nmicrobiol.2016.172

Davies, G. J., Gloster, T. M., and Henrissat, B. (2005). Recent structural insights into the expanding world of carbohydrate-active enzymes. *Curr. Opin. Struct. Biol.* 15, 637–645. doi: 10.1016/j.sbi.2005.10.008

Doyle, R. J., Chaloupka, J., and Vinter, V. (1988). Turnover of cell walls in microorganisms. *Microbiol. Rev.* 52, 554–567.

Foster, S. J. (1995). Molecular characterization and functional analysis of the major autolysin of *Staphylococcus aureus* 8325/4. *J. Bacteriol.* 177, 5723–5725. doi: 10.1128/jb.177.19.5723-5725.1995

Frankel, M. B., Hendrickx, A. P., Missiakas, D. M., and Schneewind, O. (2011). LytN, a murein hydrolase in the cross-wall compartment of *Staphylococcus aureus*, is involved in proper bacterial growth and envelope assembly. *J. Biol. Chem.* 286, 32593–32605. doi: 10.1074/jbc.M111.258863

Fuchs, R., Stoehr, P., Rice, P., Omond, R., and Cameron, G. (1990). New services of the EMBL data library. *Nucleic Acids Res.* 18, 4319–4323. doi: 10.1093/nar/18.15.4319

Gally, D., and Archibald, A. R. (1993). Cell wall assembly in *Staphylococcus aureus*: proposed absence of secondary crosslinking reactions. *J. Gen. Microbiol.* 139, 1907–1913. doi: 10.1099/00221287-139-8-1907

Gisin, J., Schneider, A., Nagele, B., Borisova, M., and Mayer, C. (2013). A cell wall recycling shortcut that bypasses peptidoglycan de novo biosynthesis. *Nat. Chem. Biol.* 9, 491–493. doi: 10.1038/nchembio.1289

Götz, F., Heilmann, C., and Stehle, T. (2014). Functional and structural analysis of the major amidase (Atl) in Staphylococcus. *Int. J. Med. Microbiol.* 304, 156–163. doi: 10.1016/j.ijmm.2013.11.006

Hengstenberg, W., Kohlbrecher, D., Witt, E., Kruse, R., Christiansen, I., Peters, D., et al. (1993). Structure and function of proteins of the phosphotransferase system and of 6-phospho-beta-glycosidases in Gram-positive bacteria. *FEMS Microbiol. Rev.* 12, 149–163.

Hill, A. D., and Reilly, P. J. (2008). Computational analysis of glycoside hydrolase family 1 specificities. *Biopolymers* 89, 1021–1031. doi: 10.1002/bip.21052

Hiramatsu, K., Katayama, Y., Matsuo, M., Sasaki, T., Morimoto, Y., Sekiguchi, A., et al. (2014). Multi-drug-resistant *Staphylococcus aureus* and future chemotherapy. *J. Infect. Chemother.* 20, 593–601. doi: 10.1016/j.jiac.2014.08.001

Kajimura, J., Fujiwara, T., Yamada, S., Suzawa, Y., Nishida, T., Oyamada, Y., et al. (2005). Identification and molecular characterization of an N-acetylmuramyl-L-alanine amidase Sle1 involved in cell separation of *Staphylococcus aureus*. *Mol. Microbiol.* 58, 1087–1101. doi: 10.1111/j.1365-2958.2005.04881.x

Katoh, K., and Standley, D. M. (2013). MAFFT multiple sequence alignment software version 7: improvements in performance and usability. *Mol. Biol. Evol.* 30, 772–780. doi: 10.1093/molbev/mst010

Komatsuzawa, H., Fujiwara, T., Nishi, H., Yamada, S., Ohara, M., Mccallum, N., et al. (2004). The gate controlling cell wall synthesis in *Staphylococcus aureus*. *Mol. Microbiol.* 53, 1221–1231. doi: 10.1111/j.1365-2958.2004.04200.x

Letunic, I., and Bork, P. (2016). Interactive tree of life (iTOL) v3: an online tool for the display and annotation of phylogenetic and other trees. *Nucleic Acids Res.* 44, W242–W245. doi: 10.1093/nar/gkw290

Litzinger, S., Duckworth, A., Nitzsche, K., Risinger, C., Wittmann, V., and Mayer, C. (2010a). Muropeptide rescue in *Bacillus subtilis* involves sequential hydrolysis by beta-N-acetylglucosaminidase and N-acetylmuramyl-L-alanine amidase. *J. Bacteriol.* 192, 3132–3143. doi: 10.1128/JB.01256-09

Litzinger, S., Fischer, S., Polzer, P., Diederichs, K., Welte, W., and Mayer, C. (2010b). Structural and kinetic analysis of *Bacillus subtilis* N-acetylglucosaminidase reveals a unique Asp-His dyad mechanism. *J. Biol. Chem.* 285, 35675–35684. doi: 10.1074/jbc.M110.131037

Litzinger, S., and Mayer, C. (2010). "Chapter 1: the murein sacculus," in *Prokaryotic Cell Wall Compounds - Structure and Biochemistry*, eds H. König, H. Claus, and A. Varma (New York, NY: Springer), 3–52.

Meeske, A. J., Riley, E. P., Robins, W. P., Uehara, T., Mekalanos, J. J., Kahne, D., et al. (2016). SEDS proteins are a widespread family of bacterial cell wall polymerases. *Nature* 537, 634–638. doi: 10.1038/nature19331

Mokhtari, A., Blancato, V. S., Repizo, G. D., Henry, C., Pikis, A., Bourand, A., et al. (2013). *Enterococcus faecalis* utilizes maltose by connecting two incompatible metabolic routes via a novel maltose 6′-phosphate phosphatase (MapP). *Mol. Microbiol.* 88, 234–253. doi: 10.1111/mmi.12183

Monteiro, J. M., Fernandes, P. B., Vaz, F., Pereira, A. R., Tavares, A. C., Ferreira, M. T., et al. (2015). Cell shape dynamics during the staphylococcal cell cycle. *Nat. Commun.* 6:8055. doi: 10.1038/ncomms9055

Postma, P. W., Lengeler, J. W., and Jacobson, G. R. (1993). Phosphoenolpyruvate:carbohydrate phosphotransferase systems of bacteria. *Microbiol. Rev.* 57, 543–594.

Ramadurai, L., Lockwood, K. J., Nadakavukaren, M. J., and Jayaswal, R. K. (1999). Characterization of a chromosomally encoded glycylglycine endopeptidase of *Staphylococcus aureus*. *Microbiology* 145(Pt 4), 801–808. doi: 10.1099/13500872-145-4-801

Reith, J., and Mayer, C. (2011). Peptidoglycan turnover and recycling in Gram-positive bacteria. *Appl. Microbiol. Biotechnol.* 92, 1–11. doi: 10.1007/s00253-011-3486-x

Schaub, R. E., and Dillard, J. P. (2017). Digestion of peptidoglycan and analysis of soluble fragments. *Bio Protoc.* 7:e2438. doi: 10.21769/BioProtoc.2438

Staedtler, P., Hoenig, S., Frank, R., Withers, S. G., and Hengstenberg, W. (1995). Identification of the active-site nucleophile in 6-phospho-beta-galactosidase from *Staphylococcus aureus* by labelling with synthetic inhibitors. *Eur. J. Biochem.* 232, 658–663. doi: 10.1111/j.1432-1033.1995.tb20857.x

Stamatakis, A. (2014). RAxML version 8: a tool for phylogenetic analysis and post-analysis of large phylogenies. *Bioinformatics* 30, 1312–1313. doi: 10.1093/bioinformatics/btu033

Stapleton, M. R., Horsburgh, M. J., Hayhurst, E. J., Wright, L., Jonsson, I. M., Tarkowski, A., et al. (2007). Characterization of IsaA and SceD, two putative lytic transglycosylases of *Staphylococcus aureus*. *J. Bacteriol.* 189, 7316–7325. doi: 10.1128/JB.00734-07

Sugai, M., Komatsuzawa, H., Akiyama, T., Hong, Y. M., Oshida, T., Miyake, Y., et al. (1995). Identification of endo-β-N-acetylglucosaminidase and N-acetylmuramyl-L-alanine amidase as cluster-dispersing enzymes in *Staphylococcus aureus*. *J. Bacteriol.* 177, 1491–1496. doi: 10.1128/jb.177.6.1491-1496.1995

Sychantha, D., Jones, C. S., Little, D. J., Moynihan, P. J., Robinson, H., Galley, N. F., et al. (2017). In vitro characterization of the antivirulence target of Gram-positive pathogens, peptidoglycan O-acetyltransferase A (OatA). *PLoS Pathog.* 13:e1006667. doi: 10.1371/journal.ppat.1006667

Takahashi, J., Komatsuzawa, H., Yamada, S., Nishida, T., Labischinski, H., Fujiwara, T., et al. (2002). Molecular characterization of an atl null mutant of *Staphylococcus aureus*. *Microbiol. Immunol.* 46, 601–612. doi: 10.1111/j.1348-0421.2002.tb02741.x

Vollmer, W., Blanot, D., and De Pedro, M. A. (2008). Peptidoglycan structure and architecture. *FEMS Microbiol. Rev.* 32, 149–167. doi: 10.1111/j.1574-6976.2007.00094.x

Wheeler, R., Turner, R. D., Bailey, R. G., Salamaga, B., Mesnage, S., Mohamad, S. A., et al. (2015). Bacterial cell enlargement requires control of cell wall stiffness mediated by peptidoglycan hydrolases. *mBio* 6:e00660. doi: 10.1128/mBio.00660-15

Witt, E., Frank, R., and Hengstenberg, W. (1993). 6-Phospho-beta-galactosidases of gram-positive and 6-phospho-beta-glucosidase B of gram-negative bacteria: comparison of structure and function by kinetic and immunological methods and mutagenesis of the *lacG* gene of *Staphylococcus aureus*. *Protein Eng.* 6, 913–920. doi: 10.1093/protein/6.8.913

Wong, W., Young, F. E., and Chatterjee, A. N. (1974). Regulation of bacterial cell walls: turnover of cell wall in *Staphylococcus aureus*. *J. Bacteriol.* 120, 837–843.

Yamada, S., Sugai, M., Komatsuzawa, H., Nakashima, S., Oshida, T., Matsumoto, A., et al. (1996). An autolysin ring associated with cell separation of *Staphylococcus aureus*. *J. Bacteriol.* 178, 1565–1571. doi: 10.1128/jb.178.6.1565-1571.1996

Yip, V. L., Thompson, J., and Withers, S. G. (2007). Mechanism of GlvA from *Bacillus subtilis*: a detailed kinetic analysis of a 6-phospho-alpha-glucosidase from glycoside hydrolase family 4. *Biochemistry* 46, 9840–9852. doi: 10.1021/bi700536p

Conflict of Interest Statement: The authors declare that the research was conducted in the absence of any commercial or financial relationships that could be construed as a potential conflict of interest.